Investigations of Pure and Derivatized Fullerenes by Mass Spectrometry

Mark Peter Barrow

Thesis submitted for the degree of Doctor of Philosophy in Chemistry

Department of Chemistry, University of Warwick, UK

September 2000

Table of Contents

Table of Figures

Acknowledgements

First of all, I wish to thank Dr. Thomas Drewello for his vital role as my supervisor. Similarly, I wish to acknowledge the support of the group members during my research, most notably Dr. Yury Vasil'ev, Tracy Brown, and Mohammed S. Al-Jafari. The crucial involvement of our collaborators must also not be overlooked. Instrument time has been provided courtesy of Dr. Monika Möder, Dr. Matthias Nüchter, Prof. Bernd Ondruschka, Dr. Gabor Czira, and Dr. Karoly Vékey, Martin Green, Erik Williams, Dr. Robert H. Bateman, Dr. Jackie Jarvis, Prof. Rainer Herzschuh, Inder Katyal, Dr. Xidong Feng, Dr. James I. Wallace, and Prof. Peter J. Derrick. Dr. Roger Taylor, Dr. Olga V. Boltalina, Prof. Carlito Lebrilla, and Prof. Andreas Hirsch have played the vital role of providing the research group with many, different fullerene derivative samples, and Prof. K. Peter Vollhardt provided the organometallic compound used as a precursor for fullerene formation. I would also like to thank Prof. Patrick W. Fowler for his friendly discussions during the course of the research.

Alex Colburn, Dr. Anastassios E. Giannakopulos, Dr. Rob Noll, Dr. Mike Belov, Dr. Julie Varney, and Dr. Richard T. Gallagher have imparted useful experience and advice with regards to mass spectrometric instrumentation. In relation to improving my understanding of Physics, I have had many enlightening discussions with Danny Chrastina, Neill Bowler, and David Gillingham. Phil Roskelly, Kirk Harris, and Neville Cosgriff, of the electronics workshop, and Ken Westwood, Marcus Grant, and Lee Butcher, of the mechanical workshop, have supplied essential support during the maintenance of the instruments.

The friendship and support of colleagues Andrew Bottrill, Ben Thomas, Liam McDonnell, Phil Green, and Dr. Helen J. Cooper has been greatly appreciated. Finally, I would like to thank my parents, Mrs. M. C. Barrow and Dr. H. G. Barrow, and my girlfriend, Elizabeth J. Hodgson, for their patience and assistance, especially during the preparation of my thesis.

Declaration

I hereby declare that this thesis represents original material and that, to the best of my knowledge, it contains material not previously created nor published by a person other than myself, unless otherwise acknowledged in the text. The material presented in this thesis has also not been submitted for an award at an establishment other than the University of Warwick; the following thesis has been submitted solely to the University of Warwick, UK, for the degree of Doctor of Philosophy.

Mark Peter Barrow

Abstract

The following thesis represents an investigation into the gas-phase behavior of fullerenes and fullerene derivatives, using mass spectrometry as an analytical method. This thesis encompasses the formation and structure elucidation of carbon-based clusters which have been formed through the ablation of fullerene derivatives, the formation of fullerenes from non-fullerene precursor material, an evaluation of the stability of solid C_{60}, the delayed ionization of pure fullerenes, and the assessment of an alternative ionization method for the direct analysis of fullerenes and fullerene derivatives. The coalescence reactivities of $C_{60}H_{36}$, oxides of C_{60} and C_{70}, metallofullerenes, fluorinated fullerenes, and three fullerene derivatives of the formula $C_{60}[C(COOEt)_2]_n$ (where n = 1, 2, and 3) have been studied. Analogously, an organometallic compound of the formula $[Cp_5CpMn(CO)_3]$ has been evaluated as a possible precursor for fullerene formation using laser ablation. The stability of C_{60} under ambient conditions, in the presence of light and air, has been studied, revealing that dimerization reactions occur following oxidation. Following analysis of the structures of coalesced species, it became apparent that time-of-flight instruments of a particular design may be prone to artifact signals originating from the delayed ionization of fullerenes; a subsequent study led to the development of a new method for examining this behavior and the findings have far reaching consequences for studies using similar instrumentation. Laser desorption/ionization and matrix-assisted laser desorption/ionization are not always suitable ionization methods due to the observation of high degrees of fragmentation or reactions with the matrix. Electrospray ionization represents an obvious solution, but an investigation into the suitability of this method was required due to the lack of successful analyses in the literature. Though the topics involved and the samples used are diverse, each investigation thus represents a mass spectrometric study into the gas-phase behavior of fullerenes and their derivatives, along one of several themes.

Publications

The following publications have been produced during the course of the research conducted by the author towards the degree of Doctor of Philosophy:

1) "Matrix-assisted laser-induced gas-phase aggregation of C_{60} oxides"

   Mark P. Barrow, Nicole J. Tower, Roger Taylor, and Thomas Drewello

   Chem. Phys. Lett., **1998**, *293*, 302-308

2) "C_{60} degrades to $C_{120}O$"

   Roger Taylor, Mark P. Barrow, and Thomas Drewello

   J. Chem. Soc. Chem. Commun., **1998**, 2497-2498

3) "Penta(cyclopentadienyl)-η^5-cyclopentadienylmanganesetricarbonyl: structure and laser-induced conversion to fullerenes"

   Mark P. Barrow, J. Kevin Cammack, Matthias Goebel, Ian M. Wasser, K. Peter C. Vollhardt, and Thomas Drewello

   J. Organomet. Chem., **1998**, *572*, 135-139

4) "Laser-induced gas-phase synthesis of dimeric C_{70} oxides"

Mohammed S. Al-Jafari, Mark P. Barrow, Roger Taylor, and Thomas Drewello

Int. J, Mass Spectrom., **1999**, *184*, L1 - L4

5) "Unimolecular Ion Dissociation and Laser-induced Coalescence of Hydrogenated Fullerenes"

Monika Möder, Matthias Nüchter, Bernd Ondruschka, Gabor Czira, Karoly Vékey, Mark P. Barrow, and Thomas Drewello

Int. J. Mass Spectrom. (Robert Squires Memorial Issue), **2000**, *195/196*, 599-607

6) "Significant Interferences in the Post Source Decay Spectra of Ion-Gated Fullerene and Coalesced Carbon Cluster Ions"

Mark P. Barrow and Thomas Drewello

Int. J. Mass Spectrom., **2000**, in press

7) "Laser-Induced Formation, Fragmentation, Coalescence and Delayed Ionization of the $C_{59}N$ Heterofullerene"

Nigel L. Clipston, Tracy Brown, Yury Vasil'ev, Mark P. Barrow, Rainer Herzschuh, Uwe Reuther, Andreas Hirsch, and Thomas Drewello

J. Phys. Chem. A, **2000**, *104*, 9171-9179

8) "Characterization of Fullerenes and Fullerene Derivatives by Nanospray"

Mark P. Barrow, Xidong Feng, James I. Wallace, Olga V. Boltalina, Roger Taylor, Peter J. Derrick, and Thomas Drewello

Chem. Phys. Lett., **2000**, *330*, 267-274

Abbreviations

B:	a magnetic sector, comes from use of letter B to denote magnetic field
CAD:	collisionally-activated dissociation (see CID)
CCD:	charge coupled device
CI:	chemical ionization
CID:	collision-induced dissociation (see CAD)
Cp:	cyclopentadiene
Da:	Dalton, the atomic mass unit
DCI:	desorption chemical ionization
E:	an electrostatic sector, comes from use of letter E to denote electrostatic field
EA:	electron affinity
EI:	electron ionization (also known as electron impact)
EPR:	electron paramagnetic resonance
ESA:	electrostatic analyzer (also see "E")
FAB:	fast atom bombardment
FD:	field desorption
FFR:	field free region
FI:	field ionization
FT:	Fourier Transform

FT-ICR:	Fourier transform ion cyclotron resonance
FWHM:	full width at half maximum (height)
HPLC:	high performance liquid chromatography (also known as high pressure liquid chromatography)
ICP:	inductively coupled plasma
ICR:	ion cyclotron resonance
IE:	ionization energy
IPR:	isolated pentagon rule
IR:	infra-red
ISC:	intersystem crossing
LD:	laser desorption
LDI:	laser desorption/ionization
LI:	laser ionization
LSIMS:	liquid secondary ion mass spectrometry
MALDI:	matrix-assisted laser desorption/ionization
MCP:	microchannel plate
MIKE:	mass-analyzed ion kinetic energy
MS:	mass spectrometry/mass spectrometer
NEXAFS:	near edge X-ray absorption fine spectra
NMR:	nuclear magnetic resonance

PAD:	post acceleration detector
PD:	plasma desorption
PSD:	post source decay
Q:	a quadrupole sector
ref:	reflectron
rf:	radio frequency
SID:	surface-induced dissociation
TD:	thermal desorption
Th:	Thomson, unit of m/z value
ToF:	time-of-flight
TS:	thermospray
UPS:	ultra-violet photoemission spectroscopy
UV:	ultra-violet

Chapter One

Introduction

1.1 Fullerenes

1.1.1 Discovery and Physical Characteristics of Fullerenes

The progress of scientific achievement is periodically marked by significant discoveries which dramatically shape the path of future research. In 1985, one such event in modern research was the discovery of a new class of carbon allotrope by Kroto et al.[1] totally unlike the two previously known allotropes, graphite and diamond. Kroto et al. had been investigating mechanisms for the formation of long chain, carbon-based molecules in interstellar space and circumstellar shells utilizing laser vaporization of graphitic surfaces. A solid disk of carbon was vaporized using a pulsed, focused Nd:YAG laser with a wavelength of 532 nm and a pulse duration of 5 ns. The resulting species were then cooled in a helium stream, where they traveled until they reached the ionization region; the mass spectra obtained by Kroto et al. are shown in Figure 1. Here, an excimer laser was used to ionize the molecules, which were then accelerated by an electrostatic field and analyzed using time-of-flight (ToF) mass spectrometry. These newly discovered carbon based structures were determined to be closed cages, consisting entirely of an even number of carbon atoms. They were composed of pentagonal and hexagonal rings, forming an icosahedral structure. During the determination of the structural characteristics of these clusters, Euler's theorem for polyhedra was invoked, which states:

$$f + v = e + 2$$

where f is the number of faces, v is the number of vertices, and e is the number of edges, for a polyhedron.

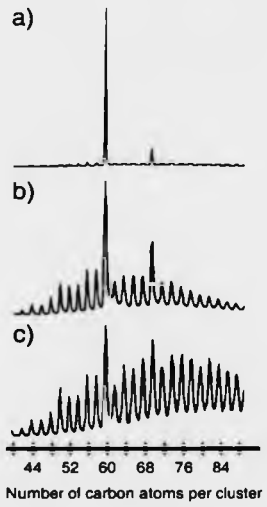

Figure 1: Three time-of-flight mass spectra arising from the laser ablation of graphite, using an ArF excimer laser. Spectrum c was obtained using helium gas at a pressure of 10 torr over the graphite target, and spectrum b was obtained after the pressure of the helium gas around the target area had been increased to 760 torr. Spectrum a was obtained under similar conditions to b, but an integration cup was incoroporated into the apparatus to increase the time between vaporization and expansion, maximizing cluster thermalization.

When considering only hexagonal and pentagonal faces, the equation becomes:

$$6(f + v - e) = p = 12$$

where p is the number of pentagonal faces of the polyhedron. Hence, all such carbon clusters which consist of only pentagonal and hexagonal faces must possess twelve pentagonal faces. Following on from this line of reasoning, it became apparent that C_{20}, a dodecahedron, is the smallest carbon cluster which may be said to possess these structural features. One year before Kroto et al.'s discovery, a group at Exxon had observed similar carbon clusters but had unfortunately not appreciated their significance.[2] The most abundant of these carbon clusters is C_{60}, which was later named "Buckminsterfullerene," after the

designer of geodesic domes, Buckminster Fuller. Further investigation revealed C_{60} to be composed of 20 hexagonal and 12 pentagonal rings, where a carbon atom was present at each vertex of the icosahedron; this structure is depicted by Figure 2. Buckminsterfullerene was found to be particularly stable due to the fact that it is the second smallest carbon cluster which satisfies what has become known as the "isolated pentagon rule," where C_{50} is the smallest fullerene satisfying this rule, and the nature of the bonding giving rise to C_{60}'s notable stability[3] has been thoroughly investigated.[4-13] The isolated pentagon rule (IPR) is used to describe the relative stabilities of particular fullerenes, such as C_{50}, C_{60}, and C_{70}, as it has been shown that increasing the number of adjacent pentagons is energetically unfavorable, due to increased strain as a result of increased curvature of the molecular structure. C_{70} was also noticeably a stable structure, typically present at 10% of the abundance of C_{60}, and it was demonstrated that C_{70} possessed a more aromatic character than C_{60}. It soon became clear that a wide range of carbon clusters existed, as evidenced by the original spectrum obtained by Kroto et al.,[1] and the name "fullerene" became synonymous with this new allotrope of carbon. It was not until 1990 that research could significantly progress, however, as it was not possible to synthesize macroscopic quantities of fullerenes. This therefore hindered empirical study of fullerenes. Krätschmer et al.[14] devised a new method for the synthesis of bulk quantities of fullerenes using graphitic electrodes during an arcing process in a helium atmosphere, and the synthesis and separation processes for fullerene production became increasingly popular topics.[15] Following the publication of these findings, fullerene research began its exponential growth.[16]

The most intensively investigated subjects associated with fullerenes were those concerning their physical structure and characteristics. The mechanism of formation of fullerenes[17-26] was investigated; the formation and stability of fullerenes has aroused much

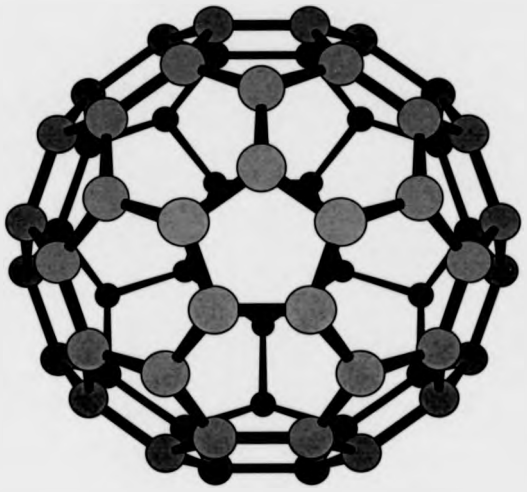

Figure 2: Three dimensional representation of Buckminsterfullerene, C_{60}.

interest and Crespo et al.[27] even conducted theoretical analysis of the analogous formation of Si_{60}, though such a molecule has not been observed. It was noticeable that an even number of carbon atoms was highly favorable and fullerenes fragmented via the loss of C_2 units. Such a fragmentation pathway became known as an indicative characteristic of all fullerenes. The "shrink wrap mechanism"[28,29] was proposed as the mechanism of fragmentation and bond formation by which fullerenes characteristically lost the C_2 units. During the course of the shrink wrap mechanism, two, adjacent carbon atoms undergo a rearrangement of bonds with other carbon atoms in the vicinity, creating two, abutting pentagons. The two carbon atoms in question, forming the base of both, abutting pentagons, are then ejected from the molecule, resulting in the formation of a C_2 leaving group and a hexagonal face where the two, adjacent pentagons once were. The carbon cage can only undergo efficient self-repair if even numbers (i.e. C_{2n}) of carbon atoms are lost in this manner. Therefore, the shrink wrap mechanism is in excellent agreement with the observation of fullerenes possessing primarily even numbers of carbon atoms, though

there are exceptions.[20] The fragmentation of fullerenes is traditionally studied using mass spectrometry, whether it is the study of fragmentation within the ion source,[30] using mass-analyzed ion kinetic energy spectra (MIKES),[31] or using collision-induced dissociation conditions with a variety of target gases.[32,33] The binding energies of C_n units,[34-38] has been a matter of disagreement, with values between 4 - 12 eV being proposed. Though there has been some debate over whether C_2 loss occurs in a concerted or a sequential manner,[35,39-42] increasing support can be found for sequential C_2 loss, with minor contributions from C_4 loss. Though the fragmentation dynamics of C_{60} have been of primary interest, the fragmentation of C_{70} has also been studied.[43] With its positive electron affinity[44,45] of approximately 1.2 eV,[45] it is notable that C_{60} readily forms anionic species[46] and is able to accept multiple charges,[47] though it has no protons to lose; C_{60} will form multiply charged species without protonation/deprotonation. The formation of multiply charged cations has also been studied[48-50] and Scheier et al. reported the observation of the sextuply charged ion C_{70}^{6+}.[51] The ionization energy of neutral C_{60} has become accepted as being approximately between 7.5 and 7.6 eV,[41,42,52-63] though there has been subsequent discussion about experiments performed for the determination of ionization potentials.[64-66] A figure closer to 7.6 eV seems to be increasingly accepted, with many references being made to experiments performed by Lichtenberger et al.,[67] Zimmerman et al.,[68] de Vries et al.,[69] and Lifshitz.[70]

1.1.2 Endohedral and Exohedral Complexes

It was not long before research began to diversify, with most efforts concentrating on characterizing the physical behavior of fullerenes. It was determined by Heath et al.[71] that atoms may be trapped inside the carbon cages, and such adducts were later to become

known as "endohedral" complexes, while fullerenes which possessed atoms or functional groups bound to the exterior of the cage became known as "exohedral" complexes. The formation of endohedral complexes became one of the major fields of investigation,[9,22,29,72-88] though exohedral interactions are also noted.[89,90] A "window mechanism"[82,91,92] became accepted as the means for formation of such complexes, where carbon-carbon bonds are cleaved until a large enough hole is present for the gas atom to enter the carbon cage, the gas atom is then captured, and the carbon-carbon bonds reform. The alternative mechanism, where gas atoms "squeeze through" a face of the fullerene following stretching of carbon-carbon bonds without cleavage occurring, was disregarded due to the requirement of a high activation energy. Nuclear magnetic resonance (NMR) became a common spectroscopic method for probing the interior of endohedral fullerenes,[93-96] as has infra-red (IR) spectroscopy,[97-100] while purely theoretical calculations were also in evidence[101] as the environment and bonding inside the cage became of interest.[102-106] While others had used collision experiments using mass spectrometers to capture gas atoms, Saunders et al.[107] also experimented with apparatus which relied upon the use of high pressures. Weiske et al. succeeded in capturing more than one atom inside the carbon cage.[91] Mass spectrometry was first used to produce such complexes, but increasingly the role of mass spectrometry was for structure elucidation.[108-110] Applications of endohedral complexes have since been proposed, one of the most original theoretical applications was that of a memory device. The theory entails the use of a nanotube and an endohedral fullerene,[111] which may be operated together as a binary device when under the influence of an electric field. Synthesis of endohedral complexes incorporating metal atoms, or "metallofullerenes," became the primary development, due to the possibility of the production of potential superconductors. Investigations into the production and physical structure of metallofullerenes gained momentum as a result.[78,110,112-119]

1.1.3 Coalescence Reactions

In 1993, a discovery was made which opened up new avenues of research with respect to fullerenes. Yeretzian et al.[120,121] observed the coalescence of carbon clusters following laser desorption/ionization (LDI) of a known fullerene sample, with analysis being performed using time-of-flight mass spectrometry. Ions which possess masses that are multiples of the mass of the starting material were found to be particularly favored. The aggregate species consisted of an even number of carbon atoms, and distinct distributions could be observed, with all signals being spaced by 24 Da (C_2). In an attempt to deduce the structure of these higher carbon clusters, Yeretzian et al.[121] collided coalesced carbon clusters with a silicon surface and no fragments were observed up to a collision energy of 200 eV. The spacing of the coalesced carbon cluster ions by C_{2n} units, a distinctive characteristic of fullerenes, and the total absence of a fragment which corresponds to the precursor compound used, together implied that the coalesced clusters were indeed larger, closed cage fullerenes and not weakly bound aggregates. During the course of similar experiments using fullerene anions, Zhu et al.[20,122] managed to also observe odd (uneven) numbered carbon clusters, though the abundance of these species was relatively low. Fowler et al. have investigated the relative stabilities of fullerenes which possess even and uneven carbon contents and it was shown that carbon clusters with an uneven carbon content were the less stable at higher temperatures.[123] Marshall and co-workers have produced carbon clusters as large as $C_{500}^{+\bullet}$ using laser desorption/ionization.[124] In addition to coalescence following laser ablation, Campbell et al. have demonstrated the possibility to induce such reactions through the collision of $C_{60}^{+\bullet}$ ions with C_{60} neutrals in a collision cell.[125] Studies performed by Jarrold and co-workers[126,127] have provided evidence for the formation of more than one dimeric species following gas-phase coalescence reactions. Experiments

performed by Tast et al. demonstrated that dissociation of selected coalescence products led to the production fragment ions which provided evidence for the formation of dimeric structures in the gas-phase.[128] Simulations were used by Xia et al. to illustrate the effect of collision energy and impact parameter upon the course of the coalescence reactions, and clearly showed that low energy collisions were more likely to result in the production of dimeric species while high energy collisions were more likely to result in the total fusion of the two entities, leading to closed caged fullerenes.[129] Investigation into the coalescence behavior of fullerenes increased.[24,126,130-132] Fabre et al.[133] managed to synthesize bridged fullerene dimers, with the structural characterization being performed using mass spectrometry. Attempts were made to deduce the mechanism behind coalescence reactions.[63,134,135] Beck et al.[63] proposed that the LDI process leads to the rapid heating of the fullerene sample, with vibrationally and perhaps electronically excited neutrals being produced; these neutrals can cool through fragmentation or autoionization, but at high enough vapor densities lead to collisions of excited neutrals which in turn can lead to coalescence. Other research[134] implied that such reactions may be accompanied by C_{2n} unit uptake as well as C_{2n} loss (assumed to be sequential for this investigation). Further heating of the excited molecules occurs following reaction, through the heat of fusion, and C_{2n} loss leads to cooling of coalesced species. A rate of reaction was proposed, based on the uptake of fragments in a dense plume after laser desorption; it was found that the predicted abundances of each coalesced species compared well with experiment. Work by Mitzner et al.[135] compared the abundances of selected coalesced species with respect to the abundance of particular fragments, for instance comparing $C_{2n+60}^{+\bullet}$ and $C_{2n}^{+\bullet}$; the role of such fragments in the coalescence mechanism could explain the greater intensity of $C_{118}^{+\bullet}$ (than $C_{120}^{+\bullet}$) as the formation of $C_{58}^{+\bullet}$ via fragmentation of C_{60} is frequently prominent. Examination of velocities of the molecules within the ion source showed that fragment

ions of lower velocity were less abundant than expected, and this was explained by ions of lower velocity having an increased probability of reaction. Ions with a greater velocity would leave the plume sooner and therefore spend less time in this region of the ion source, within which the greatest probability of collision could be found. An explanation was provided where coalescence occurs via the fusion of one neutral species (where neutrals of lower velocity have a greater chance of reaction) and one ionic species; the reactions are initiated by the fusion of a neutral sample molecule with a fragment ion, continuing via the fusion of the coalesced, ionic species and neutral molecules.[135] The coalescence reactivity of fullerene derivatives has also been studied.[136-138] Beck et al.[136] demonstrated that C_{60} oxides displayed an increased reactivity with respect to C_{60} and it was postulated that this is a result of the increased tendency for fragmentation which is observed for fullerene oxides. Deng et al.[139] have used mass spectrometry for the analysis of a bridged $C_{180}O_2$ species which was produced synthetically, rather than as a result of coalescence within the ion source, while Eisler et al.[140] have studied $C_{120}O$, $C_{120}O_2$, and $C_{130}O$, and Penn et al. also used mass spectrometry for the analysis of bridged fullerene oxide dimers.[141] Theoretical work by Fowler et al.[142] has been carried out into the structures of dimeric fullerene oxides. Other investigations have shown that the coalescence behavior of fullerene oxides varies depending on the ionization method chosen.[143,144] When the "softer" ionization process known as matrix-assisted laser desorption/ionization (MALDI) is used, non-fullerene aggregates, consisting of two moieties bound by σ C-C bonds, are formed, while use of LDI leads to the traditional fusion to form higher fullerenes, with an increased coalescence reactivity as shown by Beck et al.[136] As the study of fullerene coalescence has continued to grow, an overview of fullerene dimers and their production has recently been published by Segura and Martín.[145]

1.1.4 Delayed Ionization/Thermionic Emission

Perhaps one of the most striking features of fullerenes is a phenomenon known as "delayed ionization." First cited by Campbell et al.,[52] it was discovered that C_{60} and C_{70} exist as excited, neutral states for an order of microseconds prior to ionization. The experimental apparatus involved the use of a time-of-flight (ToF) mass spectrometer and two lasers; one laser was used for desorption of the sample and the other for the ionization. A pulsed extraction potential was then applied following a chosen delay time, and two potentials were applied prior to extraction to remove any ions which may have been "promptly" formed. Ions were still detected even after the maximum chosen delay time of 16 μs. Very shortly afterwards, the discovery that fullerenes may undergo delayed ionization was further corroborated by Wurz et al.[53] Since that time, delayed ionization has become a popular research topic. Most experiments have involved the use of laser desorption/ionization in conjunction with a ToF mass spectrometer,[54,55,60,62,146] though use has also been made of mass spectrometers incorporating electron impact (EI)[147,148] and surface induced dissociation (SID),[131] and one research group has used ASTRID, a heavy-ion storage ring.[149] Delayed ionization has also been briefly mentioned as observations during the course of studies dedicated to other topics.[35,41,42,150] Electron detachment from fullerene anions has also been studied as being similar to ionization of fullerene neutrals.[151,152] Loepfe et al. have managed to observe fullerene ions after a delay time of 120 μs using a time-of-flight mass spectrometer which employed an infra-red (IR) laser (wavelength of 10.6 μm)[61] and von Helden et al. have equally managed to observe delay times of approximately 150 μs when using an IR laser.[153] However, Hansen and Echt[154] claimed that C_{60} cations have been observed after a delay of 300 μs following multiphoton excitation using lasers with nanosecond pulse widths; a 300 μs delay has also been supported by

Deng et al.[41] Rate expressions have been estimated for delayed electron emission.[154,155] Despite intensive study, a conclusive insight into the mechanism of ionization has not been forthcoming. It is known that excited states of fullerenes are involved and it has been suggested that Rydberg states may play a role,[148,156] but triplet states[157,158] are now widely accepted as playing the most important role, though singlet states[159] may also be involved. Zhang et al.[58] noted that the ionization energy of C_{60} appeared to be approximately 5.8 eV when investigating delayed ionization, and proposed that this could be explained by the further excitation of the lowest triplet state of C_{60}, which lies at approximately 1.7 eV, and has a lifetime as great as 40 μs. Klots and Compton[160] proposed that singlet and triplet states are indeed involved in the delayed ionization process. Intersystem crossing from singlet states to triplet states prior to further excitation has been cited as one of the mechanistic steps.[161] It has been proposed that delayed ionization includes rapid conversion from singlet states to triplet states,[58,59,153,160,162] which possess a comparatively long lifetime, followed by further excitation leading to ionization. However, the greatest dispute lies in the discrimination between whether or not the process is analogous to thermionic emission, as observed in metal clusters. The leading proponent of the thermionic emission analogy has been Klots, and some of his work[160,163-166] is frequently cited during the discussions. However, there have also been notable disagreements with the theoretical model put forward by Klots.[58,59,167] Though the mechanism of delayed ionization is not yet agreed upon, the involvement of triplet states is no longer a contentious issue. Indeed, it has even been proposed that approximately 80% of the C_{60}^{+} ions detected using typical LDI conditions will have been formed through delayed ionization rather than prompt ionization.[168,169] Though a topic of intense interest, the mechanism of delayed ionization has not yet been deduced, and a review of the research into this topic has been published by Campbell and Levine.[170] No potential applications of this phenomenon have been forthcoming, but delayed

ionization has been seen as further evidence of the stability of fullerenes and their ability to accommodate to changes in their environment.

1.1.5 Fullerene Derivatives

As the characteristics and behavior of fullerenes have slowly become better understood, research has increasingly begun to focus on the synthesis and characterization of derivatives of these carbon clusters,[171,172] often with potential applications in mind. Böhme has provided insight into the reactivity of C_{60} as a function of its charge state[173] and detailed reactions such as cation-transfer reactions, surface derivatization, and polymerization. The use of computational chemistry to investigate the structure of fullerenes and fullerene derivatives has been reviewed by Andreoni.[174] Endohedral and exohedral fullerenes have attracted much attention in the past, but "heterohedral" fullerenes (or "heterofullerenes"), where one or more carbon atoms are replaced by a different element such as nitrogen, have become increasingly popular research topics.[175] Fullerenes which have been brominated,[176] chlorinated,[177] or fluorinated[178-182] have attracted interest partly because of the notion that a fluorinated carbon cluster may be an ideal lubricant and may bear some similarity to Teflon™. The most commonly synthesized fluorinated fullerenes are $C_{60}F_{18}$, $C_{60}F_{36}$, and $C_{60}F_{48}$, though various reaction products range from $C_{60}F_{27}$ to $C_{60}F_{x\leq102}$. Hydrogenated fullerenes[177,183-190] bear a close resemblance to fluorinated fullerenes, both classes of derivatives consisting of highly saturated carbon cluster, with a "spiked" appearance. The major hydrogenated products of syntheses involving C_{60} include $C_{60}H_2$, $C_{60}H_4$, $C_{60}H_6$, $C_{60}H_{18}$, $C_{60}H_{32}$, $C_{60}H_{36}$, $C_{60}H_{38}$, $C_{60}H_{40}$, $C_{60}H_{42}$, and $C_{60}H_{46}$, where $C_{60}H_{36}$ is the most common product and is the major product of the Birch reduction, one of the most common synthetic methods used. The major reaction products of hydrogenation reactions

involving C_{70} include $C_{70}H_2$, $C_{70}H_4$, $C_{70}H_{18}$, $C_{70}H_{30}$, $C_{70}H_{36}$, $C_{70}H_{38}$, $C_{70}H_{40}$, $C_{70}H_{42}$, and $C_{70}H_{48}$, where $C_{70}H_{30}$ is the major product under the Birch reduction. The potential application of hydrogenated fullerenes which is under examination is that of a means to store hydrogen safely. Perhaps the fullerene derivative field of greatest interest is that of metallofullerenes. Since the first experiments involving the inclusion of a lanthanide metal in C_{60},[71] metallofullerene research has grown dramatically, with promises of new superconducting materials. It is of no surprise then that the derivatives with the greatest, potential, commercial value become the focus of the most intensive synthetic research. Metallofullerenes were at first investigated alongside other forms of endohedral complex[84] and methods of production were developed over time.[78,114,116,119] There were initial investigations into the reactivity of metallofullerenes with such reports into the reactivity with oxygen under collision conditions, investigated using mass spectrometry, by Callahan et al.[112] Investigations of the structures and oxidation states of various metallofullerenes[118] have shown that the endohedral metal atom donates electron density to the surrounding carbon cage (typically two or three electrons, depending on the metal atom and carbon cluster size), and the enhanced stability of the carbon cage due to this interaction with the endohedral metal atom has also been demonstrated.[117] Theoretical investigations of metallofullerenes[191] are not uncommon and calculations by Kobayashi[115] have shown that $M@C_{82}$ species, which are particularly favored, obey the isolated pentagon rule, just as the pure fullerenes do. Notable discoveries during the course of these theoretical experiments were that two of the four isomers of the $Ca@C_{72}$ species were found to violate the IPR rule, and one other isomer possessed a heptagon within the carbon cage structure. Kobayashi has also shown that it is possible to fit two metal atoms inside a fullerene cage,[113] as in the cases of $Sc_2@C_{84}$ and $La_2@C_{80}$. Furthermore, the two Sc metal atoms may also oscillate within the cage, while the two La atoms may even circulate within the

cage, producing a magnetic field. As the properties of pure fullerenes have become increasingly studied,[192] the interest in possible applications of non-derivatized fullerenes has also become more aroused. Dai et al. have investigated the use of fullerenes to dope glasses[193,194] which may in turn filter out high intensity light, such as that emitted by lasers. Possible military applications[195] are amongst the most viable uses. The design of a memory device by Kwon et al.,[111] using a nanotube and a doped C_{60} molecule, is perhaps one of the most imaginative ideas.

One noticeable trend within fullerene research is that while some investigations into the physical characteristics involve the use of NMR,[93-96,107,185,189,196-199] as well as visible spectroscopy[200-203] and IR spectroscopy,[97-100,204-207] many of the experiments providing insight into the physical characteristics of fullerenes have been performed using mass spectrometers.[110,112,137,177,208-214] The discovery of Buckminsterfullerene through the use of mass spectrometry[1] and the use of mass spectrometry by Krätschmer et al. following the development of a new synthetic route for fullerene production[14] both contribute to the strong connection between the fields of fullerene research and mass spectrometry.[208,211]

1.2 Mass Spectrometry

Since its origins in the late 19th century, mass spectrometry has developed into a valuable analytical tool, capable of providing insight into the behavior of molecules in the gas-phase, as well as performing the established role of establishing relative molecular masses of samples. Traditionally, the inception of mass spectrometry has been considered to be experiments conducted by J. J. Thompson in 1912, A. J. Dempster in 1918, and F. W. Aston in 1919. Since that time it has continued to thrive,[215] with four Nobel Prizes have

been awarded which directly relate to mass spectrometry. The awarding of the Nobel Prize in 1996 to the discoverers of Buckminsterfullerene may also be claimed to be directly related to mass spectrometry, due to the important role which mass spectrometry played during the course of their work.

A mass spectrometer must essentially consist of three stages. The first stage is the generation of ions following introduction of the sample into the ion source. These ions are then extracted from the ion source and must be separated according to their mass using one or more of a variety of mass analyzers. Finally, the separated ions must be detected, and their relative molecular mass and relative abundance must be recorded. It is now common practice for the data processing and instrument control to be handled using a computer. It may also be noted that some instruments include fourth and fifth stages, where ions are fragmented during collisions (with a surface or collision gas) and the fragment ions are analyzed once again (using a second analyzer), respectively. An instrument where such stages are present is often referred to as a "tandem mass spectrometer." The nomenclature used within the field of mass spectrometry is documented,[216] and the following discussion aims to explain the terminology used and elaborate upon the instrumentation used and the principles upon which they are based.

1.2.1 Mass Analyzers

1.2.1A Sector Instruments

Ionization sources are often interchangeable for a given mass spectrometer, while the mass analyzers and detection systems for an instrument are not easily modified, by contrast. Mass spectrometers are most frequently "defined" by the type of mass analyzers

employed; four methods of mass analysis are used in following investigations and are therefore discussed in this section. The principles behind the different forms of instrumentation may be easily found in books and journal articles. The oldest designs are often referred to as "sector instruments" and these incorporate "magnetic sectors" and "electrostatic sectors;" many publications covering sector instrumentation exist.[217-222] Once an ion has been formed in the ion source, it is extracted by an "acceleration potential" or "extraction potential," where a potential difference is created between the point of ionization and the entrance to the analyzer region (ion source exit); this potential varies between different instruments but is typically of an order of 5 - 20 kV, with 8 kV being particularly common. Overviews of electromagnetism and classical mechanics may be obtained from many physics textbooks,[223] should further information be required for a fuller understanding of the following derivations. The work done on an charged particle is defined as:

$$W = qV \qquad (1)$$

where W is the work done (in Joules, J), q is the charge associated with the particle (in Coulombs, C), and V is the potential difference experienced by the particle (in Volts, V). The work done on the charged particle translates to the kinetic energy it possesses as it leaves the ion source. Kinetic energy is defined by:

$$K = \tfrac{1}{2} mv^2 \qquad (2)$$

where K is the kinetic energy of the particle (in Joules, J), m is the mass of the charged particle (in kilograms, kg) and v is its velocity (in $m\ s^{-1}$). Therefore, equating formulae (1) and (2):

$$qV = \tfrac{1}{2} mv^2 \qquad (3)$$

A charged particle moving through a magnetic field will experience a force acting on it, as shown by the Lorentz force equation. The Lorentz force considers both electrostatic and magnetic forces which may act on a charged particle:

$$F = qE + qvB \sin \theta$$

The force acting on a charged particle in the presence of only a magnetic field is therefore defined by the component:

$$F = qvB \sin \theta$$

where F is the force (in Newtons, N) and B is the magnetic field (in Teslas, T). In the case of a mass spectrometer, an ion will travel through a magnetic field which is perpendicular to the motion of the ion; the expression therefore becomes:

$$F = qvB$$

An ion traveling through a magnetic field which is perpendicular to its vector of motion will travel in a circular path. The expression for the centripetal force which must act on a body in order that it may have a circular trajectory is:

$$F = \frac{mv^2}{r} \qquad (4)$$

where r is the radius of the arc mapped by the motion of the body (in meters, m). Equating centripetal force to the force due to the magnetic field:

$$qvB = \frac{mv^2}{r} \tag{5}$$

$$mv = qBr \tag{6}$$

or:

$$r = \frac{mv}{qB} \tag{7}$$

Therefore, the equation is only satisfied by ions which possess a given momentum-to-charge ratio, as the radius of the arc of the magnetic sector is constant. Only ions of this momentum-to-charge ratio continue their path through the flight tube for a given magnetic field, B. In this way, the magnetic sector selects ions according to their momentum-to-charge ratio (equation (7)). By taking into account the relation between the momentum of an ion and the kinetic energy it is afforded by the potential in the ion source:

$$mv^2 = 2qV$$

and by combining with equation (6):

$$\frac{m}{q} = \frac{r^2B^2}{2V} \tag{8}$$

For a given radius, r, for the flight tube of an instrument and for a given accelerating potential, V, only ions of one m/q value may traverse the magnetic field, B, with the correct flight path. Thus, the magnetic sector, known to be a momentum-to-charge ratio analyzer,

may be used as a mass-to-charge ratio analyzer provided that the kinetic energy of the ions leaving the ion source is known. The application of a magnetic sector is represented in Figure 3. By varying the magnetic field, B, it is possible to scan the range of ions produced in the ion source, with different m/q values. Spectra are usually plotted as the relative intensity of the signal versus the m/z value of a given ion. Though equation (8) is in terms of an m/q ratio, it should be remembered that the total charge on the ion, q, is simply given by the multiplication of the number of charges on the ion, z, by the charge of one electron, e (in Coulombs, C). One consequence of using a magnetic sector for the selection of ions, however, is that ions of the same mass and charge may be dispersed according to their kinetic energy. By using equations (1), (2), and (7):

$$r = \frac{\sqrt{2mK}}{qB}$$

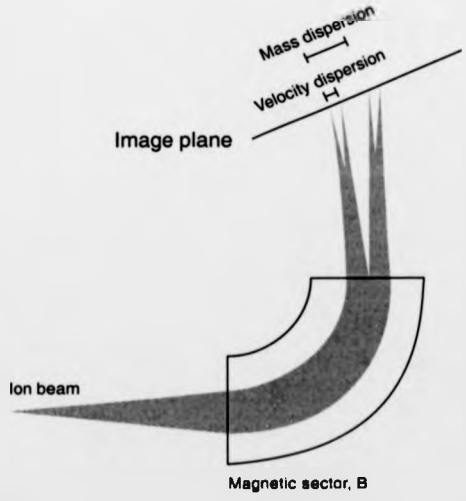

Figure 3: Schematic diagram of a magentic sector, B. Ions of two different masses and two different velocities are considered to be produced from a point source. The ions are resolved according to their momentum to charge ratio, resulting is the splitting of the ion beam into four components parts.

For mass analysis, it is desirable to select ions of a given m/q and focus them, regardless of kinetic energy, at the desired point in the instrument. Dispersion of ions of the same m/q ratio according to their kinetic energy would otherwise lead to a degradation of the operating resolution of the instrument. This disadvantage may be overcome by incorporating an electrostatic sector. The electrostatic sector produces an electrostatic field which the ion must traverse, where the electrostatic field is parallel to the vector of the resulting force, in contrast to the magnetic sector. The principles of an electrostatic sector are demonstrated in Figure 4. The resulting force acting on a charged particle due to an electrostatic field is given by:

$$F = qE \tag{9}$$

where E is the electric field (in V m^{-1}). In a manner analogous to the case of the magnetic sector, the force experienced by the ion in the electrostatic sector equates to the centripetal force required in order for the ion to follow the correct trajectory and continue its path through the flight tube. Combining equations (9) and (4):

$$qE = \frac{mv^2}{r} \tag{10}$$

and substituting to include the kinetic energy (equation (2)):

$$r = \frac{2K}{qE} \tag{11}$$

It can be seen that just as the magnetic sector acts as a momentum-to-charge ratio analyzer (equation (7)), the electrostatic analyzer acts as a kinetic energy-to-charge ratio analyzer (equation (11)). Note that neither the magnetic sector nor the electrostatic sector

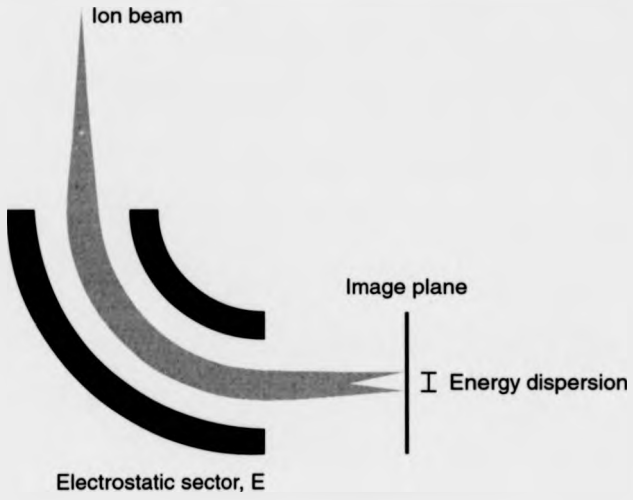

Figure 4: Schematic diagram of an electrostatic sector, E. Ions of two different masses and two different kinetic energies are considered to be produced from the point source. Ions are separated according to their kinetic energy to charge ratio, resulting in the splitting of the ion beam into two component parts.

acts as a mass analyzer. It is possible to use a magnetic sector in conjunction with an electrostatic sector so that an ion beam which is both inhomogeneous in energy and divergent in direction may be focused. By combining the two analyzers in such a way that the velocity dispersion is approximately equal and opposite when comparing the two analyzers, the velocity aberration in the focused image is greatly reduced while the directional focusing is maintained; the result is that for each mass considered, many object points become mapped on to only one image point, as illustrated by Figure 5. The directional focusing and the velocity focusing images for the desired ions (of a given mass) coincide, giving rise to the term "double focusing." Mass spectrometers which employ both types of sectors (the majority of modern instruments) are known as "double focusing mass spectrometers" as a result, and have much higher operating resolutions than a single sector instrument. For a magnet of radius 30 cm, a typical resolution of 5000 may be obtained, but a double focusing instrument can reach up to resolutions over 100,000.

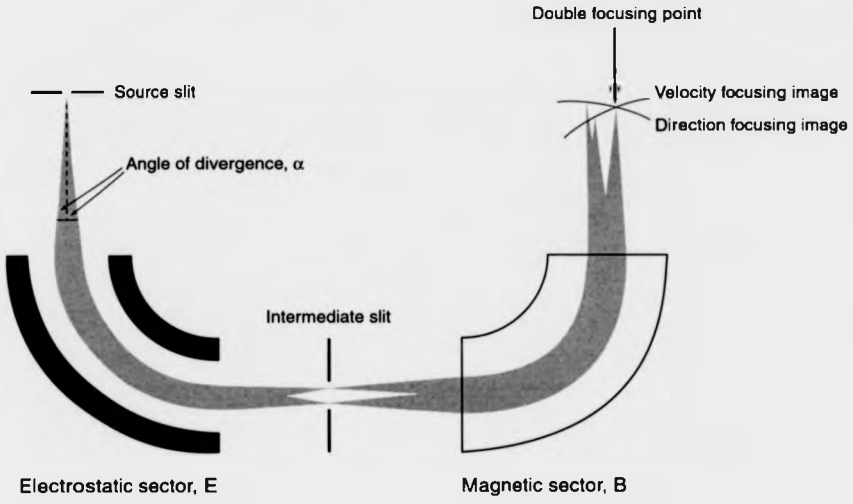

Figure 5: Schematic diagram illustrating the principle of a double focusing mass spectrometer. Ions are produced from the point source at the ion source and are separated according to their kinetic energy to charge ratio, prior to being separated according to their momentum to charge ratio. The coupling of the electrostatic and magnetic sectors results in the splitting of the ion beam into three component parts; the velocity focusing image and the direction focusing image of the ions of interest coincide at the double focusing point.

Resolution is defined as:

$$\frac{m}{\Delta m}$$

where two peaks of equal intensity are examined at masses m and m+Δm, where the height of the valley between the peaks is 10% of the height of each peak, as represented by Figure 6. This is one of the two possible definitions of resolution that are used. The other definition, the "Full Width at Half Maximum" (FWHM) definition, uses m as the mass of the ion observed and Δm is the width of the peak at half its height, as exemplified by Figure 7. The "10% valley" definition, as it is sometimes referred to, is commonly used with regards to sector and quadrupole instruments, while the FWHM method is commonly

used in conjunction with FT-ICR (Fourier Transform Ion Cyclotron Resonance) and ToF (Time-of-flight) instruments, which are described later. With regards to the design of sector instruments, mass spectrometer geometries are frequently abbreviated using the physical notation used to describe the associated fields, "B" denotes a magnetic sector and "E" denotes an electrostatic sector, for instance. For historical reasons, mass spectrometers with an "EB" geometry are known as "Mattauch-Herzog" or, more commonly, "Nier-Johnson" instruments. Instruments with a "BE" geometry are known as "reverse geometry" mass spectrometers.

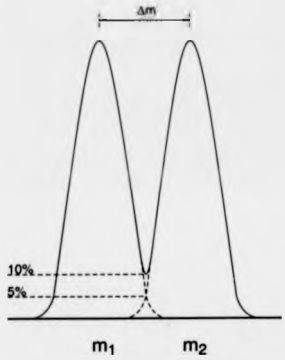

Figure 6: Illustration of the "10% valley" definition of resolution.

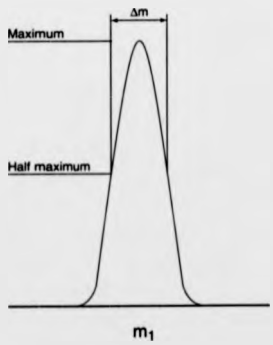

Figure 7: Illustration of the "full width at half maximum" (FWHM) definition of resolution.

1.2.1B Time-of-Flight Instruments

Another variation of mass analysis is performed using "time-of-flight" (ToF) mass spectrometry. Though a method of mass analysis developed later than sector instruments, ToF mass spectrometers have a long history. Time-of-flight mass spectrometry has spanned several decades, but has been a less viable option due to the limitations of the technology (specifically the electronic components) available. Modern ToF instruments exhibit greatly enhanced resolving powers, compared to the earliest time-of-flight instruments, as a result of two developments. The first is the implementation of Wiley-McLaren ion source designs,[224] which reduce the energy spreads of ions. The second advance in ToF instrumentation is the incorporation of a"reflectron,"[225-227] which improves resolution during mass analysis by focusing ions of the same mass but differing energies, and also enables the distinction between daughter ions and parent ions, following unimolecular dissociation in flight. An example of a typical time-of-fight instrument is illustrated by Figure 8. Due to their relative simplicity, ToF instruments are amongst the most popular candidates for home built instruments.[228-233] Many reviews of instrumentation and design principles exist.[234-241] All ions leaving an ion source should, in an ideal situation, have identical translational (kinetic) energies. Ions of the same kinetic energy but differing masses will travel at differing velocities, as demonstrated using equation (3) to obtain equation (12) below, and this difference in flight times is the basis of mass analysis in ToF mass spectrometers.

$$qV = \tfrac{1}{2} mv^2 \qquad (3)$$

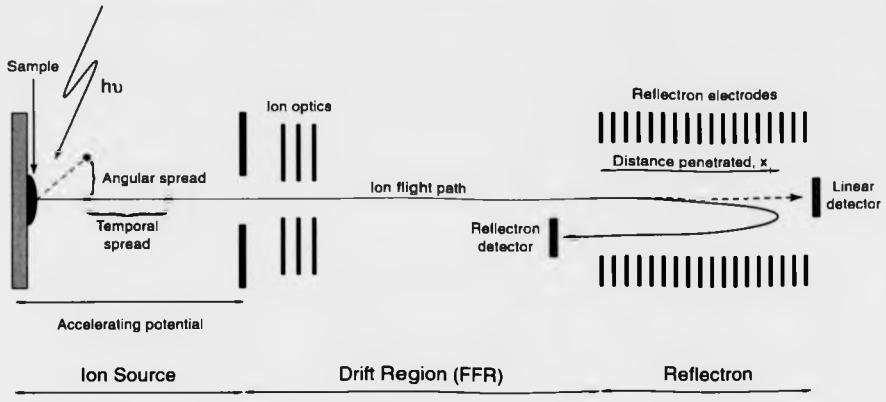

Figure 8: Schematic diagram of a typical time-of-flight mass spectrometer. Ions are generated in the ion source, most commonly following photoirradiation of the sample. The ions are extracted by the accelerating potential which exists within the ion source and enter the field free region. They are then detected at a detector at the end of the flight tube if their linear flight path is maintained. A series of electrodes termed a "reflectron" is frequently incorporated to improve resolution and to provide the possibility of tandem mass spectrometry experiments. Ions are then reflected following passage against the potential gradient and are detected at a detector positioned towards the middle of the flight tube.

or

$$v = \sqrt{\frac{2qV}{m}} \qquad (12)$$

The relationship between the displacement of a particle, s (in meters, m), and the velocity at which it travels, v (in m s^{-1}) is expressed as a function of time, t (in seconds, s):

$$s = vt$$

$$t = \frac{s}{v} \qquad (13)$$

By substituting for the value of v obtained in equation (12):

$$t = \frac{s}{\sqrt{\frac{2qV}{m}}}$$

or

$$t = \frac{s\sqrt{m}}{\sqrt{2qV}}$$

In terms of a m/q ratio:

$$t^2 = \frac{s^2}{2V}\frac{m}{q}$$

Again, it should be remembered that the charge on an ion is defined as the product of the multiplication of the number of charges on the ion, z, by the charge on an electron, e (in Coulombs, C). Thus, the m/z ratio of an ion may be determined from the calculation of the square of its flight time, t^2. Due to the fact that ions do not leave the ion source with identical kinetic energies, and hence with differing velocities for a given mass, resolution is adversely affected by such energy spreads. To compensate for this, it is possible to include a series of electrodes which create a potential gradient up which the ions must travel. This series of electrodes is commonly known as a "reflectron" and will reflect an ion towards the detector. The ions will penetrate the electric field to a depth, x (in meters, m), determined by the kinetic energy it possesses, translating all of its kinetic energy to potential energy before beginning its reverse path out of the reflectron. For the following, simple case, a reflectron will be considered which possesses a linear potential gradient.

$$qV = \tfrac{1}{2} mv^2 \qquad (3)$$

and as:

$$E = \frac{V}{x}$$

$$q(Ex) = \tfrac{1}{2} mv^2 \qquad (14)$$

$$x = \frac{mv^2}{2qE} \qquad (15)$$

At the point where the ion's velocity along the z axis, the greatest component of the ion's flight path, becomes zero when all of its translational energy has become potential energy, the ion will have traveled a depth of x meters into the reflectron. By using equation (13), the time needed to penetrate this far into the electric field is given by the distance penetrated into the reflectron divided by the mean velocity (the average of the initial velocity, when entering the reflectron, and zero velocity, at the distance x):

$$t_0 = \frac{x}{\left(\frac{v_{iz}}{2}\right)}$$

where t_0 (in seconds, s) is the time at which the ion has a velocity equal to zero along the z axis, and v_{iz} is the initial velocity along the z axis with which the ion enters the reflectron (in $m\ s^{-1}$). The ion is then accelerated out of the reflectron again by the electric field, leaving with a final kinetic energy equal to the total potential energy (which is in turn equal to the kinetic energy of the ion prior to entering the reflectron). The total time spent in the reflectron is given by:

$$t_r = 2t_0$$

or:

$$t_r = \frac{2x}{\left(\frac{v_{iz}}{2}\right)} = \frac{4x}{v_{iz}} \qquad (16)$$

where t_r is the total time spent in the reflectron (in seconds, s). To demonstrate the manner in which the reflectron may focus ions of differing kinetic energies, but of the same mass, consider two ions of mass m, with two different kinetic energies, K and K'.

$$K = \frac{m v_{iz}^{\ 2}}{2}$$

$$v_{iz} = \sqrt{\left(\frac{2K}{m}\right)} \qquad (17)$$

Consider the ratio of the two kinetic energies to be defined using a constant, c:

$$\frac{K'}{K} = c^2 \qquad (18)$$

$$K' = \frac{c^2 m v_{iz}^{\ 2}}{2}$$

$$v_{iz}' = \sqrt{\left(\frac{2Kc^2}{m}\right)} \qquad (19)$$

Comparing equations (17) and (19):

$$v_{iz}' = c v_{iz}$$

For a total path length of d (in meters, m) which is the total distance of field free flight during the flight of the ion, the time of flight will be:

$$t_d = \frac{d}{v_z} \tag{20}$$

where t_d is the time spent in the field free region (in seconds, s) at a drift velocity along the z axis, v_z (in m s^{-1}). Similarly, for the other ion:

$$t_d' = \frac{d}{v_z'} = \frac{d}{cv_z}$$

$$t_d' = \frac{t_d}{c} \tag{21}$$

Using equation (15) and equation (18) to compare kinetic energies:

$$x = \frac{K}{qE}$$

$$x' = \frac{K'}{qE} = \frac{c^2K}{qE}$$

$$x' = c^2x$$

The times spent in the reflectron by the two ions may be deduced from equation (16) and are given by:

$$t_r = \frac{4x}{v_{iz}} \tag{22}$$

$$t_r' = \frac{4x'}{v_{iz}'} = \frac{4c^2x}{cv_{iz}} = \frac{4cx}{v_{iz}}$$

$$t_r' = ct_r \qquad (23)$$

Therefore, the total flight times for each ion can be calculated using equations (20) and (22) for one ion and (21) and (23) for the other ion.

$$t_{total} = t_d + t_r$$

$$t_{total}' = \frac{t_d}{c} + ct_r$$

If c>1, the ion with the kinetic energy K' (i.e. a greater kinetic energy) will have a shorter flight time outside of the reflectron, but a longer flight time inside the reflectron. If c<1, then the ion with kinetic energy K' has a lower kinetic energy, and therefore has a longer flight time outside of the reflectron but a shorter flight time inside the reflectron. In this manner, it is possible to compensate for ions of a higher kinetic energy by increasing their flight time in relation to ions of the same mass but with a lower kinetic energy. This therefore narrows the signals recorded in each mass spectrum, which shows the relative intensity of the ion as a function of what is essentially flight time, increasing the effective resolution of the instrument. By using a correct combination of electric field in the reflectron, accelerating potential in the ion source, and the total flight path length in the field free region of the instrument, it is possible to optimize the focusing effects of the reflectron when designing the instrument. One other great advantage of a reflectron is that it enables the user to perform tandem mass spectrometry experiments. When a selected "parent ion" fragments in the field free region, the "daughter ion" continues with the same velocity as the parent ion. Without a reflectron, the fragment ion would continue with the same velocity as the parent ion, although it would possess a lower kinetic energy than the parent ion, and therefore the recorded flight times would be the same. The use of a reflectron

again enables the resolution of the ions according to their kinetic energy, and hence it become possible to distinguish between the parent ion and the daughter ion. Consider an example where a parent ion of mass m_p (in kg) fragments during flight, generating a fragment ion of mass m_f and a neutral (which will not be detected and is therefore not examined in the following). The parent ion has a kinetic energy of K_p (in Joules, J) and the daughter ion has a kinetic energy of K_f (in Joules, J), but both have the same velocity v_{iz} (in m s^{-1}). From equation (2), the kinetic energy is defined as:

$$K_p = \frac{m_p v_{iz}^2}{2}$$

$$K_f = \frac{m_f v_{iz}^2}{2}$$

$$\frac{K_p}{K_f} = \frac{m_p}{m_f}$$

$$K_f = K_p \frac{m_f}{m_p} \qquad (24)$$

Examining the depth of penetration of the two ions into the reflectron electric field, using equation (14):

$$x_p = \frac{K_p}{qE} \qquad (25)$$

$$x_f = \frac{K_f}{qE} \qquad (26)$$

Using equations (24) and (26):

$$x_f = \frac{K_p m_f}{qE m_p} \qquad (27)$$

Substituting using equations (25) and (27):

$$x_f = x_p \frac{m_f}{m_p}$$

The flight times of the ions in the reflectron may be calculated using equation (16):

$$t_{rp} = \frac{4x_p}{v_{iz}} \tag{28}$$

$$t_{rf} = \frac{4x_f}{v_{iz}} = \frac{4x_p m_f}{v_{iz} m_p} \tag{29}$$

Substituting for v_{iz} using equations (28) and (29):

$$t_{rf} = \frac{m_f}{m_p} t_{rp} \tag{30}$$

Equation (30) shows that the fragment ion will therefore spend less time in the reflectron than the parent ion. When examining the fragmentation of ions in the field free region, it is necessary to resolve the daughter ions from parent ions; two ions of different masses but with the same velocity are indeed separated by the reflectron, enabling tandem mass spectrometry experiments. Without the reflectron, a "linear detector" would simply detect daughter ions at the same flight time as the parent ions, and tandem experiments could not be performed. The separation of ions by the reflectron may be considered to be the reverse of the case mentioned earlier, where ions of the same mass but differing velocities are focused at the detector by the reflectron, enhancing the resolution of the instrument. Spengler has written a overview of tandem mass spectrometry using time-of-flight instruments,[242] where "post source decay" (PSD) experiments are performed by monitoring the metastable decay of ions in the flight tube following the exit from the ion source. Harvey et al. have shown that dissociations arising from PSD may result in the observation

of a mass shift when using a reflectron time-of-flight instrument, and an equation was developed so that it was possible to link shifted signals with the parent ion from which they originated.[243]

Instrument design is continually evolving and one such development is exhibited in design work performed by Laiko et al.[244] and Morris et al.,[245] and further elaborated by Guilhaus et al.[238] Laiko et al.[244] and Morris et al.[245] have demonstrated the use of instruments which incorporate orthogonal acceleration of ions prior to ToF analysis in order to improve resolution; by accelerating the ions orthogonally, the temporal spread of the ions, arising from differences in ion velocities and space-charge effects, is compensated for as the temporal spread is converted to angular spread. Another development is the use of quadratic field and curved field reflectrons, where the graph of the potential versus distance inside the reflectron obeys a quadratic relationship (for quadratic field reflectrons)[232] or resembles the arc of a circle (for curved field reflectrons).[246] Both designs of reflectron have the same advantage over linear field reflectrons when acquiring PSD spectra in that the complete PSD spectrum may be obtained during the course of one acquisition. Linear field reflectrons, by contrast, must acquire a PSD spectrum by acquiring data over a series of steps, varying the potentials inside the reflectron with each step, and the different spectra are "stitched" together to produce the final spectrum. One of the most recent developments is the incorporation of "delayed extraction" into ion sources. Whilst most ion sources for ToF instruments incorporate just one potential, an increasing number of sources now use two potentials. The first potential is of shallow gradient and is maintained between a given position inside the ion source and the sample substrate itself so that ions travel down the potential gradient and thus collect within a relatively smaller area. Use of ion sources without this second potential results in larger energy spreads, due to the fact that the ions

are more widely scattered throughout the source, experience varying field strengths at these different locations, and therefore leave the source with differing final kinetic energies once accelerated into the flight tube. An ion source incorporating delayed extraction employs a pulsed extraction potential, in order to allow ions to collect within a small area under the influence of the second, weaker potential prior to the acceleration process. The net result is that smaller energy spreads are observed in mass spectra, and hence resolution is greatly improved.

1.2.1C Quadrupole Instruments

Developed a few years after the ToF analysis principle was first documented, quadrupole analyzers and ion traps are a third form of analyzer used in mass spectrometry.[219,221,222,247,248] Quadrupole analyzers consist of four rods with a circular or hyperbolic cross section. The rods are maintained at a potential with a DC controlled component, U (in Volts, V), and a radio frequency (rf) controlled component. Two rods, opposite each other, are maintained at a positive potential while the other two, opposite each other too, are maintained at a negative potential. Ions travel through the analyzer along the z axis with translational energies typically under 100 eV and are forced to oscillate along the x and y axes as they traverse the electric fields within the analyzer. An example of a quadrupole mass analyzer is shown in Figure 9. The voltage applied to two rods will be described by:

$$-(U + V_0 \cos \omega t)$$

$$+(U + V_0 \cos \omega t)$$

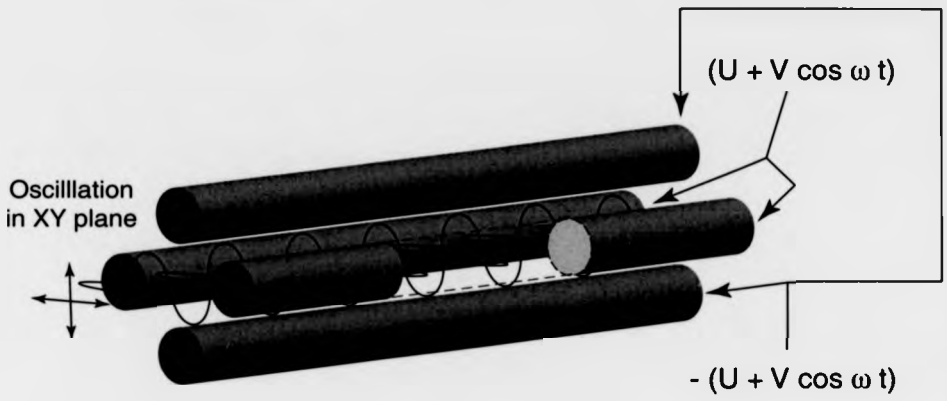

Figure 9: Schematic diagram of a quadrupole mass analyzer, consisting of four rods to which a DC and an rf potential is applied. Adjacent rods are kept at opposite polarity, and the polarities of the rods are dependent on the phase of the rf potential. Ions enter the quadrupole and oscillate in the xy plane as they travel along the z axis. As the quadrupole mass analyzer is scanned, only ions of specific mass to charge ratios possess stable trajectories and manage to traverse the mass analyzer. The quadrupole may thus be considered to act as a filter.

where U (in Volts, V) is the DC controlled component and $V_0 \cos \omega t$ (in Volts, V) is the rf controlled component, where ω (in radians per second, rad s^{-1}) is the frequency of the rf voltage and t (in seconds, s) is time. The Mathieu equations define the motion of an ion of a mass to charge ratio of m/e along the x and y axes, mutually perpendicular to the z axis:

$$\frac{d^2x}{d\left(\frac{\omega t}{2}\right)^2} + \left(a + 2q \cos 2\left(\frac{\omega t}{2}\right)\right)x = 0$$

$$\frac{d^2y}{d\left(\frac{\omega t}{2}\right)^2} - \left(a + 2q \cos 2\left(\frac{\omega t}{2}\right)\right)y = 0$$

where:

$$a = \frac{8eU}{mr_0^2\omega^2}$$

and

$$q = \frac{4eV_0}{mr_0^2\omega^2}$$

where e (in Coulombs, C) is the charge on an electron, m is the mass (in kilograms, kg) of the ion, and r_0 (in meters, m) is half the separation between opposing rods. Therefore:

$$\frac{a}{q} = \frac{2U}{V_0}$$

As long as the displacement of an ion along both the x and y axes is less than r_0, the ion may successfully traverse the analyzer. All other ions will discharge themselves against the rods of the quadrupole mass analyzer or may escape between the gaps spacing the rods. Hence, the quadrupole analyzer acts as a filter, only allowing ions of stable oscillations to pass. Ions must possess translational energies only up to several hundred eV, as ions of higher translational energies will pass through the analyzer without being properly filtered. For a fixed frequency, U and V_0 are directly proportional to the mass of the ion examined, and therefore if these potentials are scanned in a manner that keeps the ratio of a:q constant, ions of different masses will follow stable oscillations through the analyzer in turn, leading to the recording of a mass spectrum. If only an rf potential is applied, without the use of the DC component (U), then ions of all masses may pass and the quadrupole acts only as an ion guide. Quadrupole instruments can be seen to measure the mass of ions directly, rather than measuring an m/e or m/z ratio. In practice, these types of instruments are unusual in that they are frequently operated at a "unit resolution" mode, operating with a resolution of 1 Dalton (Da) throughout the mass range. This is in contrast to the traditional operation at a fixed, numerical value for resolution, where signals at higher masses are less easily resolved than those at lower masses; using a quadrupole instrument, ions of

higher mass have lower velocities and therefore spend longer in the rf field, which in turn improves resolution at higher masses. Quadrupole based instruments have the advantages that they are compact, the ion source may be kept at a low potential due to the fact that it is advantageous for ions to possess low translational energies, the analyzer may be rapidly scanned, and no slits are required in the flight tube, improving sensitivity. The upper mass limit of quadrupole instruments is approximately 2000 Da.

1.2.1D FT-ICR Instruments

The most recently developed form of mass analysis is that of ion cyclotron resonance (ICR).[219,221,222,249-258] The principle of ICR mass spectrometry is to trap ions in a cell, within which they undergo a circular orbit due to the presence of a strong magnetic field. The strong magnetic field (typically ranging from 3 - 20 T) acts parallel to the axis of flight of the ions from the ion source. Due to a the component of the ions' velocity along the x or y axis, perpendicular to the axis of the magnetic field, a force is therefore exerted on the ions acting as the centripetal force, maintaining the orbit within the cell, where the ions precess about the z axis. This orbit within the cell is known as the "cyclotron motion." As has been shown earlier, for an ion with a velocity vector component which is perpendicular to the magnetic field through which it passes:

$$qvB = \frac{mv^2}{r} \qquad (5)$$

or:

$$qB = \frac{mv}{r} \qquad (31)$$

By definition, the angular frequency, ω (in radians per second, rad s^{-1}), is defined as:

$$\omega = 2\pi f = \frac{v}{r}$$

or:

$$f = \frac{\omega}{2\pi} = \frac{v}{2\pi r} \qquad (32)$$

where f (in Hertz, Hz) is the frequency, v (in m s^{-1}) is the velocity of the ion, r (in m) is the radius of the orbit, and ω (in radians per second, rad s^{-1}) is the angular frequency. Comparing equations (32) and (31), it can be shown that:

$$f = \frac{Bq}{2\pi m}$$

or alternatively, from equation (32), this may be more commonly expressed as:

$$\omega = \frac{Bq}{m}$$

Thus, the frequency of the cyclotron motion within the cell is dependent upon the inverse of the m/q ratio. In this way, the analysis of the ions present in the cell can be performed. It is notable that the frequency is independent of the velocity of the ions. This then leads to the observation that the frequency is also independent of the kinetic energy of the ions as a result. While kinetic energy spreads can adversely affect the resolution of ToF and sector instruments, no such disadvantage can be found for ICR analysis. In part due to this phenomenon, ICR mass spectrometers are characterized by their high resolution, typically of the order of 10^6, compared to 100,000 for sector instruments and approximately 2000 for many ToF and quadrupole-based instruments.

To prevent ions from escaping from the cell during analysis, which would greatly reduce sensitivity, two plates are mounted perpendicularly to the magnetic field at each end of the cell. A potential is applied to these plates so that a potential well is created along the z axis, restraining the ions' movement parallel to the magnetic field once they have entered the cell. Ions undergo simple harmonic motion along the z axis between these trapping plates. Considering the simple case of a cell which is cuboid in shape, the trapping plates occupy positions at the two ends of the z axis. Two more electrodes occupy the ends of the x axis, and two further electrodes are placed at the ends of the y axis as well. Two opposing electrodes of the four are used for the purposes of excitation of the ions within the cell, while the other two opposing plates are used for the purposes of detection. Ions entering the instrument cell have a low kinetic energy, typically less than 1 eV. The radius of the ions' orbits is too small to be measured, and therefore must be increased. This is done by applying an rf controlled voltage to the two excitation plates, exciting ions of the same m/q value to a coherent circular motion, of equal radius, closer to the detection plates. Broadband excitation may be employed in order to excite ions over a wide m/z range; this is effected by applying many frequencies during excitation, most commonly performed using a rapid frequency sweep, also known as an "rf chirp." The ions spiral outwards to larger orbits when their cyclotron frequency is in resonance with the frequency of the rf controlled potential of the two excitation plates; ions which are not resonant with the rf controlled potential remain at the center of the cell. If the rf controlled voltage were applied continuously, the ions would continue to spiral outwards until they strike one of the four plates, and so the excitation is terminated once the ions are close enough to the detection plates for analysis to be performed. Detection of the ions is, unlike other mass spectrometers, non-destructive. The ions pass two detection plates, which are connected electrically, during their orbit, and as they do so the ions induce the

movement of electrons in the plate; as the ions pass the other detection plate, the electrons move from the former plate to the latter. The result is that the ions induce a sinusoidal current known as an "image current." This current can be amplified and processed using a computer. A typical FT-ICR mass spectrometer is illustrated in Figure 10.

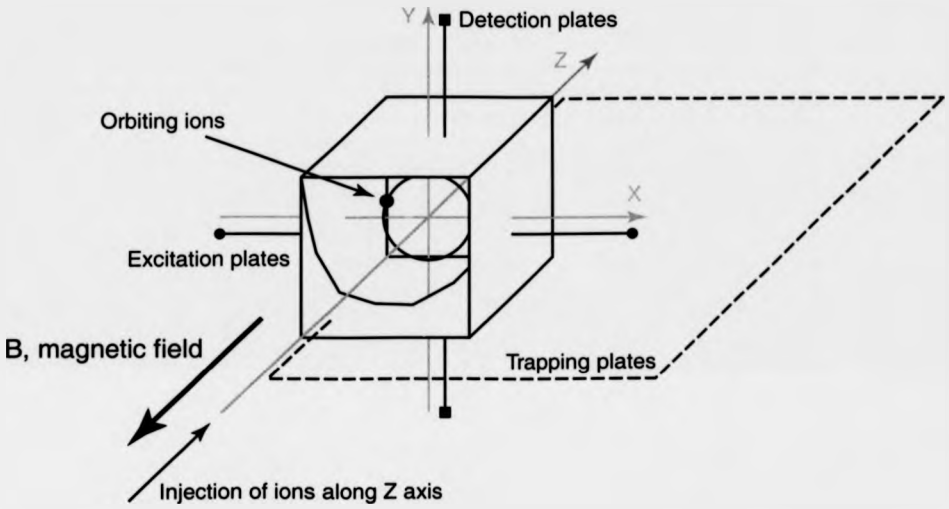

Figure 10: Schematic representation of an FT-ICR mass spectrometer cell. Ions are injected along the z axis and precess about the center of the cell, in the xy plane, due to the presence of the magnetic field. Excitation plates are used to excite the ions to an orbit of suitable radius in order that their proximity may be detected by the two detector plates.

The trapping motion and cyclotron motion of the ions are not coupled. However, the potential inside the cell arising from the two detection plates, two excitation plates, and two trapping plates assumes a three dimensional nature. The potential is greatest at the center of the cell, along the z axis, repelling ions to the edges of the xy plane; the electrostatic potential is roughly radially repulsive from the center of the cell in the xy plane. The trapping plates meanwhile constrain the motion of the ions along the z axis.

The force acting on the ions due to the presence of the magnetic field, meanwhile, also serves to prevent the ions from being accelerated into the edges of the xy plane (cell walls) by the electrostatic potential. The ions therefore undergo cyclotron motion, the center of which precesses about the center of the cell due to the additional magnetron motion, resulting in two orbits: the orbit labeled the cyclotron motion, and the orbit of the center of the cyclotron motion about the center of the xy plane known as the "magnetron motion." The radius of the magnetron motion is determined by the deviation of the ion's flight path from the z axis, running perpendicular to center of the cell, upon injection. The frequency of the magnetron motion, unlike the frequency of cyclotron motion, is independent of the mass to charge ratio of the ion, and also does not serve any analytical purpose. It is possible to minimize the magnetron motion by injecting ions as precisely as possible along the principal axis of the cell, running parallel to the magnetic field. It should be noted that the radius of the cyclotron motion is usually much greater than the radius of the magnetron motion during detection, and that the magnetron motion is exaggerated for the purposes of illustration in the diagram; magnetron frequencies are typically of the order of 1 - 100 Hz, while cyclotron frequencies are of an order of 5 kHz - 5 MHz. Figure 11 shows the 3D potential surface, in the xy plane of the cell, and is based upon a plot published by Amster;[257] Figure 12 illustrates the ion motion within the cell, and is based upon diagrams used by Amster[257] and Jacoby et al.[255]

It is more efficient to apply many excitation frequencies at once during the excitation event, so that not only ions of one m/q value may be excited and detected. However, in doing so, the image current detected is then a function of many ions with different m/q values, and therefore the image is a composite of many, different sinusoids and amplitudes. By applying a Fourier Transform (FT) to the time domain transient, frequency components

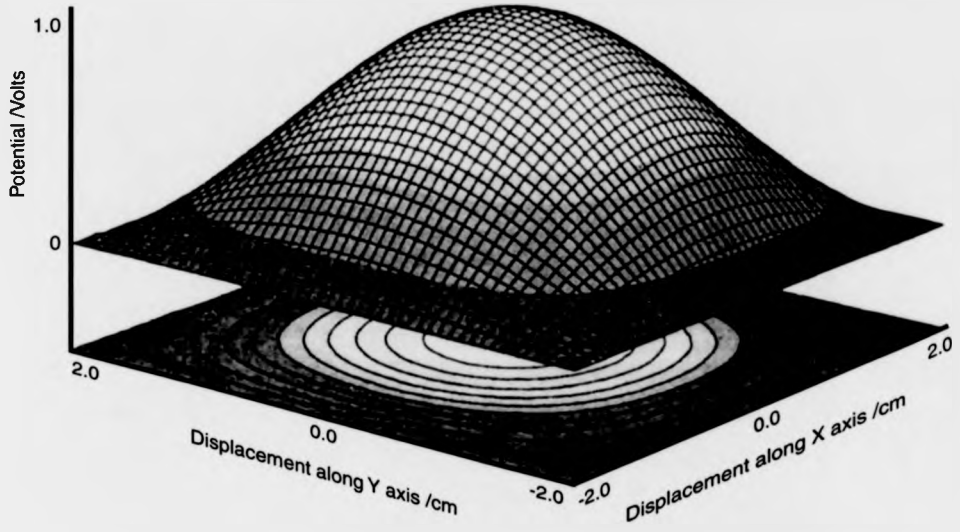

Figure 11: Three dimensional plot of the potential surface, in the xy plane, which is experienced by the ions. The detection plates (y axis) and excitation plates (x axis) are maintained at earth potential. A voltage is applied to the trapping plates (z axis) which used to trap ions within the cell, resulting in a non-zero potential at the center of the cell along the z axis. This non-zero potential at the center of the cell thus results in the potential surface within the xy plane shown here.

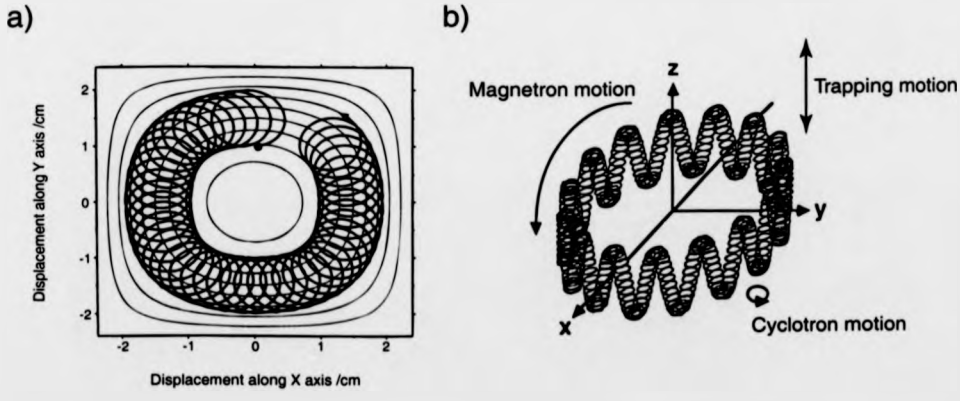

Figure 12: Illustration of the motion of ions within the cell. Diagram a demonstrates the cyclotron motion of the ions, offset from the center of the cell by the magnetron motion which results from the potential experienced in the xy plane. Diagram b is a three dimensional representation of the three types of motion which the ions undergo: the magnetron motion, cyclotron motion, and trapping motion.

of the signal are obtained and use of a calibration formula derived from the cyclotron frequency equation then translates this data into the form of a mass spectrum. This technique is known as Fourier Transform Ion Cyclotron Resonance (FT-ICR) mass spectrometry, and requires the use of powerful computers for the purpose of signal processing. One other potential difficulty of this technique is the reliance on the repeated detection of ions within the cell. Ions must therefore be prevented from undergoing collisions within the cell, and this means maintaining the cell under very high vacuum conditions, typically 10^{-9} Torr (a pressure of one to two orders of magnitude lower than is typical for sector and ToF instruments).

1.2.2 Detectors

Detection systems for mass spectrometers most typically rely on the destructive detection of ions, where ions must collide with a surface to induce the flow of electrons. The notable exception to this rule is the method of detection employed by FT-ICR mass spectrometers, where the movement of charge past a detection plate induces a current to counteract the effect of the proximity of the charge. This non-destructive detection is one of the advantages of FT-ICR mass spectrometry. However, other instrument designs employ the use of detection systems which rely on electron multiplication following collision of the ion with a surface within the detector instrumentation.[221,222,236,259,260]

1.2.2A Electron Multipliers

One of the most common types of detector is the "electron multiplier," an example of which is shown in Figure 13. Discrete dynode multipliers are connected in series via a chain of resistors, and a high voltage is applied to the system, where the same potential

difference should be present between adjacent dynodes. The dynodes are most commonly constructed using beryllium/copper, although aluminum may also be used. The first dynode is maintained at a negative potential (when monitoring positive ions) with respect to the final dynode in order that electrons may be accelerated down the chain, eventually arriving at an amplifier. Following the impact of an ion upon the first dynode, secondary electrons are liberated from the dynode surface which are accelerated towards the next dynode and the collision of these electrons proceeds to liberate further electrons, and so on down the dynode chain. The resulting cascade of electrons results in a measurable current which may be amplified, producing a signal which may be measured for the determination of the relative intensity of a given ion. One disadvantage of the electron multiplier system is that the detector may become saturated with electrons if the ion signal is intense enough, which would in turn limit the sensitivity of the system. A multiplier gain of between 10^7 - 10^8 is typically achievable, though gain does deteriorate with time and electron multiplier detectors will require eventual replacement.

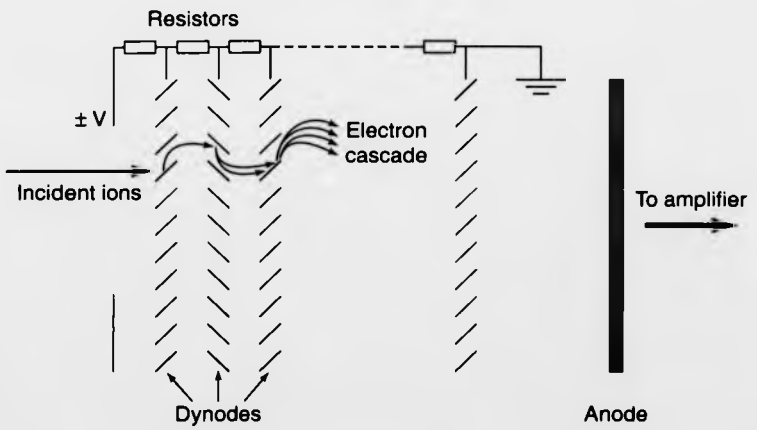

Figure 13: Schematic diagram of an electron multiplier. The impact of ions upon the dynodes liberates electrons, which in turn impact upon other dynodes, until a current is registered at the anode and amplified.

1.2.2B Microchannel Plates

A variation of the electron multiplier detector involves the use of "microchannel plates" (MCP's). An example of a microchannel plate arrangement is illustrated by Figure 14. MCP's consist of a plate in which parallel, cylindrical channels have been incorporated. Millions of such channels may be present in a single MCP, with channel diameters ranging from 4 - 25 μm, with a spacing of approximately 6 - 32 μm between the centers of the channels. The principle of a microchannel plate is analogous to that of the electron multiplier described previously, with a potential is applied between the front and back of the plate and the production of secondary electrons following the impact of an ion, and each microchannel plate may be considered to be a miniaturized electron multiplier system. One disadvantage is that a single microchannel plate provides a lower gain than a traditional electron multiplier system, but MCP's have the advantage of being much more compact. Use of a single MCP results in an experimental gain of approximately 10^5, while the use of several plates, typically in a "chevron assembly," can result in gains of up to 10^8.

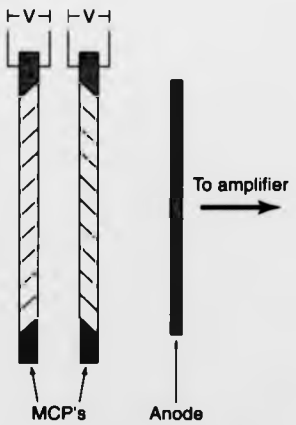

Figure 14: Schematic representation of two multichannel plates. Electrons are liberated, following the impact of ions upon the multichannel plate, and arrive at the anode, where the current is amplified.

1.2.2C Post Acceleration Detectors

Though not yet fully substantiated, there is growing interest in the hypothesis that ions must have a velocity equal to or greater than a threshold value in order for secondary electrons to be produced by electron multiplier systems.[236,259,260] The theory is centered around the concept that secondary electron production depends upon the momentum of incident ions rather than kinetic energy, and hence larger ions will possess a lower velocity and therefore a lower momentum than smaller ions with a higher velocity, but equal kinetic energy. While the matter is still of some debate, if proven to be well founded, the hypothesis has serious implications for biological mass spectrometry, which involves the investigation of molecules with masses of an order of kDa. One possible solution is the use of "post acceleration detectors" (PAD's), as shown in Figure 15. As the ion beam passes through a resolving slit of the instrument, the ions are accelerated towards an off-axis target which is frequently constructed using polished aluminum. Impact with the target liberates electrons which are then accelerated to an electron multiplier. If the target surface were flat, secondary electrons would tend to curve away from the multiplier axis, due to the fact that the field above the target surface is convex. This may be prevented by constructing a concave target surface, which has the effect of focusing secondary electrons into the electron multiplier. The target surface is usually maintained at a potential between ±8 - ±30 kV (negative potentials when studying cations, positive potentials when studying anions), and therefore the ions will be accelerated orthogonally with a resulting momentum great enough to liberate secondary electrons effectively. By accelerating the ions orthogonally, the velocity of the ions along the flight path axis is not significant for the generation of secondary electrons and by utilizing a high enough potential, ions with a high mass may be detected efficiently. PAD's may also be used during tuning of sector instruments; a

PAD may be switched on the determine the optimization of the ion beam at a given point, and then switched off to allow the passage of ions through the flight tube again. In this manner, the user may proceed in a logical manner, optimizing the signal at each stage of the instrument in order to maximize the ion intensity at the final detector.

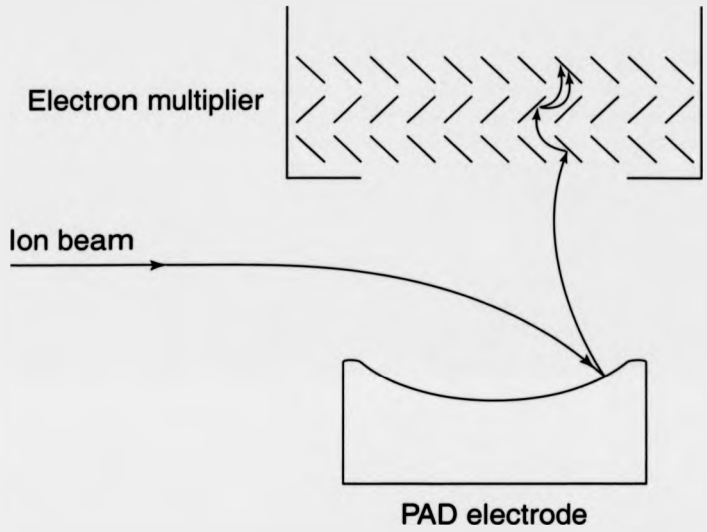

Figure 15: Schematic representation of a postacceleration detector (PAD). The ion beam is deflected by an off-axis electrode. The impact of the ions upon the electrode results in the liberation and repulsion of electrons, which then arrive at dynodes within an electron multiplier and produce a current which is later amplified.

1.2.2D Array Detectors

A variation of the use of electron multipliers may be found in array detection systems, an example of which is shown in Figure 16.[221,222,259,260] Microchannel plates are employed as the first stage in such a set up, and the resulting secondary electrons are then used to generate photons following collision with a phosphor screen. Photons are then transferred

via a fiber optic coupling to a charge coupled device (CCD), where each channel of the CCD is typically 25 μm wide and 2.5 mm long. The photons are converted to charge, integrated, and stored. Due to the fact that the detection system uses discrete channels, it is possible to resolve signals arising from different ions which impact upon the MCP's. Commonly, 4% mass range may be detected by an array detector, with a resolution of a few thousand. Sector instruments are known for their low sensitivity, due to the fact that scanning of the ion beam is required, rejecting the vast majority of the ions generated; a 4% mass range for a sector instrument would represent a considerable improvement. As a result, array detectors are almost always used in conjunction with sector instruments, providing them with a sensitivity increase of over two orders of magnitude.

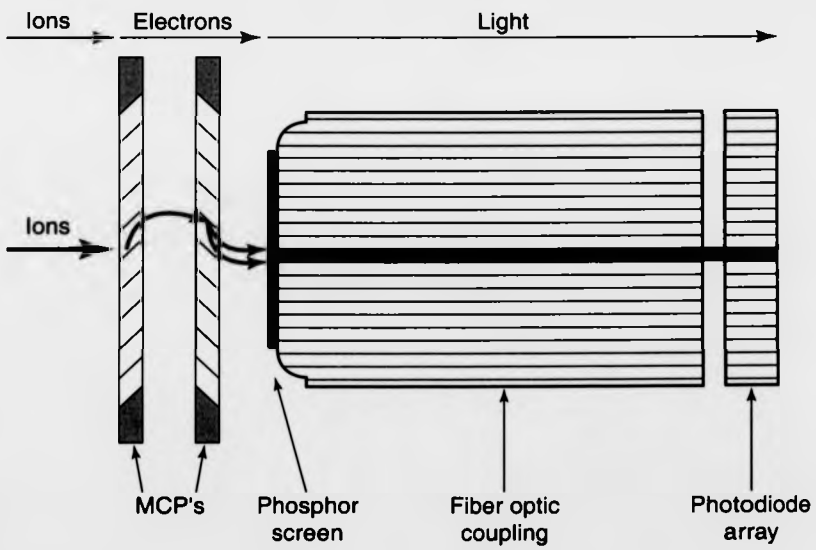

Figure 16: Schematic diagram of an array detector. Collision of ions upon multichannel plates results in the production of electrons which arrive at a phosphor screen, causing it to glow. The resulting light is channeled by fiber optic connections and arrives at one of an array of photodiodes, where it is detected.

1.2.3 Ionization Methods

Another critical feature of a mass spectrometer is the ionization technique used. The choice of ionization method can exert a great influence on appearance of the mass spectrum obtained, independently of the chosen method of mass analysis. Current ionization techniques include: electron ionization (also known as electron impact) (EI), chemical ionization (CI), laser desorption/ionization (LDI), matrix-assisted laser desorption/ionization (MALDI), electrospray ionization (ESI), thermospray (TS), inductively coupled plasma (ICP), field desorption (FD), field ionization (FI), plasma desorption (PD), fast atom bombardment (FAB), and liquid secondary ion mass spectrometry (LSIMS). Ion sources which are pulsed by nature, such as LDI and MALDI, are most often coupled to mass spectrometers which use analyzers that rely on the measurement of packets of ions, such as time-of-flight instruments. Ion sources which continuously ionize sample neutrals, such as EI and CI, are most suited to use with instruments which implement continuous detection, such as sector instruments. As a result, the choice of ion source is often closely correlated with the type of mass analyzer utilized, though it is possible to devise methods for coupling ion sources to mass analyzers which had previously been considered to be "less suitable." Of particular relevance to following discussions are ionization techniques of: electron ionization, laser desorption/ionization, matrix-assisted laser desorption/ionization, liquid secondary ion mass spectrometry, and electrospray ionization.

1.2.3A Electron Ionization (EI)

EI is the oldest form of sample ionization. A typical EI source is shown in Figure 17. The sample is first loaded into a probe, the probe inserted into the ion source, and the

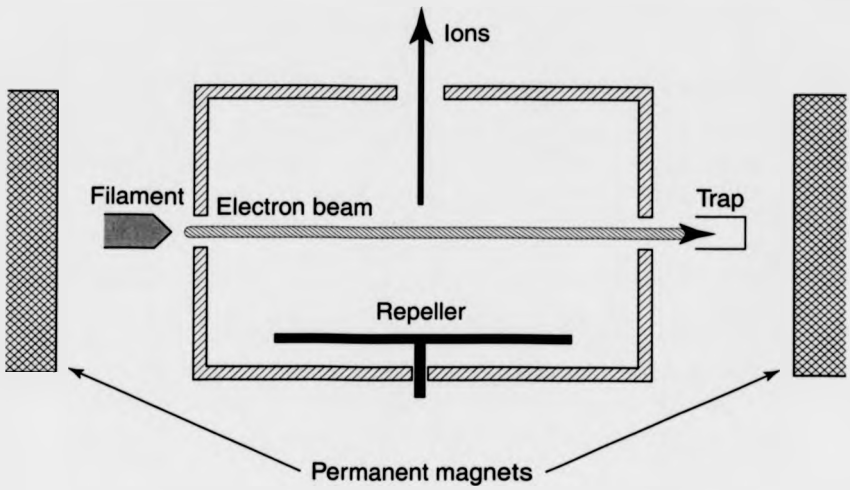

Figure 17: Schematic diagram of an electron ionization (EI) ion source.

sample is vaporized by heating; the sample vapor then enters the ionization chamber. A filament, typically made of tungsten or rhenium, is used to create a beam of electrons via thermionic emission. A potential is applied to the ionization chamber which acts to accelerate the electrons towards it, and some of the electrons enter the chamber through a slit; magnets placed behind the filament and on the opposite side of the ionization chamber act to guide the electrons in a narrow, helical path. The electrons which enter the ionization chamber may collide with neutrals in the sample vapor; approximately less than 1/100 of the total electrons interact with the sample molecules. Interaction between the electrons and the sample neutrals may lead to the removal of an electron from the sample molecule, leading to cation formation, or the neutrals may capture electrons, leading to anion formation. The electron current may be regulated using a "trap" on the opposing side of the chamber, which provides feedback of the number of electrons reaching it. By varying the accelerating potential acting on the electrons, it is possible to vary the electron energy and hence control the internal energy imparted to the sample molecules upon collision.

Increasing the internal energy of a neutral increases the probability of fragmentation within the ion source. Electron energies are most frequently varied when studying the ion intensity of a chosen species versus electron energy to produce a breakdown curve; otherwise, mass spectra are typically recorded at an electron energy of 70 eV. Electron impact is considered to be one of the most harsh ionization techniques available, and tends to induce a high degree of fragmentation.

1.2.3B Laser Desorption/Ionization (LDI)

LDI has the advantage of being a relatively simple technique. The sample is usually deposited on a target, such as a stainless steel slide, as a solution and the solution is allowed to dry, leaving behind a solid layer of the sample. The sample is then ablated by a laser. The precise mechanism underlying laser desorption/ionization is not yet understood, though insight has been provided into the processes which must occur.[261,262] All of the steps considered must occur within a short time scale, typically nanoseconds, and within a small area, typically square micrometers, in order to avoid thermal decomposition. Laser irradiation of the sample leads to the formation of an excited solid, and ionization may occur at this stage or later; this excited solid then undergoes desorption,as demonstrated by Figure 18. It is assumed that desorption occurs on a large scale, rather than via individual molecules. The ions and molecules must traverse what is referred to as the "selvedge region," where the outer boundary is defined as being the distance from the target past which no ion-molecule reactions occur and only unimolecular dissociations may occur. Within the selvedge region, photochemistry and radical chemistry is believed to take place. The plume of different species continues to expand under the forces exerted due to Coulombic repulsion. The varying species may now be considered to be truly of the

gas-phase, and are then accelerated out of the ion source into the flight tube of the mass spectrometer. Control of the energy imparted to the sample is maintained by tuning the frequency of the photons emitted from the laser in some cases, or, in the majority of cases, the intensity of the laser light is governed by a filter which controls the transmission of the beam, restricting the total number of photons allowed to arrive at the target.

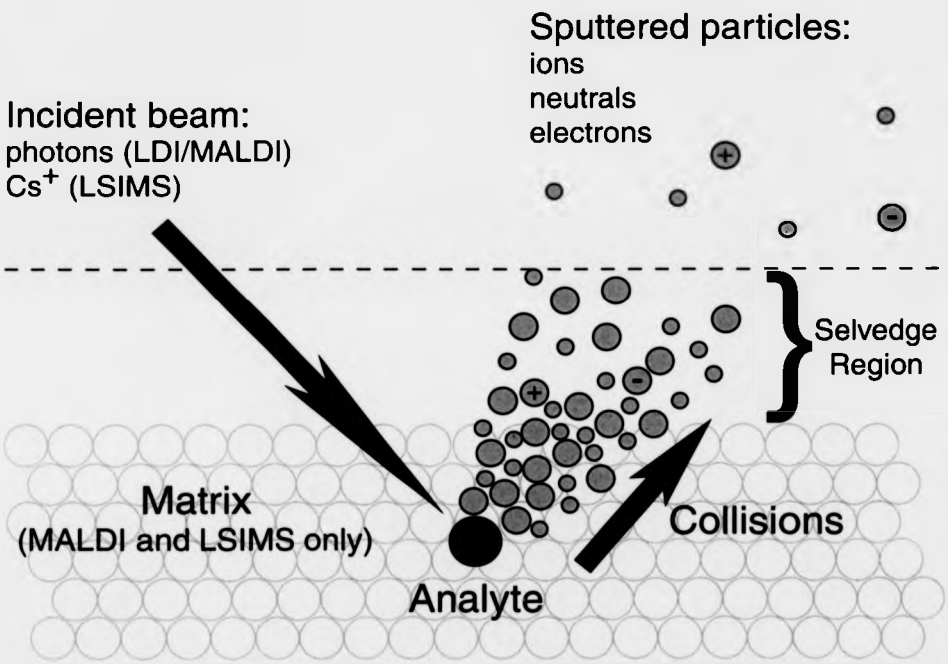

Figure 18: Illustration of the principles underlying desorption/ionization, as applied by LSIMS, LDI, and MALDI. An incident beam results in the desorption of neutrals and ions from the target surface. Collisions and interactions between particles continue until leaving the Selvedge region. Ions, neutrals, and electrons are considered to be sputtered into the ion source. Ions are then extracted by an acceleration potential within the ion source, and enter the mass analyzer.

When thin layers of sample are used, the substrate will also be ablated into the plume and will therefore also interact with the sample of interest. Optimum conditions

may be obtained by using a frequency for which the sample undergoes a strong, resonant absorption. Gentle desorption may be performed when the analyte displays a strong, resonant absorption (linear absorption) at the respective laser wavelength.[261,263] Derived from the Beer-Lambert Law, the energy transferred to the analyte per unit volume is proportional to the product of the molar extinction coefficient, the molar concentration multiplied, and the energy per unit area deposited by the laser.

The Beer-Lambert Law states:

$$\frac{I}{I_0} = 10^{-\varepsilon c l}$$

or:

$$\log \frac{I}{I_0} = -\varepsilon c l$$

where I_0 is the intensity of the incident radiation, I is the intensity of the transmitted radiation, ε is the molar absorption coefficient (in $M\ cm^{-1}$, or moles $dm^{-3}\ cm^{-1}$), c is the molar concentration (in M or moles dm^{-3}), and l is the path length which is equal to the thickness of the absorbing material (in centimeters, cm).

Following on from this expression, Hillenkamp[261] stated the relationship:

$$\text{Energy per unit volume of sample} = 2.3 \times \varepsilon \times c \times H$$

and H, the radiant exposure (measured in terms of total energy per unit area) is equal to:

$$H = \text{laser irradiance} \times \tau$$

where the laser irradiance describes the power per unit area (frequently described in terms of W cm^{-2}) and τ is the pulse width of the laser (typically in the region of nanoseconds).

When such a linear relationship exists, the energy deposited in the analyte may be easily controlled by changing the laser irradiance (in J s^{-1} cm^{-2} or W cm^{-2}) (note: "laser fluence," in J cm^{-2}, is also a frequently used term and is independent of the duration of the laser pulse width). For samples which do not show a strong, resonant absorption, non-linear absorption processes occur at high laser fluences, the amount of energy absorbed by the sample becomes much more difficult to regulate, and it is likely that plasma formation occurs at the sample. The role of infra-red (IR) lasers under optimum desorption conditions is not yet clear, although ultra-violet (UV) lasers are known to induce electronic transitions within the desorbed molecules. Evidence exists for the photoionization of the sample in the condensed phase, as the primary channel for ionization, when using UV lasers.[261] Slow heating of a sample, with energy equilibration amongst all available degrees of freedom would result in thermal decomposition. The desorption process involved in laser desorption/ionization, however, may be considered to be a non-equilibrium process. Lasers of short pulse widths, of an order of a few nanoseconds, are typically used and in this way, compounds which are liable to thermal decomposition may be analyzed using LDI based techniques. Other ionization techniques which require vaporization through heating of the sample, such as EI and CI, are therefore not as suitable. Variations of the LDI technique exist. One such variation is the use of two lasers, one for the laser desorption (LD) process and one for the direct photoionization, or "laser ionization" (LI), of the molecules within the vapor. Perhaps the most well known variation is that of matrix-assisted laser desorption/ionization (MALDI).

1.2.3C Matrix-Assisted Laser Desorption/Ionization (MALDI)

The originators of MALDI are indeterminate as two groups, Tanaka et al.[264] and Karas et al.,[265] published papers almost simultaneously. Karas et al. used a sample protein in conjunction with nicotinic acid, a UV absorbing matrix, and a UV laser and demonstrated that the use of a matrix had improved the sensitivity of labile, high mass compound. Nicotinic acid was found to have a high absorption coefficient at 266 nm, the wavelength of the UV laser used. A mixture of aqueous solutions of a protein and nicotinic acid were then deposited and dried, leading to the formation of a mixed solid. The matrix would absorb the UV light efficiently, leading to desorption, and this in turn led to the efficient desorption of the analyte. Tanaka et al. obtained similar findings, though based on a different principle, using a mixture of a protein sample with glycerol, a liquid matrix, and a fine, metal powder. Glycerol was used to suspend both the protein sample and the metal powder, and was transparent to the UV laser (337 nm). The metal powder had dimensions smaller than the wavelength of the irradiating laser, resulting in the heating of the powder due to the currents induced by the laser. The metal particles acted to couple the laser irradiation and the liquid matrix and resulted in the heating of the sample. The mechanisms behind both methods are still not yet fully understood. However, Karas et al.'s method was 1000 times more sensitive than Tanaka et al.'s. Mass spectra displayed by Karas et al. also exhibited a higher signal-to-noise ratio than those demonstrated by Tanaka et al, and so the former method rather than the latter became the method upon which MALDI is now based.

The principle of MALDI is to selectively deposit energy from the photoirradiation process into the matrix. A large excess of matrix to analyte is used in order to disrupt

intermolecular forces between analyte molecules. The matrix absorbs the energy from the laser and is responsible for the break up of the condensed phase assisting the analyte molecules into the gas-phase. It has been noted that increasing the irradiance frequently results in the broadening of signals when using ToF mass spectrometry. This results from the fact that more energy is deposited into the system, increasing the temporal and angular spreads amongst the ions, and these discrepancies lead to differing flight times. One group used various protein samples and matrices to conduct an investigation into the velocity distributions of ions within the ion source following laser ablation,[266] determining the initial velocities to be of an order of hundreds of meters per second. It was found that the most important factor was the matrix used, that the molecular weight of the proteins studied had relatively little effect (for masses over 5 kDa), and that there was no dependence on the wavelength (266 nm and 337 nm tested) of the laser used. Little is known about the mechanisms of desorption and ionization involved in MALDI, although it is currently believed to be similar to LDI (as shown in Figure 18), in that chemical interactions in the selvedge region lead to reactions and ionization in addition to such processes within the condensed phase immediately following ablation; the matrix's major role is believed to be the preferential absorption of the incident photons to enable the gentle desorption of the analyte, and possible chemical interactions following desorption.

Overviews of MALDI as an analytical technique[267-269] have gained increasing interest, though the mechanisms involved during the desorption/ionization process are still relatively little understood. It is known that a potential matrix must absorb photons of the wavelength produced by the laser for a given instrument, as the energy must be deposited in the matrix and not the analyte. In terms of specific applications, it is favorable for the potential matrix to dissolve in the same solvent used to create the analyte solution. Finally, an ideal

matrix will not react with the sample; matrices which tend to act as oxidizing agents are particularly unsuitable for use with many biochemicals for instance. However, though a matrix may meet these known requirements, it still may not be experimentally useful. It has been stated that by 1992, though over 300 matrices had been investigated, only seven were actually found to be of use.[268] Matrix-assisted laser desorption/ionization has become one of the most common ionization techniques used in modern times, largely due to its simplicity and its suitability for use with the relatively inexpensive and easy to use time-of-flight mass spectrometers. The typical applications of MALDI are the analyses of polymers[270,271] and biological samples,[261-263,268] though other samples such as calixarenes[272] and fullerenes[213] have also been investigated, to name but a few, selected examples. Ionization techniques based on the laser ablation of a target always carry with them the problem of shot-to-shot reproducibility; inhomogeneities within a target surface can lead to starkly differing profiles being accumulated, and therefore sample preparation has become a subject of investigation. Axelsson et al.[273] attempted to increase reproducibility by using a process analogous to electrospray for the application of the sample to the target. As a result of the possibility of decomposition of the analyte during the spraying process, others have attempted to use spraying methods which do not require high voltages, such as the use of a standard, artist's airbrush.[274] With the increasing attention paid to MALDI and ToF mass spectrometry, one group has pioneered the use of a liquid matrix with sector instruments.[275] The matrix reforms its shape after each laser pulse, regenerating the homogeneous layer on the target which would be lacking when using a solid phase matrix. The renewal of the sample surface is of special importance as the position of irradiance is usually fixed when using sector instruments.

1.2.3D Liquid Secondary Ion Mass Spectrometry (LSIMS)

LSIMS is another "soft" ionization technique used in mass spectrometry when it is undesirable to provide a labile sample with a high internal energy and when a high degree of fragmentation is not required. The sample is dissolved in a liquid matrix, such a 3-nitrobenzyl alcohol (NBA) or glycerol, and mounted on the tip of a probe. The probe is inserted into the ion source, and the analyte/matrix mixture is bombarded with ions of high kinetic energy, typically cesium ions at 30 - 35 keV, which have been generated using filament ionization sources or plasma discharge sources. A liquid matrix is used in order that the surface may be renewed following each collision with a cesium ion. Relatively more is understood about the LSIMS ionization process than those behind the LDI and MALDI processes.[221,222,262] Requirements for a good matrix include a low volatility, solvent/analyte solubility, and a low acid/base or redox reactivity. Assuming an interaction time of 0.1 ns during the collision process, the power involved is approximately equal to 6×10^{-5} W, or an energy of 6×10^{-15} J (37449 eV). It is thought that a Cs^+ ion impacts upon the surface, leading to a series of collisions within the matrix as the energy is transferred from the impacting ion. This series of collisions leads to the ejection of molecular species as a result of the "sputtering" process, as shown in Figure 18.

Ionization occurs during the cascade of collisions immediately after collision and in acid/base or redox reactions as the analyte molecules leave the surface of the analyte/matrix mixture. Acid/base reactions, photolytic reactions (where the necessary light is provided by the particle source in the LSIMS source), and bombardment induced reactions occur within the sample solution. Redox reactions also occur in an environment that includes strong potentials and electrons liberated during the collision processes. Ions and molecules

1.2.3D Liquid Secondary Ion Mass Spectrometry (LSIMS)

LSIMS is another "soft" ionization technique used in mass spectrometry when it is undesirable to provide a labile sample with a high internal energy and when a high degree of fragmentation is not required. The sample is dissolved in a liquid matrix, such a 3-nitrobenzyl alcohol (NBA) or glycerol, and mounted on the tip of a probe. The probe is inserted into the ion source, and the analyte/matrix mixture is bombarded with ions of high kinetic energy, typically cesium ions at 30 - 35 keV, which have been generated using filament ionization sources or plasma discharge sources. A liquid matrix is used in order that the surface may be renewed following each collision with a cesium ion. Relatively more is understood about the LSIMS ionization process than those behind the LDI and MALDI processes.[221,222,262] Requirements for a good matrix include a low volatility, solvent/analyte solubility, and a low acid/base or redox reactivity. Assuming an interaction time of 0.1 ns during the collision process, the power involved is approximately equal to 6×10^{-5} W, or an energy of 6×10^{-15} J (37449 eV). It is thought that a Cs^+ ion impacts upon the surface, leading to a series of collisions within the matrix as the energy is transferred from the impacting ion. This series of collisions leads to the ejection of molecular species as a result of the "sputtering" process, as shown in Figure 18.

Ionization occurs during the cascade of collisions immediately after collision and in acid/base or redox reactions as the analyte molecules leave the surface of the analyte/matrix mixture. Acid/base reactions, photolytic reactions (where the necessary light is provided by the particle source in the LSIMS source), and bombardment induced reactions occur within the sample solution. Redox reactions also occur in an environment that includes strong potentials and electrons liberated during the collision processes. Ions and molecules

which leave the solution must then traverse the selvedge region, referred to earlier. The pressure drops from that experienced within the condensed phase to that of a free vacuum, and it is between these two regions that the selvedge region is located, where ions may undergo association and dissociation reactions. It can therefore be seen that LSIMS involves the transition of highly energized molecules to a more interactive plume of species in the selvedge region, through a process of rapid expansion away from the target surface. Resulting spectra typically exhibit the presence of $[M+H]^+$ or $[M-H]^-$ species, with even electron configurations, and the ionization technique is known for inducing very low degrees of fragmentation, making it suitable for use with labile species, including high mass molecules such as proteins, though MALDI has become increasingly widespread for the analysis of such analytes, as MALDI is the more efficient desorption/ionization process for large molecules.

1.2.3E Electrospray Ionization (ESI)

Another recent development during the search for softer ionization techniques is a method known as electrospray ionization.[221,222,276-280] An electrospray is obtained by applying a strong electrostatic field to a liquid flowing with a low velocity through a metal capillary, where the liquid typically flows through the capillary at a rate of an order of 1-10 $\mu L\ min^{-1}$. The electrostatic field exists between the metal capillary and the aperture to the mass spectrometer. When used in the positive-ion mode, the metal capillary acts as an anode. Anions in solution drift towards the capillary walls, while cations are repelled; the aperture to the mass spectrometer may be considered to act in an analogous manner to a cathode. This charge redistribution within the solution acts to counter the field arising within the solution. The positive ions destabilize the liquid surface, as they collect at this point, but

are unable to escape. The surface of the liquid becomes drawn downfield, away from the capillary, forming a conical shape; such a feature is known as a "Taylor cone." At high fields, the tip of the Taylor cone is drawn out further into a liquid filament and, further downfield, droplets are emitted, consisting of many positive ions in solution; as the electrostatic field strength is increased, the length of the liquid filament is decreased due to the increasing instability which is induced at the Taylor cone tip. Once the droplets have formed, they are accelerated towards the accelerating potential of the mass spectrometer; this principle is illustrated by Figure 19. When using the instrument in the negative-ion mode, the behaviors are analogous, where the polarity of the ions and electrodes discussed are simply reversed. During flight, the droplets continuously evaporate solvent molecules, resulting in the formation of smaller and smaller droplets.

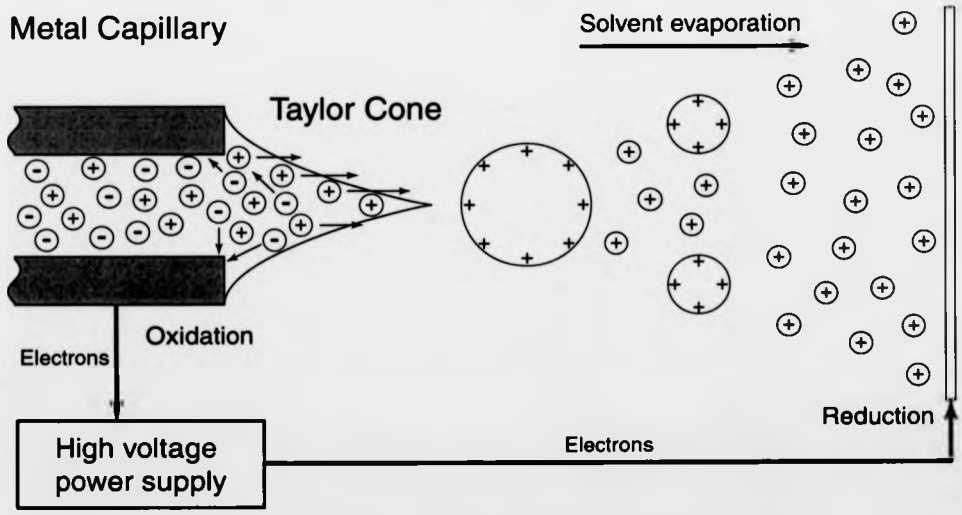

Figure 19: Schematic representation of the electrospray ionization process. Redox reactions occur at the metal capillary surface and ions of one polarity (cations in the case of the above Figure) are attracted towards the counter electrode positioned at the entrance to the flight tube, while ions of the opposite polarity (anions in this case) are repelled. The attraction of ions towards the counter electrode results in the formation of the Taylor Cone, from which droplets containing solvent molecules and analyte ions are ejected. Solvent evaporation occurs as the droplets are accelerated towards the counter electrode.

The mechanism of electrospray ionization is not fully understood. The first component of the electrospray process is the formation of ions. The electrospray arrangement has been compared to part of an electrolytic cell,[281-285] where the capillary and aperture of the mass spectrometer constitute the electrodes of opposing polarity. It has been shown that ion production may be dependent on the concentration of analytes,[283,286] concentration of added electrolytes,[283] resistance of the solution,[285] the distance between the electrical contact and the end of the needle,[285] needle diameter,[285] the flow rate of the solution,[282-284] and the time taken for the analyte to diffuse to the needle wall.[284] Electrochemical processes occur which result in the formation ions in solution; positive ions and negative ions, once formed, behave in the manner discussed earlier; Charbonnier et al. have investigated the nature of redox reactions within the needle and at the counter electrode (entrance to mass analyzer region).[287,288] As ions of one polarity are emitted from the capillary, in order to maintain an equilibrium, an ion of the opposite polarity must undergo a redox reaction at the capillary wall. It has been observed that this charge balancing process results in the electrochemical oxidation/reduction of the electrospray components. Reduction/oxidation of ions at the aperture of the mass spectrometer effectively completes the electrical circuit, and leads to the detection of the current measured to gauge the flow of ions entering the instrument. The other component of the electrospray process is the manner in which the droplets evaporate during flight. It is known that for the extraction of ions from the liquid, the repulsion arising from to the charges in close proximity must overcome the surface tension of the liquid holding the droplet together.[221,280-282,289] It was noticed, however, that evaporation still occurred at a lower threshold than would be predicted using Rayleigh's equation. Gomez and Tang[290] showed that breakdown of droplets may occur before the limit set by the Rayleigh equation is reached (approximately 80% of the normal limit), due to deformation of the droplet. This deformation, leading to a "tail" or

filament similar to the one observed in a Taylor cone, reduces the electrostatic repulsion required for the evaporation of ions. Gomez and Tang also observed that evaporation does not proceed via even fission of the parent droplet, but occurs via the production of uneven sized daughter droplets. With regard to the mechanism of evaporation between the capillary and the entrance to the mass spectrometer, two varieties of mechanism have so far been proposed. The first mechanism[291] involves the formation of very small droplets which incorporate a single ion. Solvent evaporation from this droplet leads to the production of a single, gas-phase ion. The second mechanism was proposed by Iribarne and Thompson[292,293] and involves the emission of ions from small, highly charged droplets. The droplets do not undergo fission, but emit gas-phase ions, and it is not therefore necessary to produce droplets which are so small as to contain only one ion. Neither mechanism has received total acceptance, and the precise nature of the evaporation and desorption of ions is still under investigation.

The development of electrospray ionization has provided an analytical tool which is suitable for even the most labile of samples. Little internal energy is imparted to the analyte, due to the lack of any heating, photoirradiation, or collision event, and hence little fragmentation is induced. The result is that ESI is the premier "soft" ionization technique, and is particularly suitable for the investigation of polymers, proteins, and carbohydrates. It may be noted that should a species not readily ionize under ESI conditions, it is possible to aid the process by the formation of sodium, potassium, ammonia, or other adducts. Mass spectra recorded using ESI most frequently exhibit protonated species when using the instrument in the positive-ion mode, and, in a similar manner, deprotonated species in the negative-ion mode; these observations are in line with the theory that ions are formed as a result of electrochemical processes in solution, as proton transfer is amongst the most

common of electrochemical reactions. Van Berkel et al. were the first to observe radical cation signals[294] when using electrospray ionization for the study of porphyrin-based species. The other major advantage of ESI is the ability to produce multiply charged ions. Mass spectrometers are hindered by upper mass limits, with the limit being governed mainly by the choice of mass analyzer. For an ion of a given mass, increasing the number of charges present on the ion lowers the m/z ratio. As sector and FT-ICR instruments measure the m/z ratio, this effect of lowering the mass to charge ratio means that high mass ions may be investigated; it would otherwise not be possible to analyze singly charged ions of high mass. One disadvantage, however, is the relatively large sample quantities consumed during acquisition. Continuous spraying of a sample solution over a period of minutes may rapidly consume a valuable sample material. Relatively new variations of the electrospray ionization method have been developed, namely "micro-electrospray" and "nano-electrospray." By reducing the sample quantity required for analysis and providing an analytical technique where the sample undergoes almost no fragmentation, the variations of electrospray ionization have become an increasingly formidable ionization technique.

1.2.4 Tandem Mass Spectrometry Techniques

1.2.4A Metastable Ions

It is well known that ions and neutrals in the ionization source will undergo dissociations, leading to the formation of fragment ions; the information obtained by studying such fragment ions may be used for structure elucidation purposes. Ions which dissociate between the ion source and the detector are known as "metastable ions." Such species are often associated with processes which require low activation energies, and when the dissociation occurs in a field free region, that is outside of an electrostatic or

magnetic field, the dissociations of a metastable ion will be detected.[221,222,247,295] Metastable ions typically have a lifetime of an order of 10^{-6} to 10^{-5} seconds and typically have an internal energy of 0.1 - 1 eV above the threshold. Under the correct conditions, such metastable ions may be detected.

Equation (3) states:

$$qV = \tfrac{1}{2} mv^2$$

and thus this leads to equation (12) which states:

$$v = \sqrt{\frac{2qV}{m}}$$

The correct magnetic field strength must be employed in order for an ion of a specific m/q ratio to traverse the magnetic sector, as shown by equation (5):

$$qvB = \frac{mv^2}{r}$$

Hence:

$$B = \frac{mv}{qr} \qquad (33)$$

Combining equations (12) and (33), the following expression is derived:

$$B = \frac{m}{qr}\sqrt{\frac{2qV}{m}} \qquad (34)$$

Dissociation of metastable parent ions occur in a field free region (FFR) of the flight tube, where the field free regions are located between the ion source and the first sector,

and between sectors. Consider a sector instrument of EB geometry. If an ion leaves the ion source and dissociates in the first field free region (FFR1), which is located between the ion source and the electrostatic sector, the daughter ion will not reach the magnetic sector. The daughter ion will possess the same velocity as the parent ion, but will possess a lower kinetic energy due to the lower mass and will thus be filtered out by the electrostatic analyzer, which acts as a kinetic energy-to-charge ratio analyzer. It can therefore be seen that metastable ions will only be detected if they are formed in the second field free region (FFR2) which is located between the electrostatic and magnetic sectors. Now consider an instrument of BE geometry. An fragment ion, formed via the dissociation of a parent ion in between the ion source and the magnetic sector (FFR1 for a reversed geometry instrument), will have a lower momentum than an ion of the same mass (m_f) which was formed in the ion source rather than in the flight tube. Hence, it is possible for the metastable ions to traverse a magnetic sector as long as the dissociation occurs within the correct region of the flight tube for the particular mass spectrometer; FFR1 (between the ion source and first sector) for a reversed geometry instrument and in FFR2 (between the two sectors) for a Nier-Johnson geometry instrument. In either case, this fragment ion will traverse the magnetic sector having an "apparent mass," due to the decreased the momentum-to-charge ratio. Equation (34) may be used as the basis for the understanding of this principle.

For a parent ion of mass m_p (in kilograms, kg):

$$B_p = \frac{m_p}{qr}\sqrt{\frac{2qV}{m_p}} \qquad (35)$$

For a fragment ion of mass m_f (in kilograms, kg), formed through the dissociation of the parent ion:

$$B_f = \frac{m_f}{qr}\sqrt{\frac{2qV}{m_p}} \tag{36}$$

as the velocity, defined by equation (12), of the fragment ion is identical to that of the parent ion.

The fragment ion resulting from dissociation in the flight tube will appear to possess an apparent mass, m* (in kilograms, kg):

$$B_{apparent} = \frac{m^*}{qr}\sqrt{\frac{2qV}{m^*}} = \sqrt{\frac{m^*}{q}}\frac{1}{r}\sqrt{2V} \tag{37}$$

As

$$B_f = B_{apparent}$$

then equating equations (36) and (37) leads to:

$$\frac{m_f}{qr}\sqrt{\frac{2qV}{m_p}} = \sqrt{\frac{m^*}{q}}\frac{1}{r}\sqrt{2V}$$

$$\frac{m_f}{qr}\sqrt{\frac{q}{m_p}}\sqrt{2V} = \sqrt{\frac{m^*}{q}}\frac{1}{r}\sqrt{2V}$$

$$m_f \frac{1}{q}\sqrt{q}\sqrt{\frac{1}{m_p}} = \sqrt{m^*}\sqrt{\frac{1}{q}}$$

$$m_f\sqrt{\frac{1}{m_p}} = \sqrt{m^*}$$

The relationship between the "apparent mass" of a metastable ion, m*, its actual mass, m_f, and the mass of the associated parent ion, m_p, may finally be described as:

$$m^* = \frac{m_f^{\,2}}{m_p} \qquad (38)$$

This illustration has consider the case of fragment ions which possess the same velocity as the parent ion. However, kinetic energy releases frequently occur during the fragmentation process, leading to daughter ions which possess differing kinetic energies. Such kinetic energy releases may be studied using mass-analyzed ion kinetic energy spectra (MIKES) and involve the scanning of the electrostatic sector to monitor the kinetic energy of the ions.

1.2.4B Mass-Analyzed Ion Kinetic Energy Spectra (MIKES)

Mass-analyzed ion kinetic energy spectra sample the unimolecular dissociations of metastable ions. The formation of daughter ions can be promoted via collision-induced dissociation.[221,222,247,295] MIKE spectra may be obtained using sector instruments of reverse geometry (BE) or a sector based tandem mass spectrometer, typically consisting of three or more sectors. Consider an ion of mass m_p which fragments after the magnetic sector

and prior to the electrostatic sector. The region in which it fragments, in between sectors, is known as a field free region. The daughter ion, of mass m_d, has a velocity equal to that of the parent ion, v_p. From the discussion earlier, it has been shown that the kinetic energy of an ion, K, is equal to the work done on the ion by the accelerating potential within the ion source:

$$qV = \tfrac{1}{2} mv^2 \qquad (3)$$

For the parent ion:

$$K_p = \frac{m_p v_p^{\,2}}{2}$$

For the daughter ion:

$$K_d = \frac{m_d v_p^{\,2}}{2}$$

Thus the ratio of the kinetic energies may be expressed as:

$$\frac{K_p}{K_d} = \frac{\left(\frac{m_p v_p^{\,2}}{2}\right)}{\left(\frac{m_d v_p^{\,2}}{2}\right)} = \frac{m_p}{m_d}$$

and the kinetic energies of the parent and daughter ions are therefore directly proportional to the masses of the ions. However, as daughter ions possess a lower kinetic energy than would be imparted to it through the acceleration process, the daughter ion will not be

observed, as it will not traverse the electrostatic sector. It is possible though to vary the electrostatic field strength deliberately so that such daughter ions may be observed. The electrostatic field strength equates to the centripetal force required for an ion to traverse the sector:

$$qE = \frac{mv^2}{r} \qquad (10)$$

For the parent ion:

$$qE_p = \frac{m_p v_p^2}{r}$$

For the daughter ion:

$$qE_d = \frac{m_d v_p^2}{r}$$

Thus, the electrostatic field strengths required for the observation of the parent ion and the daughter ion are directly proportional:

$$\frac{E_p}{E_d} = \frac{\left(\frac{m_p v_p^2}{rq}\right)}{\left(\frac{m_d v_p^2}{rq}\right)} = \frac{m_p}{m_d} \qquad (39)$$

When the ratio of E_p/E_d and the mass of the parent ion, m_p, are known, it is possible to determine the mass of the fragment, m_d, which is observed. It is possible to select ions

of interest, using the magnetic sector, and then scan the electrostatic sector. By doing so, an energy spectrum effectively results. Broad peaks are observed for the fragment ions, where kinetic energy releases are observed; the upper and lower kinetic energies of the daughter ions will be equal to the predicted kinetic energy of the daughter ion plus or minus, respectively, a kinetic energy release arising during fragmentation. The kinetic energy is affected by the orientation of the parent ion during fragmentation, so that if a daughter ion is ejected along the reverse of the axis of flight, its kinetic energy will be reduced, while a daughter ion ejected forwards along the axis of flight will possess an increased kinetic energy. These energy releases during fragmentation account for the frequently broad signals encountered during acquisition of MIKE spectra.

1.2.4C B/E Linked Scan

For the investigation of metastable ions and daughter ions arising from collision-induced dissociation, a further technique is of use. This technique is known as a B/E linked scan and is used in order to scan for all daughter ions produced following metastable decay or collision-induced fragmentation of a parent ion.[219,221,222,247,295] B/E scans are used therefore in the determination of daughter ions following dissociation of a selected ion. Consider a parent ion, analyzed by an instrument of BE geometry, which fragments between the ion source and magnetic sector. The force due to the magnetic field acting on the moving, charged particle equates to the centripetal force required for it to traverse the magnetic sector:

$$qvB = \frac{mv^2}{r} \qquad (5)$$

or, by substituting and rearranging:

For the parent ion:

$$qB_p = \frac{m_p v_p}{r}$$

For the daughter ion:

$$qB_d = \frac{m_d v_p}{r} \qquad (40)$$

Comparing the two equations:

$$\frac{B_p}{B_d} = \frac{\left(\frac{m_p v_p}{rq}\right)}{\left(\frac{m_d v_p}{rq}\right)} = \frac{m_p}{m_d} \qquad (41)$$

It can be seen that the ratio of the magnetic field strengths required to pass the parent ion and the daughter ion is proportional to the masses of the parent ion and the daughter ion. This relationship is similar to the use of electrostatic sectors for MIKE scans. By comparing equation (41) with equation (39):

$$\frac{E_p}{E_d} = \frac{m_p}{m_d} = \frac{B_p}{B_d}$$

or:

$$\frac{B_p}{E_p} = \frac{B_d}{E_d} = \text{Constant} \qquad (42)$$

Equation (42), therefore, is the principle behind the B/E linked scan, and exhibits a relationship with a chosen parent ion. The magnetic and electrostatic sectors are scanned simultaneously, keeping the ratios between the magnetic and electrostatic field strengths constant; for a normal mass spectrum the electrostatic sector is kept constant while the magnetic sector is scanned. Once a parent ion has been chosen by the user and selected using the instrument, by keeping B/E equal to a constant during simultaneous scanning, it is possible to detect all daughter ions during the acquisition. It is also noticeable from equation (42) that it is possible to obtain a B/E scan using either a Nier-Johnson or a reversed geometry mass spectrometer. Due to the fact that double focusing is maintained, the operating resolution for a B/E scan is much greater than for a MIKE spectrum. However, the two techniques serve different purposes, and a B/E linked scan cannot yield information about kinetic energy releases arising during fragmentation, as only a small velocity spread of the daughter ions generated is allowed to pass both sectors. Historically, the B/E linked scan was developed for use with Nier-Johnson geometry instruments, providing the only opportunity to perform tandem mass spectrometry experiments using such instrumentation. The B/E scan later found important roles during the course of peptide sequencing using four sector instruments, where both the parent ion selection and the daughter ion analysis were performed under high resolution conditions. More recently, the high resolution of the daughter ions of the B/E scan provided valuable information regarding the formation of endohedral fullerene complexes in high energy collision experiments.[72,75,91]

1.2.4D B^2/E Linked Scan

Similar to the B/E linked scan is the B^2/E linked scan. The difference is that while B/E scans are used to examine daughter ions produced following dissociation, B^2/E scans

are used in a manner which may be seen as the reverse, determining parent ions.[219,221,222] A fragment ion which is generated in the ion source will have the same kinetic energy as intact parent ions leaving the source. A daughter ion which is generated in the first field free region, after leaving the source but before reaching the first sector, possesses a velocity equal to that of its parent ion. The daughter ion therefore has a different kinetic energy from the parent ion, due to the difference in mass. It is possible to distinguish between fragmentation occurring in the ion source and metastable decay. Using the equations derived earlier which demonstrate the relationship between centripetal force and the forces acting on the ion in the electrostatic and magnetic sectors:

$$qE = \frac{mv^2}{r} \tag{10}$$

For a fragment ion generated in the ion source:

$$qE_{d\ source} = \frac{m_d v_d^{\ 2}}{r} \tag{43}$$

For a daughter ion produced in the first field free region:

$$qE_{d\ FFR} = \frac{m_d (v_d')^2}{r} \tag{44}$$

Combining equations (43) and (44):

$$\frac{E_{d\ source}}{E_{d\ FFR}} = \frac{m_d v_d^{\ 2}}{m_d (v_d')^2}$$

where v_d' is the velocity (in m s^{-1}) of a daughter ion produced in the FFR.

As the kinetic energies of an intact parent ion and a fragment ion produced in the ion source are equal:

$$m_d v_d^2 = m_p v_p^2 \tag{45}$$

As the velocity of a daughter ion formed in the FFR is equal to that of the parent ion from which it was produced:

$$m_d (v_d')^2 = m_d v_p^2 \tag{46}$$

$$\frac{E_{d\ source}}{E_{d\ FFR}} = \frac{m_p v_p^2}{m_d v_p^2} = \frac{m_p}{m_d} \tag{47}$$

For the magnetic sector:

$$qB = \frac{mv}{r'} \qquad \text{derived from (40)}$$

where r' is the radius of the circular motion through the magnetic sector (in meters, m).

For a fragment ion produced in the ion source:

$$qB_{d\ source} = \frac{m_d v_d}{r'} \tag{48}$$

For a daughter ion produced in the FFR:

$$qB_{d\ FFR} = \frac{m_d v_d'}{r'} \tag{49}$$

Combining equations (48) and (49):

$$\frac{B_{d\ source}}{B_{d\ FFR}} = \frac{m_d v_d}{m_d v_d'}$$

and using equation (46) and substituting:

$$\frac{B_{d\ source}}{B_{d\ FFR}} = \frac{m_d v_d}{m_d v_p} = \frac{v_d}{v_p}$$

Using equation (45):

$$\frac{v_d^{\,2}}{v_p^{\,2}} = \frac{m_p}{m_d}$$

$$\frac{v_d}{v_p} = \sqrt{\frac{m_p}{m_d}}$$

$$\frac{B_{d\ source}}{B_{d\ FFR}} = \sqrt{\frac{m_p}{m_d}} \qquad (50)$$

Finally, comparing equations (47) and (50), a relationship is obtained as follows:

$$\frac{B_{d\ source}^{\,2}}{E_{d\ source}} = \frac{B_{d\ FFR}^{\,2}}{E_{d\ FFR}} = \text{Constant} \qquad (51)$$

Equation (51) exhibits a relationship which depends on the choice of fragment ion. Once the user has chosen a fragment ion of interest and the instrument is used to select this fragment ion, by scanning the magnetic and electrostatic sectors simultaneously, maintaining a constant ratio of B^2/E, it is possible to determine the corresponding precursor ions for a given fragment ion. Due to the fact that the constant is dependent upon B^2, the magnetic field strength must be accurately controlled in order to observe the desired signals as small deviations from the desired magnetic field strength can lead to accentuated experimental error, and this can become a disadvantage of the technique.

1.2.4E Collision-Induced Dissociation (CID)

Some mass spectrometers incorporate a collision cell into their design, where a chamber may be partly filled with a choice of inert target gas with the intent of colliding ions leaving the ion source. Inducing collisions can lead to the increased fragmentation of sample ions with the intent of gaining structural or energetic insight, charge stripping reactions, or gas-phase reactions of another nature within the collision cell. The experimental technique has become known as "collision-induced dissociation" (CID) or "collisionally-activated dissociation" (CAD) and has become one of the most common techniques used in conjunction with mass spectrometry.[221,222,247,295-300] Collision cells frequently possess the ability to be "floated" at desired potential, and by doing so at a voltage chosen by the user, it is possible to control the kinetic energy of the ions entering the cell, as ions must continue their flight against this potential gradient between the collision cell and the ion source. As will be demonstrated by the following discussion, controlling the kinetic energy of ions entering the collision cell enables the user to exert control over the kinetic energy which may be converted to internal energy. In this manner, the user may increase or decrease the degree of fragmentation. It may be noted that experimentally, the quantity of collision gas allowed into the collision cell and the degree of fragmentation spectra are referred to in terms of ion beam attenuation (e.g. 30% beam intensity) in order to make such experiments easily reproducible. Consider the case of an ion of mass m_1 which collides with a gas atom of mass m_2, as shown in Figure 20. It is possible to determine the kinetic energy available for conversion to internal energy by assuming an observation point off of the collision axis. The distance D_1, from the observation point to the center of the gravity m_1, may be defined as the sum the distances D_c and d_1, which lie along axes

which are orthogonal to one another (note that quantities labeled with the notation "D_x" are vectors). Similarly, D_2 is equal to the sum of D_c and d_2.

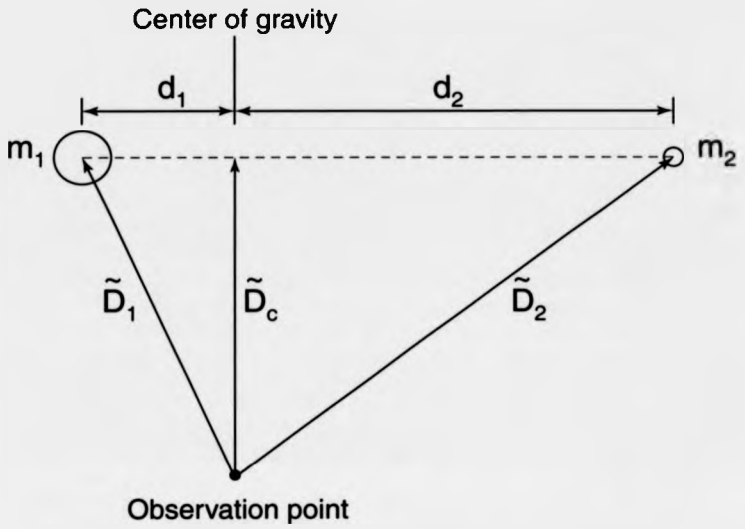

Figure 20: Representation of the center of mass framework, relative to a fixed observation point. An ion of mass m_1 is considered to approach, and collide with, a stationary target (such as a gas atom) of mass m_2, the position vectors of which are labeled accordingly.

$$\tilde{D}_1 = \tilde{D}_c + d_1 \tag{52}$$

$$\tilde{D}_2 = \tilde{D}_c + d_2 \tag{53}$$

The center of mass may be determined as follows:

$$m_1 d_1 = -m_2 d_2$$

From the observation point frame of reference, the total mass, m_1+m_2, acts through the center of gravity, and as:

$$m_1\tilde{D}_c = m_1\tilde{D}_1 - m_1d_1$$

and

$$m_2\tilde{D}_c = m_2\tilde{D}_2 - m_2d_2$$

then this equates as follows:

$$(m_1 + m_2)\tilde{D}_c = m_1\tilde{D}_1 - m_1d_1 + m_2\tilde{D}_2 - m_2d_2$$

or:

$$(m_1 + m_2)\tilde{D}_c = m_1\tilde{D}_1 + m_2\tilde{D}_2 \qquad (54)$$

By substituting using equations (52) and (54):

$$(m_1 + m_2)\left(\tilde{D}_1 - d_1\right) = m_1\tilde{D}_1 + m_2\tilde{D}_2$$

$$d_1 = \tilde{D}_1 - \frac{m_1\tilde{D}_1 + m_2\tilde{D}_2}{(m_1 + m_2)}$$

$$d_1 = \frac{\tilde{D}_1(m_1 + m_2)}{(m_1 + m_2)} - \frac{m_1\tilde{D}_1 + m_2\tilde{D}_2}{(m_1 + m_2)}$$

$$d_1 = \frac{m_2\left(\tilde{D}_1 - \tilde{D}_2\right)}{\left(m_1 + m_2\right)}$$

Similarly, substituting using equations (53) and (54):

$$\left(m_1 + m_2\right)\left(\tilde{D}_2 - d_2\right) = m_1\tilde{D}_1 + m_2\tilde{D}_2$$

$$d_2 = \tilde{D}_2 - \frac{m_1\tilde{D}_1 + m_2\tilde{D}_2}{\left(m_1 + m_2\right)}$$

$$d_2 = \frac{\tilde{D}_2\left(m_1 + m_2\right)}{\left(m_1 + m_2\right)} - \frac{m_1\tilde{D}_1 + m_2\tilde{D}_2}{\left(m_1 + m_2\right)}$$

$$d_2 = -\frac{m_1\left(\tilde{D}_1 - \tilde{D}_2\right)}{\left(m_1 + m_2\right)}$$

Differentiating displacement with respect to time leads to:

$$u_1 = \frac{m_2\left(v_1 - v_2\right)}{\left(m_1 + m_2\right)} \tag{55}$$

and

$$u_2 = -\frac{m_1\left(v_1 - v_2\right)}{\left(m_1 + m_2\right)} \tag{56}$$

where u is the velocity component (in m s^{-1}) along the center of mass axis and v is the velocity component (in m s^{-1}) along the axis joining the center of mass of a particle to the observation point. To simplify, the term (v_1-v_2) will be referred to as g, where:

$$g = \frac{u_1(m_1 + m_2)}{m_2} \tag{57}$$

and

$$g = -\frac{u_2(m_1 + m_2)}{m_1} \tag{58}$$

Combining equations (57) and (58):

$$m_1u_1 = -m_2u_2$$

or:

$$m_1u_1 + m_2u_2 = 0$$

Thus, the total momentum of the system is equal to zero with respect to the center of mass frame. The maximum kinetic energy available for conversion to internal energy is equal to the total kinetic energy along the center of mass frame, K_{COM} (in Joules, J).

$$K_{COM} = \frac{(m_1u_1^2 + m_2u_2^2)}{2}$$

Substituting using equations (55) and (56):

$$K_{COM} = \frac{m_1}{2}\left(\frac{m_2g}{(m_1 + m_2)}\right)^2 + \frac{m_2}{2}\left(\frac{-m_1g}{(m_1 + m_2)}\right)^2$$

$$K_{COM} = \frac{m_1}{2}\left(\frac{m_2^2 g^2}{(m_1 + m_2)^2}\right) + \frac{m_2}{2}\left(\frac{m_1^2 g^2}{(m_1 + m_2)^2}\right)$$

$$K_{COM} = \frac{m_1 m_2 g^2}{(m_1 + m_2)2}$$

$$K_{COM} = \frac{m_1 m_2 (v_1 - v_2)^2}{(m_1 + m_2)2} \qquad (59)$$

It is possible to simplify this expression by referring to a term μ, the "reduced mass" (in kilograms, kg), and obtaining the following equation:

$$K_{COM} = \frac{\mu g^2}{2}$$

where

$$\mu = \frac{m_1 m_2}{(m_1 + m_2)}$$

Equation (59) may be rearranged as:

$$K_{COM} = \frac{m_1 m_2 v_1^2 - 2m_1 m_2 v_1 v_2 + m_1 m_2 v_2^2}{(m_1 + m_2)2}$$

As the velocity of the target atom, v_2, is assumed to be zero,

$$K_{COM} = \frac{m_1 m_2 v_1^2}{(m_1 + m_2)2} \qquad (60)$$

The initial kinetic energy of the ion is equal to that imparted to it during the acceleration process in the ion source and may be expressed as:

$$K_{m_1} = \frac{m_1 v_1^2}{2}$$

The final expression for the maximum amount of kinetic energy available for conversion to internal energy, during the collision of an ion with a stationary target atom in a collision cell, is therefore:

$$K_{COM} = K_{m_1} \frac{m_2}{(m_1 + m_2)} \qquad (61)$$

Collisions where the total kinetic energy is conserved are termed "elastic collisions," of which collisions between billiard balls is a prime example. "Inelastic collisions" are those where the total kinetic energy is not constant, though momentum must be conserved; a rubber ball hitting a hard surface and deforming upon impact is an example of an inelastic collision, as energy is lost upon deformation. It is therefore possible to describe the conversion of kinetic energy to internal energy during the collision process by introducing a term which expresses the amount of internal energy which is converted. During an elastic collision between molecules, from equation (60):

$$K_{COM} = K_{COM}' \Rightarrow \frac{m_1 m_2 v_1^2}{(m_1 + m_2)2} = \frac{m_1 m_2 v_1'^2}{(m_1 + m_2)2}$$

During an inelastic collision, part of the collision energy is converted to internal energy, defined as Q (in Joules, J):

$$K_{COM} = K_{COM}' + Q \Rightarrow \frac{m_1 m_2 v_1^2}{(m_1 + m_2)2} = \frac{m_1 m_2 v_1'^2}{(m_1 + m_2)2} + Q \qquad (62)$$

While equation (61) is used to derive the maximum amount of energy available for conversion to internal energy, equation (62) is used to express the conservation of energy, in terms of the total initial kinetic energy, and the final kinetic energy and energy which is converted to internal energy during the collision, which becomes available for fragmentation and/or reaction. The use of the term Q has been implemented in explanations of the collisional activation of large, organic ions[301,302] for instance, and Vékey has studied internal energy effects in mass spectrometry.[303] The internal energy of a system is crucial as it dictates which fragmentation pathways are accessible, as outlined by Rice-Ramsperger-Kassel-Marcus (RRKM) theory, also known as quasiequilibrium theory (QET).[303,304]

The choice of collision gas also has a direct influence upon the collision energy. Thus, for a C_{60}^{+} ion with a kinetic energy of 8 keV, use of helium (RAM: 4 Da) results in a center of mass collision energy of approximately 44 eV, while use of argon (RAM: 40 Da) yields a collision energy of approximately 421 eV. CID has many uses and allows for structure elucidation, energy release investigations, fragment ion analysis, parent ion analysis, and allows charge stripping reactions and covalent/non-covalent interactions to be conducted in the gas-phase. Disadvantages include the facts that sensitivity is lost as ions are scattered by collision events and that instrument design is frequently made more complex.

1.2.4F Post Source Decay (PSD)

While ions which fragment during flight after exiting the ion source have been traditionally referred to as "metastable ions" when using sector instruments, such species are usually referred to as "post source decay" (PSD) fragments when using time-of-flight

instruments. As discussed earlier, a reflectron must be incorporated into the design of the instrument in order to resolve parent ions from daughter ions, due to the fact that fragment ions possess the same velocity as the parent ions and would thus have the same flight time in a linear instrument. Though CID is also an available technique for use with ToF instruments,[298] post source decay has become an increasingly popular technique used during the structural determination of ions using ToF mass spectrometry.[221,222,234,242,243,246,272] It is debatable whether or not PSD is distinct from metastable ion monitoring. Recommendations are sometimes made to increase the pressure inside the flight tube of an instrument in order to increase the probability of post source decay. This also complicates the distinction between PSD and CID as it is likely that increasing the pressure within the flight tube simply increases the probability of high energy collisions within the flight tube. Due to the relatively simple instrumental design, time-of-flight mass spectrometry has become increasingly popular, and as a result of the fact that PSD is a relatively inexpensive technique, such studies have become increasingly common.

1.3 Experimental Results

The elucidation of the behavior and physical chemistry of fullerenes are key areas of current concern and, as has been shown, mass spectrometry provides invaluable tools during the course of such research. The following chapters detail the use of mass spectrometric methods to investigate important topics such as coalescence, delayed ionization, and the derivatization of fullerenes. Five chapters concern the study of derivatized fullerenes and their behavior in the gas-phase, while a sixth investigates the viability of ESI as an ionization method for the study of fullerene derivatives. The coalescence reactivities of fullerene derivatives are of particular interest. The fragmentation

dynamics of hydrogenated fullerenes are studied using a variety of instruments, demonstrating that fragmentation occurs via the loss of C_mH_n species. Laser desorption/ionization time-of-flight mass spectrometry is used to examine the coalescence reactivity, resulting in the conclusion that hydrogenated fullerenes display a lower degree of reactivity in this respect. The fragmentation dynamics of fluorinated fullerenes are also initially examined using LDI ToF MS, leading to the discovery of their remarkable coalescence reactivity, exhibiting a behavior not dissimilar to the laser ablation of graphite. This leads to a study of fluorinated fullerene coalescence reactions with respect to the laser irradiance used and the fluorine content of the derivatives. Fullerene oxides are initially investigated using MALDI in order to determine the oxygen content, and are later coalesced under LDI and MALDI conditions, resulting in different species being produced depending on the ionization method used. Higher fullerenes, devoid of the presence of oxygen, are generated under LDI conditions, while dimeric species bridged by oxygen atoms are produced through the employment of MALDI conditions. An attempt to characterize three metallofullerene samples leads to the instant discovery that the metallofullerenes show a significantly enhanced coalescence reactivity. Not only do the three samples coalesce at much lower laser irradiances than pure fullerenes, but the energy required is so low that it is nearly impossible to characterize the samples without contributions from species generated in the gas-phase. Three ligand bearing fullerene samples, incorporating one, two, or three bis(ethoxycarbonyl)methylene ligands, are analyzed using a hybrid mass spectrometer of EBE ToF geometry and an LDI source. The coalescence behavior of these species is investigated, resulting in the formation of pure carbon clusters, and such higher entities are then fragmented through collision-induced dissociation in order to determine their structures; the reason for such interest in the structures of the higher fullerenes formed in the gas-phase is that it is known that the

precursors undergo fragmentation prior to reaction, but in many cases one or more carbon atoms from the ligands remain attached to the fullerene core. Finally, due to the difficulties encountered during structure elucidation of the derivatives and due to the fact that electrospray ionization of fullerenes has remained an elusive goal, the suitability of ESI for use in conjunction with fullerene samples is assessed. In contradiction to the literature, it is shown that ESI is indeed a viable ionization method, resulting in the formation of radical species without the need for protonation/deprotonation. Such a discovery has implications for the current understanding of the ionization mechanisms involved.

The synthesis of fullerene derivatives is one of the most intensive areas of investigation within the field of fullerene research. Potential applications mean that this has become an area of rapid growth in interest, especially within the realms of nanotechnology and superconductivity. Following on from research into fullerene oxides, the stability of pure fullerenes in air, with particular respect to oxidation, is studied. Though it is known that fullerenes may oxidize in the presence of light and air at room temperature, the remarkable discovery is made that such oxides dimerize under ambient conditions. There are obvious implications for applications of fullerene research, as the potential for oxidation and dimerization even at room temperature must not become a concern. In keeping with the themes of fullerene formation and coalescence in the gas-phase following laser ablation, a eighth chapter deals with the attempt to form fullerenes using an organometallic precursor. The Krätschmer-Huffman method of fullerene production has become well established as the most effective method for fullerene production, but due to the increasing interest in fullerene research, new methods of production are constantly being considered. The results of the investigation show that it is indeed possible to generate fullerenes in the gas-phase using laser ablation of an organometallic precursor, but the

efficiency of such a synthetic route is too low to become a preferred method of the future. The ninth and final chapter involves the examination of the abilities of pure fullerenes to undergo delayed ionization when employing LDI conditions. Whilst initially a study of the structure of coalesced fullerenes using PSD in conjunction with ToF mass spectrometry, it soon becomes apparent that significant artifact signals, which could lead to misinterpretation of the results obtained, are due to delayed ionization. The findings have implications for studies of fullerenes which involve the use of ToF instruments that employ a time based ion gate for the mass selection of ions, as well as clearly demonstrating that delayed ionization is a significant phenomenon associated with fullerenes. Together, the nine chapters cover topics such as: the delayed ionization of pure fullerenes, the degradation of pure fullerenes under mild conditions, the study of fullerene derivatives in the gas-phase and the viability of an ionization method for this purpose, and the formation of larger, carbon-based entities in the gas-phase from fullerene, fullerene derivative, and non-fullerene precursors.

1.4 References

1) Kroto, H. W.; Heath, J. R.; O' Brien, S. C. O.; Curl, R. F.; Smalley, R. E. *Nature* **1985**, *318*, 162-163.

2) Rohlfing, E. A.; Cox, D. M.; Kaldor, A. *J. Chem. Phys.* **1984**, *81*, 3322-3330.

3) Laskin, J.; Lifshitz, C. *Int. J. Mass Spectrom. Ion Processes* **1994**, *138*, 95-106.

4) Klein, D. J.; Seitz, W. A.; Schmalz, T. G. *Nature* **1986**, *323*, 703-706.

5) Schmalz, T. G.; Seitz, S. A.; Klein, D. J.; Hite, G. E. *Chem. Phys. Lett.* **1986**, *130*, 203-207.

6) Schmalz, T. G.; Seitz, W. A.; Klein, D. J.; Hite, G. E. *J. Am. Chem. Soc.* **1988**, *110*, 1113-1127.

7) Wakabayashi, T.; Kikuchi, K.; Shiromaru, H.; Suzuki, S.; Achiba, Y. *Supplement to Z. Phys. D.* **1993**, *26*, S 258-260.

8) Wang, X. Q.; Wang, C. Z.; Zhang, B. L.; Ho, K. M. *Supplement to Z. Phys. D.* **1993**, *26*, S 264-266.

9) Callahan, J., H.; Ross, M. M.; Weiske, T.; Schwarz, H. *J. Phys. Chem.* **1993**, *97*, 20-22.

10) Surjan, P. R. *Theochem - Journal of Molecular Structure* **1995**, *338*, 215-223.

11) Aihara, J. *J. Phys. Chem.* **1995**, *99*, 12739-12742.

12) Austin, S. J.; Fowler, P. W.; Manolopoulos, D. E.; Orlandi, G.; Zerbetto, F. *J. Phys. Chem.* **1995**, *99*, 8076-8081.

13) Aihara, J.-i. *J. Am. Chem. Soc.* **1995**, *117*, 4130-4136.

14) Krätschmer, W.; Lamb, L. D.; Fostiropoulos, K.; Huffman, D. R. *Nature* **1990**, *347*, 354-357.

15) Liu, S.; Vu, R.; Yee, A.; Bussell, A.; Chang, R. P. H.; Michel, R.; Richard, S.; Bräuchle, G.; Weis, P.; Beck, R.; Kappes, M. M. *Supplement to Z. Phys. D.* **1993**, *26*, S 267-269.

16) Braun, T. *Magyor Kemiai Folyoivat* **1993**, *99*, 212-215.

17) Ebbesen, T. W.; Tabuchi, J.; Tanigaki, K. *Chem. Phys. Lett.* **1992**, *191*, 336-338.

18) McElvany, S. W.; Ross, M. M.; Goroff, N. S.; Diederich, F. *Science* **1993**, *259*, 1594-1596.

19) Campbell, E. E. B.; Tellgmann, R.; Wahl, F.; Prinzbach, H. *Int. J. Mass Spectrom. Ion Processes* **1994**, *136*, 209-214.

20) Zhu, L.; Wang, S.; Li, Y. *J. Chem. Phys.* **1994**, *101*, 8592-8595.

21) Fadeenko, Y. I. *Powder Metallurgy and Metal Ceramics* **1994**, *33*, 397-400.

22) Tomanek, D.; Wang, Y.; Ruoff, R. S. *J. Phys. Chem. Solids* **1993**, *54*, 1679-1684.

23) Abdourazak, A. H.; Marcinow, Z.; Sygula, A.; Sygula, R.; Rabideau, P. W. *J. Am. Chem. Soc.* **1995**, *117*, 6410-6411.

24) Xie, Z. X.; Liu, Z. Y.; Wang, C. R.; Huang, R. B.; Lin, F. C.; Zheng, L. S. *J. Chem. Soc. - Faraday Transactions* **1995**, *91*, 987-990.

25) Kubler, B.; Millon, E.; Gaumet, J. J.; Muller, J. F. *Fullerene Science and Technology* **1996**, *4*, 1247-1261.

26) Alexandrov, A. L.; Schweigert, V. A. *Chem. Phys. Lett.* **1996**, *263*, 551-558.

27) Crespo, R.; Piqueras, M. C.; Tomás, F. *Synthetic Metals* **1996**, *77*, 13-15.

28) Curl, R. F.; Smalley, R. E. *Scientific American*, **October 1991**, *265*, 32-41.

29) Schwarz, H.; Weiske, T.; Böhme, D. K.; Hrusák, J. *Exo- and Endohedral Fullerene Complexes in the Gas Phase*; Billups, W. E. and Ciufolini, M. A., Ed.; VCH Publishers: New York, 1993, pp 257-283.

30) Kolodney, E.; Tsipinyuk, B.; Budrevich, A. *J. Chem. Phys.* **1995**, *102*, 9263-9275.

31) Matt, S.; Sonderegger, M.; David, R.; Echt, O.; Scheier, P.; Laskin, J.; Lifshitz, C.; Märk, T. D. *Int. J. Mass Spectrom.* **1999**, *185/186/187*, 813-823.

32) Mathur, D.; Brink, C.; Hvelplund, P.; Jensen, N.; Yu, D. H. *Rapid Commun. Mass Spectrom.* **1995**, *9*, 114-118.

33) Ehlich, R.; Westerburg, M.; Campbell, E. E. B. *J. Chem. Phys.* **1996**, *104*, 1900-1911.

34) Joyes, P.; Tarento, R. J.; Van De Walle, J. *Supplement to Z. Phys. D.* **1993**, *26*, S 270-272.

35) Beck, R. D.; Rockenberger, J.; Weis, P.; Kappes, M. *J. Phys. Chem.* **1996**, *104*, 3638-3650.

36) Barran, P. E.; Firth, S.; Stace, A. J.; Kroto, H. W.; Hansen, K.; Campbell, E. E. B. *Int. J. Mass Spectrom. Ion Processes* **1997**, *167/168*, 127-133.

37) Laskin, J.; Hadas, B.; Märk, T. D.; Lifschitz, C. *Int. J. Mass Spectrom.* **1998**, *177*, L9-L13.

38) Lifshitz, C. *Int. J. Mass Spectrom.* **2000**, *198*, 1-14.

39) Hansen, K.; Campbell, E. E. B. *J. Chem. Phys.* **1996**, *104*, 5012-5018.

40) Scheier, P.; Dünser, B.; Wörtgötter, R.; Muigg, D.; Matt, S.; Echt, O.; Foltin, M.; Märk, T. D. *Phys. Rev. Lett.* **1996**, *77*, 2654-2657.

41) Deng, R.; Littlefield, G.; Echt, O. *Z. Phys. D.* **1997**, *D 40*, 355-360.

42) Foltin, M.; Echt, O.; Scheier, B.; Dünser, B.; Wörgötter, R.; Muigg, D.; Matt, S.; Märk, T. D. *J. Chem. Phys.* **1997**, *107*, 6246-6256.

43) Drewello, T.; Asmus, K.-D.; Herzschuh, R. *Eur. Mass Spectrom.* **1995**, *1*, 237-241.

44) Burba, M. E.; Lim, S. K.; Albrecht, A. C. *J. Phys. Chem.* **1995**, *99*, 11839-11843.

45) Chen, G.; Ma, S.; Cooks, R. G.; Bronstein, H. E.; Best, M. D.; Scott, L. T. *J. Mass Spectrom.* **1997**, *32*, 1305-1309.

46) Moriwaki, T.; Shiromaru, H.; Achiba, Y. *Supplement to Z. Phys. D.* **1993**, *26*, S 320-322.

47) Boyd, P. D. W.; Bhyrappa, P.; Paul, P.; Stinchcombe, J.; Bolskar, R. D.; Sun, Y. P.; Reed, C. A. *J. Am. Chem. Soc.* **1995**, *117*, 2907-2914.

48) Javahery, G.; Petrie, S.; Wang, J.; Bohme, D. K. *Chem. Phys. Lett.* **1992**, *195*, 7-10.

49) Fieber-Erdmann, M.; Krätschmer, W.; Ding, A. *Supplement to Z. Phys. D.* **1993**, *26*, S 308-310.

50) Sai Baba, M.; Lakshmi Narasimhan, T. S.; Balasubramanian, R.; Matthews, C. K. *J. Phys. Chem.* **1995**, *99*, 3020-3032.

51) Scheier, P.; Mark, T. D. *Int. J. Mass Spectrom. Ion Processes* **1994**, *133*, L5-L9.

52) Campbell, E. E. B.; Ulmer, G.; Hertel, I. V. *Phys. Rev. Lett.* **1991**, *67*, 1986-1988.

53) Wurz, P.; Lykke, K. R. *J. Chem. Phys.* **1991**, *95*, 7008-7010.

54) Campbell, E. E. B.; Ulmer, G.; Hertel, I. V. *Z. Phys. D.* **1992**, *24*, 81-85.

55) Wurz, P.; Lykke, K. R. *J. Phys. Chem.* **1992**, *96*, 10129-10139.

56) Yoo, R. K.; Ruscic, B.; Berkowitz, J. *J. Chem. Phys.* **1992**, *96*, 911-918.

57) Dresselhaus, M. S.; Dresselhaus, G.; Eklund, P. C. *J. Mater. Res.* **1993**, *8*, 2054-2097.

58) Zhang, Y.; Stuke, M. *Phys. Rev. Lett.* **1993**, *70*, 3231-3234.

59) Jones, A. C.; Dale, M. J.; Banks, M. R.; Gosney, I.; Langridge-Smith, P. R. R. *Molecular Physics* **1993**, *80*, 583-600.

60) Ding, D.; Compton, R. N.; Haufler, R. E.; Klots, C. E. *J. Phys. Chem.* **1993**, *97*, 2500-2504.

61) Loepfe, M.; Siegmann, C.; Sattler, K. *Supplement to Z. Phys. D.* **1993**, *D 26*, S 311-313.

62) Walder, G.; Kennedy, K. W.; Echt, O. *Supplement to Z. Phys. D.* **1993**, *26*, S 288-290.

63) Beck, R. D.; Weis, P.; Bräuchle, G.; Kappes, M. M. *J. Chem. Phys.* **1994**, *100*, 262-270.

64) Scheier, P.; Lezius, M.; Dünser, B.; Robl, R.; Schiestl, B.; Märk, T. D. *Int. J. Mass Spectrom. Ion Processes* **1993**, *125*, R17-R19.

65) Sai Baba, M.; Lakshmi Narasimhan, T. S.; Balasubramanian, R.; Matthews, C. K. *Int. J. Mass Spectrom. Ion Processes* **1994**, *130*, L5-L6.

66) Sai Baba, M.; Lakshmi Narasimhan, T. S.; Balasubramanian, R.; Matthews, C. K. *Int. J. Mass Spectrom. Ion Processes* **1994**, *130*, L1-L4.

67) Lichtenberger, D. L.; Nebesny, K. W.; Ray, C. D.; Huffman, D. R.; Lamb, L. D. *Chem. Phys. Lett.* **1991**, *176*, 203-208.

68) Zimmerman, J. A.; Eyler, J. R.; Bach, S. B. H.; McElvany, S. W. *J. Chem. Phys.* **1991**, *94*, 3556-3562.

69) de Vries, J.; Steger, H.; Kamke, B.; Menzel, C.; Weisser, B.; Kamke, W.; Hertel, I. V. *Chem. Phys. Lett.* **1992**, *188*, 159-162.

70) Lifshitz, C. *Mass Spectrom. Rev.* **1993**, *12*, 261-284.

71) Heath, J. R.; O'Brien, S. C.; Zhang, Q.; Liu, Y.; Curl, R. F.; Kroto, H. W.; Tittel, F. K.; Smalley, R. E. *J. Am. Shem. Soc.* **1985**, *107*, 7779-7780.

72) Ross, M. M.; Callahan, J. H. *J. Phys. Chem.* **1991**, *95*, 5720-5723.

73) Weiske, T.; Böhme, D. K.; Schwarz, H. *J. Phys. Chem.* **1991**, *95*, 8451-8452.

74) Caldwell, K. A.; Giblin, D. E.; Hsu, C. S.; Cox, D.; Gross, M. L. *J. Am. Chem. Soc.* **1991**, *113*, 8519-8521.

75) Weiske, T.; Böhme, D. K.; Hrusák, J.; Krätschmer, W.; Schwarz, H. *Angew. Chem. Int. Ed. Engl.* **1991**, *30*, 884-886.

76) Mowrey, R. C.; Ross, M. M.; Callahan, J. H. *J. Phys. Chem.* **1992**, *96*, 4755-4761.

77) Weiske, T.; Wong, T.; Krätschmer, W.; Terlouw, J. K.; Schwarz, H. *Angew. Chem. Int. Ed. Engl.* **1992**, *31*, 183-185.

78) Gillan, E. G.; Yeretzian, C.; Min, K. S.; Alvarez, M. M.; Whetten, R. L.; Kaner, R. B. *J. Phys. Chem.* **1992**, *96*, 6869-6871.

79) Caldwell, K. A.; Giblin, D. E.; Gross, M. L. *J. Am. Chem. Soc.* **1992**, *114*, 3743-3756.

80) Breton, J.; Gonzalezplatas, J.; Girardet, C. *J. Chem. Phys.* **1993**, *99*, 4036-4040.

81) Ugarte, D. *Chem. Phys. Lett.* **1993**, *209*, 99-103.

82) Saunders, M.; Jiménez-Vázquez, H. A.; Cross, R. J.; Poreda, R. J. *Science* **1993**, *259*, 1428-1430.

83) Pederson, M. R.; Laouini, N. *Phys. Rev. B.* **1993**, *48*, 2733-2737.

84) Bethune, D. S.; Johnson, R. D.; Salem, J. R.; de Vries, M. S.; Yannoni, C. S. *Nature* **1993**, *366*, 123-128.

85) Holleman, I.; Boogaarts, M. G. H.; Meijer, G. **1994**, *113*, 543-546.

86) Davey, S. N.; Leigh, D. A.; Moody, A. E.; Tetler, L. W. *J. Chem. Soc. Chem. Commun.* **1994**, 7-8.

87) Nemecek, S. *Scientific American* **October 1995**, 273, 18-19

88) Dagani, R. *C&E News* **1995**, *73*, 9.

89) Ali, R.; Berry, H. G.; Cheng, S.; Dunford, R. W.; Esbensen, H.; Gemmel, D. S.; Kanter, E. P.; Lebrun, T.; Young, L.; Bauer, W. *Nuclear Instruments & Methods in*

Physics Research Section B Beam Interactions with Materials and Atoms **1995**, *96*, 545-549.

90) Cooper, H. J.; Gallagher, R. T.; Greenwood, P. F.; Vulpius, T.; Derrick, P. J. *J. Chem. Soc. Chem. Commun.* **1995**, 1459-1460.

91) Weiske, T.; Schwarz, H.; Giblin, D. E.; Gross, M. L. *Chem. Phys. Lett.* **1994**, *227*, 87-90.

92) Juha, L.; Hamplova, V.; Engst, P.; Kubat, P.; Koudoumas, E.; Couris, S. *J. Phys. Chem.* **1995**, *99*, 8200-8201.

93) Smith III, A. B.; Strongin, R. M.; Brard, L.; Romanow, W. J.; Saunders, M.; Jiménez-Vázquez, H. A.; Cross, R. J. *J. Am. Chem. Soc.* **1994**, *116*, 10831-10832.

94) Saunders, M.; Jiménez-Vázquez, H. A.; Cross, R. J.; Mroczkowski, S.; Freedberg, D. I.; Anet, F. A. L. *Nature* **1994**, *367*, 256-257.

95) Bühl, M.; Thiel, W.; Jiao, H.; von Ragué Schleyer, P.; Saunders, M.; Anet, F. A. L. *J. Am. Chem. Soc.* **1994**, *116*, 6005-6006.

96) Bühl, M.; Thiel, W. *Chem. Phys. Lett.* **1995**, *233*, 585-589.

97) Joslin, C. G.; Gray, C. G.; Goddard, J. D.; Goldman, S.; Yang, J.; Poll, J. D. *Chem. Phys. Lett.* **1993**, *213*, 377-382.

98) Joslin, C. G.; Yang, J.; Gray, C. G.; Goldman, S.; Poll, J. D. *Chem. Phys. Lett.* **1993**, *211*, 587-594.

99) Joslin, C. G.; Yang, J.; Gray, C. G.; Goldman, S.; Poll, J. D. *Chem. Phys. Lett.* **1993**, *208*, 86-92.

100) Joslin, C. G.; Gray, C. G.; Goldman, S. *Chem. Phys. Lett.* **1995**, *244*, 93-99.

101) Kolb, M.; Thiel, W. *Journal of Computational Chemistry* **1993**, *14*, 37-44.

102) Jackson, K.; Kaxiras, E.; Pederson, M. R. *J. Phys. Chem.* **1994**, *98*, 7805-7810.

103) Hernandezrojas, J.; Breton, J.; Llorente, J. M. G. *Chem. Phys. Lett.* **1995**, *235*, 160-162.

104) Son, M.-S.; Sung, Y. K. *Chem. Phys. Lett.* **1995**, *245*, 113-118.

105) Hernandezrojas, J.; Breton, J.; Llorente, J. M. G. *Chem. Phys. Lett.* **1995**, *243*, 587-588.

106) Braun, T. *Ach - Models in Chemistry* **1995**, *132*, 245-263.

107) Saunders, M.; Jiménez-Vázquez, H. A.; Cross, R. J.; Mroczkowski, S.; Gross, M. L.; Giblin, D. E.; Poreda, R. J. *J. Am. Chem. Soc.* **1994**, *116*, 2193-2194.

108) Lorents, D. C.; Yu, D. H.; Brink, C.; Jensen, N.; Hvelplund, P. *Chem. Phys. Lett.* **1995**, *236*, 141-149.

109) Laskin, J.; Jimenezvazquez, H. A.; Shimshi, R.; Saunders, M.; Devries, M. S. *Chem. Phys. Lett.* **1995**, *242*, 249-252.

110) Laskin, J.; Peres, T.; Khong, A.; Jiménez-Vázquez, H. A.; Cross, R. J.; Saunders, M.; Bethune, D. S.; de Vries, M. S.; Lifshitz, C. *Int. J. Mass Spectrom.* **1999**, *185/186/187*, 61-73.

111) Kwon, Y.-K.; Tománek, D.; Iijima, S. *Phys. Rev. Lett.* **1999**, *82*, 1470-1473.

112) Callahan, J. H.; McElvany, S. W.; Ross, M. M. *Int. J. Mass Spectrom. Ion Processes* **1994**, *138*, 221-239.

113) Kobayashi, K.; Nagase, S.; Akasaka, T. *Chem. Phys. Lett.* **1996**, *261*, 502-506.

114) Hopwood, F. G.; Fisher, K. J.; Greenhill, P.; Willett, G. D.; Zhang, R. *J. Phys. Chem. B.* **1997**, *101*, 10704-10708.

115) Kobayashi, K.; Nagase, S.; Yoshida, M.; Osawa, E. *J. Am. Chem. Soc.* **1997**, *119*, 12693-12694.

116) Kuran, P.; Krause, M.; Bartl, A.; Dunsch, L. *Chem. Phys. Lett.* **1998**, *292*, 580-586.

117) Stevenson, S.; Burbank, P.; Harich, K.; Sun, Z.; Dorn, H. C.; van Loosdrecht, P. H. M.; de Vries, M. S.; Salem, J. R.; Kiang, C.-H.; Johnson, R. D.; Bethune, D. S. *J. Phys. Chem. A* **1998**, *102*, 2833-2837.

118) Kobayashi, K.; Nagase, S. *Chem. Phys. Lett.* **1998**, *282*, 325-329.

119) Kimura, T.; Sugai, T.; Shinohara, H. *Int. J. Mass Spectrom.* **1999**, *188*, 225-232.

120) Yeretzian, C.; Hansen, K.; Diederich, F.; Whetten, R. L. *Nature* **1992**, *359*, 44-47.

121) Yeretzian, C.; Hansen, K.; Diederich, F.; Whetten, R. L. *Supplement to Z. Phys. D.* **1993**, *26*, S 300-304.

122) Zhu, L.; Wang, S.; Li, Y.; Zhang, Z.; Hou, H.; Qin, Q. *Appl. Phys. Lett.* **1994**, *65*, 702-704.

123) Fowler, P. W.; Heine, T.; Zerbetto, F. *J. Phys. Chem. A* **2000**, *104*, 9625-9629.

124) Wood, T. D.; Van Cleef, G. W.; Mearini, M. A.; Coe, J. V.; Marshall, A. G. *Rapid Commun. Mass Spectrom.* **1993**, *7*, 304-311.

125) Campbell, E. E. B.; Schyja, V.; Ehlich, R.; Hertel, I. V. *Phys. Rev. Lett.* **1993**, *70*, 263-266.

126) Hunter, J. M.; Fye, J. L.; Bolvin, N. M.; Jarrold, M. F. *J. Phys. Chem.* **1994**, *98*, 7440-7443.

127) Shvartsburg, A. A.; Hudgins, R. R.; Dugourd, P.; Jarrold, M. F. *J. Phys. Chem. A* **1997**, *101*, 1684-1688.

128) Tast, F.; Malinowski, N.; Billas, I. M. L.; Heinebrodt, M.; Branz, W.; Martin, T. P. *J. Chem. Phys.* **1997**, *107*, 6980-6985.

129) Xia, Y.; Xing, Y.; Tan, C.; Mei, L. *Phys. Rev. B* **1996**, *53*, 13871-13876.

130) Liu, Z.-Y.; Wang, C.-R.; Huang, R.-B.; Zheng, L.-S. *Int. J. Mass Spectrom. Ion Processes* **1995**, *145*, 1-7.

131) Beck, R. D.; Weis, P.; Rockenberger, J.; Kappes, M. M. *Surface Review Letters* **1996**, *3*, 771-775.

132) Onoe, J.; Takeuchi, K. *J. Mass Spectrom.* **1998**, *33*, 387-391.

133) Fabre, T. S.; Treleaven, W. D.; McCarley, T. D.; Newton, C. L.; Landry, R. M.; Saraiva, M. C.; Strongin, R. M. *J. Org. Chem.* **1998**, *63*, 3522-3523.

134) Hansen, K.; Yeretzian, C.; Whetten, R. L. *Chem. Phys. Lett.* **1994**, *218*, 462-466.

135) Mitzner, R.; Winter, B.; Kusch, C.; Campbell, E. E. B.; Hertel, I. V. *Z. Phys. D* **1995**, *37*, 89-95.

136) Beck, R. D.; Stoermer, C.; Schulz, C.; Michel, R.; Weis, P.; Bräuchle, G.; Kappes, M. M. *J. Chem. Phys.* **1994**, *101*, 3243-3249.

137) Beck, R. D.; Weis, P.; Hirsch, A.; Lamparth, I. *J. Phys. Chem.* **1994**, *98*, 9683-9687.

138) Zhao, L.; Zhang, J.; Zhang, R.; Li, Y.; Chen, Y.; Cai, R.; Huang, Z. *Chem. Phys. Lett.* **1996**, *263*, 235-240.

139) Deng, J.-P.; Mou, C.-Y.; Han, C.-C. *Chem. Phys. Lett.* **1996**, *256*, 96-100.

140) Eisler, H.-J.; Hennrich, F. H.; Werner, E.; Hertwig, A.; Stoermer, C.; Kappes, M. M. *J. Phys. Chem.* **1998**, *102*, 3889-3897.

141) Penn, S. G.; Costa, D. A.; Balch, A. L.; Lebrilla, C. B. *Int. J. Mass Spectrom. Ion Processes* **1997**, *169/170*, 371-386.

142) Fowler, P. W.; Mitchell, D.; Taylor, R.; Seifert, G. *J. Chem. Soc. Perkin Trans. 2* **1997**, 1901-1905.

143) Barrow, M. P.; Tower, N. J.; Taylor, R.; Drewello, T. *Chem. Phys. Lett.* **1998**, *293*, 302-308.

144) Al-Jafari, M. S.; Barrow, M. P.; Taylor, R.; Drewello, T. *Int. J. Mass Spectrom.* **1999**, *184*, L1-L4.

145) Segura, J. L.; Martin, N. *Chem. Soc. Rev.* **2000**, *29*, 13-25.

146) Kennedy, K. W.; Echt, O. *J. Phys. Chem.* **1993**, *97*, 7088-7091.

147) Gallogly, E. B.; Bao, Y.; Han, K.; Lin, H.; Jackson, W. M. *J. Phys. Chem.* **1994**, *98*, 3121-3125.

148) Lin, H.; Han, K.-L.; Bao, Y.; Gallogly, E. B.; Jackson, W. M. *J. Phys. Chem.* **1994**, *98*, 12495-12500.

149) Andersen, J. U.; Brink, C.; Hvelplund, P.; Larsson, M. O.; Bech Nielsen, B.; Shen, H. *Phys. Rev. Lett.* **1996**, *77*, 3991-3994.

150) Aumayr, F.; Betz, G.; Märk, T. D.; Scheier, P.; Winter, H. P. *Int. J. Mass Spectrom. Ion Processes* **1998**, *174*, 317-328.

151) Arslanbekov, T. U.; Koval, A. V.; Pazdzersky, V. A. *Laser Physics* **1997**, *7*, 689-691.

152) Bekkerman, A.; Tsipinyuk, B.; Kolodney, E. *Int. J. Mass Spectrom.* **1999**, *185/186/187*, 773-786.

153) von Helden, G.; Holleman, I.; van Roij, A. J. A.; Knippels, G. M. H.; van der Meer, A. F. G.; Meijer, G. *Phys. Rev. Lett.* **1998**, *81*, 1825-1828.

154) Hansen, K.; Echt, O. *Phys. Rev. Lett.* **1997**, *78*, 2337-2340.

155) Weis, P.; Rockenberger, J.; Beck, R. D.; Kappes, M. M. *J. Chem. Phys.* **1996**, *104*, 3629-3637.

156) Remacle, F.; Levine, R. D. *Phys. Lett. A* **1993**, *173*, 284-287.

157) Jeoung, S. C.; Kim, D.; Kim, S.; Kim, S. K. *Chem. Phys. Lett.* **1995**, *241*, 528-532.

158) Sauve, G.; Dimitrijevic, N. M.; Kamat, P. V. *J. Phys. Chem.* **1995**, *99*, 1199-1203.

159) Vandenheuvel, D. J.; Vandenberg, G. J. B.; Groenen, E. J. J.; Schmidt, J.; Holleman, I. *J. Phys. Chem.* **1995**, *99*, 11644-11649.

160) Klots, C. E.; Compton, R. N. *Phys. Rev. Lett.* **1996**, *76*, 4092-4093.

161) Ding, D.; Huang, J.; Compton, R. N.; Klots, C. E.; Haufler, R. E. *Phys. Rev. Lett.* **1994**, *73*, 1084-1087.

162) van Heijnsbergen, D.; von Helden, G.; Sartakov, B.; Meijer, G. *Chem. Phys. Lett.* **2000**, *321*, 508-513.

163) Klots, C. E. *Chem. Phys. Lett.* **1991**, *186*, 73-76.

164) Klots, C. E. *Z. Phys. D* **1991**, *20*, 105-109.

165) Klots, C. E. *J. Chem. Phys.* **1994**, *100*, 1035-1039.

166) Klots, C. E.; Compton, R. N. *Surface Rev. Lett.* **1996**, *3*, 535-540.

167) Lykke, K. R. *Phys. Rev. Lett.* **1995**, *75*, 1234-1235.

168) Beck, R. D.; Weis, P.; Rockenberger, J.; Kappes, M. M. *J. Phys. Chem.* **1995**, *99*, 3990-3999.

169) Winter, B.; Mitzner, R.; Kusch, C.; Campbell, E. E. B.; Hertel, I. V. *J. Chem. Phys.* **1996**, *104*, 9179-9190.

170) Campbell, E. E. B.; Levine, R. D. *Annu. Rev. Phys. Chem.* **2000**, *51*, 1-34.

171) Hirsch, A. *Synthesis - Stuttgart* **1995**, 895-913.

172) Kan, S. Z.; Byun, Y. G.; Lee, S. A.; Freiser, B. S. *J. Mass Spectrom.* **1995**, *30*, 194-200.

173) Böhme, D. K. *Can. J. Chem.* **1999**, *77*, 1453-1464.

174) Andreoni, W. *Annu. Rev. Phys. Chem.* **1998**, *49*, 405-439.

175) Wang, S.-H.; Chen, F.; Fann, Y.-C.; Kashani, M.; Malaty, M.; Jansen, S. A. *J. Phys. Chem.* **1995**, *99*, 6801-6807.

176) Peel, J. B.; Rothwell, R. G. *Aust. J. Chem.* **1994**, *47*, 131-141.

177) Rogner, I.; Birkett, P.; Campbell, E. E. B. *Int. J. Mass Spectrom.* **1996**, *156*, 103-108.

178) Fritz, H. P.; Hiemeyer, R. *Carbon* **1995**, *33*, 1601-1609.

179) Boltalina, O. V.; Borschevskii, A. Y.; Sidorov, L. N.; Street, J. M.; Taylor, R. *J. Chem. Soc. Chem. Commun.* **1996**, 529-530.

180) Boltalina, O. V.; Sidorov, L. N.; Bagryantsev, V. F.; Seredenko, V. A.; Zapol'skii, A. S.; Street, J. M.; Taylor, R. *J. Chem. Soc. Perkin Trans. 2* **1996**, 2275-2278.

181) Cozzolino, R.; Belgachem, O.; Drewello, T.; Käseberg, L.; Herzschuh, R.; Suslov, S.; Boltalina, O. *Eur. Mass Spectrom.* **1997**, *3*, 407-414.

182) Boltalina, O. V. *J. Fluorine Chem.* **2000**, *101*, 273-278.

183) Banks, M. R.; Dale, M. J.; Gosney, I.; Hodgson, P. K. G.; Jennings, R. C. K.; Jones, A. C.; Lecoultre, J.; Langridge-Smith, P. R. R.; Maier, J. P.; Scrivens, J. H.; Smith,

M. J. C.; Smyth, C., J.; Taylor, A. T.; Thorburn, P.; Webster, A. S. *J. Chem. Soc. Chem. Commun.* **1993**, 1149-1152.

184) Austin, S. J.; Batten, R. C.; Fowler, P. W.; Redmond, D. B.; Taylor, R. *J. Chem. Soc. Perkin Trans. 2* **1993**, 1383-1386.

185) Bühl, M.; Thiel, W.; Schneider, U. *J. Am. Chem. Soc.* **1995**, *117*, 4623-4627.

186) Darwish, A. D.; Abdul-Sada, A. a. K.; Langley, G. J.; Kroto, H. W.; Taylor, R.; Walton, D. R. M. *J. Chem. Soc. Perkin Trans. 2* **1995**, 2359-2365.

187) Lobach, A. S.; Perov, A. A.; Rebrov, A. I.; Roshchupkina, O. S.; Tkacheva, V. A.; Stepanov, A. N. *Russian Chem. Bulletin* **1997**, *46*, 641-648.

188) Gol'dshleger, N. F.; Moravskii, A. P. *Russian Chem. Rev.* **1997**, *66*, 323-342.

189) Billups, W. E.; Gonzalez, A.; Gesenberg, C.; Luo, W.; Marriott, T.; Alemany, L. B.; Saunders, M.; Jiménez-Vázquez, H. A.; Khong, A. *Tetrahedron Lett.* **1997**, *38*, 175-178.

190) Möder, M.; Nüchter, M.; Ondruschka, B.; Czira, G.; Vékey, K.; Barrow, M. P.; Drewello, T. *Int. J. Mass Spectrom.* **2000**, *195/196*, 599-607.

191) Östling, D.; Rosén, A. *Supplement to Z. Phys. D* **1993**, *26*, S 279-281.

192) Schluter, A. D. *Abstracts of Papers of the American Chemical Society* **1995**, *209*, 294-POLY.

193) Dai, S.; Compton, R. N.; Young, J. P.; Mamantov, G. *J. Am. Ceram. Soc.* **1992**, *75*, 2865-2866.

194) Dai, S.; Compton, R. N.; Young, J. P.; Mamantov, G. *C&EN* **1995**, 29.

195) Mattes, B. R.; Koskelo, A. *C&EN* **1994**, 36.

196) Mizoguchi, K.; Maniwa, Y.; Kume, K. *Materials Science and Engineering B - Solid State Materials for Advanced Technology* **1993**, *19*, 146-153.

197) Scanlon, J. C.; Brown, J. M.; Ebert, L. B. *J. Phys. Chem.* **1994**, *98*, 3921-3923.

198) Smith, A. B.; Strongin, R. M.; Brard, L.; Furst, G. T.; Romanow, W. J.; Owens, K. G.; Goldschmidt, R. J.; King, R. C. *J. Am. Chem. Soc.* **1995**, *117*, 5492-5502.

199) Wang, G.-W.; Komatsu, K.; Murata, Y.; Shiro, M. *Nature* **1997**, *387*, 583-586.

200) Kato, T. *LASER Chemistry* **1994**, *14*, 155-160.

201) Diehl, M.; Degen, J.; Schmidtke, H. H. *J. Phys. Chem.* **1995**, *99*, 10092-10096.

202) Dwivedi, R. K.; Thareja, R. K. *Phys. Rev. B* **1995**, *51*, 7160-7167.

203) Mitzner, R.; Campbell, E. E. B. *J. Chem. Phys.* **1995**, *103*, 2445-2453.

204) Schettino, V.; Salvi, P. R.; Bini, R.; Cardini, G. *J. Chem. Phys.* **1994**, *101*, 11079-11081.

205) Dixon, D. A.; Chase, B. E.; Fitzgerald, G.; Matsuzawa, N. *J. Phys. Chem.* **1995**, *99*, 4486-4489.

206) Gallagher, S. H.; Armstrong, R. S.; Lay, P. A.; Reed, C. A. *J. Phys. Chem.* **1995**, *99*, 5817-5825.

207) Kuzmany, H.; Winkler, R.; Pichler, T. *J. Phys. - Condensed Matter* **1995**, *7*, 6601-6624.

208) McElvany, S. W.; Ross, M. M. *J. Am. Soc. Mass Spectrom.* **1992**, *3*, 268-280.

209) Stry, J. J.; Garvey, J. F. *Int. J. Mass Spectrom. Ion Processes* **1994**, *138*, 241-261.

210) Popovic, A.; Drazic, G.; Marsel, J. *Rapid Commun. Mass Spectrom.* **1994**, *8*, 985-990.

211) Dunsch, L.; Kirbach, U.; Klostermann, K. *Journal of Molecular Structure* **1995**, *348*, 381-384.

212) Saldi, F.; Marie, Y.; Gao, Y.; Simon, C.; Migeon, H. N.; Begin, D.; Mareche, J. F. *Eur. Mass Spectrom.* **1995**, *1*, 487-492.

213) Cordero, M. M.; Cornish, T. J.; Cotter, R. J. *J. Am. Soc. Mass Spectrom.* **1996**, *7*, 590-597.

214) Aumayr, F.; Vana, M.; Winter, H.; Drexel, H.; Grill, V.; Senn, G.; Matt, S.; Scheier, P.; Märk, T. D. *Int. J. Mass Spectrom. Ion Processes* **1997**, *163*, L1-14.

215) Beynon, J. H. *Biomed. Mass. Spectrom.* **1981**, *8*, 380-383.

216) Todd, J. F. J. *Pure and Applied Chemistry* **1991**, *63*, 211-232.

217) McDowell, C. A. *Mass Spectrometry*; McGraw-Hill Book Company Inc., 1963, pp 639.

218) Rumpf, B. A.; Derrick, P. J. *Int. J. Mass Spectrom. Ion Processes* **1988**, *82*, 239-257.

219) Jennings, K. R.; Dolnikowski, G. G. *Methods in Enzymology* **1990**, *193*, 37-61.

220) Trainor, J. R.; Derrick, P. J. *Sectors and Tandem Sectors*; Gross, M. L., Ed.; Kluwer Academic Publishers: Netherlands, 1992; Vol. Chapter 1, pp 3-27.

221) Chapman, J. R. *Practical Organic Mass Spectrometry: A Guide for Chemical and Biochemical Analysis*; 2nd ed.; John Wiley and Sons Ltd.: Chichester, 1993.

222) de Hoffmann, E.; Charette, J.; Stroobant, V. *Mass Spectrometry: Principles and Applications*; John Wiley and Sons Ltd.: Chichester, 1996.

223) Serway, R. A. *Physics for Scientists and Engineers with Modern Physics*; 4th ed.; Saunders College Publishing:, 1996.

224) Wiley, W. C.; McLaren, J. H. *Rev. Sci. Instrum.* **1955**, *26*, 1150-1157.

225) Alikhanov, S. G. *Sov. Phys. JETP* **1957**, *4*, 452-453.

226) Mamyrin, B. A.; Karatev, V. I.; Shmikk, D. V.; Zagulin, V. A. *Sov. Phys. JETP* **1973**, *37*, 45-48.

227) Mamyrin, B. A. *Int. J. Mass Spectrom. Ion Processes* **1994**, *131*, 1-19.

228) Bergmann, T.; Martin, T. P.; Schaber, H. *Rev. Sci. Instrum.* **1989**, *60*, 792-793.

229) Bergmann, T.; Martin, T. P.; Schaber, H. *Rev. Sci. Instrum.* **1989**, *60*, 347-349.

230) Bergmann, T.; Martin, T. P.; Schaber, H. *Rev. Sci. Instrum.* **1990**, *61*, 2592-2600.

231) Bergmann, T.; Martin, T. P.; Schaber, H. *Rev. Sci. Instrum.* **1990**, *61*, 2585-2591.

232) Cotter, R. J. *Time-of-Flight Mass Spectrometry: Instrumentation and Applications in Biological Research*; ACS Professional Reference Books: Washington DC, 1997.

233) Giannakopulos, A. E.; Reynolds, D. J.; Chan, T.-W. D.; Colburn, A. W.; Derrick, P. J. *Int. J. Mass Spectrom. Ion Processes* **1994**, *131*, 67-86.

234) Tang, X.; Beavis, R.; Ens, W.; Lafortune, F.; Schueler, B.; Standing, K. G. *Int. J. Mass Spectrom. Ion Processes* **1988**, *85*, 43-67.

235) Wollnik, H.; Grüner, U.; Li, G. *Time-Of-Flight Mass Spectrometers*; Gross, M. L., Ed.; Kluwer Academic Publishers: Netherlands, 1992; Vol. Chapter 6, pp 117-131.

236) Guilhaus, M. *J. Mass Spectrom.* **1995**, *30*, 1519-1532.

237) Weickhardt, C.; Moritz, F.; Grotemeyer, J. *Mass Spectrom. Rev.* **1996**, *15*, 139-162.

238) Guilhaus, M.; Mlynski, V.; Selby, D. *Rapid Commun. Mass Spectrom.* **1997**, *11*, 951-962.

239) Schriemer, D. C.; Li, L. *Anal. Chem.* **1997**, *69*, 4176-4183.

240) Schriemer, D. C.; Li, L. *Anal. Chem.* **1997**, *69*, 4169-4175.

241) Doroshenko, V. M.; Cotter, R. J. *J. Am. Soc. Mass Spectrom.* **1999**, *10*, 992-999.

242) Spengler, B. *J. Mass Spectrom.* **1997**, *32*, 1019-1036.

243) Harvey, D. J.; Hunter, A. P.; Bateman, R. H.; Brown, J.; Critchley, G. *Int. J. Mass Spectrom.* **1999**, *188*, 131-146.

244) Laiko, V. V.; Dodonov, A. F. *Rapid Commun. Mass Spectrom.* **1994**, *8*, 720-726.

245) Morris, H. R.; Paxton, T.; Panico, M.; McDowell, R.; Dell, A. *J. Protein Chem.* **1997**, *16*, 469-479.

246) Cordero, M. M.; Cornish, T. J.; Cotter, R. J.; Lys, I. A. *Rapid Commun. Mass Spectrom.* **1995**, *9*, 1356-1361.

247) de Hoffmann, E. *J. Mass Spectrom.* **1996**, *31*, 121-137.

248) March, R. E. *J. Mass Spectrom.* **1997**, *32*, 351-369.

249) Comisarow, M. B.; Marshall, A. G. *Chem. Phys. Lett.* **1974**, *25*, 282-283.

250) Comisarow, M. B.; Marshall, A. G. *Can. J. Chem.* **1974**, *52*, 1997-1999.

251) Comisarow, M. B.; Marshall, A. G. *Chem. Phys. Lett.* **1974**, *26*, 489-490.

252) Marshall, A. G.; Comisarow, M. B. *Anal. Chem.* **1975**, *47*, 491A-504A.

253) Comisarow, M. B.; Marshall, A. G. *J. Chem. Phys.* **1976**, *64*, 110-119.

254) Comisarow, M. B. *J. Chem. Phys.* **1978**, *69*, 4097-4104.

255) Jacoby, C. B.; Holliman, C. L.; Gross, M. L. *Fourier Transform Mass Spectrometry: Features, Principles, Capabilities, and Limitations*; Gross, M. L., Ed.; Kluwer Academic Publishers: Netherlands, 1992; Vol. Chapter 5, pp 93-116.

256) Comisarow, M. B. *Hyperfine Interactions* **1993**, *81*, 171-178.

257) Amster, I. J. *J. Mass Spectrom.* **1996**, *31*, 1325-1337.

258) Marshall, A. G.; Hendrickson, C. L.; Jackson, G. S. *Mass Spectrom. Rev.* **1998**, *17*, 1-35.

259) Evans, S. *Methods in Enzymology* **1990**, *193*, 67-86.

260) Geno, P. W. *Ion Detection in Mass Spectrometry*; Gross, M. L., Ed.; Kluwer Academic Publishers: Netherlands, 1992; Vol. Chapter 7, pp 133-141.

261) Hillenkamp, F.; Ehring, H. *Laser Desorption Mass Spectrometry Part I: Basic Mechanisms and Techniques*; Gross, M. L., Ed.; Kluwer Academic Publishers: Netherlands, 1992; Vol. Chapter 9, pp 165-179.

262) Busch, K. L. *J. Mass Spectrom.* **1995**, *30*, 233-240.

263) Karas, M.; Bahr, U.; Ingendoh, A.; Nordhoff, E.; Stahl, B.; Strupat, K.; Hillenkamp, F. *Analytica Chimica Acta* **1990**, *241*, 175-185.

264) Tanaka, K.; Waki, H.; Ido, Y.; Akita, S.; Yoshida, Y.; Yoshida, T. *Rapid Commun. Mass Spectrom.* **1988**, *2*, 151.

265) Karas, M.; Hillenkamp, F. *Anal. Chem.* **1988**, *60*, 2299-2301.

266) Juhasz, P.; Vestal, M. L.; Martin, S. A. *J. Am. Soc. Mass Spectrom.* **1997**, *8*, 209-217.

267) Overberg, A.; Hassenbürger, A.; Hillenkamp, F. *Laser Desoprtion Mass Spectrometry Part II: Performance and Applications of Matrix-Assisted Laser Desorptio/Ionization*

of Large Biomolecules; Gross, M. L., Ed.; Kluwer Academic Publishers: Netherlands, 1992; Vol. Chapter 10, pp 181-197.

268) Beavis, R. C. *Org. Mass Spectrom.* **1992**, *27*, 653-659.

269) Fitzgerald, M. C.; Parr, G. R.; Smith, L. M. *Anal. Chem.* **1993**, *65*, 3204-3211.

270) Bahr, U.; Deppe, A.; Karas, M.; Hillenkamp, F. *Anal. Chem.* **1992**, *64*, 2866-2869.

271) Hoberg, A.-M.; Haddleton, D. M.; Derrick, P. J. *Eur. Mass. Spectrom.* **1997**, *3*, 471-473.

272) Linnemayr, K.; Allemaier, G. *Eur. Mass Spectrom.* **1997**, *3*, 141-149.

273) Axelsson, J.; Hoberg, A.-M.; Waterson, C.; Myatt, P.; Shield, G. L.; Varney, J.; Haddleton, D. M.; Derrick, P. J. *Rapid Commun. Mass Spectrom.* **1996**.

274) Haddleton, D. M.; Waterson, C.; Derrick, P. J. *Eur. Mass Spectrom.* **1998**, *4*, 203-207.

275) Kumar Kolli, V. S.; Orlando, R. *Anal. Chem.* **1997**, *69*, 327-332.

276) Yamashita, M.; Fenn, J. B. *J. Phys. Chem.* **1984**, *88*, 4671-4675.

277) Yamashita, M.; Fenn, J. B. *J. Phys. Chem.* **1984**, *88*, 4451-4459.

278) Fenn, J. B.; Mann, M.; Meng, C. K.; Wong, S. F.; Whitehouse, C. M. *Science* **1989**, *246*, 64-71.

279) Mann, M. *Electrospray Mass Spectrometry*; Gross, M. L., Ed.; Kluwer Academic Publishers: Netherlands, 1992; Vol. Chapter 8, pp 145-163.

280) Gaskell, S. J. *J. Mass Spectrom.* **1997**, *32*, 677-688.

281) Kebarle, P.; Tang, L. *Anal. Chem.* **1993**, *65*, 972 A-985 A.

282) Van Berkel, G. J. *The Electrolytic Nature of Electrospray*; Cole, R. B., Ed.; John Wiley: New York, 1997; Vol. Chapter 2, pp 65-105.

283) Enke, C. G. *Anal. Chem.* **1997**, *69*, 4885-4893.

284) McCarley, T. D.; Lufaso, M. W., .; Curtin, L. S.; McCarley, R. L. *J. Phys. Chem. B* **1998**, *102*, 10078-10086.

285) Jackson, G. S.; Enke, C. G. *Anal. Chem.* **1999**, *71*, 3777-3784.

286) Tang, L.; Kebarle, P. *Anal. Chem.* **1993**, *65*, 3654-3668.

287) Charbonnier, F.; Nicolas, J.-P.; Berthelot, L.; Hapiot, P.; Pinson, J.; Rolando, C. *Red-Ox Chemistry in the Electrospray Mist*: Orlando, Florida, 1998, pp 426.

288) Charbonnier, F.; Berthelot, L.; Rolando, C. *Anal. Chem.* **1999**, *71*, 1585-1591.

289) Fenn, J. B.; Rosell, J.; Meng, C. K. *J. Am. Mass Spectrom.* **1997**, *8*, 1147-1157.

290) Gomez, A.; Tang, K. Q. *Phys. Fluids* **1994**, *6*, 404-414.

291) Dole, M.; Mack, L. L.; Hines, R. L.; Mobley, R. C.; Ferguson, L. D.; Alice, M. B. *J. Chem. Phys.* **1968**, *49*, 2240-2249.

292) Iribarne, J. V.; Thompson, B. A. *J. Chem. Phys.* **1976**, *64*, 2287-2294.

293) Thompson, B. A.; Iribarne, J. V. *J. Chem. Phys.* **1979**, *71*, 4451-4463.

294) Van Berkel, G. J.; McLuckey, S. A.; Glish, G. L. *Anal. Chem.* **1991**, *63*, 1098-1109.

295) Levsen, K. *Fundamental Aspects of Organic Mass Spectrometry*; 1 ed.; Verlag Chemie: Weinheim, 1978; Vol. 4.

296) Neumann, G. M.; Sheil, M. M.; Derrick, P. J. *Z. Naturforsch.* **1984**, *39a*, 584-592.

297) Hayes, R. N.; Gross, M. L. *Methods in Enzymology* **1990**, *193*, 237-263.

298) Cornish, T. J.; Cotter, R. J. *Anal. Chem.* **1993**, *65*, 1043-1047.

299) Bradley, C.; Curtis, J. M.; Derrick, P. J.; Sheil, M. M. *J. Chem. Soc. Faraday Trans.* **1994**, *90*, 239-247.

300) Cooks, R. G. *J. Mass Spectrom.* **1995**, *30*, 1215-1221.

301) Uggerud, E.; Derrick, P. J. *J. Phys. Chem.* **1991**, *95*, 1430-1436.

302) Cooper, H. J.; Derrick, P. J.; Jenkins, H. D. B.; Uggerud, E. *J. Phys. Chem.* **1993**, *97*, 5443-5444.

303) Vékey, K. *J. Mass Spectrom.* **1996**, *31*, 445-463.

304) Baer, T.; Mayer, P. M. *J. Am. Soc. Mass Spectrom.* **1997**, *8*, 103-115.

Chapter Two

Laser-Induced Fullerene Production Using the Organometallic Precursor Penta(cyclopentadienyl)-η^5-cyclo pentadienylmanganesetricarbonyl

2.1 Introduction

Laser vaporization of graphite became the first method of fullerene production, albeit accidentally.[1] It is unsurprising then that the most common method of analysis of fullerenes has been the use of laser desorption/ionization coupled with mass spectrometry. Yeretzian et al.[2,3] first discovered that laser ablation of a fullerene target resulted in coalescence which in turn led to the formation of higher fullerenes. Typically, the coalesced clusters display a tendency to consist of multiples of the precursor molecule used,[4,5] though clusters possessing uneven numbers of carbon atoms have also been observed.[6] Experiments have involved the use of different fullerene precursors, such as C_{60}, C_{70}, and C_{84}, and it has been found that the products of such coalescence reactions depend on the precursor material used[7,8] and the formation mechanism has been investigated.[9-13] Fullerene derivatives have also been investigated[14] and fullerene oxides in particular have displayed unusual tendencies.[15] Fullerene oxides undergo coalescence at much lower laser powers than pure fullerenes and form pure, higher carbon clusters. However, under matrix-assisted laser desorption/ionization conditions, the fullerene oxides undergo more gentle coalescence and dimeric species are formed where fullerene moieties are bridged by furnanoid rings,[16,17] comprising of one σ C-C bond and one C-O-C bond, as discussed in detail in Chapter Six.

Generation of fullerenes from non-fullerene precursors has also become an area of interest.[18] Recent examples include the production of metallofullerenes following laser ablation of pyrolyzed dried algae residues,[19] fullerene formation following coalescence of cyclo[n]carbons,[20] and fullerene formation from dodecahedrane derivatives;[21] polycyclic aromatic hydrocarbons[22] appear to be a particularly common choice of precursor, due to their resemblance to a partial fullerene. It has been shown that not only is the presence of

a sufficient amount of carbon important, but also that the presence of certain structural features facilitates fullerene formation. With this in mind, a recently synthesized organometallic compound seemed suitable for the generation of fullerenes in the gas-phase. Penta(cyclopentadienyl)-η^5-cyclopentadienylmanganesetricarbonyl, or $[Cp_5CpMn(CO)_3]$, possesses a π ligand which may provide a suitable precursor. Cp_5Cp ($C_{30}H_{25}$) is very similar to semi-buckminsterfullerene ($C_{30}H_{10}$),[23] where the arrangement of six pentagons satisfies the isolated pentagon rule,[24] and is therefore structurally favorable. Laser desorption/ionization (LDI) mass spectrometry can therefore be envisaged as being a suitable experimental method for the possible generation and analysis of fullerenes. Production of metallofullerenes, where the manganese atom is enclosed by the fullerene cage, may also be considered possible. X-Ray crystallography and LDI mass spectrometry were used for structural analysis of the precursor, and LDI mass spectrometry was further used in order to attempt to produce fullerenes in the gas-phase from the organometallic precursors.

2.2 Experimental

The organometallic compound was synthesized by K. Vollhardt's group (University of California at Berkeley, Berkeley, California, USA) during the collaborative effort on this topic. $[Cp_5CpMn(CO)_3]$ is obtained as a mixture of 1,3- and 1,4-cyclopentadiene tautomers. Slow crystallization of one isomer proceeds at -20 °C in hexanes as yellow crystals. These crystals could then be analyzed using X-Ray crystallography. Mass spectrometric analysis was performed using two different instruments. Most analysis was performed using a Kratos Kompact MALDI IV. The ion source incorporates a nitrogen laser (337 nm, 3 ns pulse width). Ions created following laser ablation are then accelerated

into the flight tube by a 20 kV accelerating potential. Mass analysis is performed by time-of-flight analysis, and a curved field reflectron is incorporated to improve mass resolution. An "ion gate," consisting of two deflecting electrodes, may be used to select ions of interest; application of a potential to these electrodes deflects ions (at times correlating with the arrival of ions that are not of interest at the ion gate) and then the potential is no longer applied when ions of interest are allowed to traverse the ion gate. During the course of the following experiments, the ion gate has been used on two occasions. This was due to instrumental reasons of the time, where the reflectron detector of the mass spectrometer was prone to reduced sensitivity when large numbers of ions were produced across a broad mass range, due to saturation of the detector.[25] Selection of a narrower mass range results in enhanced sensitivity, which was particularly important for the following experiments where low intensity signals were examined. Each spectrum shown is the result of the accumulation of 200 profiles, each generated by a single laser pulse. As it was found that the sample would degrade at room temperature, sample solutions were freshly prepared shortly before each experiment, and the sample compound was otherwise stored at low temperature and in the absence of light. To prepare a sample for analysis, the solid was dissolved in dichloromethane, and the resulting solution was then spotted on to a stainless steel target slide and the solvent was allowed to evaporate. The slide was then inserted into the ion source.

Further mass spectrometric analysis was carried out using a Micromass TofSpec E with the assistance of E. Williams (Micromass Ltd., Manchester, UK), shown in Figure 1. The TofSpec E uses a nitrogen laser for laser desorption/ionization (LDI) just as the Kompact MALDI IV does. Ions are accelerated by a 20 kV accelerating potential, and mass analysis is based on time-of-flight analysis. One difference between the TofSpec E and the Kompact

MALDI IV is the fact that the TofSpec E uses a linear field reflectron. It may be noted that the TofSpec E has a higher resolution than the Kompact MALDI IV, but that the curved field reflectron of the Kompact MALDI IV makes it more suitable for post source decay (PSD) experiments; during the course of experiments, PSD was not investigated, but the higher resolution was necessary for establishing the parent ion and fragmentation reactions. For a more comprehensive description of the Kratos Kompact MALDI IV, see Chapter Three. Samples were prepared for analysis in a near identical manner to the Kompact MALDI IV experiments.

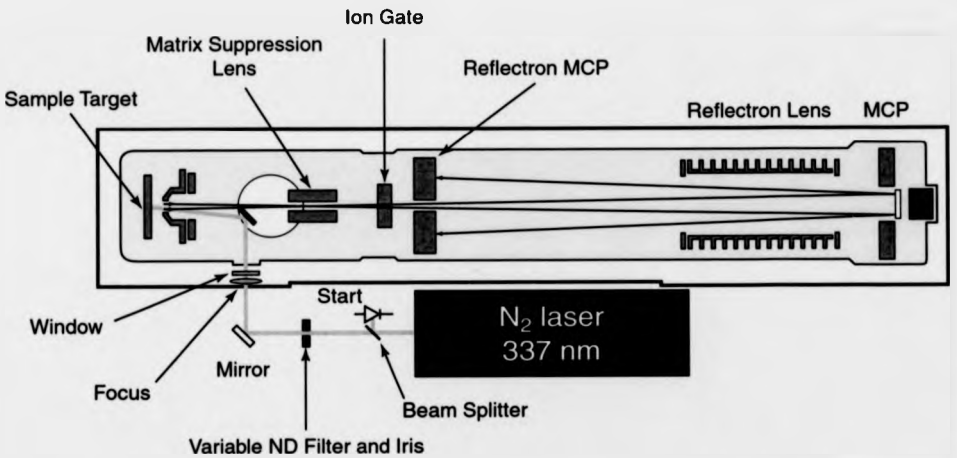

Figure 1: Schematic diagram of the Micromass TofSpec E

2.3 Results and Discussion

A reaction scheme for the production of penta(cyclopentadienyl)-η^5-cyclopentadienylmanganesetricarbonyl is shown in Figure 2, and Figure 3 shows the structure of the compound, determined by X-Ray crystallography. It must be noted that

the X-Ray analysis was performed entirely by the the Vollhardt group at the University of California at Berkeley, and the results are presented here to provide a clearer understanding of the compound of interest. Bond lengths were also established during X-Ray analysis and some of these values are: C(4) - C(9) 1.475(6) Å, C(9) - C(10) 1.459(6) Å, C(10) - C(11) 1.378 (7) Å, C(11) - C(12) 1.410(8) Å, C(12) - C(13) 1.489(6) Å, C(9) - C(13) 1.357(7) Å, C(8) - C(29) 1.478(6) Å, C(29) - C(30) 1.480(7) Å, C(30) - C(31) 1.446(7) Å, C(31) - C(32) 1.371(7) Å, C(32) - C(33) 1.469(7) Å, and C(29) - C(33) 1.354(6) Å. An alternating tautomeric pattern is observed for the five Cp rings, where C(14), C(19), and C(29) mark the terminus of the diene unit, while C(9) and C(24) are their internal analogs. The absence of coplanarity amongst the Cp units is notable, where dihedral angles range from 42.2° to 46.4° and bending angles (of carbon atoms attached from the least squares plane of C(4) - C(8)) average 10°. While the average distance of the α carbon atoms in neighboring Cp substituents is approximately 3.3 Å, Spartan modeling of the all coplanar conformer narrows this angle to approximately 2.2 Å.

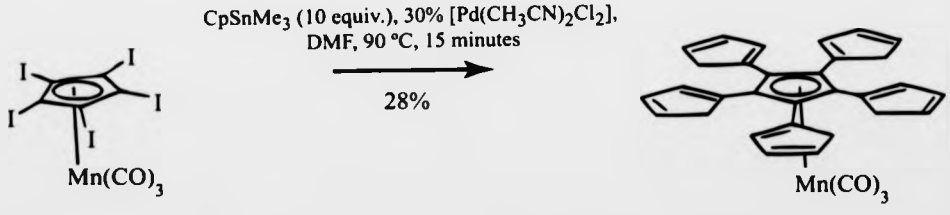

Figure 2: Reaction scheme for the production of the penta(cyclopentadienyl)-η^6-cyclopentadienylmanganesetricarbonyl compound.

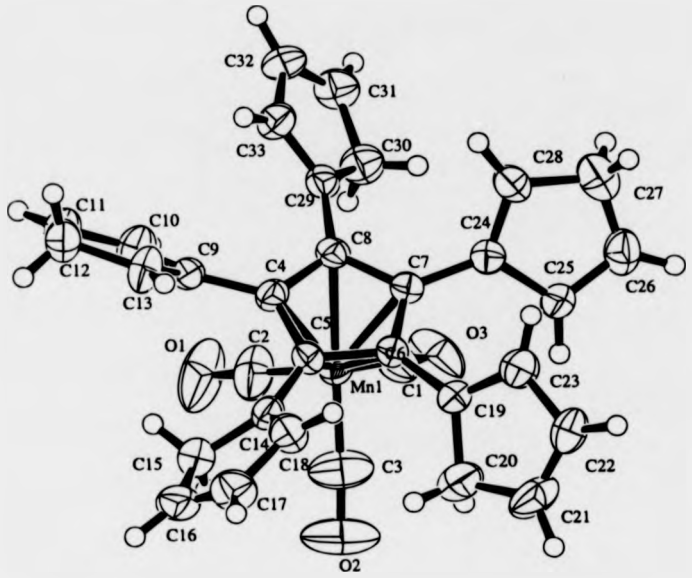

Figure 3: X-Ray crystallography structure of penta(cyclopentadienyl)-η^5-cyclopentadienylmanganesetricarbonyl

Figure 4 shows the positive-ion mass spectrum of the $[Cp_5CpMn(CO)_3]$ sample, obtained at just above a threshold laser irradiance on a Micromass TofSpec E. Signals are observed for $C_{25}H_{17}^{+\bullet}$ (m/z 317), $C_{30}H_{25}^{+\bullet}$ (i.e. Cp_5Cp) (m/z 385), $C_{30}H_{25}Mn^{+\bullet}$ (i.e. Cp_5CpMn) (m/z 440), and $C_{30}H_{22}Mn(CO)_2^{+\bullet}$ (i.e. $Cp_5CpMn(CO)_2 - H_2$) (m/z 493). Another experiment (spectrum not shown) was performed using a deuterated version of the compound, $[C_{30}D_{25}Mn(CO)_3]$, in order to verify the mass assignment. The use of a deuterated version of the sample confirmed the mass assignment shown in Figure 4 as the signals were found to shift to masses predicted in correlation with the use of deuterium instead of hydrogen. Using both the hydrogenated and the deuterated samples, it is notable that the parent ions could not be detected, and the fragment with the largest mass resulted from the loss of one carbonyl group. Under electron ionization (EI) conditions, using electrons with the standard energy of 70 eV, the molecular ion has a relative intensity of 56%, and the signal arising

from $Cp_5CpMn^{+\bullet}$ is the base peak. It can therefore be seen that use of LDI leads to more pronounced fragmentation.

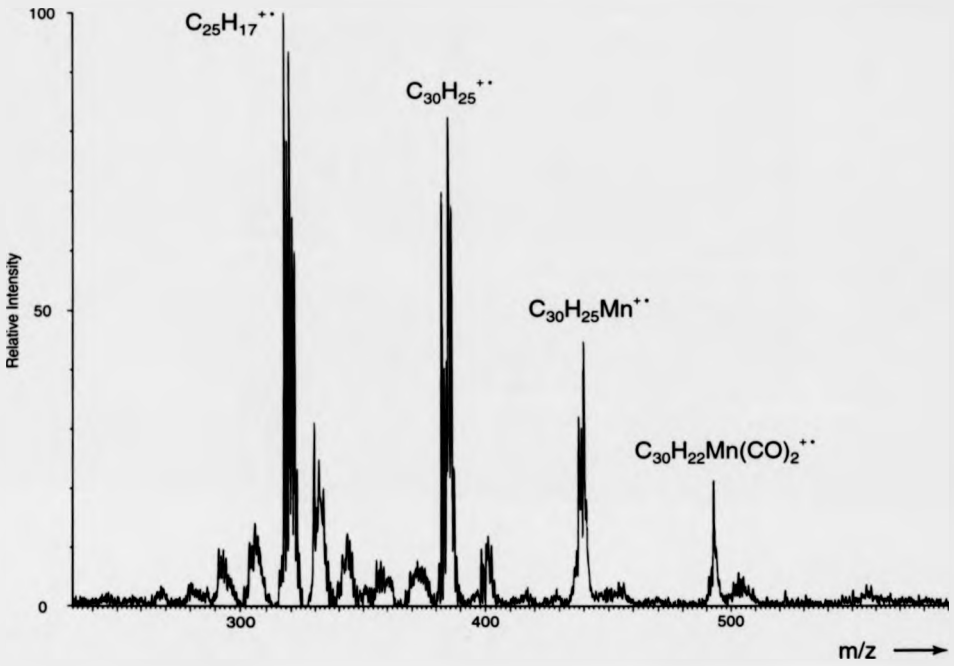

Figure 4: Positive-ion mass spectrum obtained on the Micromass ToFSpec E showing the fragmentation pattern of the organometallic precursor

The Cp_5Cp ligand, composed of $C_{30}H_{25}$, represents an interesting geometrical subunit. C_{30} is exactly half C_{60}, and it was perceived that it may be possible, through fragmenting the organometallic compound under LDI conditions, to generate highly energized fragments which may coalesce to generate fullerenes. The coalescence experiments have been conducted with the Kratos Kompact MALDI IV mass spectrometer and the resulting positive-ion LDI mass spectra are depicted in Figure 5 as a function of increasing laser irradiances. The laser irradiances required were significantly higher than that used in Figure 4 for a normal mass spectrum. As referred to earlier, the ion gate was used during

the course of these experiments, namely for the three spectra shown in Figure 5, in order to enhance the sensitivity of the instrument; this method prevents the reduction in sensitivity due to saturation of the detector. In this manner, the fullerenes formed in the gas-phase, produced in low abundances, may be more readily observed.

Figure 5a was recorded at a laser irradiance of 3.8×10^7 W cm^{-2} and Figure 5b was recorded using a laser irradiance of 6.6×10^7 W cm^{-2}, and the ion gate had been used to select ions between m/z 600 and m/z 900 in both cases. Figure 5c was obtained at a laser irradiance of 1.4×10^8 W cm^{-2}, after the ion gate had selected ions between m/z 600 and m/z 1200. The laser irradiance values are approximate, as they do not take into account possible degradation of the laser over time, and the laser was up to one year old at the time of these experiments. Figure 5a clearly shows that the generation of fullerenes occurs, with carbon cluster signals, spaced by 24 Da (C_2), being detected. $C_{50}^{+\bullet}$ is the most intense peak, while, surprisingly, $C_{60}^{+\bullet}$ and $C_{70}^{+\bullet}$ do not appear to be particularly favored. Figure 5b shows a similar tendency, but $C_{60}^{+\bullet}$ and $C_{70}^{+\bullet}$ are more pronounced than in Figure 5a, relative to adjacent signals. However, the signal-to-noise level can clearly be seen to be decreased with respect to Figure 5a. Indeed, the signals obtained at the higher laser irradiance used in Figure 5b were less intense than those obtained in Figure 5a, at a lower laser irradiance. At the highest laser irradiance, shown in Figure 5c, fullerenes are generated over a wider mass range, but the signal-to-noise ratio is at its lowest. A probable explanation for the trends observed is that increasing the laser irradiance increases the degree of fragmentation of the Cp_5Cp ligand. At the lowest irradiance, coalescence is likely to result in the formation of particular structures; Figure 4 shows an abundance of $C_{25}H_{17}^{+\bullet}$, for instance, and so $C_{50}^{+\bullet}$ is one of the most probable products, and it may be noted that $C_{50}^{+\bullet}$ is also a "magic number"[26,27] in $C_{60}^{+\bullet}$ dissociations. As the fragmentation increases, smaller

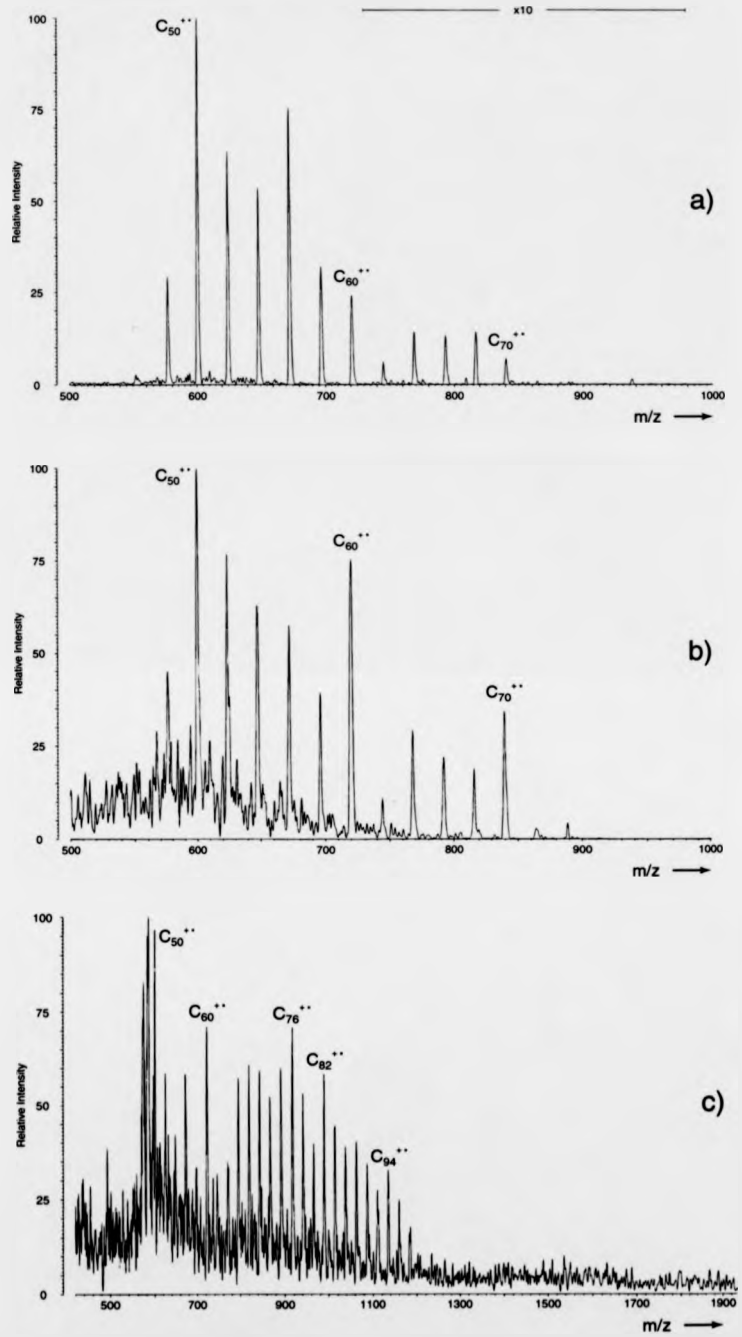

Figure 5: Positive-ion mass spectra obtained on the Kratos Kompact MALDI IV comparing the coalescence reactions as a function of increasing laser irradiance. Spectra a, b, and c were acquired using laser irradiances of 3.8×10^7 W cm^{-2}, 6.6×10^7 W cm^{-2}, and 1.4×10^8 W cm^{-2}, respectively.

carbon fragments are produced. With a large number of small carbon fragments being produced, the "selectivity" of the coalescence reactions changes, and the most stable carbon clusters become favored. However, at the same time the signal-to-noise ratio decreases because the formation process becomes less efficient. As the mean size of the particles decreases, the probability of a sufficient amount of collisions which result in reactions is reduced. Also, at increasing laser irradiances, the tendency of coalesced clusters to fragment also increases.

No metallofullerenes were detected in any of the spectra obtained. It is likely that the Cp_5Cp ligand is lost from the metal atom prior to further fragmentation, and this can account for the lack of presence of manganese in any of the fullerenes produced. Fullerene production, using the $[Cp_5CpMn(CO)_3]$ precursor, can be estimated to be two orders of magnitude lower than that observed when using pure fullerenes to generate higher fullerenes under LDI conditions. Unfortunately, the resolution of the Kompact MALDI IV is not sufficient to rule out the presence of hydrogen in the carbon clusters generated. The fact that the signals are narrow implies that any hydrogen content is likely to be very low, if there is indeed any hydrogen present at all. The experiments have revealed that coalescence does occur, resulting in the production of fullerenes (with a possible hydrogen content), following fragmentation of the organometallic precursor. Loss of the metal atom appears to precede further fragmentation, explaining the lack signals arising from metallofullerenes. The low yield of fullerenes overall is most likely to be due to the facile fragmentation of Cp_5Cp, making simple coalescence reactions less probable. At higher laser irradiances, fragmentation occurs to a greater extent and therefore more reactive collisions are required to build fullerene structures from smaller carbon fragments. The high degree of σ bonded hydrogen atoms may also play a role in reducing the yield of pure fullerenes, in an analogous

manner to $C_{60}H_{36}$ displaying a reduced tendency to coalesce to form higher fullerenes,[28] compared to pure C_{60}, as discussed in Chapter Four.

2.4 Summary

X-Ray crystallography revealed the structure of the compound $[Cp_5CpMn(CO)_3]$ and laser desorption/ionization mass spectrometry was used in an attempt to generate fullerenes from the organometallic precursor. The presence of hydrogen in the fullerenes generated could not be discounted, but due to the limitations of the instrumentation, it was not possible to establish whether or not an hydrogen was indeed present. No metallofullerenes were observed, which can be explained by the loss of the manganese atom during activation of the organometallic sample. At low laser irradiances, structures such as $C_{50}^{+\bullet}$ are clearly favored, and as the laser irradiance is increased, more commonly observed fullerenes such as $C_{60}^{+\bullet}$ and $C_{70}^{+\bullet}$ become increasingly intense. Increasing the laser irradiance further results in the formation of a range of fullerenes of higher mass, but another trend was observed where increasing the laser power decreases the signal-to-noise ratio. This can be explained by the greater number of interactions required for fullerene formation, as fragments become smaller due to the increased energy imparted to the organometallic precursor. The low yields for fullerene generation mirror the reduced tendency for $C_{60}H_{36}$ to undergo coalescence to form higher fullerenes,[28] and the large number of σ bonded hydrogen atoms in both $C_{60}H_{36}$ and $[Cp_5CpMn(CO)_3]$ may be partly responsible. Dissociation of the ligand bearing favorable structural features for the generation of fullerenes might also be of relevance to the low net yield of fullerenes. Due to the fact that the yield was so low, it is unlikely that the organometallic compound could be employed in future as a precursor for fullerene generation. It should be mentioned that fullerene

formation in these experiments is not determined purely by the carbon content of the target material. Recent coalescence experiments, performed in follow up by the group at the University of Warwick, which utilized polyaromatic hydrocarbons have provided clear evidence of the prevailing influence of the structure of the target material on the fullerene formation. This in turn provides support for the hypothesis correlating the geometric features of the Cp_5Cp ligand with the formation of fullerenes.

2.5 References

1) Kroto, H. W.; Heath, J. R.; O' Brien, S. C. O.; Curl, R. F.; Smalley, R. E. *Nature* **1985**, *318*, 162-163.

2) Yeretzian, C.; Hansen, K.; Diederich, F.; Whetten, R. L. *Nature* **1992**, *359*, 44-47.

3) Yeretzian, C.; Hansen, K.; Diederich, F.; Whetten, R. L. *Supplement to Z. Phys. D.* **1993**, *26*, S 300-304.

4) Hunter, J. M.; Fye, J. L.; Bolvin, N. M.; Jarrold, M. F. *J. Phys. Chem.* **1994**, *98*, 7440-7443.

5) Xie, Z. X.; Liu, Z. Y.; Wang, C. R.; Huang, R. B.; Lin, F. C.; Zheng, L. S. *J. Chem. Soc. - Faraday Transactions* **1995**, *91*, 987-990.

6) Zhu, L.; Wang, S.; Li, Y. *J. Chem. Phys.* **1994**, *101*, 8592-8595.

7) Liu, Z.-Y.; Wang, C.-R.; Huang, R.-B.; Zheng, L.-S. *Int. J. Mass Spectrom. Ion Processes* **1995**, *145*, 1-7.

8) Kubler, B.; Millon, E.; Gaumet, J. J.; Muller, J. F. *Fullerene Science and Technology* **1996**, *4*, 1247-1261.

9) Beck, R. D.; Weis, P.; Bräuchle, G.; Kappes, M. M. *J. Chem. Phys.* **1994**, *100*, 262-270.

10) Hansen, K.; Yeretzian, C.; Whetten, R. L. *Chem. Phys. Lett.* **1994**, *218*, 462-466.

11) Mitzner, R.; Winter, B.; Kusch, C.; Campbell, E. E. B.; Hertel, I. V. *Z. Phys. D* **1995**, *37*, 89-95.

12) Alexandrov, A. L.; Schweigert, V. A. *Chem. Phys. Lett.* **1996**, *263*, 551-558.

13) Onoe, J.; Takeuchi, K. *J. Mass Spectrom.* **1998**, *33*, 387-391.

14) Beck, R. D.; Weis, P.; Hirsch, A.; Lamparth, I. *J. Phys. Chem.* **1994**, *98*, 9683-9687.

15) Beck, R. D.; Stoermer, C.; Schulz, C.; Michel, R.; Weis, P.; Bräuchle, G.; Kappes, M. M. *J. Chem. Phys.* **1994**, *101*, 3243-3249.

16) Barrow, M. P.; Tower, N. J.; Taylor, R.; Drewello, T. *Chem. Phys. Lett.* **1998**, *293*, 302-308.

17) Al-Jafari, M. S.; Barrow, M. P.; Taylor, R.; Drewello, T. *Int. J. Mass Spectrom.* **1999**, *184*, L1-L4.

18) Hopwood, F. G.; Fisher, K. J.; Greenhill, P.; Willett, G. D.; Zhang, R. *J. Phys. Chem. B.* **1997**, *101*, 10704-10708.

19) Rose, H. R.; Dance, I. G.; Fisher, K. J.; Smith, D. R.; Willett, G. D.; Wilson, M. A. *J. Chem. Soc. Chem. Commun.* **1993**, 941.

20) McElvany, S. W.; Ross, M. M.; Goroff, N. S.; Diederich, F. *Science* **1993**, *259*, 1594-1596.

21) Campbell, E. E. B.; Tellgmann, R.; Wahl, F.; Prinzbach, H. *Int. J. Mass Spectrom. Ion Processes* **1994**, *136*, 209-214.

22) Chen, G.; Ma, S.; Cooks, R. G.; Bronstein, H. E.; Best, M. D.; Scott, L. T. *J. Mass Spectrom.* **1997**, *32*, 1305-1309.

23) Abdourazak, A. H.; Marcinow, Z.; Sygula, A.; Sygula, R.; Rabideau, P. W. *J. Am. Chem. Soc.* **1995**, *117*, 6410-6411.

24) Aihara, J.-i. *J. Am. Chem. Soc.* **1995**, *117*, 4130-4136.

25) Cozzolino, R.; Belgachem, O.; Drewello, T.; Käseberg, L.; Herzschuh, R.; Suslov, S.; Boltalina, O. *Eur. Mass Spectrom.* **1997**, *3*, 407-414.

26) Zimmerman, J. A.; Eyler, J. R.; Bach, S. B. H.; McElvany, S. W. *J. Chem. Phys.* **1991**, *94*, 3556-3562.

27) Laskin, J.; Lifshitz, C. *Int. J. Mass Spectrom. Ion Processes* **1994**, *138*, 95-106.

28) Möder, M.; Nüchter, M.; Ondruschka, B.; Czira, G.; Vékey, K.; Barrow, M. P.; Drewello, T. *Int. J. Mass Spectrom.* **2000**, *195/196*, 599-607.

Chapter Three

Delayed Ionization as the Cause of Interference Signals Observed in the Post Source Decay Spectra of Coalesced Carbon Clusters

3.1 Introduction

Coalescence of fullerenes is a well-known phenomenon,[1,2] typically studied using a laser desorption/ionization (LDI) ion source and often in conjunction with a time-of-flight (ToF) mass spectrometer. Time-of-flight mass spectrometry is perfectly suited to this type of experiment, due to the "pulsed" nature of ion generation. LDI-ToF instruments are used in fullerene research often because of the suitability of laser desorption/ionization as an ionization technique and also because of the additional possibility of using a matrix for "soft" ionization.[3-10] Use of a matrix results in the ionization technique known as matrix-assisted laser desorption/ionization (MALDI), which makes it possible to study more labile species, with particular attention being paid to fullerene derivatives. In order to prepare a target surface for laser desorption/ionization, a solid-phase fullerene coating must be applied to a slide which can then be inserted into the ion source; this is usually prepared by dissolving the desired fullerene in toluene, and then spotting the resulting solution on to a metal slide, allowing the solvent to evaporate and leave the thin, fullerene layer behind. The sample is irradiated by the laser, and a plume of neutral species and ions expands away from the target surface. It is in this plume that coalescence reactions occur. The mechanism for coalescence is of current research interest,[11-13] and is believed to involve fusion of at least one ionic species and one neutral species[13] or the fusion of two, excited, neutral species.[12] Sample quantity is important for such reactions, as enough sample must be desorbed for collisions to occur in the gas-phase before coalescence can occur. The newly formed carbon cluster may then undergo cooling via the loss of successive C_2 units (a characteristic associated with fullerenes), and the loss of C_{2n} units is possible as well, albeit to a lesser extent.[14-16] Uptake of C_2 units by coalesced species can also occur, resulting in carbon clusters consisting of a higher number of carbon atoms than would be obtained

via the simple fusion of two precursor fullerenes. By studying the fragmentation pattern of such coalesced species, it is possible to gain further insight into its structure and the mechanism of their formation.

The structure of coalesced species is a subject that attracts much interest. Mass spectrometry is one of the leading analytical methods in the investigation of fullerenes, and so it is natural that mass spectrometry is used for structure elucidation of coalesced species in the gas-phase. Post source decay (PSD)[17,18] experiments would be performed in order to investigate the stability of the coalesced species and to determine the structure of the carbon cluster, through examination of the fragmentation pattern. Post source decay is an important, new method in mass spectrometry, used for structure elucidation. This method competes with collision-induced dissociation (CID)[19-22] as a method for analyzing the fragmentation of ions after they have left the ion source. PSD involves the selection of an ion or ions (via the use of appropriate instrumentation), so that all other ions, such as the fragments generated in the ion source, are filtered out. The resulting spectrum should consist entirely of only the selected ion or ions, and any fragment ions that arose from fragmentation during flight through the flight tube once the ions have left the ion source, hence the term "post source decay." Fragment ions formed in the ion source should be accelerated into the flight tube with the maximum kinetic energy provided by the accelerating potential. However, any daughter ions that result from fragmentation in the flight tube (i.e. after acceleration) will continue with the same velocity as the parent ion, albeit with a lower kinetic energy. Should the flight path be linear, the daughter ion will arrive at the detector at the same time as the parent ion would have, and so, when using a time-of-flight analyzer, the resulting spectrum will appear to show signals resulting from the parent ion alone. It is therefore necessary to separate the ions by kinetic energy when

conducting a PSD experiment, so that it is possible to distinguish between the parent ion and the daughter ions produced during flight. This separation is achieved using a "reflectron."[23-29] A reflectron is a series of electrodes in a straight path, which are used to define a potential gradient, which may be of a linear or a curved gradient. Ions with high kinetic energy penetrate further into the field than those ions of a lower kinetic energy before being reflected out of the reflectron again. This has two consequences. The first consequence is that when two ions of the same mass, but of slightly different kinetic energy, enter the reflectron they will do so at slightly different times due to the difference in their velocities. It is possible to focus the ions so that they reach the detector at the same time, by taking advantage of the difference in distances penetrated into the reflectron field.[30,31] This improves resolution, as the energy spread for ions of the same mass is compensated for. The second consequence of the use of a reflectron is that ions of the same velocity but different mass (such as a daughter ion, produced through PSD, and a parent ion) will be separated out. The ions enter the reflectron at the same time, due to their identical velocities, but as they possess differing kinetic energies, the ions travel different distances against the field in the reflectron. As a result, the ions are separated out in the reflectron so that they will reach the detector at different times. The result is that it is then possible to distinguish between daughter ions formed via post source decay and their respective parent ions. In general, experiments in which daughter ions are sampled from a selected parent ion is commonly referred to as "tandem mass spectrometry" or "MS/MS."

While CID involves the use of collision gases to convert part of the particle's translational energy to internal energy, resulting in fragmentation of the selected ion or ions, PSD does not. Post source decay involves the decomposition of metastable ions.

Some instrumentational arrangements allow for air to be bled gently into the flight tube, to increase the internal pressure slightly, so that fragmentation is facilitated; the definitions of PSD and CID then become less distinct. A "normal" mass spectrum will include signals arising from the parent ions and a variety of fragmentation processes. A PSD spectrum will exhibit the fragmentation pattern of only the selected ion(s), and therefore provide information on the stability and structure of the selected species alone.

The initial intention of this investigation was to deduce whether coalesced species were larger, closed-shell fullerenes, or whether they were "dumb-bell shaped" structures, composed of two distinct, fullerene moieties connected to one another via bridging bonds. All the evidence to date appeared to signify that pure fullerenes coalesce to form larger, closed-shell fullerenes, although dumb-bell structures may be formed during the course of some reactions, such as the photoirradiation of certain fullerene derivatives. Post source decay was the experimental technique of choice, as it would be possible to correlate fragments with their respective parent ions, and so an LDI ToF mass spectrometer could be used for the generation and analysis of coalesced species. Should the most stable fragments resemble the precursor species used during coalescence, this would indicate that the structure of the coalesced species was dumb-bell like. The coalesced species would consist of two precursor structures, bonded to one another by a small number of bridging bonds which are the most likely candidates for bond cleavage upon fragmentation. If most fragmentation occurred via C_2 loss and the most stable fragments at lower masses were simply the most favorable structures (such as C_{60}) regardless of what precursor was used during the fusion process, this would appear to indicate that the coalesced species had no memory of its precursor components; the structure would be likely to be a closed shell fullerene. However, during the course of the experiments, results were obtained that

appeared to contradict all previous evidence in the literature, and seemed to signify that the coalesced carbon cluster possessed a "memory" of the precursor species. Further examination was required in order to resolve the apparently conflicting evidence.

3.2 Experimental

Most experiments were performed using a Kratos Kompact MALDI IV mass spectrometer. A schematic diagram of the instrument is shown in Figure 1. This instrument consists of an LDI source, used in conjunction with a ToF analyzer. A nitrogen laser (337 nm, 3 ns pulse width) is used for the desorption/ionization of the sample, and the resulting ions are accelerated out of the source into the flight tube using a potential of either 5 kV or 20 kV, with 20 kV being the potential of choice and is used throughout the course of these experiments. A curved field reflectron[32] is employed in the instrument; curved field reflectrons are preferred over linear field reflectrons in instruments where PSD studies are to be conducted. This is due to the fact that reflectrons which use a curved field do not need to be "stepped" as for linear field reflectrons, in order to direct all fragment ions to the detector. A curved field reflectron focuses all fragment ions on to the detector during a single spectrum acquisition. The final PSD spectrum derived from an instrument which uses a linear field reflectron actually consists of two or more "stitched" spectra, where the reflectron potentials were varied. The disadvantage of a curved field reflectron is the decrease in sensitivity, compared to a linear field reflectron. An "ion gate" is positioned in the flight tube, before the reflectron, and consists of two electrodes. When the ion gate is in operation, a potential is applied to these electrodes in order to deflect all ions. The gate is on when all ions other than the selected ion(s) would reach the ion gate position at that point in time; the gate is off at the time when the selected ion(s) would reach the ion gate.

Hence, the mass selection of ions is time based, for the reason that the final mass analysis (and hence the principle of the ToF instrument) is time based. The resulting spectrum, when the ion gate is operated, should display only the selected ions and any daughter ions produced by fragmentation in the flight tube, after having passed the ion gate. The instrument can be used in either "linear" mode (bypassing the reflectron, where all ions have a straight path down the flight tube) or "reflectron" mode (where the reflectron reflects all ions, which then travel towards a separate electron multiplier). It is necessary to use reflectron mode in order to operate the ion gate, however. Figure 2 shows a test of the selectivity of the ion gate, using a polyethyleneglycol (PEG) sample. Figure 2a shows the distribution associated with this sample of PEG 1000. In Figure 2b, the ions of mass 1010 Da are selected, and one additional signal corresponding to ions of mass 966 Da is observed. The margin of error associated with the ion gate in this instrument can be taken as being no greater than ±44 Da therefore. This is a large margin of error, but is sufficient for the purposes of these experiments, though signals may be of an order of a few Th (Thomson, the unit relating to m/z values) wide.

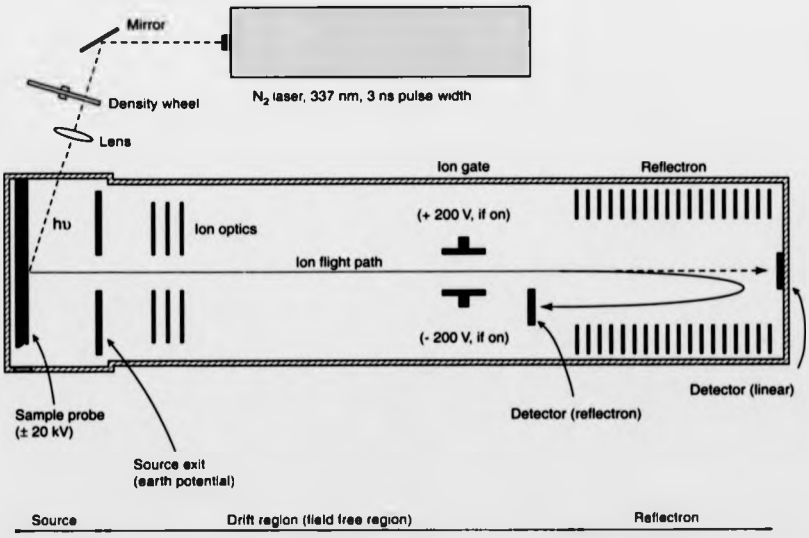

Figure 1: Schematic diagram of the Kratos Kompact MALDI IV

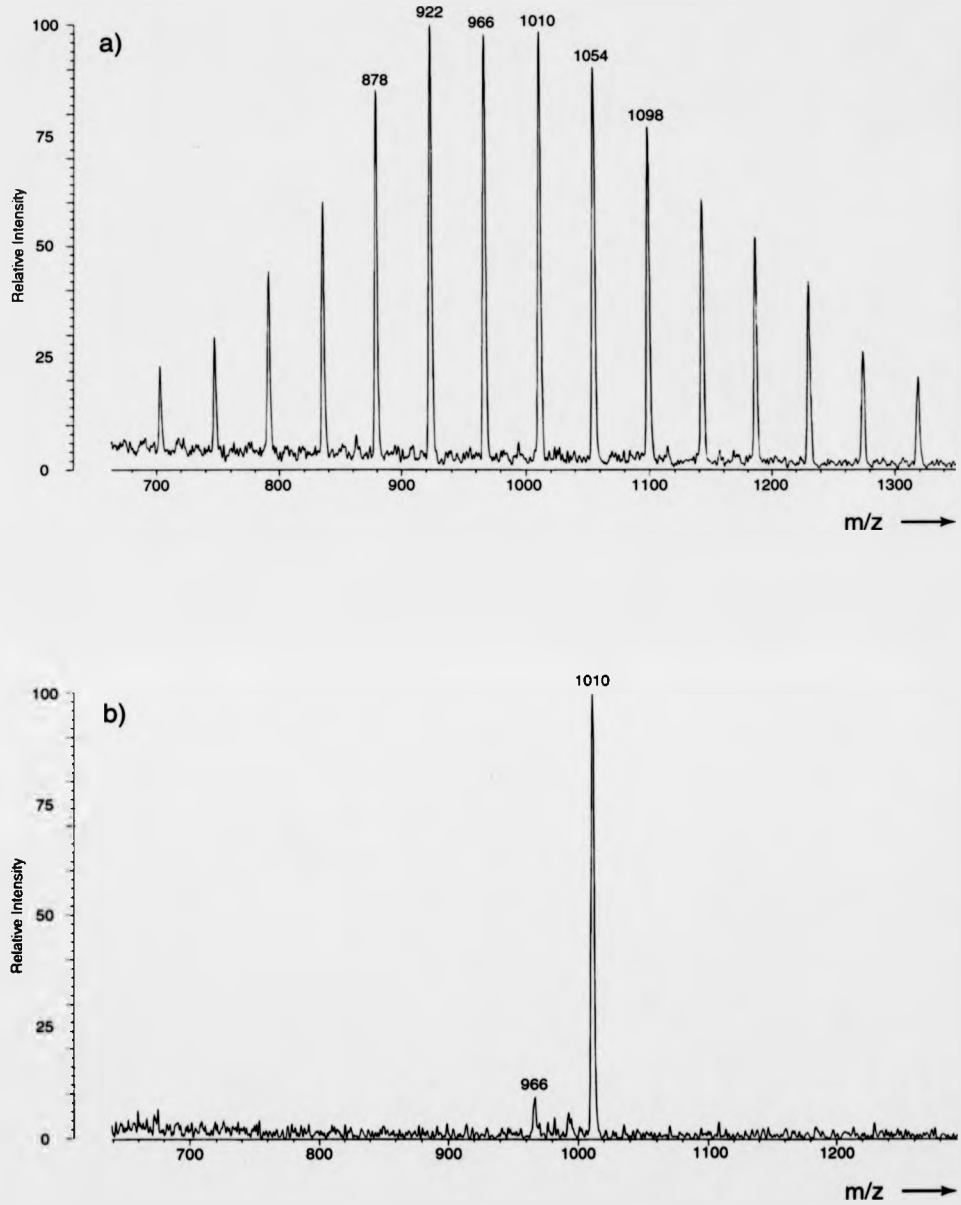

Figure 2: Positive-ion mode mass spectra obtained used polyethyleneglycol (PEG) 1000. Spectrum a was recorded as a normal mass spectrum, while spectrum b was obtained using the ion gate to select ions of m/z 1010 only. The selectivity of the ion gate is thus demonstrated, as is the fact that the ion gate is working as expected.

Further experiments were performed using a Micromass AutoSpec oa-ToF, and the spectra were obtained with the assistance of M. Green (Micromass Ltd., Manchester, UK). The instrument uses a EBE ToF geometry where the ToF analyzer is orthogonal to the previous flight path, and an LDI ion source was used. Figure 3 shows the instrumental set up used. Ions were generated using a nitrogen laser and then accelerated by an 8 kV accelerating potential. Ions of a selected energy (usually 8 keV) must first traverse the first electrostatic sector, E1, and then ions of a certain mass may be selected by the magnetic sector, B. Alternatively, all ions (of the selected energy) may be allowed the traverse the magnetic sector by using a "bypass tube" which bypasses the magnetic sector. Ions then pass through the second electrostatic sector, E2. Ions may then be decelerated (resulting in an energy of 800 eV in the present case) upon entry to a collision cell, which is used for collision-induced dissociation experiments. The collision cell precedes the pusher electrode, which is used to accelerate orthogonally all ions along the axis of the ToF analyzer for the final time-of-flight analysis. All ions then continue to the orthogonal ToF analyzer, where they are accelerated perpendicularly from their flight path by a "pusher" electrode. The orthogonal ToF arrangement has the advantage that a slight energy spread (and hence differing temporal displacements) is compensated for; the paths of the ions of differing energies (but of the same "ion packet") run parallel to one another, whereas before the paths were along the same axis but with a lag between the ions of different energies. Angular spread (which becomes a temporal spread, following orthogonal acceleration) is not compensated for by an orthogonal ToF arrangement, but angular spread is more easily minimized by use of Einzel lenses duirng flight.

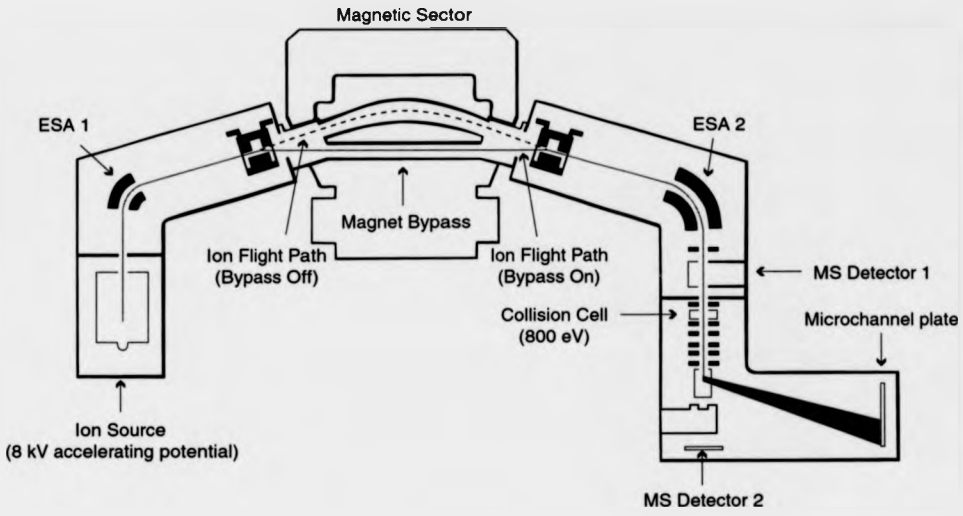

Figure 3: Schematic diagram of the Micromass AutoSpec oa-ToF

3.3 Results and Discussion

The LDI mass spectrum of $C_{60}^{+\bullet}$ can be seen in Figure 4a. The distribution of coalesced species can clearly be seen, with the loss or uptake of successive C_2 (and/or C_{2n}) units also visible. The loss of C_2 units from the coalesced species provides strong evidence that it is indeed a larger fullerene that has been formed. Figures 4b and 4c show the resulting PSD spectra when a region of the dimeric coalesced species and the trimeric species are selected using the ion gate. The intensity of the $C_{60}^{+\bullet}$ signals in each case is unexpected, and would seem to indicate that the coalesced species are in fact very unstable and dissociate very efficiently. This is in direct contradiction to the literature. The mass shift associated with these signals (~50 Da and ~100 Da respectively) was also unexpected, and was initially assigned to a calibration fault associated with calibration for PSD spectra. Though mass shifts can occasionally occur, particularly with linear field reflectron instruments, due to

metastable decay of ions in the flight tube,[18] mass shifts of such magnitude are unheard of. It also became apparent that the mass shift would increase as the ion gate was used to select higher masses. The validity of the assignment of the signal associated with $C_{60}^{+\bullet}$ was verified by counting successive C_2 losses from the coalesced species, and the fragmentation pattern fitted that which is expected for $C_{60}^{+\bullet}$. Figure 4c also exhibits an enhanced $C_{50}^{+\bullet}$ signal, as is often associated with the fragmentation of $C_{60}^{+\bullet}$ at high laser fluences. The intensities of the fullerene daughter ion signals seem to imply that the trimeric and dimeric species decay very efficiently under the applied PSD conditions. The extent to which this apparent fragmentation is observed is unexpected as the parent ions are not collisionally-activated to promote dissociation. The results seem to indicate that $C_{60}^{+\bullet}$ is the fragment which is preferentially formed as the coalesced species dissociates, and this may be due either to the dimeric species consisting of two, distinct moieties, leading to a "memory" of the precursor. Alternatively, at this stage of the investigation, the observation of $C_{60}^{+\bullet}$ may simply reflect this daughter ion as being amongst the most energetically favored structures. However, the observation of C_2 loss from these coalesced species, by contrast, supports the theory that they are indeed larger fullerenes.

Further investigation involved the use of C_{70} and C_{84} as precursors for coalescence, forming their respective dimeric species. A comparison of PSD experiments conducted using C_{60}, C_{70}, and C_{84} would provide additional insight into whether the dimers possessed a memory of their respective precursors, or whether the most energetically favored fragment (C_{60} for instance) would predominate in every case. Figure 5 shows the PSD spectra of the C_{60}, C_{70}, and C_{84} dimers, respectively. A region of each dimeric distribution is selected using the ion gate. Figures 5a, 5b, and 5c show strong signals for the fragments of $C_{60}^{+\bullet}$, $C_{70}^{+\bullet}$, and $C_{84}^{+\bullet}$, respectively, along with their distinctive fragmentation patterns. The

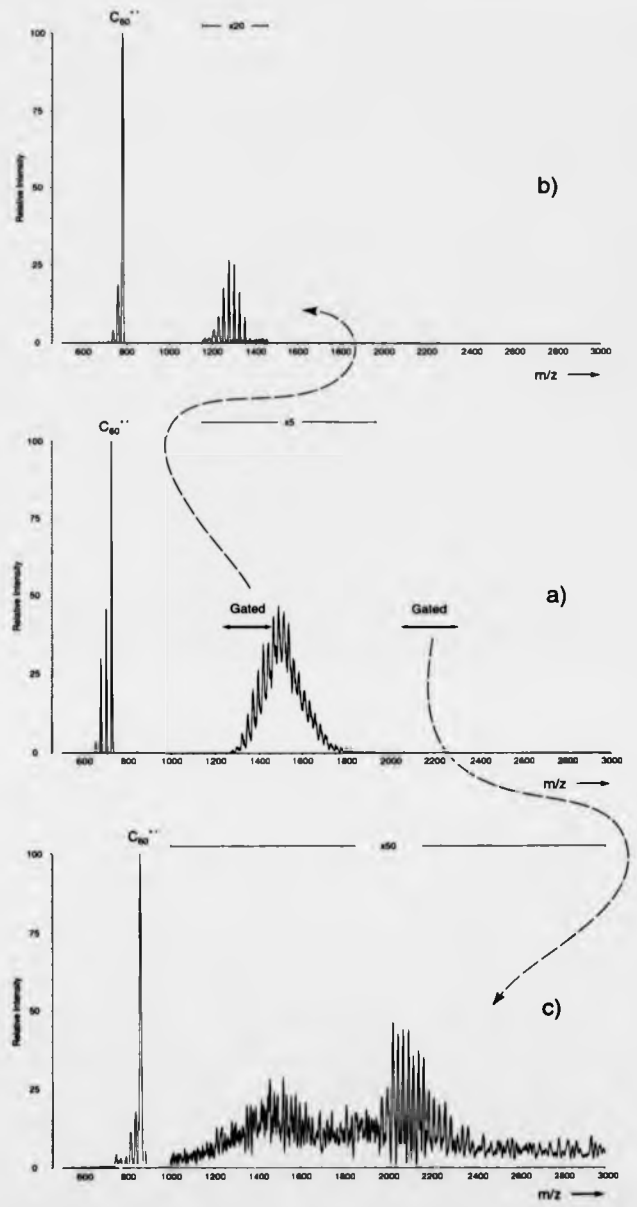

Figure 4: Time-of-flight mass spectra recorded following the laser desorption/ ionization of C_{60}. Spectrum a clearly shows the presence of coalescence products which result from reactions within the ion source. Spectrum b resulted from the selection of ions constituting some of the dimeric products; an intense apparent fragment ion signal can be observed which is attributed to $C_{60}^{+\bullet}$. Spectrum c was recorded following the selection of ions which corresponded with trimeric species; an intense fragment ion signal attributed to $C_{60}^{+\bullet}$ is again observed. In each case, C_2 loss may be observed as a prominent fragmentation channel.

assignment of these signals is unambiguous, as their individual fragmentation patterns are very distinctive. However, these conclusions then strongly lead to the deduction that each of the dimeric species retains structural elements of their respective precursors, which is in contrast to the literature. The enhanced intensity of the fragment ion signals is again unexpected and seem improbable, but again lead to the possible conclusion that the coalesced species are very labile. The mass shifts that were observed are far greater than would be expected should there be a calibration problem. These discrepancies with the known masses occasionally reach 300 Da, and these mass shifts do not occur when non-fullerene samples were tested. Slight mass shifts can be observed when conducting PSD experiments, due to errors associated with the temporal focusing of daughter ions arising from metastable decay, but such mass shifts almost never rise above tens of Daltons, and typically consist of about 5 Da. It is therefore not likely to be a calibration fault, and the mass shifts appear to be associated only with fullerene samples; such artifacts have not been observed using non-fullerene samples. The intensity of the fragment ion signals, the significant mass shifts, and the contradiction of the literature all lead to the conclusion that the "fragment ion signals" observed cannot be explained as resulting from post source decay of the coalesced species.

To test this theory, a series of PSD spectra of $C_{84}^{+\bullet}$ was recorded where C_{60} and C_{70} were used to dope some of the C_{84} samples. Three PSD spectra are shown in Figure 6. Figure 6a shows the spectrum recorded using C_{84} alone on the slide, and the fragmentation pattern is that which would be expected for a C_{84} sample. Figure 6b shows the spectrum obtained when the C_{84} sample was doped with an equal amount of C_{60}, and Figure 6c shows the resulting spectrum when the C_{84} sample was doped with an equal amount of C_{70}. While Figure 6a resembles a spectrum of $C_{84}^{+\bullet}$ alone, with its resulting fragments, Figures

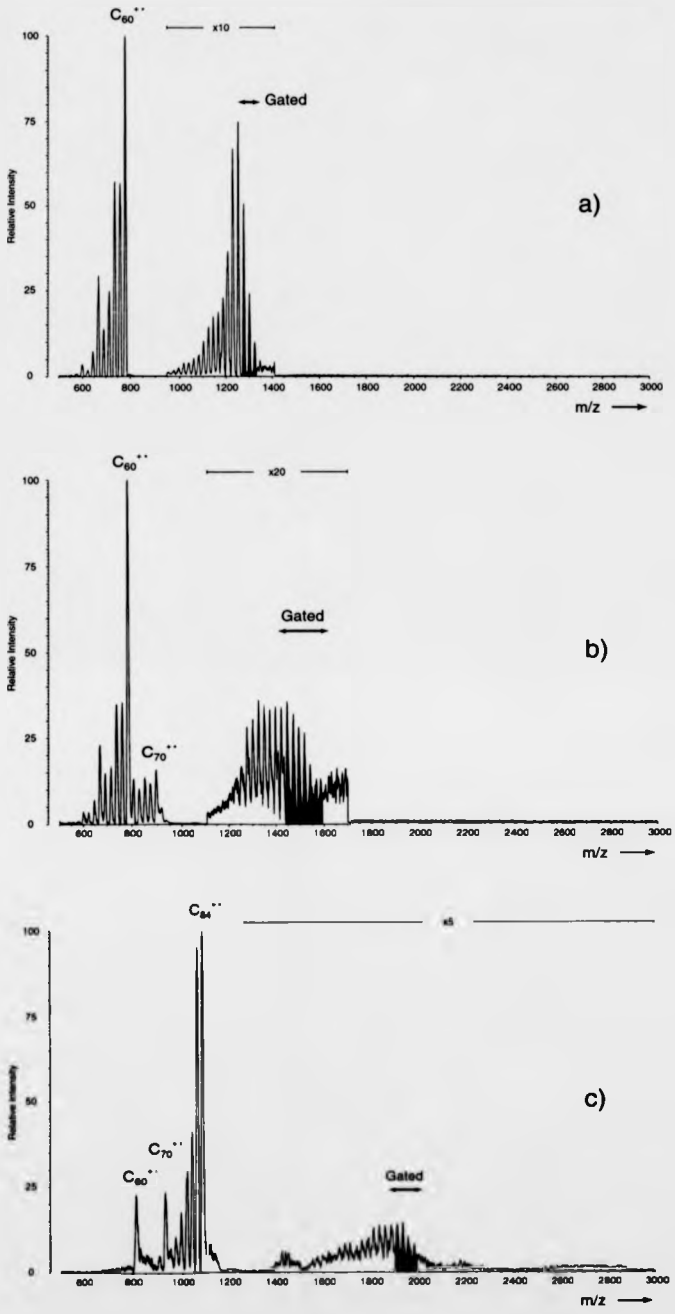

Figure 5: Post source decay (PSD) spectra recorded following the selection of dimeric species. Spectrum a was obtained using C_{60} as the sample for ablation, while spectrum b was recorded using C_{70}, and spectrum c was obtained using C_{84}. In each case, an intense fragment ion is observed which appears to correspond to the precursor material used.

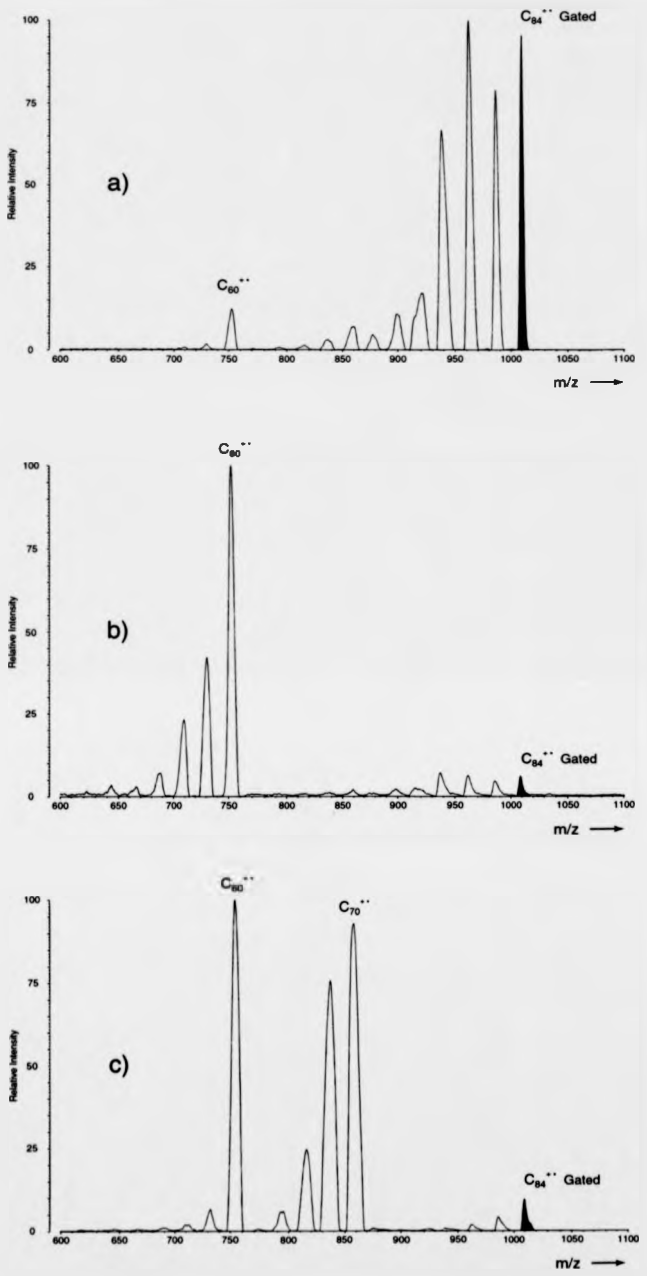

Figure 6: Post source decay spectra recorded following the selection of the C_{84}^{2+} ion. Spectrum a was obtained using a pure C_{84} sample, while spectra b and c were acquired after the C_{84} sample had been doped with C_{60} and C_{70}, respectively. Doping the target material has a significant effect on the appearance of the PSD spectrum, though the ion gate should prevent interference from the dopant material.

6b and 6c resemble such a spectrum but with the corresponding C_{60} or C_{70} spectrum overlaid. The intensity of the fragments ion signals from $C_{84}^{+\bullet}$ differs slightly between the three spectra, but this can be attributed to experimental error caused by poor spot-to-spot reproducibility. The significant increase in the intensity of the $C_{60}^{+\bullet}$ and the $C_{70}^{+\bullet}$ signals in Figures 6b and 6c respectively are a clear indication that the ion gate is not preventing the passage of such ions, as the fragmentation of C_{84} should not increase by adding a dopant. Neither should adding a particular dopant increase the probability of C_{84} dissociating to form the ionic form of that dopant. However, referring back to Figure 2, it is clear that there is no fault with the ion gate's performance, and even an error of ±44 Da is not enough to account for the passage of the $C_{60}^{+\bullet}$ and $C_{70}^{+\bullet}$ ions. Mass shifts are again evident in each of the three spectra, when looking at the $C_{60}^{+\bullet}$ and $C_{70}^{+\bullet}$ ions and their corresponding fragments. This should not normally be the case for a PSD spectrum. The conclusion that can be drawn is that neither the $C_{60}^{+\bullet}$ ions nor the $C_{70}^{+\bullet}$ ions (and their fragments) result from PSD, and that the signals do not arise from poor selectivity of the ion gate. Nevertheless, these ions are not filtered out by using the ion gate, and they must therefore be produced in the ion source and pass the ion gate at the same time as the selected ion.

If the C_{60} and C_{70} neutral species were to be longer lived in the ion source than expected, ionize, and then be accelerated out into the flight tube at a later time than normal, then two "time delays" would be involved. The first time delay would be simply due to the delay in ionization, where the neutral must exist as an excited species prior to ionization. Indeed "delayed ionization" is a known phenomenon associated with fullerenes, first cited by Campbell et al.[33,34] Since that time, delayed ionization has become an increasingly cited observation.[16,35-38] Most delayed ionization studies are performed using variations of LDI-ToF arrangements,[15,39-43] although EI has also been utilized as an alternative ionization

method,[44,45] and the radiative cooling of C_{60} in a storage ring has also been investigated.[46] Though most LDI experiments are performed using ultra-violet (UV) lasers, some investigations into the delayed ionization of various fullerenes have been conducted with infra-red (IR) lasers.[47-51] The delayed ionization of higher fullerenes has been studied[52] and such a phenomenon has also been observed for smaller fullerenes such as C_{36}.[15] In analogy to the delayed electron detachment from neutral C_{60}, delayed electron detachment from C_{60}^{*} has also been studied.[53] Fullerenes have been shown to exist as excited neutral species for tens of microseconds in many LDI-ToF experiments, but in some cases, lifetimes of an order of hundreds of microseconds have been cited,[43,47,50,54] and Hansen et al. observed ions after a 300 μs delay.[43] The exact mechanism for delayed ionization is not yet understood, but is the focal point of such investigative work. Indeed, despite such interest in the mechanism, Campbell and Levine recently published a review of the topic and appealed for further experiments to be conducted.[55] The shape of the asymmetric tail has been investigated with the hope of providing more information about the rate constants involved.[34,40,50,56] It has often been proposed that more than one rate constant is involved and that even a continuum of rate constants may be required to describe the tail's appearance.[43,57] Currently, two main models exist, where one is based on an analog of thermionic emission,[58] and one is based on the existence of long lived triplet states, although the involvement of Rydberg states has also been proposed.[44,45,59] Regardless, it is widely agreed that autoionization occurs, where coupling is required between vibrational and electronic energy modes.[60] It is the latter model which tends to attract more support, although both have strong advocates. Comparisons have been drawn between delayed ionization in fullerenes and thermionic emission from metal clusters. Klots' finite heat bath model for thermionic emission[61-64] is frequently cited as a suitable model.[34,40] Though there is a lack of consensus for the mechanism of delayed ionization, it has become generally

accepted that it involves the formation of triplet states.[35,41] This more commonly cited mechanism, involving triplet states, is outlined in Figure 7. As a photon is absorbed after photoirradiation of the sample, the fullerene is excited to a singlet state, with less electronic energy than the ionization threshold (7.6 eV); the first singlet state exists at approximately 2 eV[41,50,65,66] and the lowest triplet state exists at approximately 1.7 eV.[35,67] Unless continuous wave lasers are used, a time delay between laser pulses of the order of nanoseconds is most frequently involved and each time-of-flight experiment is the result of a single laser pulse. Excited states will not exist for the full length of time between laser pulses and, therefore, all excitation and energy redistribution processes must occur within the timeframe of each time-of-flight experiment, which will typically last for an order of tens of microseconds. Intersystem crossing (ISC)[36] can occur within this time scale and this leads to the formation of a triplet state of lower energy, with a near unit quantum yield.[41] This process continues until the fullerene exists in a very low energy triplet state, with the first triplet state existing at approximately 1.7 eV. As a result, most of the total energy put into the system ends up as vibrational energy. It may be noted as an example that the lifetime of the lowest triplet state, with a total vibronic energy of 4 eV, has been determined to be 40 μs.[68] Due to high number of degrees of freedom possessed by fullerenes, it is possible for this vibrational energy to be accommodated without the occurrence of fragmentation; the excess energy is accommodated as vibrational energy; there is evidence that C_{60} may accommodate up to 50 eV in internal energy,[40,51,69,70] as, with 174 degrees of freedom, the number of quanta excited per mode is relatively low.[70] Competing processes are involved during the photoirradiation of a fullerene sample. If there is a rapid uptake of photons by the fullerene before ISC can occur, the fullerene will be electronically excited beyond the ionization threshold and ionization will occur (left hand side of the Figure). If ISC occurs before another photon can be absorbed (middle section of the Figure), then the low energy

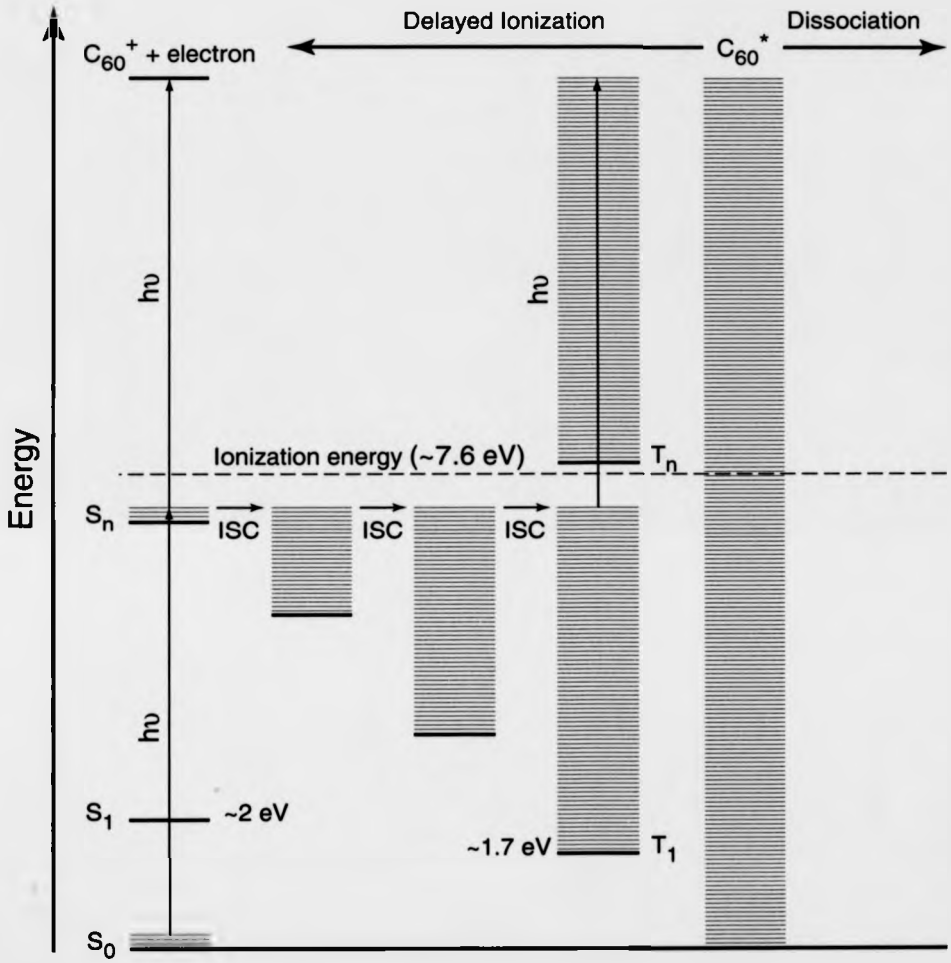

Figure 7: Representation of the excited states of C_{60}. Competing energetic processes are shown, following the absorption of photons. Excitation to a singlet state which lies below the ionization threshold is the primary step, followed by either further excitation, leading to ionization, or rapid intersystem conversion to triplet states of lower energy; excess energy is converted to vibrational energy. The involvement of singlet and triplet states may also be compared to the electronic ground state, where all internal energy provided by photoirradiation is converted to vibrational energy.

triplet states will be formed, and further excitation will electronically excite enough to ionize the fullerene, while the increased vibrational energy means that fragmentation may also occur. Should all energy be converted to vibrational energy (right hand side of the Figure), and the fullerene exists in a superexcited ground state, the fullerene will undergo dissociation or autoionization.

The second time delay incurred would result from the movement of the excited neutral as part of the expanding plume away from the target, and hence with a velocity vector towards the source exit. This would then mean that at the time of ionization, the neutral would be at a position of lower potential in the source, and after its acceleration out of the source following ionization, it would enter the flight tube with a lower kinetic energy than other ions. The final result of this second effect is that the ion possesses a lower velocity than normal. The coupling of these two "delays" (a delay in ionization, and then a possession of a lower velocity by the ion) could facilitate the possibility of a "delayed ion" reaching the ion gate, which is purely time based, at the same time as the selected ion or ions. However, upon passing the ion gate, the delayed ion would still possess a higher velocity than the selected ion (even when allowing for the slightly decreased kinetic energy of the delayed ion), and so the delayed ion would still reach the detector before the selected ion. This means that when using the ion gate to select an ion at an arbitrary m/z value, even if no ion is present at that m/z value, a C_{60} neutral may still undergo a delay in ionization, pass the ion gate at the time when the electrodes are at earth potential (i.e. when the gate is "open"), and then reach the detector. Such a species would be recorded at a much lower mass than the "selected ion," due to its greater velocity than the selected ion of higher mass. Thus, the fullerene ion may appear to be a fragment ion in a PSD spectrum. Figure 8 illustrates this hypothesis pictorially.

a)

m_1 drifts as a neutral, m_2 enters flight tube following ionization and acceleration

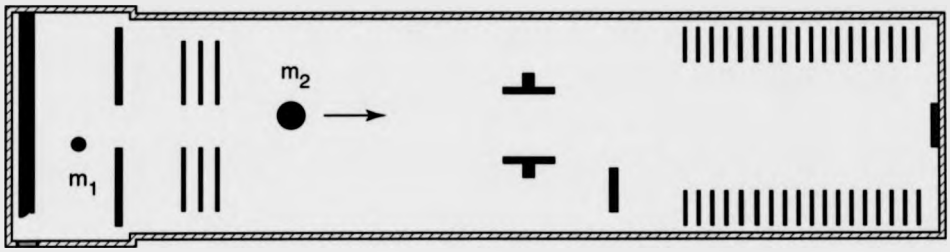

b)

m_1 ionizes and accelerates into flight tube, ions arrive at ion gate at same time

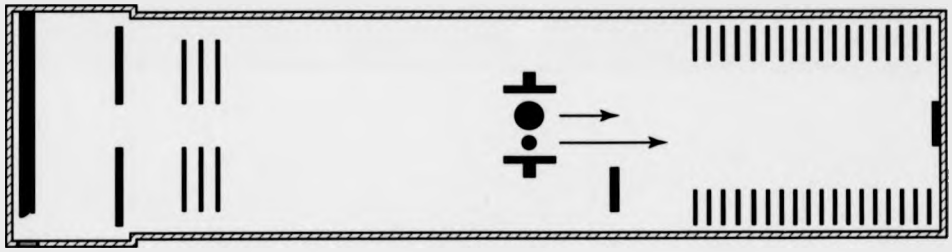

c)

ions traverse ion gate, but reach detector at different times due to different velocities

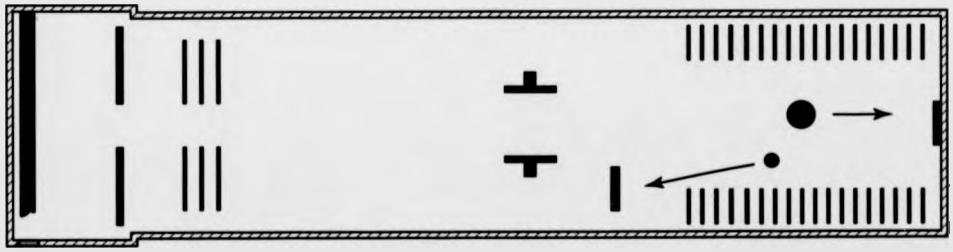

Figure 8: Schematic representation of the flight of delayed ions through the instrument in relation to the flight of prompt ions, according to the proposed theory.

As the ion gate is set to pass ions of increasing mass, the mass shift of interference signals, such as those arising from $C_{60}^{+\bullet}$, becomes greater; this would be because the total delay time needed for $C_{60}^{+\bullet}$ to pass the ion gate would increase. The delay time for ionization and the velocity of the delayed ion are therefore coupled, and both factors combine to influence the total flight time of the species. It is also notable that as the ion gate is positioned at higher masses, the intensity of the delayed ions decreases. This is because the probability of ionization decreases with time, and so ions that have existed for long periods as excited neutrals are less abundant than ions that have ionized promptly. It must be emphasized that these findings cannot be explained by such an energy deficit, as mentioned above. The artifacts observed when using fullerene samples are not observed when using non-fullerene samples; in addition, such artifact signals are not observed when using fullerene derivative samples. A further test of the delayed ionization hypothesis is to record spectra under similar conditions but using the negative-ion mode, as delayed ionization can only occur during cation formation. In consistency with the hypothesis, no artifacts are observed in the negative-ion mode, when using the same sample, the same laser irradiance, and the same gate setting. Even by altering the parameters, such as the laser irradiance, it is still impossible to observe this phenomenon in the negative-ion mode. In summary, the phenomenon is observed only for pure fullerene samples which are analyzed in the positive-ion mode.

In order to further discredit the argument that the results could be explained by an energy spread alone (albeit only for fullerenes and only in the positive-ion mode), calculations were used to test the energy spread theory. The motion of the molecule may be considered in three stages. The first stage consists of the neutral molecule drifting in the ion source prior to ionization, with a set drift velocity (also referred to as the initial

velocity) following laser ablation. For most molecules, the time spent as a neutral in the ion source is extremely short and is insignificant. For delayed ions, this time is of an order of microseconds and is therefore significant, as the total flight time is typically of an order of about 10^{-5} seconds. The second stage of motion of the molecule is acceleration in the ion source after ionization. The final kinetic energy of the ion depends on how long the ion is accelerated for. "Prompt" ions will ionize at or very close to the target where the field will be close to or equal to 20 kV, while "delayed" ions will move through the ion source as a neutral, ionize at a lower potential, and therefore leave the ion source with less than 20 keV. The final stage of the molecule's flight, for a linear flight path, will be its motion through the field free region (FFR), representing the flight tube of the instrument, with a constant, final velocity. For the purposes of these calculations, the reflectron does not need to be modeled, as the region of interest in the instrument is between the target (in the ion source) and the ion gate in the FFR; the aim of the calculations is to demonstrate how delayed ions may arrive at the ion gate at the same time as a prompt ion of greater mass.

For the purposes of the following calculations, the motion of the molecule will be considered in three separate stages. At time t_0, the laser ablates the surface of the target and the molecule exists as a neutral until time t_i, at which point it undergoes ionization. The neutral drifts with a velocity of v_d; the magnitude of the drift velocity has been discussed earlier. Between the time of ionization, t_i, and the time at which the ion exits the ion source, t_e, acceleration occurs, due to the force acting on the ion which is due to the accelerating potential in the ion source. The ion then leaves the ion source with a final velocity v_f, and travels with constant velocity in the FFR, arriving at the ion gate at time t_g (not referred to in the following calculations). Graphs may be plotted to describe the three

stages of motion of the molecule, and by overlaying plots for ions of different mass or delay times, it is possible to compare the relative positions of the neutrals/ions in the mass spectrometer at any point in time.

In general, velocity may be expressed as:

$$v(t) = \int_{t_1}^{t_2} a(t) \cdot dt \qquad (1)$$

where a is the acceleration (in m s^{-2}) of the particle and t corresponds to time (in seconds).

Displacement, s (in m), may in turn be described by:

$$s(t) = \int_{t_1}^{t_2} v(t) \cdot dt = \int_{t_1}^{t_2} \left(v_d + a(t - t_1)\right) \cdot dt \qquad (2)$$

where v is the velocity (in m s^{-1}) of the particle and t corresponds to time (in seconds).

The motion of a particle during the time period from photoirradiation to a chosen time after leaving the ion source may be considered in three stages. The first stage is drift through the ion source prior to ionization; for prompt ionization, this time may be estimated to be nearly zero. For delayed ionization, where the particle exists as an excited neutral for a considerable period, this drift time may be equal to several microseconds. The second stage is the acceleration of the particle following ionization. The third and final stage is the motion of the ion with a constant velocity. Once the ion has reached its final kinetic energy and left the ion source, the ion travels with a constant, final velocity through the flight tube, as it heads towards the ion gate.

1. Drift as an excited neutral

For $t_0 \leq t \leq t_i$

$$s(t') = \int_{t_0}^{t} v_d \cdot dt' = \left[v_d t'\right]_{t_0}^{t}$$

As t_0, the start time, is equal to zero, the term becomes:

$$s(t') = v_d t - v_d t_0 = v_d t \qquad (3)$$

2. Acceleration within the ion source

For $t_i \leq t \leq t_e$

From equation (2):

$$s(t') = \int_{t_i}^{t} \left(v_d + a(t' - t_i)\right) \cdot dt'$$

$$s(t') = \int_{t_i}^{t} \left(v_d + at' - at_i\right) \cdot dt'$$

$$s(t') = \left[\left(v_d t' + \frac{1}{2} at'^2 - at_i t'\right)\right]_{t_i}^{t_e}$$

$$s(t') = \left(v_d t + \frac{1}{2} at^2 - at_i t\right) - \left(v_d t_i + \frac{1}{2} at_i^2 - at_i^2\right)$$

$$s(t') = v_d t - v_d t_i + \frac{1}{2} at^2 - at_i t + \frac{1}{2} at_i^2$$

$$s(t') = v_d t - v_d t_i + \frac{1}{2} a\left(t^2 - 2t_i t + t_i^2\right)$$

$$s(t') = v_d t - v_d t_i + \frac{1}{2} a(t - t_i)^2 \qquad (4)$$

3. Constant velocity after leaving ion source:

For $t_e \le t \le t_g$

$$v_3 = v_f = v_d + a(t_e - t_i)$$

$$s(t') = \int_{t_i}^{t} \left(v_d + a(t_e - t_i)\right) \cdot dt'$$

$$s(t') = \left[\left(v_d t' + at' (t_e - t_i)\right)\right]_{t_e}^{t'}$$

$$s(t') = \left(v_d t + at(t_e - t_i)\right) - \left(v_d t_e + at_e(t_e - t_i)\right)$$

$$s(t') = v_d t - v_d t_e + at(t_e - t_i) - at_e(t_e - t_i)$$

$$s(t') = v_d t - v_d t_e + a(t_e - t_i)(t - t_e) \qquad (5)$$

4. Combining the three components:

$$s(t') = \int_{t_0}^{t_i} v_d \cdot dt' + \int_{t_i}^{t_e} v_2 \cdot dt' + \int_{t_e}^{t} v_f \cdot dt' \qquad (6)$$

By analogy with the derivations of equations (3), (4), and (5):

$$s(t') = v_d t_i + v_d t_e - v_d t_i + \frac{1}{2} a(t_e - t_i)^2 + v_d t - v_d t_e + a(t_e - t_i)(t - t_e)$$

$$s(t') = v_d t + \frac{1}{2} a(t_e - t_i)^2 + a(t_e - t_i)(t - t_e)$$

$$s(t') = v_d t + \frac{1}{2} a(t_e - t_i)\left((t_e - t_i) + 2(t - t_e)\right) \qquad (7)$$

Determining variables for use with equation (7) prior to plotting results:

Determining t_e:

The time the ion leaves the ion source, t_e, is not known, and must be defined before equation (7) may be used. By equating $s(t_e)$ and d_s, using equations (3) and (4), the length of the ion source (in m), it is possible to determine t_e:

$$d_s = \int_{t_0}^{t_i} v_d \cdot dt' + \int_{t_i}^{t_e} \left(v_d + a(t' - t_i)\right) \cdot dt'$$

$$d_s = \left[v_d t_i\right] + \left[v_d t_e - v_d t_i + \frac{1}{2} a(t_e - t_i)^2\right]$$

$$d_s = v_d + \frac{1}{2} a(t_e^2 - 2t_i t_e + t_i^2)$$

$$d_s = v_d t_e + \frac{1}{2} a t_e^2 - a t_i t_e + \frac{1}{2} t_i^2$$

Rearranging to form a quadratic function,

$$\frac{1}{2} a t_e^2 + (v_d - a t_i) t_e + \frac{1}{2} a t_i^2 - d_s = 0$$

As

$$x = \frac{-b \pm \sqrt{b^2 - 4ac}}{2a} \qquad \text{if} \qquad ax^2 + bx + c = 0$$

then by analogy,

$$t_e = \frac{(-v_d + at_i) \pm \sqrt{(v_d - at_i)^2 - 4 \cdot \frac{1}{2} \cdot a\left(\frac{1}{2} at_i^2 - d_s\right)}}{2 \cdot \frac{1}{2} a}$$

$$t_e = \frac{(-v_d + at_i) \pm \sqrt{v_d^2 - 2v_d at_i + a^2 t_i^2 - a^2 t_i^2 + 2ad_s}}{a}$$

Simplifying, one of the two solutions becomes:

$$t_e = t_i - \frac{v_d}{a} + \frac{1}{a}\sqrt{v_d^2 + 2a(d_s - v_d t_i)} \qquad (8)$$

(the other solution is not viable)

Determining acceleration:

The acceleration, a, is used throughout these equations, and may be defined in the following manner:

$$F = ma$$

where F is the force (in N), m is the mass of the particle (in kg), and a is the acceleration on the particle due to the net force (in m s^{-2})

and

$$F = qE$$

where F is the force (in N), q is the charge on the ion (in C), and E is the electric field strength (in V m^{-1})

Equating the two:

$$qE = ma$$

and therefore,

$$a = \frac{qE}{m} \qquad (9)$$

The electric field strength may be defined by:

$$E = \frac{V}{d}$$

where V is the potential difference (in V) between two points and d is the distance between those two points (in m)

Rearranging,

$$a = \frac{qV}{dm}$$

More specifically, an ion will experience an acceleration of:

$$a = \frac{qV}{md_s} \qquad (10)$$

where d_s is the length of the ion source (in m), V is the potential inside the ion soucre (20000 V), and m is the mass of the ion (in kg).

Once equation (7) has been obtained and the variables a and t_c have been defined with relation to known data, it is possible to plot graphs that demonstrate the displacement of prompt and delayed ions as a function of time, where the delay in ionization can be chosen manually. The potential gradient inside the ion source is linear, and therefore this expression may be used for delayed ions as well. The net result is that the ions leave with a lower velocity and therefore lower kinetic energy. Using equations (3), (4), (7), and (10), it is possible to plot the displacement of a molecule as a function of time, and such graphs are shown in Figure 9. It is also of great importance that the inconsistency in the argument which is in favor of an energy spread alone is noted; using this high value for a drift velocity, in order to produce a difference in kinetic energy, a delay time of the order of microseconds is first required. In effect, as a delay of an order of microseconds is a prerequisite for a significant energy spread to result, delayed ionization is required for an energy spread to arise that is large enough to account for the observations. Figure 9 shows graphs which plot the displacement of $C_{60}^{+\bullet}$, $C_{120}^{+\bullet}$, and a delayed $C_{60}^{+\bullet}$ ion as a function of time. Studies of initial velocities[71] of fullerene neutrals within an ion source, following laser ablation, can be found within the literature, and neutral velocities typically range between the lower and upper limits of 100 m s^{-1} and 1000 m s^{-1}, respectively.[13,72-74] Relying on these values, Figure 9a shows the resulting graph using a drift velocity of 1000 m s^{-1} and Figure 9b shows the resulting graph using a drift velocity of 100 m s^{-1}. As appropriate examples, the displacement of a delayed $C_{60}^{+\bullet}$ species is compared with a $C_{120}^{+\bullet}$ species, as it has been the dimeric coalesced species which have been of primary importance during the course of these experiments. It can be seen that a delay time between approximately 1.1 μs (for a neutral with a drift velocity of 1000 m s^{-1}) and 1.2 μs (for a neutral with a drift velocity of 100 m s^{-1}) is required for a delayed $C_{60}^{+\bullet}$ species to coincide with $C_{120}^{+\bullet}$ at the ion gate. It must be noted that the graph illustrates the flight of the ions for the first few

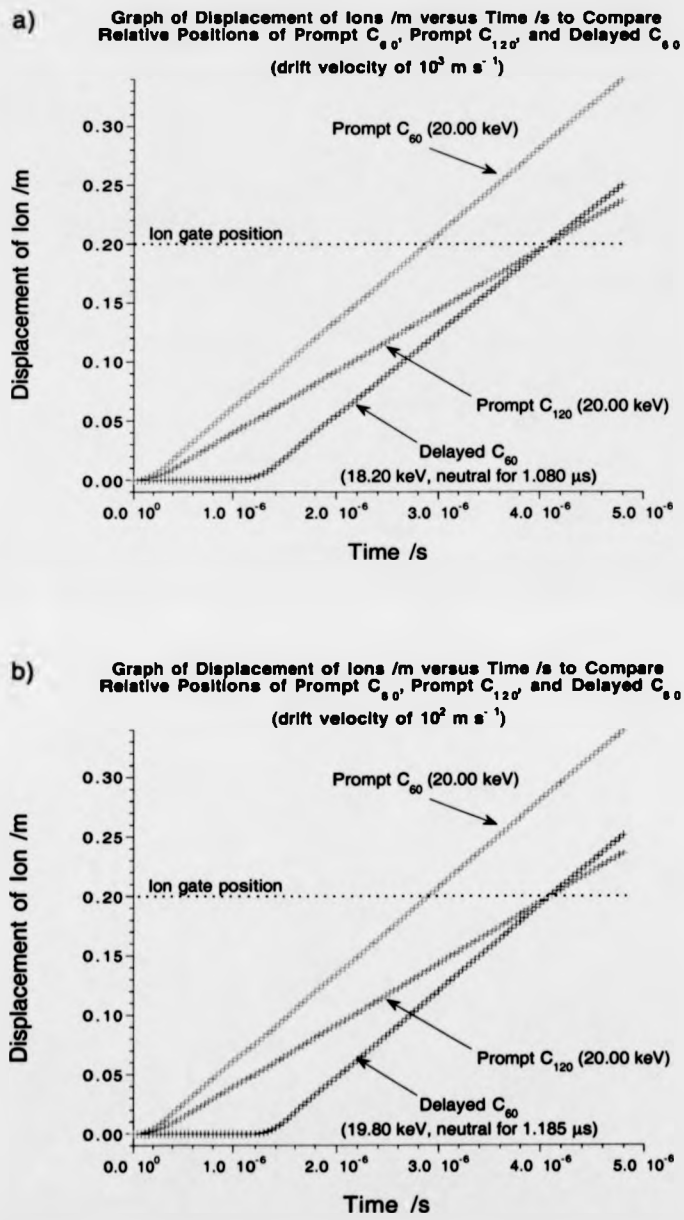

Figure 9: Graphs of displacement as a function of time for three ions; a C_{60} ion which has undergone delayed ionization, a C_{120} ion which has been promptly ionized, and, for comparison, a promptly ionized C_{60} species. Graph a assumes a drift velocity of 1000 m s^{-1} for neutral C_{60} species, whereas graph b assumes a drift velocity of 100 m s^{-1}. A comparison of the two graphs reveals that the delays prior to ionization, required for the delayed C_{60}^{+} ion to coincide with the C_{120}^{+} ion at the ion gate, are similar, regardless of the order of magnitude difference between the drift velocities.

stages inside the mass spectrometer, and takes into account the design of the ion source but does not involve the use of a reflectron, as it is only the acceleration and drift of the ions up to the position of the ion gate that is of importance here. Using estimates of the drift velocities of the neutral species, in conjunction with knowledge of the instrument design, it is possible to determine the maximum delay times which can be observed. After a delay of 12 μs for neutrals traveling at 1000 m s^{-1} and after a delay of 120 μs for neutrals with a drift velocity of 100 m s^{-1}, the neutral species will have left the ion source without undergoing ionization and will thus not be detected.

The delayed ions will therefore interfere with any PSD spectrum of a fullerene or fullerene derivative, and ToF instruments that select ions on a time of flight basis cannot be relied upon for PSD data of such compounds. ToF instruments could be reliably used for PSD analysis of fullerenes and their derivatives if a different or additional ion selection method were to be employed, such as an electrostatic sector to select only ions of the full kinetic energy imparted by the accelerating potential in the ion source. Equally, use of a pulsed extraction ion source could also minimize interference from delayed ion signals. For the experiments which led to the spectra shown in Figure 10, C_{70} was used as the sample, and the ion gate was used to select $C_{64}^{+\bullet}$, one of the fragments produced in the ion source; the ion gate is set to a mass that is deliberately close to the mass of C_{60} (720 Da). It becomes apparent that the signal composed of $C_{60}^{+\bullet}$ ions has a fine structure, divided into three components. By measuring the exact flight times of $C_{66}^{+\bullet}$, $C_{64}^{+\bullet}$, $C_{62}^{+\bullet}$, and component a) of the $C_{60}^{+\bullet}$ signal, it is clear that these are fragment ions produced in the ion source. $C_{66}^{+\bullet}$ will pass the ion gate due to the uncertainty associated with the selectivity of the ion gate, and indeed the asymmetric tails on the $C_{64}^{+\bullet}$ and $C_{62}^{+\bullet}$ signals imply that while these signals may largely originate from PSD, there will be a contribution from the poor selectivity

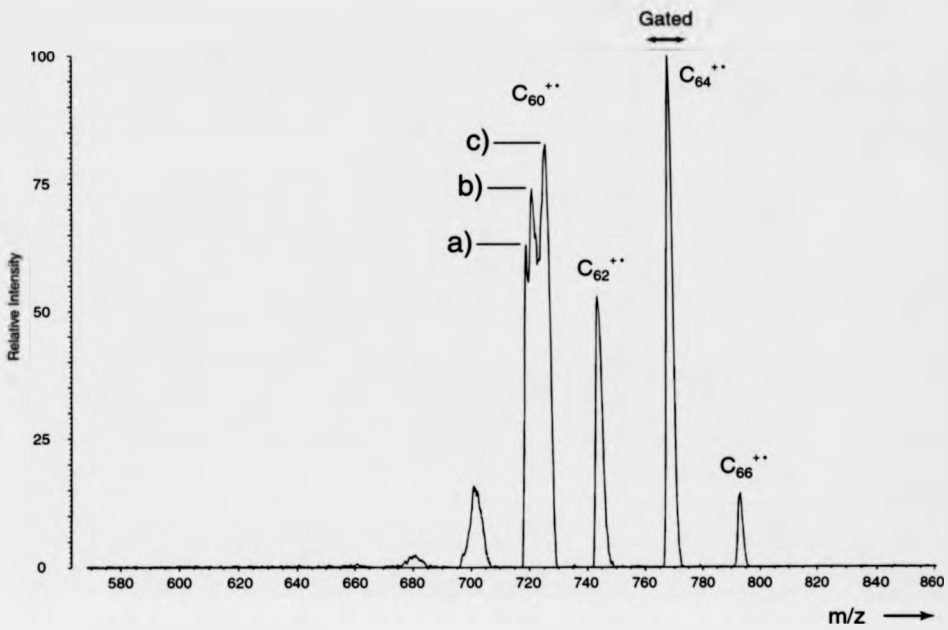

Figure 10: Positive-ion mass spectrum obtained using a C_{70} sample, following the selection of the $C_{64}^{+\bullet}$ fragment ion. The $C_{60}^{+\bullet}$ signal observed is split into three components.

of the ion gate and/or delayed ionization. By positioning the ion gate at such a close proximity to m/z 720, $C_{60}^{+\bullet}$ ions that have been generated as fragments in the ion source will pass the ion gate purely due to the width of the signal and the error associated with its selectivity, and this component is attributed to component a). A C_{60} fragment that undergoes delayed ionization would be shifted in mass due to both the delay in its ionization and also by the longer flight time if it possesses a lower velocity when it leaves the ion source. Analysis of the flight times of the three components of the $C_{60}^{+\bullet}$ signal results in the conclusion that the difference in flight time between component a) and component c) would be the required delay time for a $C_{60}^{+\bullet}$ ion to reach the ion gate at the same time as a $C_{64}^{+\bullet}$ ion. Component c) is therefore assigned as resulting from the delayed ionization of a

C_{60} fragment in the ion source. Component b) cannot be unambiguously assigned, but may well be a signal of $C_{60}^{+\bullet}$ fragment ion produced via post source decay of $C_{66}^{+\bullet}$, $C_{64}^{+\bullet}$, or $C_{62}^{+\bullet}$.

To further verify the hypothesis that the anomalous results are due to artifacts rather than being caused by the dissociation of the selected ion, coalescence of C_{70} and subsequent daughter ion analysis of the dimeric species was conducted on a different instrument. A Micromass AutoSpec oa-ToF of EBE-ToF geometry was used, coupled with an LDI ion source. Coalescence of C_{70} was achieved through laser desorption. Using the bypass option, ions were accelerated perpendicularly to their previous flight path in the orthogonal time-of-flight analyzer. The pulse used for this purpose was aimed for ions with m/z 1560 ($C_{130}^{+\bullet}$), and, due to the error associated with the pushing electrode, led to orthogonal acceleration of ions with a ±4% deviation from this mass, resulting in the recording of a partial mass spectrum centered around $C_{130}^{+\bullet}$. Ions with increasing mass deviation from this ±4% uncertainty are decreasingly likely to be accelerated into the oa-ToF region. In turn, following the selection of $C_{130}^{+\bullet}$, $C_{70}^{+\bullet}$ could only be detected if the parent ion were to dissociate following CID/PSD or if $C_{70}^{+\bullet}$ had the same arrival time at the pushing electrode as the selected ion, as may occur following delayed ionization. $C_{70}^{+\bullet}$ is clearly not observed in Figure 11a, indicating that large coalesced carbon clusters do not undergo unimolecular dissociation which leads to the formation of this ion. Even when the internal energy of the selected ion is increased by collision with xenon, resulting in the spectrum shown in Figure 11b, no $C_{70}^{+\bullet}$ fragment ions are formed, though, efficient C_2 losses are observed. These experiments thus provide a clear indication that large carbon clusters produced from the coalescence of C_{70} are in fact higher fullerenes and do not possess any structural moieties which feature C_{70} as a subunit, which could in turn lead to a "memory effect" and therefore

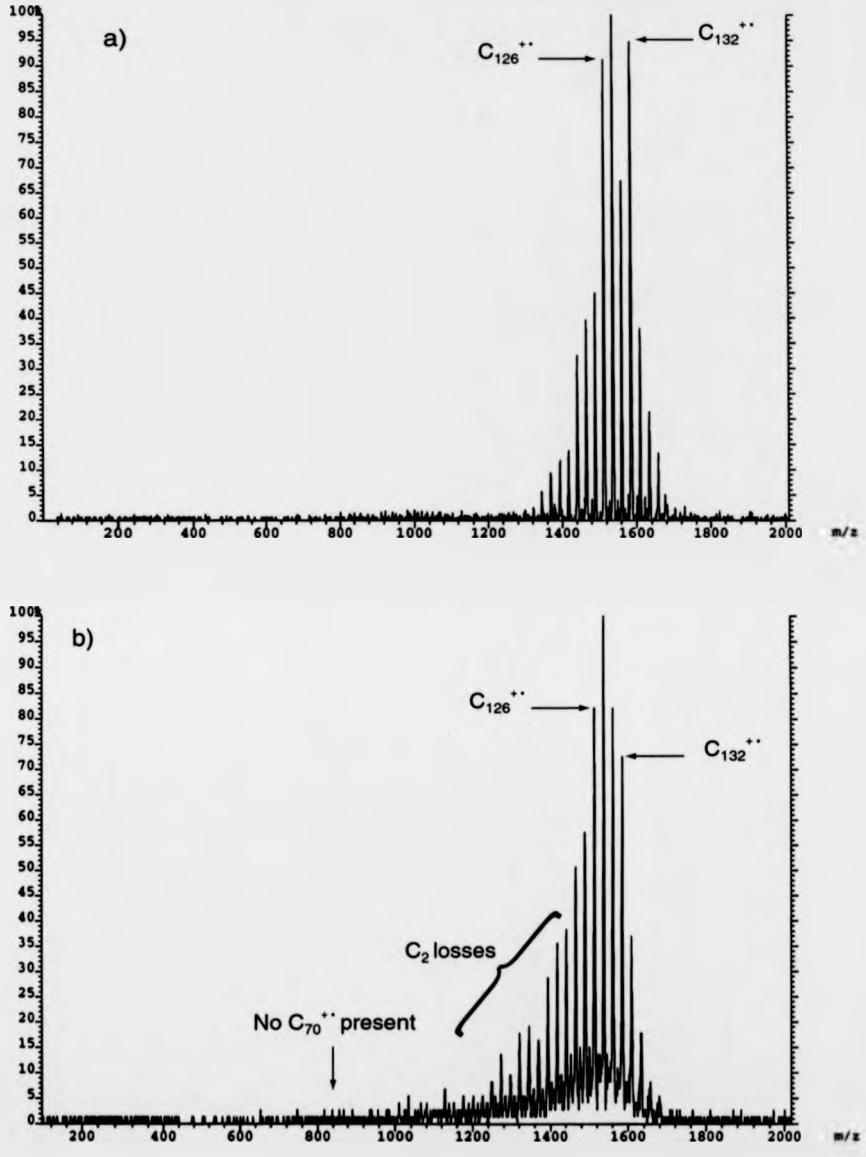

Figure 11: Positive-ion time-of-flight mass spectra acquired following laser desorption/ionization of a C_{70} sample using the Micromass AutoSpec oa-ToF. Spectrum a clearly demonstrates that the dimeric species do not undergo post source decay and that the coalesced carbon clusters are indeed stable. Spectrum b is a collision-induced dissociation spectrum obtained using xenon as the collision gas; even under these more violent conditions, no fragmentation is observed and the coalesced carbon clusters are demonstrated to be stable fullerene structures.

the observation of $C_{70}^{+\bullet}$ as a major daughter ion. The total absence of what may be assigned as "delayed ions" can be explained by two instrumental factors. The first factor is the fact that the flight length to the pusher electrode within the AutoSpec oa-ToF is much greater than the distance to the ion gate within the Kompact MALDI IV. With an accelerating potential of 8 kV, a C_{70} neutral which undergoes delayed ionization and arrives at the pusher electrode at the same time as a selected $C_{130}^{+\bullet}$ species, therefore also taking part in the time-of-flight analysis and being properly analyzed as having a mass of 840 Da, must undergo a delay prior to ionization of much greater magnitude than observed on the Kompact MALDI IV. Under the present conditions, the abundance of delayed $C_{70}^{+\bullet}$ ions is so low that very little signal would be detected. The second instrumental difference is that the AutoSpec-oa ToF uses electrostatic analyzers, which may discriminate against "delayed ions,"which may possess a lower kinetic energy than the full 8 keV. As the delay times required for the observation of delayed species on the AutoSpec oa-ToF are much greater than those required using the Kompact MALDI IV, the distance traveled as a neutral species within the ion source will be greater. This in turn leads to a greater, proportional reduction in the final kinetic energy of the ion. The electrostatic sectors of the instrument would almost certainly filter out such ions, due to the increased, proportional, kinetic energy deficit that would result.

Returning to the discussion of experiments performed using the reflectron time-of-flight mass spectrometer, Figure 12 shows a mass spectrum of $C_{60}^{+\bullet}$, but without the use of the ion gate and without the application of the usual data processing, such as baseline minimization and signal smoothing. It is important that the data processing is minimized as it can dramatically affect the appearance of the mass spectrum obtained; when data processing is applied to the spectrum shown in Figure 12, the asymmetric tails

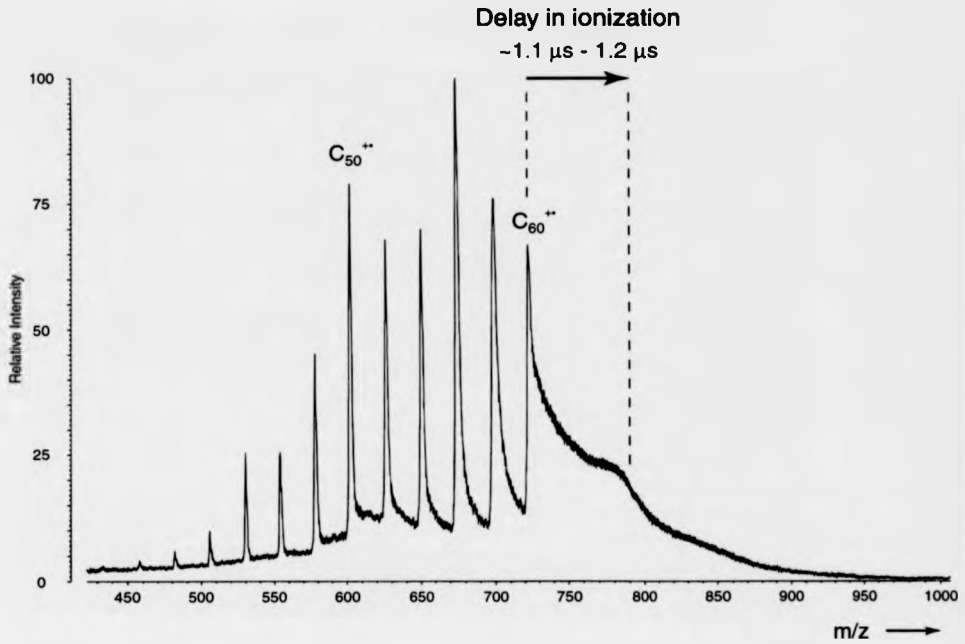

Figure 12: Time-of-flight mass spectrum obtained using a C_{60} sample on the Kratos Kompact MALDI IV; data processing features have been disabled to demonstrate the significance of the delayed ionization phenomenon. The spectrum is similar to others found in the literature and the delay time required for a $C_{60}^{+\bullet}$ ion to coincide with $C_{120}^{+\bullet}$ at the ion gate. The nominal m/z value that would be observed for this delayed ion, following use of the ion gate for the selection of $C_{120}^{+\bullet}$ in this manner, is shown.

would all but disappear, disguising the true appearance of the spectrum and thus preventing the procurement of valuable insight into the gas-phase behavior of the fullerene sample. The difference is significant, and each signal can be seen to have a tail at the high mass end, which results from the arrival of the delayed ions of the same mass. This tailing was first noticed by Campbell et al.,[33,34] and the characteristic "hump" in the $C_{60}^{+\bullet}$ tail is frequently cited. It has been postulated that the shape is determined by competing processes, which may be described by two or more rate constants. The tailing is most pronounced on the $C_{60}^{+\bullet}$ signal, and then decreases in significance with each, lower mass fragment. C_{60} is the fullerene most well known for its ability to undergo delayed ionization, although other

fullerenes can also undergo delayed ionization to varying extents. Figure 12 clearly shows the significance of delayed ionization, with the tail of the C_{60}^{++} signal extending for approximately 300 Da. The delay prior to ionization, required for the production of ions which would coincide with the C_{120} at the ion gate is labeled on the spectrum. This time delay is within the range of approximately 1.1 μs to 1.2 μs, depending on the initial velocity of the neutral species, as detailed earlier. The intensity of the tail merges with the noise level at approximately 1000 Da and by performing calculations which evaluate the delay times involved, it is reasonable to estimate that, during the course of these experiments, delays prior to ionization of no greater than approximately 4 μs have been observed.

3.4 Summary

It has been found that the PSD spectrum of fullerenes and their derivatives, obtained using an ion gate for the selection of parent ions in conjunction with a continuous acceleration potential, can be interfered with by artifact signals which result from the delayed ionization of pure fullerene samples. This finding is of particular importance as, in principle, any PSD spectrum of a fullerene sample may be falsely interpreted as exhibiting intense fragment ion signals. Fullerene derivative parent ions do not exhibit this tendency. However, pure fullerene fragments which arise through the dissociation of the fullerene derivative sample may in turn undergo delayed ionization, and these signals may be incorrectly assigned. Pure fullerene and fullerene derivative samples show no sign of this phenomenon in the negative-ion mode, and non-fullerene samples do not display similar tendencies in either the positive-ion mode or the negative-ion mode. These facts may be seen as strong evidence in support of the proposed explanation of the artifact signals, which is based upon delayed ionization. The careful elucidation of the interferences

observed leads to the conclusion that the delayed ionization phenomenon is the major cause of such artifact signals in these PSD spectra. For instance, kinetic energy deficits in the ion arising from the position of ionization within the source can indeed play a major role, but can only do so when accompanied by a delay in ionization; for an ion to move a sufficient distance for a noticeable energy difference to occur, the time required during drift as a neutral is of an order of μs, based on initial velocity measurements of fullerenes cited in the literature. In turn, the findings discussed here may lead to a new method which may be deliberately employed for the study of delayed ionization. In fact, additional studies based on these results are currently under way within the research group to make use of these observations and to study the behavior of fullerene based materials with regards to the delayed ionization phenomenon. Though less dramatic, but of significance nonetheless, the experiments further corroborate the theory that coalescence products, formed following laser ablation of pure fullerenes, are indeed large, closed cage fullerenes, and do not consist of more than one moiety.

3.5 References

1) Yeretzian, C.; Hansen, K.; Diederich, F.; Whetten, R. L. *Nature* **1992**, *359*, 44-47.

2) Yeretzian, C.; Hansen, K.; Diederich, F.; Whetten, R. L. *Supplement to Z. Phys. D.* **1993**, *26*, S 300-304.

3) Cordero, M. M.; Cornish, T. J.; Cotter, R. J. *J. Am. Soc. Mass Spectrom.* **1996**, *7*, 590-597.

4) Rogner, I.; Birkett, P.; Campbell, E. E. B. *Int. J. Mass Spectrom.* **1996**, *156*, 103-108.

5) Gromov, A.; Lebedkin, S.; Ballenweg, S.; Avent, A. G.; Taylor, R.; Krätschmer, W. *J. Chem. Soc. Chem. Commun.* **1997**, 209-210.

6) Lebedkin, S.; Ballenweg, S.; Gross, J.; Taylor, R.; Krätschmer, W. *Tetrahedron Lett.* **1995**, *36*, 4971-4974.

7) Cozzolino, R.; Belgachem, O.; Drewello, T.; Käseberg, L.; Herzschuh, R.; Suslov, S.; Boltalina, O. *Eur. Mass Spectrom.* **1997**, *3*, 407-414.

8) Penn, S. G.; Costa, D. A.; Balch, A. L.; Lebrilla, C. B. *Int. J. Mass Spectrom. Ion Processes* **1997**, *169/170*, 371-386.

9) Barrow, M. P.; Tower, N. J.; Taylor, R.; Drewello, T. *Chem. Phys. Lett.* **1998**, *293*, 302-308.

10) Al-Jafari, M. S.; Barrow, M. P.; Taylor, R.; Drewello, T. *Int. J. Mass Spectrom.* **1999**, *184*, L1-L4.

11) Hansen, K.; Yeretzian, C.; Whetten, R. L. *Chem. Phys. Lett.* **1994**, *218*, 462-466.

12) Beck, R. D.; Weis, P.; Bräuchle, G.; Kappes, M. M. *J. Chem. Phys.* **1994**, *100*, 262-270.

13) Mitzner, R.; Winter, B.; Kusch, C.; Campbell, E. E. B.; Hertel, I. V. *Z. Phys. D* **1995**, *37*, 89-95.

14) Scheier, P.; Dünser, B.; Wörtgötter, R.; Muigg, D.; Matt, S.; Echt, O.; Foltin, M.; Märk, T. D. *Phys. Rev. Lett.* **1996**, *77*, 2654-2657.

15) Deng, R.; Littlefield, G.; Echt, O. *Z. Phys. D.* **1997**, *D 40*, 355-360.

16) Foltin, M.; Echt, O.; Scheier, B.; Dünser, B.; Wörgötter, R.; Muigg, D.; Matt, S.; Märk, T. D. *J. Chem. Phys.* **1997**, *107*, 6246-6256.

17) Spengler, B. *J. Mass Spectrom.* **1997**, *32*, 1019-1036.

18) Harvey, D. J.; Hunter, A. P.; Bateman, R. H.; Brown, J.; Critchley, G. *Int. J. Mass Spectrom.* **1999**, *188*, 131-146.

19) Neumann, G. M.; Sheil, M. M.; Derrick, P. J. *Z. Naturforsch.* **1984**, *39a*, 584-592.

20) Hayes, R. N.; Gross, M. L. *Methods in Enzymology* **1990**, *193*, 237-263.

21) Bradley, C.; Curtis, J. M.; Derrick, P. J.; Sheil, M. M. *J. Chem. Soc. Faraday Trans.* **1994**, *90*, 239-247.

22) Cooks, R. G. *J. Mass Spectrom.* **1995**, *30*, 1215-1221.

23) Mamyrin, B. A.; Karatev, V. I.; Shmikk, D. V.; Zagulin, V. A. *Sov. Phys. JETP* **1973**, *37*, 45-48.

24) Tang, X.; Beavis, R.; Ens, W.; Lafortune, F.; Schueler, B.; Standing, K. G. *Int. J. Mass Spectrom. Ion Processes* **1988**, *85*, 43-67.

25) Bergmann, T.; Martin, T. P.; Schaber, H. *Rev. Sci. Instrum.* **1990**, *61*, 2592-2600.

26) Wollnik, H.; Grüner, U.; Li, G. *Time-Of-Flight Mass Spectrometers*; Gross, M. L., Ed.; Kluwer Academic Publishers: Netherlands, 1992; Vol. Chapter 6, pp 117-131.

27) Cornish, T. J.; Cotter, R. J. *Anal. Chem.* **1993**, *65*, 1043-1047.

28) Weickhardt, C.; Moritz, F.; Grotemeyer, J. *Mass Spectrom. Rev.* **1996**, *15*, 139-162.

29) Cotter, R. J. *Time-of-Flight Mass Spectrometry: Instrumentation and Applications in Biological Research*; ACS Professional Reference Books: Washington DC, 1997.

30) Chapman, J. R. *Practical Organic Mass Spectrometry: A Guide for Chemical and Biochemical Analysis*; 2nd ed.; John Wiley and Sons Ltd.: Chichester, 1993.

31) de Hoffmann, E.; Charette, J.; Stroobant, V. *Mass Spectrometry: Principles and Applications*; John Wiley and Sons Ltd.: Chichester, 1996.

32) Cordero, M. M.; Cornish, T. J.; Cotter, R. J.; Lys, I. A. *Rapid Commun. Mass Spectrom.* **1995**, *9*, 1356-1361.

33) Campbell, E. E. B.; Ulmer, G.; Hertel, I. V. *Phys. Rev. Lett.* **1991**, *67*, 1986-1988.

34) Campbell, E. E. B.; Ulmer, G.; Hertel, I. V. *Z. Phys. D.* **1992**, *24*, 81-85.

35) Ding, D.; Compton, R. N.; Haufler, R. E.; Klots, C. E. *J. Phys. Chem.* **1993**, *97*, 2500-2504.

36) Ding, D.; Huang, J.; Compton, R. N.; Klots, C. E.; Haufler, R. E. *Phys. Rev. Lett.* **1994**, *73*, 1084-1087.

37) Beck, R. D.; Rockenberger, J.; Weis, P.; Kappes, M. *J. Phys. Chem.* **1996**, *104*, 3638-3650.

38) Aumayr, F.; Betz, G.; Märk, T. D.; Scheier, P.; Winter, H. P. *Int. J. Mass Spectrom. Ion Processes* **1998**, *174*, 317-328.

39) Wurz, P.; Lykke, K. R. *J. Chem. Phys.* **1991**, *95*, 7008-7010.

40) Wurz, P.; Lykke, K. R. *J. Phys. Chem.* **1992**, *96*, 10129-10139.

41) Jones, A. C.; Dale, M. J.; Banks, M. R.; Gosney, I.; Langridge-Smith, P. R. R. *Molecular Physics* **1993**, *80*, 583-600.

42) Beck, R. D.; Weis, P.; Rockenberger, J.; Kappes, M. M. *Surface Review Letters* **1996**, *3*, 771-775.

43) Hansen, K.; Echt, O. *Phys. Rev. Lett.* **1997**, *78*, 2337-2340.

44) Gallogly, E. B.; Bao, Y.; Han, K.; Lin, H.; Jackson, W. M. *J. Phys. Chem.* **1994**, *98*, 3121-3125.

45) Lin, H.; Han, K.-L.; Bao, Y.; Gallogly, E. B.; Jackson, W. M. *J. Phys. Chem.* **1994**, *98*, 12495-12500.

46) Andersen, J. U.; Brink, C.; Hvelplund, P.; Larsson, M. O.; Bech Nielsen, B.; Shen, H. *Phys. Rev. Lett.* **1996**, *77*, 3991-3994.

47) Loepfe, M.; Siegmann, C.; Sattler, K. *Supplement to Z. Phys. D.* **1993**, *D 26*, S 311-313.

48) von Helden, G.; Holleman, I.; Knippels, G. M. H.; van der Meer, A. F. G.; Meijer, G. *Phys. Rev. Lett.* **1997**, *79*, 5234-5237.

49) von Helden, G.; Holleman, I.; Putter, M.; van Roij, A. J. A.; Meijer, G. *Chem. Phys. Lett.* **1999**, *299*, 171-176.

50) von Helden, G.; Holleman, I.; van Roij, A. J. A.; Knippels, G. M. H.; van der Meer, A. F. G.; Meijer, G. *Phys. Rev. Lett.* **1998**, *81*, 1825-1828.

51) van Heijnsbergen, D.; von Helden, G.; Sartakov, B.; Meijer, G. *Chem. Phys. Lett.* **2000**, *321*, 508-513.

52) Kennedy, K. W.; Echt, O. *J. Phys. Chem.* **1993**, *97*, 7088-7091.

53) Bekkerman, A.; Tsipinyuk, B.; Kolodney, E. *Int. J. Mass Spectrom.* **1999**, *185/186/187*, 773-786.

54) Walder, G.; Kennedy, K. W.; Echt, O. *Supplement to Z. Phys. D.* **1993**, *26*, S 288-290.

55) Campbell, E. E. B.; Levine, R. D. *Annu. Rev. Phys. Chem.* **2000**, *51*, 1-34.

56) Weis, P.; Rockenberger, J.; Beck, R. D.; Kappes, M. M. *J. Chem. Phys.* **1996**, *104*, 3629-3637.

57) Lifshitz, C. *Int. J. Mass Spectrom.* **2000**, *198*, 1-14.

58) Fujii, T. *Eur. Mass Spectrom.* **1996**, *2*, 91-114.

59) Remacle, F.; Levine, R. D. *Phys. Lett. A* **1993**, *173*, 284-287.

60) Lykke, K. R. *Phys. Rev. Lett.* **1995**, *75*, 1234-1235.

61) Klots, C. E. *Chem. Phys. Lett.* **1991**, *186*, 73-76.

62) Klots, C. E. *Z. Phys. D* **1991**, *20*, 105-109.

63) Klots, C. E. *J. Chem. Phys.* **1994**, *100*, 1035-1039.

64) Klots, C. E.; Compton, R. N. *Surface Rev. Lett.* **1996**, *3*, 535-540.

65) Dauw, X. L. R.; Bronsveld, M. V.; Krüger, A.; Warntjes, J. B. M.; Witjes, M. R.; Groenen, E. J. J. *J. Chem. Phys.* **1998**, *109*, 9332-9339.

66) Sassara, A.; Zerza, G.; Chergui, M.; Ciulin, V.; Ganière, J.-D.; Deveaud, B. *J. Chem. Phys.* **1999**, *111*, 689-697.

67) Zhang, Y.; Stuke, M. *Phys. Rev. Lett.* **1993**, *70*, 3231-3234.

68) Haufler, R. E.; Wang, L.-S.; Chibante, L. P. F.; Jin, C.; Conceicao, J.; Chai, Y.; Smalley, R. E. *Chem. Phys. Lett.* **1991**, *179*, 449-454.

69) Arslanbekov, T. U.; Koval, A. V.; Pazdzersky, V. A. *Laser Physics* **1997**, *7*, 689-691.

70) von Helden, G.; Holleman, I.; Meijer, G.; Sartakov, B. *Optics Express* **1999**, *4*, 46-52.

71) Juhasz, P.; Vestal, M. L.; Martin, S. A. *J. Am. Soc. Mass Spectrom.* **1997**, *8*, 209-217.

72) Wurz, P.; Lykke, K. R.; Pellin, M. J.; Gruen, D. M.; Holmes Parker, D. *Vacuum* **1992**, *43*, 381-385.

73) Beck, R. D.; Weis, P.; Rockenberger, J.; Kappes, M. M. *J. Phys. Chem.* **1995**, *99*, 3990-3999.

74) Winter, B.; Mitzner, R.; Kusch, C.; Campbell, E. E. B.; Hertel, I. V. *J. Chem. Phys.* **1996**, *104*, 9179-9190.

Chapter Four

Unimolecular Dissociation and Gas-Phase Coalescence of Hydrogenated Fullerenes

4.1 Introduction

Hydrogenated fullerenes have been produced for some years, using a variety of approaches. Synthetic methods have included Birch reduction,[1] radical induced hydrogenation,[2] transfer hydrogenation of C_{60} by 9,10-dihydroanthracene,[3] or Zn/Cl reduction,[4] and the most common product of these methods is $C_{60}H_{36}$. Attempts to produce hydrogenated fullerenes which were based upon larger, fullerene cores, such as C_{76}, C_{78}, and C_{84}, resulted in the abundant production of $C_{60}H_{36}$ following cage degradation, which indicates that $C_{60}H_{36}$ is a particularly favorable structure.[5] Thermolysis of $C_{60}H_{36}$ leads to the production of $C_{60}H_{18}$,[4] which can also be generated selectively by transfer hydrogenation. The favorability of certain hydrogen contents is analogous to the favorability of certain fluorine contents in the case of fluorinated fullerenes and is a topic of much investigation using mass spectrometry,[6,7] nuclear magnetic resonance (NMR),[8] X-Ray diffraction,[9] and theoretical work.[10-14] A comprehensive overview of the synthesis, properties, and structures of fullerene hydrides has been produced by Gol'dshleger and Moravskii.[15] $C_{60}F_{18}$,[16] $C_{60}F_{36}$,[16,17] and $C_{60}F_{48}$[16,18] are particularly favored. The similarity between fluorinated and hydrogenated fullerenes does not end with "magic numbers." Recently, the structure of $C_{60}H_{36}$ was elucidated in light of the known $C_{60}F_{36}$ geometry, and the two geometries were found to be identical[19]; equally, parallels between the geometry of $C_{60}H_{18}$ and $C_{60}F_{18}$ have also been drawn.[13,14] A comparison between fluorinated fullerenes and hydrogenated fullerenes is therefore inevitable.

$C_{60}F_x$ based compounds are amongst the most stable fullerene derivatives with respect to temperature, while $C_{60}H_x$ based compounds are amongst the most thermolabile derivatives. These contrasting characteristics present different problems when analysis is to be carried out, and makes comparison using identical analytical methods very difficult.

Mass spectrometry has always been a favored tool in the analysis of fullerenes and represents one of the obvious choices for the investigation of $C_{60}H_{36}$. With the increasing wealth of fullerene derivatives, many of which are labile and susceptible to degradation under harsh ionization conditions and/or vigorous heating, a major goal for mass spectrometrists analyzing fullerenes has been to reduce fragmentation. Field desorption (FD) and matrix-assisted laser desorption/ionization (MALDI) have been used during attempts to record mass spectra that are relatively free of fragmentation. Indeed, FD[20] and MALDI[21] have been employed during studies of $C_{60}H_{36}$ during the course of which there was only a low degree of fragmentation. Recently, it has been shown that electrospray ionization (ESI) is also a viable technique,[22] contrary to previous beliefs, and this ionization method will almost undoubtedly become a favored approach for the analysis of fullerene derivatives in future. Despite these facts, utilization of ESI for the study of $C_{60}H_{36}$ at the University of Warwick has not yielded results thus far. Electron impact (EI) may represent a relatively harsh ionization technique, but valuable physical data may be obtained using this method, especially when examining fragmentation dynamics, in cases where ESI may prove to be too gentle. EI has been used previously during the characterization of hydrogenated fullerenes, but a variant known as "desorption chemical ionization" was used[4] and this technique will be further discussed later. The greatest difficulty faced when using EI as an ionization technique when examining hydrogenated fullerenes is the fact that heating is required to vaporize the sample, prior to bombardment by electrons.

Although $C_{60}H_{36}$ has been produced for some period of time, little is known about its gas-phase behavior. It is important to develop an understanding of how modification of a fullerene core affects its reactivity and stability. In this way, future applications may be pursued and tailor made syntheses may be developed with these applications in mind.

With these concerns, an investigation into the gas-phase behavior of $C_{60}H_{36}$ was performed using a variety of instruments. Particular attention was paid to the fragmentation dynamics of the sample and also to the coalescence reactivity, as pure fullerenes are well known for their ability to be fused under laser desorption/ionization (LDI) conditions, resulting in higher carbon clusters. A sector instrument of BE geometry, with an EI ionization source, was used to study the ability to form multiply charged ions and to record mass-analyzed ion kinetic energy (MIKE) scans for the study of the fragmentation behavior. A variation of the EI source known as a "Desorption Chemical Ionization" (DCI)[4,23,24] source was used; note that though the term "chemical ionization" is used, the ionization process itself bears a much closer resemblance to EI. A drop of the sample solution solution is applied to a platinum wire and the solvent is evaporated. Once the probe (to which the wire is attached) is inserted into the instrument, the platinum wire is heated. DCI is believed to be different to EI in that the sample undergoes evaporation followed by rapid ionization, direct ionization on the surface of the filament, direct ion desorption, and/or pyrolysis followed by ionization when heating the filament to high temperatures. It is known that the effective temperature used is reduced by an order of hundreds of degrees Celsius.[24] A hybrid instrument of BEqQ geometry, using an LSIMS ion source, was used to further substantiate the fragmentation tendencies observed. Finally, a time-of-flight mass spectrometer equipped with a laser desorption/ionization (LDI) ion source was used to study the coalescence reactivity of the $C_{60}H_{36}$ sample in the gas-phase. Both striking contrasts and similarities have been found between hydrogenated and fluorinated fullerene compounds.

4.2 Experimental

The $C_{60}H_{36}$ sample was synthesized using the Birch reduction and provided courtesy of B. Ondruschka and M. Nüchter (Friedrich-Schiller-Universität, Jena, Germany). A variety of mass spectrometers was used during the course of the investigation in order that a more comprehensive overview may be obtained. All electron impact (EI) mass spectra and mass-analyzed ion kinetic energy (MIKE) scans were recorded using a Finnigan MAT-95, which is a double focusing sector instrument of reversed geometry, and were provided courtesy of M. Möder (Umweltforschungzentrum Leipzig Halle GmbH, Leipzig, Germany). Samples were prepared by spotting the toluene solution on to the platinum wire of a desorption chemical ionization (DCI) probe tip, the solvent was allowed to evaporate, and then the probe would enter the ion source, which was maintained at 260 °C. The platinum wire was heated for two minutes at a rate of 175 °C min^{-1} and then kept at 350 °C for one minute while the scans were obtained. As mentioned earlier, the use of DCI has the advantage in this case of requiring less heat to be transferred to the sample and that the ionization occurs close to or at the surface of the wire. These factors are necessary in order to overcome the difficulties posed by the analysis of a thermolabile compound under EI conditions. For every spectrum recorded, the electron emission was 1 mA and the electron energy was 70 eV, and the resulting ions were accelerated by a 5 kV accelerating potential.

Low energy collision-induced dissociations (CID) were performed using the rf-only quadrupole (q) of a VG Instruments ZAB-SEQ, shown in Figure 1, and the spectra were obtained with the assistance of G. Czira and K. Vékey (Central Research Institute for Chemistry, Hungarian Academy of Sciences, Budapest, Hungary). The ZAB-SEQ is a

hybrid instrument of BEqQ geometry where reactions/collisions are carried out in the quadrupole sector labeled "q," and mass analysis is performed in the quadrupole sector labeled "Q." A liquid secondary ion mass spectrometry (LSIMS) ion source was used for ionization. A small quantity of sample was dissolved in a droplet of 3-nitrobenzylalcohol (NBA), which acts as a matrix, and then placed on the probe tip, which then entered the ion source. The sample and matrix were then bombarded with a beam of cesium ions with an energy of 30 keV. An accelerating potential of 8 kV was employed to extract the ions from the ion source.

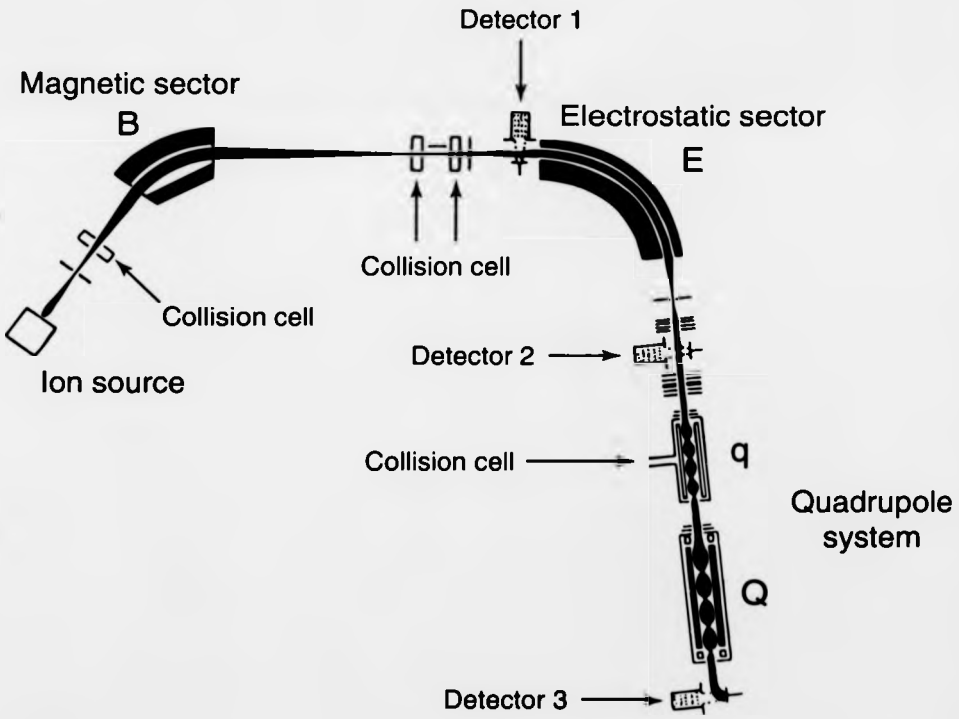

Figure 1: Schematic diagram of the VG ZAB-SEQ

Laser desorption/ionization (LDI) was used to coalesce $C_{60}H_{36}$ in the ion source, and these experiments were performed using a Kratos Kompact MALDI IV, which is a reflectron time-of-flight mass spectrometer. The ion source of the MALDI IV uses a nitrogen laser (337 nm, 3 ns pulse width) and ions are extracted by an accelerating potential of 20 kV. Each spectrum shown represents the accumulation of profiles resulting from 200 laser pulses, and the reflectron was used in each case. For the selection of ions over a desired mass range, an ion gate is used, which consists of two deflecting electrodes positioned inside the flight tube. Use can be made of the ion gate to minimize the chances of saturation of the detector, and hence may also be used to increase sensitivity, and the ion gate was used in this manner during one experiment. Sample preparation was carried out by dissolving the $C_{60}H_{36}$ sample in toluene, spotting the solution on to a stainless steel target slide, evaporating the solvent, and then the slide was inserted into the ion source.

4.3 Results and Discussion

While much is known about the fragmentation dynamics of pure fullerenes, little is known about the fragmentation of hydrogenated fullerenes. Extensive hydrogen loss in the gas-phase following vaporization and ionization has presented problems in the analysis of the synthetic product using mass spectrometry. However, the results of this investigation demonstrate that hydrogen loss is not the only fragmentation channel. Figure 2 shows a typical EI mass spectrum of $C_{60}H_{36}$, obtained using a MAT-95. Figure 2a clearly shows that doubly charged, triply charged, and even quadruply charged species are observed. A small contribution from $C_{60}H_{36}O^{+\bullet}$ may be observed, and this is attributed to oxidation of the sample on standing. This ability to undergo multiple ionization bears a closer resemblance to the behavior of pure fullerenes rather than fullerene derivatives, although

the generation of dications is known for fluorinated fullerenes. The spacing between signals arising from the ^{13}C isotopes were spaced by m/z 0.50, m/z 0.33, and m/z 0.25 for the doubly, triply, and quadruply charged species respectively, as would be expected. $C_{60}H_{36}$ was observed as a singly, doubly, and triply charged ion, but the quadruply charged ion had a maximum hydrogen content of only 28 hydrogen atoms. As the charge on the ion increases, it is found that the lower hydrogen content becomes favored, and this strongly suggests that further increasing the charge state is accompanied by increasing extent of fragmentation.

Fragmentation of $C_{60}H_{36}$ differs from the fragmentation of organic fullerene derivatives in that such derivatives tend to lose their ligands before cage shrinkage may occur via the characteristic C_2 loss mechanism. Figure 2b shows an enlarged view of the dication region of Figure 2a, and signals resulting from the detection of C_{60}^{2+} (m/z 360), C_{58}^{2+} (m/z 348), and C_{56}^{2+} (m/z 336) are clearly evident. Such fragments can only be produced via the loss of $C_{2n}H_x$ from hydrogenated fullerenes or following C_{2n} loss from pure fullerenes which are generated after previous fragmentation. Maxima are observed approximately every m/z 6 between m/z 336 and m/z 360, and it is unlikely that this pattern can be explained by even numbered carbon cores with varying hydrogen content. It is more probable that the difference of m/z 6 represents the formal loss of a single carbon atom, as part of a neutral C_nH_x moiety which is expelled from the $C_{60}H_n^{2+}$ ion. Therefore, fragmentation proceeds not only via the loss of hydrocarbon-like neutrals containing an even number of carbon atoms, but also via the loss of moieties which contain an uneven number of carbon atoms.

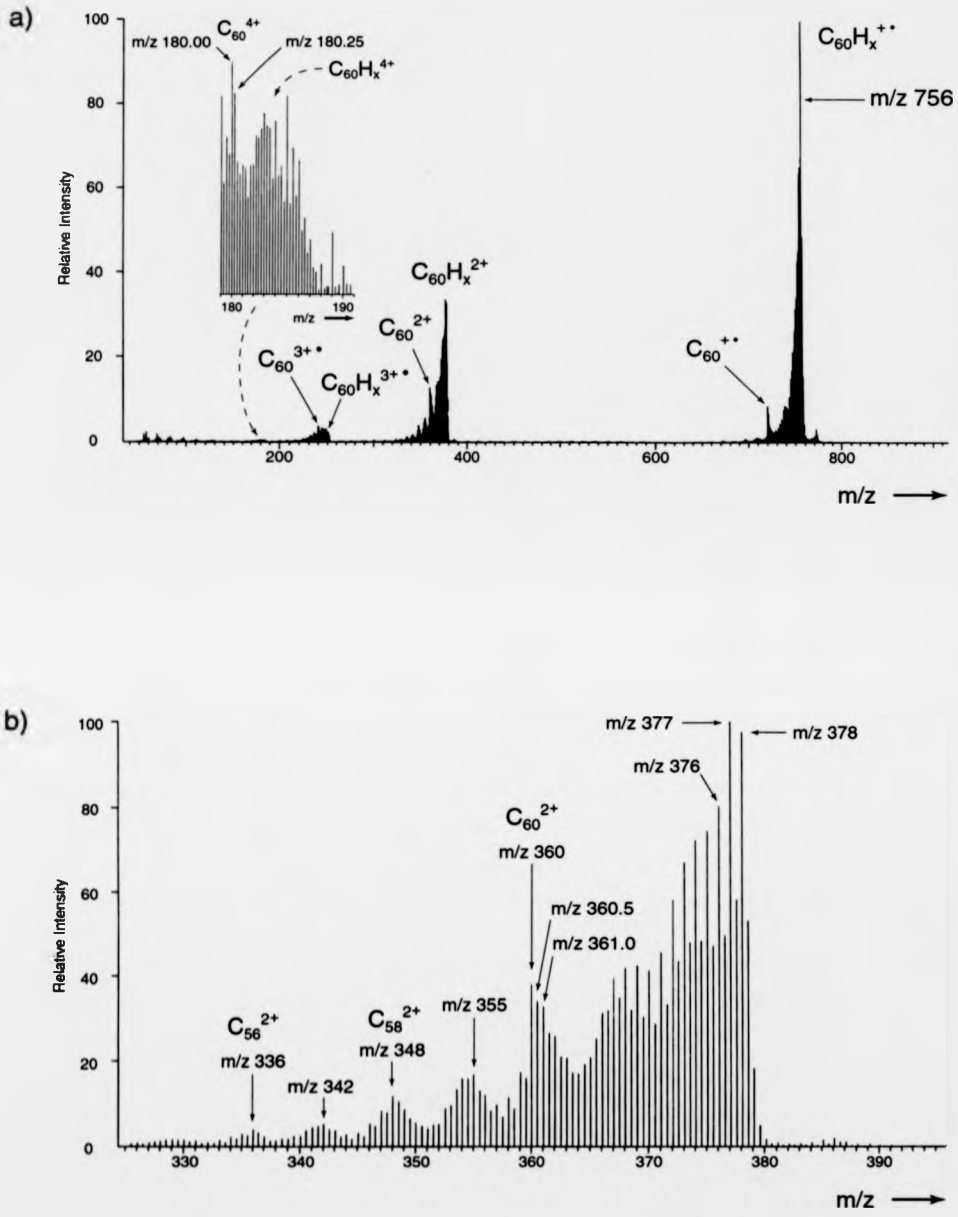

Figure 2: Positive-ion mass spectra obtained using the Finnigan MAT-95, in conjunction with use of electron ionization (EI). Spectrum a clearly shows the presence of multiply charged hydrogenated C_{60} ions, with the inset showing an enlarged mass region to indicate the presence of $C_{60}H_n^{4+}$. Spectrum b shows an enlarged mass region of the doubly charged ions.

Further investigation proceeded by studying the unimolecular fragmentation of ions of varying hydrogen content and charge state, performing MIKE scans using tandem mass spectrometry. Figure 3 shows the resulting spectra, following experiments performed on the MAT-95. Figures 3a to 3c show the results of MIKE scans carried out using a double focusing sector instrument, where the magnet was used to select the precursor ion and the electrostatic sector was scanned for daughter ion analysis. The main beam signal and those daughter ion signals arising from the loss of up to four hydrogen atoms are off scale to allow a more detailed presentation of the other fragment ion signals. The precursor ions for Figures 3a, 3b, and 3c were $C_{60}H_{36}^{+\bullet}$, $C_{60}H_{36}^{2+}$, and $C_{60}H_{18}^{+\bullet}$ respectively; $C_{60}H_{18}^{+\bullet}$ was produced using a sample where $C_{60}H_{18}$ was the main product following the hydrogenation reaction.

Figure 3a shows the fragmentation of the $C_{60}H_{36}^{+\bullet}$ ion. The most intense peak that is on scale is approximately 5 - 6 Da wide, and the peak center is located at the position corresponding to the loss of 15 Da (assigned as the loss of CH_x neutrals). The next peak is centered at a position correlating with the loss of 28 Da, and is 8 - 9 Da wide (assigned as the loss of C_2H_x neutrals). The final daughter ion signals are observed to be centered around the loss of 42 Da, attributed as resulting from the loss of C_3H_x neutrals, and is approximately 5 - 6 Da wide. It appears that in contrast to the pure carbon neutrals (e.g. C_2) lost from pure fullerenes and many derivatized fullerenes, loss of CH_x, C_2H_x, and C_3H_x also occurs. Due to the limiting resolution of the electrostatic sector, the exact hydrogen content of each distribution of daughter ion signals cannot be established; broadening of the signals may also occur following kinetic energy release during fragmentation. Another factor limiting exact structural assignment is the fact that interference may occur between isobaric ions; for instance, the ^{13}C contribution cannot be ruled out. Regardless of this,

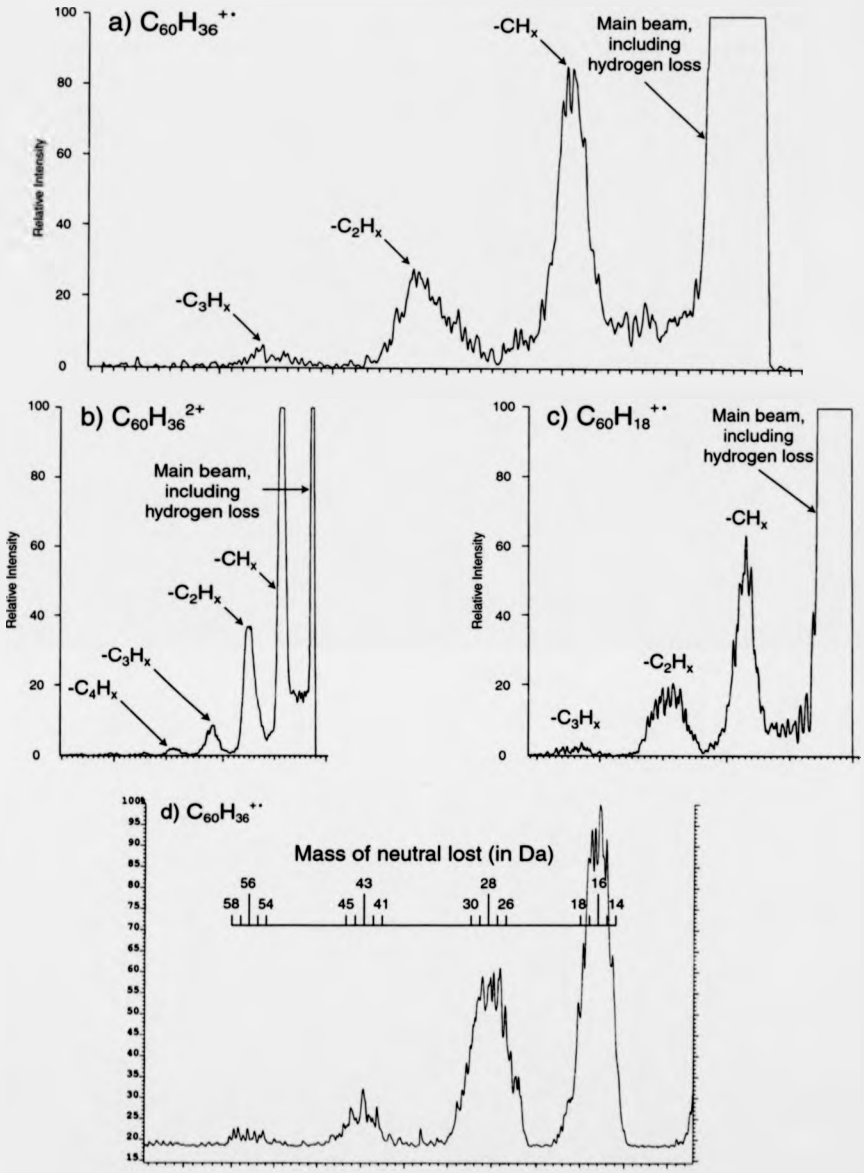

Figure 3: Positive-ion mode mass spectra illustrating the unimolecular dissociation behavior of hydrogenated C_{60} ions. Spectra a, b, and c are mass-analyzed kinetic energy spectra obtained on the Finnigan MAT-95, following the selection of $C_{60}H_{36}^{+\bullet}$, $C_{60}H_{36}^{2+}$, and $C_{60}H_{18}^{+\bullet}$, respectively. It can be seen that the fragmentation dynamics of the ions are similar, providing indications that the unimolecular dissociation behavior of hydrogenated C_{60} is independent of charge state and hydrogen content. Spectrum d was obtained on the VG ZAB-SEQ and represents a low energy collision-induced dissociation spectrum of $C_{60}H_{36}^{+\bullet}$, using argon as the collision gas and involving a collision energy of 170 eV.

certain structures are more probable than others. For instance, by simple probability calculations it can be shown that the loss of 16 Da from $C_{60}H_{36}^{+\bullet}$ is more likely to correspond to the loss of a $^{12}CH_4$ neutral rather than a $^{13}CH_3$ neutral. These concerns also hold true for the Figures 3b and 3c. Figure 3b displays a similar pattern of fragmentation, with the loss of C_nH_x neutrals, but the extent of fragmentation is greater. While Figure 3a showed the fragmentation of $C_{60}H_{36}^{+\bullet}$ proceeded by up to a loss of C_3H_x, Figure 3b shows the fragmentation of $C_{60}H_{36}^{2+}$ proceeds along similar pathways, but a maximum neutral size of C_4H_x is observed. This is further evidence that fragments of lower hydrogen content are observed as the charge state of the precursor ion increases. Figure 3c shows the fragmentation of $C_{60}H_{18}^{+\bullet}$, which occurs analogously to the fragmentation of $C_{60}H_{36}^{+\bullet}$, and the largest neutral ejected (C_3H_x) is also the same in both cases. Thus, reducing the hydrogen content of the fullerene derivatives from 36 to 18 hydrogen atoms does not lead to significantly different fragmentation pathways. For $C_{60}H_{18}^{+\bullet}$, the efficient loss of up to C_3H_x units is observed, for example. It is obvious that, for such a reaction to occur, hydrogen migration and fragmentation of the carbon cage is required. The hydrogen migration might not be efficient enough to account for these findings, assuming an even distribution of hydrogen around the fullerene structure. One might, therefore, speculate that hydrogen is not evenly distributed over the entire surface of the carbon cluster. Interestingly, this is in line with recent work on the structure elucidation of $C_{60}H_{18}$, bearing a C_{3v} symmetry in which all 18 hydrogen atoms are located adjacent to each other on "one side" of the fullerene.[25]

One further concern regarding interference from other species relates to the dissociation of ions in front of the magnet (see Chapter One for more details concerning metastable ions). As commented on earlier, Figure 2a shows that an ion of higher mass is

also present, which is assigned as being an oxide of the hydrogenated fullerene. Theoretically, such a species could dissociate in front of the magnet, and a daughter ion may have a similar momentum as the ion selected by the magnet. As a result, this daughter ion could traverse the magnetic field along with the selected ion, and would appear in the spectrum at a lower translational energy than $C_{60}H_{36}^{+\bullet}$, implying that is was a fragment ion. As this possibility could not be discounted, further research was performed using a hybrid instrument. $C_{60}H_{36}^{+\bullet}$ was dissociated in an rf-only quadrupole of a BEqQ instrument, following momentum-to-charge ratio and kinetic-energy-to-charge ratio analysis by the magnetic and electrostatic sectors, respectively. Using this arrangement, it is not possible for interferences to arise from daughter ions produced in front of the magnet. Figure 3d shows the spectrum obtained using the rf-only quadrupole for low energy CID; argon was used as the collision gas, with a cell pressure of 5×10^{-7} mbar and a laboratory collision energy of 170 eV. Four peaks were observed. These peaks were centered around the loss of 16 Da (CH_x neutral loss), 28 Da (C_2H_x neutral loss), 43 Da (C_3H_x neutral loss), and 56 Da (C_4H_x neutral loss). Comparison with the MIKE scans reveals that these results support the hypothesis stated earlier, and that fragmentation does indeed appear to occur via the loss of neutral C_nH_x species. C_4H_x loss is observed for $C_{60}H_{36}^{2+}$ (Figure 3b) due to the higher charge state, but not for $C_{60}H_{36}^{+\bullet}$ (Figure 3a); the reason why C_4H_x loss is observed when selecting $C_{60}H_{36}^{+\bullet}$ using the ZAB-SEQ is that a collision gas was used in order to encourage fragmentation, and so the degree of fragmentation has been increased slightly. In similarity with the MIKE scans, the peaks correlating with the daughter ions are broad (5 - 9 Da wide), and so, again, the establishment of the exact hydrogen content is not possible. For instrumental reasons, LSIMS was used as the ionization method coupled with the ZAB-SEQ, and this fact prevented an analogous investigation of the dication ($C_{60}H_{36}^{2+}$). An analogous investigation of $C_{60}H_{18}$ was also not possible, but this was due to

sample availability. Despite these facts, clear evidence has been provided supporting the theory that loss of C_nH_x from $C_{60}H_{36}^{+\bullet}$ occurs.

As stated previously, this fragmentation behavior (loss of C_nH_x) differs from that of most organic ligand bearing fullerenes. Most derivatized fullerenes undergo ligand loss, before fragmenting further via the loss of C_2 units. There are a few exceptions, such as the loss of CO and CO_2 from fullerene oxides, but otherwise this tendency is frequently observed. Fluorinated fullerenes bear similarity to hydrogenated fullerenes with regards to their gas-phase behavior. Besides the loss of $F^{\bullet}$, fluorinated fullerenes may also undergo loss of perfluoroalkyl radicals of the structure C_nF_x; this is analogous to the behavior of hydrogenated fullerenes in many respects. Although the precise structures of the neutrals lost could not be assigned beyond doubt, the close resemblance between the two cases is noteworthy.

Coalescence of pure fullerenes in the gas-phase following laser desorption/ionization is well documented.[26-32] Fusion of fullerene and fullerene fragments leads to the production of higher carbon clusters. The mechanism behind such a reaction is of current research interest[33-35] and is believed to involve the collision and fusion of energized, neutral species and ionic species[35] or the collision of two highly energized, neutral species,[34] followed by C_2 loss or C_2 uptake, resulting in a distribution of higher carbon clusters. C_2 loss is characteristic of a fullerene, and observation of this behavior can be used as part of the evidence in support of the generation of higher fullerenes. Coalescence of fullerene derivatives[36-39] is of interest from a mechanistic point of view, as the aggregates formed are not always pure fullerenes, with closed carbon cages. One example of such a case is the use of fullerene oxides as precursors,[38,39] with MALDI being the ionization method

selected, and the aggregates formed consist of bridged species. The products are made up of two or more fullerene moieties which are bound to each other by a bridge which resembles a furanoid ring; each bridge consists of one C-O-C bond and one σ C-C bond, as discussed in Chapter Six. Other derivatives form pure carbon clusters, but with an enhanced reactivity. An example of such behavior would be the use of fluorinated fullerenes for the formation of higher carbon clusters. In the positive-ion mode, it is evident that loss of fluorine radicals is accompanied by the efficient generation of carbon cluster radicals, which are highly suitable precursors for higher fullerene production. Coalescence leads to a much larger distribution of species than normally observed when examining only molecular ions of pure fullerene samples. Due to the similar gas-phase behavior of fluorinated and hydrogenated fullerenes, and the similarity in structure (both fluorine and hydrogen atoms are bound to the carbon cage through σ bonds, and the fluorine content is typically 18, 36, or 48 fluorine atoms) it it therefore of particular interest to establish the reactivity of hydrogenated fullerenes with respect to higher carbon cluster generation.

Figure 4 shows a comparison between two LDI mass spectra obtained using the Kratos Kompact MALDI IV, where Figure 4a shows a spectrum obtained using a C_{60} sample, and Figure 4b depicts a spectrum recorded using a $C_{60}H_{36}$ sample. The coalescence of C_{60} is well known,[26,27] and the spectrum shown in Figure 4a is typical of this behavior. C_2 loss from C_{60} can be seen, and higher carbon clusters are present at higher mass, with the most intense cluster being $C_{112}^{+\bullet}$. As seen in Figure 4b, the laser desorption/ionization of $C_{60}H_{36}$ resulted in the generation of many pure carbon fragments and fragments which also contained hydrogen, and it may also be noted that when examining the hydrogen containing species, uneven hydrogen content was observed with stronger intensity than even hydrogen content, as has been reported previously. Coalescence of the hydrogenated

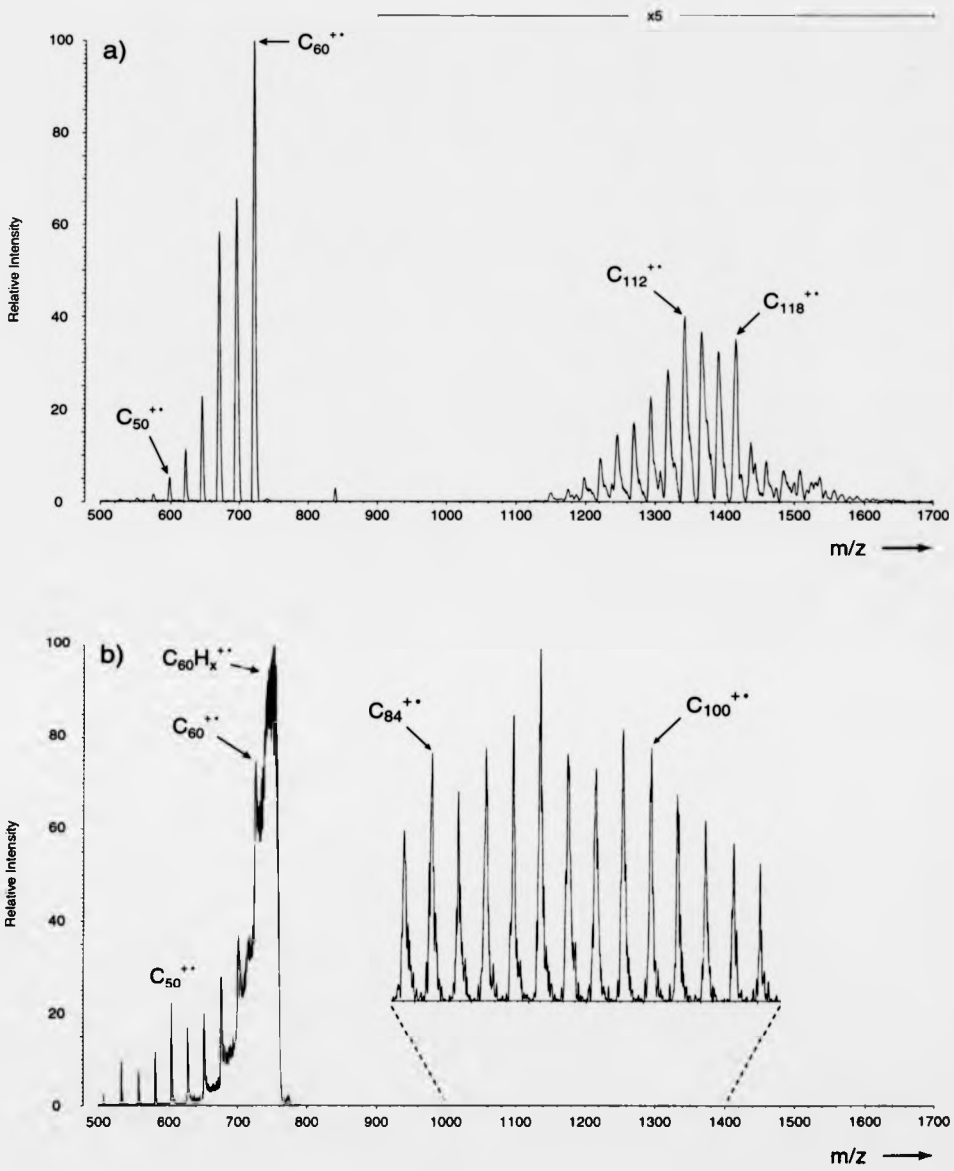

Figure 4: Positive-ion mode mass spectra showing the results of coalescence reactions using pure and hydrogenated C_{60}, respectively. Spectrum a was acquired using a pure C_{60} sample, where coalescence products are clearly in evidence with the characteristic distribution. Spectrum b was obtained using a $C_{60}H_{36}$ sample and clearly demonstrates the reduced efficiency of coalescence when using hydrogenated C_{60}.

fullerene species was indeed observed, but the signals were very weak. In order to increase the sensitivity of the instrument, the ion gate was employed to select only ions formed by coalescence reactions, so that the detector would not be saturated by the fragment ions which were much more intense. The result of this experiment is shown as the inset for Figure 4b. Further evidence for the reduced reactivity, with respect to coalescence, is the fact that a much higher laser fluence was required before higher carbon clusters could be generated with the intensity shown in the inset. Although it is difficult to quantify the relative reactivities, it is estimated that the intensities of the carbon clusters generated using $C_{60}H_{36}$ were two orders of magnitude lower than the corresponding carbon clusters generated using C_{60}. Though the signals were weak, it was still possible to establish that the carbon cluster signals were spaced by 24 Da, which leads to the conclusion that this is indicative of C_2 loss and therefore the species generated are pure carbon clusters. However, because of the poor resolving power of the Kompact MALDI IV, it is not possible the categorically state that these are pure carbon clusters; it is possible that hydrogen may be present. It must also be noted that the intensities within the distribution of fused species do not match the expected pattern, which would be expected to be centered around masses which represent multiples of C_{60}. Fusion of pure fullerenes results in distributions of products as shown in Figure 4a, where certain structures are more favorable than others. When using $C_{60}H_{36}$, it was notable that no such pattern was observed and there was no clear preference for specific structures, and this more closely resembles the behavior of fluorinated fullerenes. Although the lack of preferred structures is similar, the decreased reactivity is in stark contrast to the behavior of fluorinated fullerenes, which undergo coalescence to a much greater degree than pure fullerenes. Fluorinated fullerene targets display a much more enhanced tendency to undergo coalescence reactions than their hydrogenated counterparts. The reason for this lies in the fact that fluorine is readily

liberated from the C_{60} core, and the carbon core may then undergo fusion reactions, resulting in the generation of higher fullerene species in the gas-phase. As can be seen in Figure 4b, laser ablation of the $C_{60}H_{36}$ target leads to the observation of ions where the major signals represent carbon clusters which still possess hydrogen. It must therefore be concluded that hydrogen attachment amongst such ionic species adversely affects laser-induced coalescence reactions. It is interesting to note that fluorinated fullerenes possess a higher ionization potential than their respective, pure fullerenes, while hydrogenated fullerenes possess a lower ionization potential than the respective, pure fullerenes. For example, the ionization potential of $C_{60}F_{48}$ has been determined to be 12.0 eV,[40,41] and the ionization energy of $C_{60}F_{36}$ has been found to be 11.0 eV;[41] the ionization potential of $C_{60}F_{18}$ is still under investigation but is believed to be between 10 and 11 eV.[42] C_{60} is well known to possess an ionization potential of 7.6 eV.[43-46] Requiring the lowest energy input, the ionization energy of $C_{60}H_{36}$ is believed to be approximately 7.4 eV.[42] Thus, fluorinated fullerenes must acquire a greater internal energy in order to ionize, representing the absorption of a greater number of photons. The acquisition of a larger internal energy prior to ionization will lead to competition between ionization and dissociation channels, where it appears that fluorine radical loss is favored. This would account for the predominant observation of pure fullerene species rather than fluorinated species under LDI conditions. The lowered ionization energy of $C_{60}H_{36}$ would appear to lead to a favoring of ionization over fragmentation, explaining the observation of ionic species which still possess hydrogen. The decreased number of π bonds available for bonding found amongst ionic species which still possess a significant number of exohedrally bound atoms may be one possible reason hydrogenated fullerenes do not undergo such reactions in the gas-phase. The differences in ionization potential of the three species may explain the differences in observed coalescence behavior due to the initial differences in internal energy of the neutrals

(hence, differing extents of fragmentation), and therefore formation of different precursors for fusion reactions within the ion source.

4.4 Summary

The gas-phase behavior of a hydrogenated fullerene sample, $C_{60}H_{36}$, was investigated using a variety of mass spectrometers and ionization techniques. A sector instrument of BE geometry, coupled with EI, was used to obtain mass spectra which show the presence of multiply charged ions up to $C_{60}H_x^{4+}$ and also to obtain MIKE spectra which revealed information about the fragmentation dynamics. Use was made of a hybrid instrument of BEqQ geometry, coupled with LSIMS as the ionization technique, has further corroborated the results. It has been shown that fragmentation occurs via the loss of C_nH_x neutrals, although the exact hydrogen content could not be established for instrumental reasons. The fragmentation behavior closely resembles that of fluorinated fullerenes, rather than that of organic fullerene derivatives. Attempts to coalesce the hydrogenated fullerene under LDI conditions, using a ToF instrument, revealed a greatly reduced tendency to undergo coalescence reactions with respect to pure fullerenes. It is assumed that the lower ionization potential with respect to pure and fluorinated fullerenes results in lower internal energies of the neutrals, which are therefore less likely to undergo fragmentation. As a result, the ionic species will possess a significant number of hydrogen atoms and the lack of sufficient number of double bonds (π orbitals) for efficient fusion reactions is likely to hinder coalescence.

4.5 References

1) Haufler, R. E.; Conceicao, J.; Chibante, L. P. F.; Chai, Y.; Byrne, N. E.; Flanagan, S.; Haley, M. M.; O'Brien, S. C.; Pan, C.; Xiao, Z.; Billups, W. E.; Ciufolini, M. A.; Hauge, R. H.; Margrave, J. L.; Wilson, L. J.; Curl, R. F.; Smalley, R. E. *J. Phys. Chem.* **1990**, *94*, 8634-8636.

2) Attalla, M. I.; Vassallo, A. M.; Tattam, B. N.; Hanna, J. V. *J. Phys. Chem.* **1993**, *97*, 6329.

3) Lobach, A. S.; Perov, A. A.; Rebrov, A. I.; Roshchupkina, O. S.; Tkacheva, V. A.; Stepanov, A. N. *Russian Chem. Bulletin* **1997**, *46*, 641-648.

4) Darwish, A. D.; Abdul-Sada, A. a. K.; Langley, G. J.; Kroto, H. W.; Taylor, R.; Walton, D. R. M. *J. Chem. Soc. Perkin Trans. 2* **1995**, 2359-2365.

5) Darwish, A. D.; Kroto, H. W.; Taylor, R.; Walton, D. R. M. *J. Chem. Soc. Perkin Trans. 2* **1996**, 1415-1418.

6) Banks, M. R.; Dale, M. J.; Gosney, I.; Hodgson, P. K. G.; Jennings, R. C. K.; Jones, A. C.; Lecoultre, J.; Langridge-Smith, P. R. R.; Maier, J. P.; Scrivens, J. H.; Smith, M. J. C.; Smyth, C., J.; Taylor, A. T.; Thorburn, P.; Webster, A. S. *J. Chem. Soc. Chem. Commun.* **1993**, 1149-1152.

7) Möder, M.; Nüchter, M.; Ondruschka, B.; Czira, G.; Vékey, K.; Barrow, M. P.; Drewello, T. *Int. J. Mass Spectrom.* **2000**, *195/196*, 599-607.

8) Billups, W. E.; Gonzalez, A.; Gesenberg, C.; Luo, W.; Marriott, T.; Alemany, L. B.; Saunders, M.; Jiménez-Vázquez, H. A.; Khong, A. *Tetrahedron Lett.* **1997**, *38*, 175-178.

9) Hall, L. E.; McKenzie, D. R.; Attalla, M. I.; Vassallo, A. M.; Davis, R. L.; Dunlop, J. B.; Cockayne, D. J. H. *J. Phys. Chem.* **1993**, *97*, 5741-5744.

10) Dunlap, B. I.; Brenner, D. W.; Mintmire, J. W.; Mowrey, R. C.; White, C. T. *J. Phys. Chem.* **1991**, *95*, 5763-5768.

11) Austin, S. J.; Batten, R. C.; Fowler, P. W.; Redmond, D. B.; Taylor, R. *J. Chem. Soc. Perkin Trans. 2* **1993**, 1383-1386.

12) Bühl, M.; Thiel, W.; Schneider, U. *J. Am. Chem. Soc.* **1995**, *117*, 4623-4627.

13) Fowler, P. W.; Sandall, J. P. B.; Taylor, R. *J. Chem. Soc. Perkin Trans. 2* **1997**, 419-423.

14) Heine, T.; Fowler, P. W.; Rogers, K. M.; Seifert, G. *J. Chem. Soc. Perkin Trans. 2* **1999**, 707-711.

15) Gol'dshleger, N. F.; Moravskii, A. P. *Russian Chem. Rev.* **1997**, *66*, 323-342.

16) Boltalina, O. V. *J. Fluorine Chem.* **2000**, *101*, 273-278.

17) Boltalina, O. V.; Borschevskii, A. Y.; Sidorov, L. N.; Street, J. M.; Taylor, R. *J. Chem. Soc. Chem. Commun.* **1996**, 529-530.

18) Boltalina, O. V.; Sidorov, L. N.; Bagryantsev, V. F.; Seredenko, V. A.; Zapol'skii, A. S.; Street, J. M.; Taylor, R. *J. Chem. Soc. Perkin Trans. 2* **1996**, 2275-2278.

19) Boltalina, O. V.; Bühl, M.; Khong, A.; Saunders, M.; Street, J. M.; Taylor, R. *J. Chem. Soc. Perkin Trans. 2* **1999**, 1475-1479.

20) Rüchardt, C.; Gest, M.; Ebenhoch, J.; Beckhaus, H.-D.; Campbell, E. E. B.; Tellgmann, R.; Schwarz, H.; Weiske, T.; Pitter, S. *Angew. Chem. Int. Ed. Engl.* **1993**, *32*, 584-586.

21) Rogner, I.; Birkett, P.; Campbell, E. E. B. *Int. J. Mass Spectrom.* **1996**, *156*, 103-108.

22) Liu, T.-Y.; Shiu, L.-L.; Luh, T.-Y.; Her, G.-R. *Rapid Commun. Mass Spectrom.* **1995**, *9*, 93-96.

23) Chapman, J. R. *Practical Organic Mass Spectrometry: A Guide for Chemical and Biochemical Analysis*; 2nd ed.; John Wiley and Sons Ltd.: Chichester, 1993.

24) de Hoffmann, E.; Charette, J.; Stroobant, V. *Mass Spectrometry: Principles and Applications*; John Wiley and Sons Ltd.: Chichester, 1996.

25) Darwish, A. D.; Avent, A. G.; Taylor, R.; Walton, D. R. M. *J. Chem. Soc. Perkin Trans. 2* **1996**, 2051-2054.

26) Yeretzian, C.; Hansen, K.; Diederich, F.; Whetten, R. L. *Nature* **1992**, *359*, 44-47.

27) Yeretzian, C.; Hansen, K.; Diederich, F.; Whetten, R. L. *Supplement to Z. Phys. D.* **1993**, *26*, S 300-304.

28) Hunter, J. M.; Fye, J. L.; Bolvin, N. M.; Jarrold, M. F. *J. Phys. Chem.* **1994**, *98*, 7440-7443.

29) Zhu, L.; Wang, S.; Li, Y. *J. Chem. Phys.* **1994**, *101*, 8592-8595.

30) Liu, Z.-Y.; Wang, C.-R.; Huang, R.-B.; Zheng, L.-S. *Int. J. Mass Spectrom. Ion Processes* **1995**, *145*, 1-7.

31) Xie, Z. X.; Liu, Z. Y.; Wang, C. R.; Huang, R. B.; Lin, F. C.; Zheng, L. S. *J. Chem. Soc. - Faraday Transactions* **1995**, *91*, 987-990.

32) Onoe, J.; Takeuchi, K. *J. Mass Spectrom.* **1998**, *33*, 387-391.

33) Hansen, K.; Yeretzian, C.; Whetten, R. L. *Chem. Phys. Lett.* **1994**, *218*, 462-466.

34) Beck, R. D.; Weis, P.; Bräuchle, G.; Kappes, M. M. *J. Chem. Phys.* **1994**, *100*, 262-270.

35) Mitzner, R.; Winter, B.; Kusch, C.; Campbell, E. E. B.; Hertel, I. V. *Z. Phys. D* **1995**, *37*, 89-95.

36) Beck, R. D.; Stoermer, C.; Schulz, C.; Michel, R.; Weis, P.; Bräuchle, G.; Kappes, M. M. *J. Chem. Phys.* **1994**, *101*, 3243-3249.

37) Beck, R. D.; Weis, P.; Hirsch, A.; Lamparth, I. *J. Phys. Chem.* **1994**, *98*, 9683-9687.

38) Barrow, M. P.; Tower, N. J.; Taylor, R.; Drewello, T. *Chem. Phys. Lett.* **1998**, *293*, 302-308.

39) Al-Jafari, M. S.; Barrow, M. P.; Taylor, R.; Drewello, T. *Int. J. Mass Spectrom.* **1999**, *184*, L1-L4.

40) Steger, H.; Mische, U.; Kamke, W.; Ding, A.; Fieber-Erdmann, M.; Drewello, T. *Chem. Phys. Lett.* **1997**, *276*, 39-46.

41) Vasil'ev, Y. V.; Boltalina, O. V.; Tuktarov, R. F.; Mazunov, V. A.; Sidorov, L. N. *Int. J. Mass Spectrom. Ion Processes* **1998**, *173*, 113-125.

42) Vasil'ev, Y. V., personal communication

43) Lichtenberger, D. L.; Nebesny, K. W.; Ray, C. D.; Huffman, D. R.; Lamb, L. D. *Chem. Phys. Lett.* **1991**, *176*, 203-208.

44) Zimmerman, J. A.; Eyler, J. R.; Bach, S. B. H.; McElvany, S. W. *J. Chem. Phys.* **1991**, *94*, 3556-3562.

45) de Vries, J.; Steger, H.; Kamke, B.; Menzel, C.; Weisser, B.; Kamke, W.; Hertel, I. V. *Chem. Phys. Lett.* **1992**, *188*, 159-162.

46) Lifshitz, C. *Mass Spectrom. Rev.* **1993**, *12*, 261-284.

35) Mitzner, R.; Winter, B.; Kusch, C.; Campbell, E. E. B.; Hertel, I. V. *Z. Phys. D* **1995**, *37*, 89-95.

36) Beck, R. D.; Stoermer, C.; Schulz, C.; Michel, R.; Weis, P.; Bräuchle, G.; Kappes, M. M. *J. Chem. Phys.* **1994**, *101*, 3243-3249.

37) Beck, R. D.; Weis, P.; Hirsch, A.; Lamparth, I. *J. Phys. Chem.* **1994**, *98*, 9683-9687.

38) Barrow, M. P.; Tower, N. J.; Taylor, R.; Drewello, T. *Chem. Phys. Lett.* **1998**, *293*, 302-308.

39) Al-Jafari, M. S.; Barrow, M. P.; Taylor, R.; Drewello, T. *Int. J. Mass Spectrom.* **1999**, *184*, L1-L4.

40) Steger, H.; Mische, U.; Kamke, W.; Ding, A.; Fieber-Erdmann, M.; Drewello, T. *Chem. Phys. Lett.* **1997**, *276*, 39-46.

41) Vasil'ev, Y. V.; Boltalina, O. V.; Tuktarov, R. F.; Mazunov, V. A.; Sidorov, L. N. *Int. J. Mass Spectrom. Ion Processes* **1998**, *173*, 113-125.

42) Vasil'ev, Y. V., personal communication

43) Lichtenberger, D. L.; Nebesny, K. W.; Ray, C. D.; Huffman, D. R.; Lamb, L. D. *Chem. Phys. Lett.* **1991**, *176*, 203-208.

44) Zimmerman, J. A.; Eyler, J. R.; Bach, S. B. H.; McElvany, S. W. *J. Chem. Phys.* **1991**, *94*, 3556-3562.

45) de Vries, J.; Steger, H.; Kamke, B.; Menzel, C.; Weisser, B.; Kamke, W.; Hertel, I. V. *Chem. Phys. Lett.* **1992**, *188*, 159-162.

46) Lifshitz, C. *Mass Spectrom. Rev.* **1993**, *12*, 261-284.

Chapter Five

Coalescence of Fluorinated Fullerenes Using Laser Desorption/Ionization

5.1 Introduction

Amongst the variety of fullerene derivatives, fluorinated fullerenes represent some of the most investigated. Different synthetic methods used for the formation of fluorinated fullerenes have been tested. Fluorination using F_2 leads to the production of highly fluorinated fullerenes, such as $C_{60}F_n$, where n = 4 and 48. The use of metal fluorides during the synthesis of fluorinated fullerenes leads to the formation of more specific products such as $C_{60}F_n$ where n = 18, 36, and 48. An overview of fluorinated fullerene synthesis has recently been published by Boltalina.[1] Fluorination of C_{60} raises the ionization energy, though, in contrast, hydrogenation seems to lower the ionization potential of the compound. While $C_{60}H_{36}$ ionizes at approximately 7.4 eV,[2] $C_{60}F_{48}$ ionizes at 12.0 eV,[3,4] $C_{60}F_{36}$ ionizes at 11.0 eV,[4] and $C_{60}F_{18}$ is thought to ionize between 10 and 11 eV,[2] though this is still under investigation; C_{60} is well known to ionize at 7.6 eV.[5-8] Near edge X-ray absorption fine spectra (NEXAFS) and ultra-violet photoemission spectroscopy (UPS) have been used to study fluorinated fullerenes,[9] and the electronic structure of $C_{60}F_{48}$ has been studied using X-ray fluorescence spectroscopy.[10] There are also structural parallels between fluorinated and hydrogenated fullerenes. The structure of $C_{60}H_{36}$ was found to be identical to that of $C_{60}F_{36}$.[11] The geometries of $C_{60}H_{18}$ and $C_{60}F_{18}$ have also been compared.[12,13] The reasons for such similarities is still a subject of intense investigation, comparing structures of $C_{60}X_n$ where X = F or H.[13] When comparing $C_{60}X_{36}$ analogs where X = F or H , the fluorinated compound is found to be more stable than its hydrogenated counterpart. Following semi-empirical calculations, an explanation was provided that fluorination relieves the steric strain on the carbon cage to a greater extent than hydrogenation; near planarity is achieved with the four remaining arene rings of the fullerene core.[12] It is now known that $C_{60}F_{48}$, $C_{60}F_{36}$, and $C_{60}F_{18}$ possess four, three, and one benzenoid rings,

respectively; the π electrons are delocalized in each of these benzenoid rings and contributes to the stability of the system.[14] Noting that fluorine is more electron withdrawing than hydrogen, it was concluded that enhancing the stability of the system is better achieved through the reduction in strain than increasing the degree aromaticity.

It is clear that mass spectrometry has always played a unique role in the investigation of fullerenes and their derivatives, just as it played a role in the initial discovery of C_{60} by Kroto et al.[15] In particular, electron ionization (EI), liquid secondary ion mass spectrometry (LSIMS), and laser desorption/ionization (LDI) have been used predominantly as ionization techniques. Tuinman et al. investigated the character and stability of highly fluorinated fullerenes using UV-vis spectroscopy and mass spectrometry, making use of a variety of ionization techniques that included field desorption (FD), thermal desorption (TD), electron ionization (EI) and laser desorption ionization (LDI).[16] Under LDI conditions, fluorinated fullerenes were observed to undergo fluorine loss in the negative-ion mode while the carbon core remained largely intact; in both the positive-ion and negative-ion modes, fluorine loss also predominated when using thermal desorption. Using EI, loss of perfluoroalkyl groups, C_mF_n, was observed and losses of $CF_3^{\bullet}$, $C_2F_5^{\bullet}$, and $C_3F_7^{\bullet}$ were found to be particularly common. Collision-induced dissociation led to similar results, but the loss of $F^{\bullet}$ was also noted, as well as the loss of even electron species such as CF_2, CF_4, C_2F_6, and C_3F_8.

Coalescence of pure fullerenes is a known phenomenon which was first discovered by Yeretzian et al.,[17,18] and since then, many studies into the coalescence have been performed.[19-23] While the mechanism of coalescence is still under investigation, it is believed to involve the fusion of excited, neutral species[24] or the fusion of a neutral and an ion,[25] but in either case, loss of C_2 units is a known cooling channel following coalescence. Following

the discovery of coalescence of pure fullerenes, studies into the fusion of fullerene derivatives became increasingly abundant.[26-29] The unimolecular dissociation behavior of ionized fluorinated fullerenes differs dramatically from the behavior observed for pure fullerene cation radicals. In addition to the loss of $F^{\bullet}$, the dissociation pattern is governed by the loss of perfluoroalkyl radicals such as $CF_3^{\bullet}$, $C_2F_5^{\bullet}$, and $C_3F_7^{\bullet}$ as revealed by Tuinman et al.[16] and further demonstrated by Cozzolino et al.[30] Upon dissociation, ionized fluorinated fullerenes thus generate an array of ions possessing unusual carbon compositions such as $C_{59}F_x^+$ and $C_{57}F_x^+$. In principle, these species might also be formed under LDI conditions and take part in coalescence reactions to form coalesced species of unusual structures. Fluorinated fullerenes can exhibit an almost complete coverage of the carbon core by the heteroatom and the question of steric hindrance during such fusion reactions may therefore be raised. It is also possible that the strong C-F bond weakens the bonding within the carbon core, thus facilitating C-C bond cleavage and leading to a partial rupture of the cage. It is known that fusion of fullerene and fullerene fragments leads to the production of higher carbon clusters, but there has been a question concerning whether or not "Teflon balls,"[31] which have traditionally been a source of great interest, may be produced. The mechanism behind such a reaction is of current research interest.[24,25,32] Coalescence of fullerene derivatives[26-29] is of interest from a mechanistic point of view, as the aggregates formed are not always pure fullerenes, with closed carbon cages. One example of such a case is the use of fullerene oxides as precursors.[28,29] Indeed, Cozzolino et al. have shown that it is also possible to form higher fullerenes under LDI conditions using fluorinated fullerenes as the precursor material.[30]

The coalescence of fluorinated fullerenes has not previously been investigated in detail. Those experiments previously performed using fluorinated fullerenes[30] were

restricted for instrumental reasons to a very narrow mass range, and variation of the target material was also not possible due to the lack of availability of a wide variety of fluorinated fullerene compounds at the time of investigation. The objective of the following investigation is to obtain further insight into the coalescence of such species such as $C_{60}F_{18}$, $C_{60}F_{36}$, $C_{60}F_{48}$, and $C_{70}F_x$ (where the sample contains a mixture of fluorinated C_{70} species). A time-of-flight (ToF) mass spectrometer, equipped with an LDI ion source, was used throughout the course of the investigation. Comparisons were made between the coalesced species formed in the gas-phase as a function of the fluorine content. As will be demonstrated, due to the increased energy requirements for the ionization and dissociation of each compound as the fluorine content increases, there is also a close correlation between the fluorine content, for a given carbon core size, and the laser irradiance required. By studying the coalescence reactions of the different samples, it is possible to obtain further insight into the reaction mechanisms involved.

5.2 Experimental

A Kratos Kompact MALDI IV reflectron time-of-flight mass spectrometer was used during the course of the experiments. The instrument uses a nitrogen laser, operating with a wavelength of 337 nm and a pulse width of 3 ns, for desorption/ionization of the sample. After the sample has been ablated, the ions formed are extracted into the flight tube by a 20 kV accelerating potential. Selection of an ion or a range of ions is possible by making use of two deflecting electrodes which constitute the "ion gate." The ion gate is activated to deflect unwanted ions and is then switched off to allow the passage of the desired ions, and then switches on once more to deflect all other ions. Whether or not the selection of ions is performed, the ions continue their flight in the flight tube until they are reflected by

a curved field reflectron, the presence of which enhances the operating resolution of the instrument, and the ions are then detected by an electron multiplier. Samples were prepared by dissolving the solid material in toluene to form a saturated solution. The solutions were then pipetted on to target slides, ensuring that a sufficient and visible quantity of material has been deposited. The solvent was allowed to evaporate and a slide would then be inserted into the ion source of the instrument prior to analysis. The reason for the use of saturated solutions and for depositing a large amount of sample on each slide is that the coalescence reactions of fullerenes are heavily dependent upon the density of the plume produced following laser desorption/ionization (LDI) of the sample. Increasing the density of the ions and neutrals in the plume increases the probability of collisions in the gas-phase and hence coalescence as well, which in turn increases the signal intensity of coalesced species.

Three samples of fluorinated fullerenes were used during the following experiments: $C_{60}F_{18}$, $C_{60}F_{36}$, and $C_{60}F_{48}$. All three samples were provided by O. Boltalina (Moscow State University, Moscow, Russia), who wished to acknowledge the support from A. Yu. Lukonin and A. S. Zapol'skii during the syntheses of the samples. $C_{60}F_{48}$ was prepared by reaction of C_{60} with elemental fluorine at 350 °C for four hours in a nickel flow reactor.[33] $C_{60}F_{36}$ was formed during the reaction between C_{60} and MnF_3 at 380 °C, and this reaction yields almost a single product.[34] The $C_{60}F_{18}$ sample was synthesized by reacting C_{60} with K_2PtF_6 at 460 °C, resulting in a 90% yield of $C_{60}F_{18}$ and 10% $C_{60}F_{36}$, and purification may be performed using high performance liquid chromatography (HPLC).[35] Both $C_{60}F_{36}$ and $C_{60}F_{18}$ were prepared under vacuum and the reagents were used in a stoichiometric ratio, ground up, and loaded into a glass reactor.

5.3 Results and Discussion

Four samples were to be analyzed: $C_{60}F_{18}$, $C_{60}F_{36}$, $C_{60}F_{48}$, and $C_{70}F_x$ (where the most abundant fluorine contents are thought to be x = 52 and 56). It should first be noted that $C_{60}F_{36}$, $C_{60}F_{48}$, and $C_{70}F_x$ were initially all analyzed within three consecutive days of each other. The sample of $C_{60}F_{18}$, also analyzed at the same time as the other samples, had been shown to contain traces of C_{60} while the other samples were pure, and so the resulting $C_{60}F_{18}$ spectra could not be counted as reliable evidence. A new sample was prepared and HPLC was used for the separation of the products to ensure its purity; this sample was analyzed one year later. During that time, a new laser cartridge was installed in the instrument, which made it difficult to make direct comparisons of the laser irradiances used for each of the samples. The laser irradiance was estimated by assuming that the newly installed laser cartridge closely follows the manufacturer's performance specifications of the correlation between the actual laser irradiance and the "laser power" setting (in arbitrary units) chosen using the software. The appearance of spectra obtained using both the old and the new laser cartridges were then compared in order to estimate the laser irradiances used in practice. Figure 1 shows the mass spectra obtained using $C_{60}F_{18}$ at two different laser irradiances. Figure 1a shows the spectrum obtained at a laser irradiance of approximately 4.42×10^7 W cm^{-2}, and it should be noted that for this spectrum alone, the ion gate was used to select ions of mass 600 - 3000 Da in order to enhance the sensitivity of the instrument, by decreasing the chances of saturation of the detector. Near complete loss of the fluorine atoms from the fullerene cage can be observed. It is interesting to note that $C_{60}F_{17}^{+\bullet}$, $C_{60}F_{15}^{+\bullet}$, and $C_{60}F_{13}^{+\bullet}$ can be observed, as radical cations of fluorinated species have not been observed in any LDI experiments prior to this investigation. Fluorinated species can be observed in the negative-ion mode, but use of the positive-ion mode almost

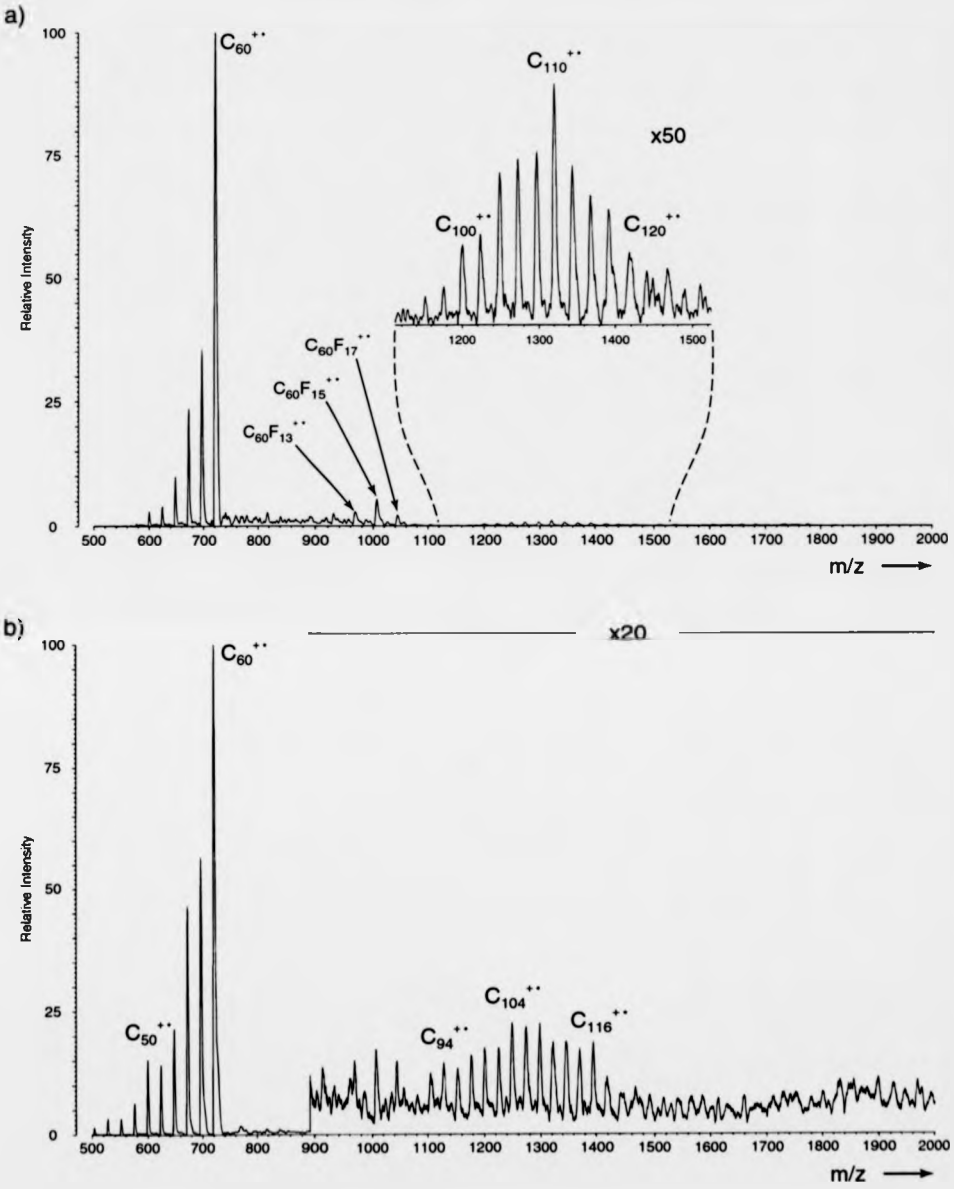

Figure 1: Positive-ion mode mass spectrum obtained using $C_{60}F_{18}$. Laser irradiances of 4.42×10^7 W cm^{-2} and 8.12×10^7 W cm^{-2} were used to produce spectra a and b, respectively.

always results in the observation of only pure fullerene ions. It is known from the literature that dissociation of the molecular ion occurs via the loss of atomic fluorine radicals and the loss of perfluoroalkyl radicals,[16,30] and in many ways, such gas-phase behavior is analogous to the results obtained when using hydrogenated fullerenes, which is discussed in Chapter Four. At higher mass, the coalesced species can be observed. These aggregates are indeed pure carbon clusters, spaced by C_2 (24 Da) as expected for pure carbon clusters; no presence of fluorine can be reliably discerned. The distribution of products is centered around $C_{110}^{+\bullet}$ and such a distribution is very similar in appearance to coalesced species produced using C_{60} as the target material. The differences are that the distribution of aggregates formed using C_{60} tends to be centered more closely around $C_{118}^{+\bullet}$ or $C_{120}^{+\bullet}$, and that coalescence can be induced (using C_{60}) at a laser irradiance of approximately 2.40×10^7 W cm^{-2} with the present instrument. The laser irradiance required for the coalescence of fluorinated fullerenes would be expected to be greater, due to the need to remove the fluorine atoms from the carbon cage prior to the formation of clusters, and therefore a greater energy input is required. Figure 1b shows a mass spectrum of $C_{60}F_{18}$ recorded at a laser irradiance of approximately 8.12×10^7 W cm^{-2}, and the ion gate is not used. The fluorinated fullerene radical cations are no longer detected, and the degree of fragmentation of $C_{60}^{+\bullet}$ has been greatly increased. Another change is the shape of the distribution of higher carbon clusters. Whereas at the lower laser irradiance (Figure 1a) the appearance resembles that of a Gaussian distribution, at the higher laser irradiance, the intensity of the different clusters is more even, resulting in a pattern which no longer resembles a Gaussian distribution. The clusters are also centered around a slightly lower mass. This may be attributable to both the slightly increased fragmentation of the fullerene precursors, with the coalescence of smaller fragments leading to the generation of smaller carbon clusters,

and also due to the increased internal energy of coalesced species, leading to fragmentation following coalescence.

Analysis of $C_{60}F_{36}$ led to the attainment of quite different results. Figure 2a shows the mass spectrum of $C_{60}F_{36}$ recorded at a laser irradiance of about 7.02×10^{7} W cm^{-2}. In stark contrast to the spectra recorded using $C_{60}F_{18}$, there is no well-defined cluster formation located around the mass expected for a C_{60} dimer. Instead, a particularly intense range of higher fullerenes is observed between the masses of about 800 Da and 1400 Da, and carbon clusters of roughly even intensity can be seen stretching from 1400 Da to 4000 Da. The presence of fluorine was not apparent and the clusters are spaced by 24 Da (C_2) as would be expected for fullerenes. The laser irradiance required in order to record this spectrum is higher than that used in Figure 1a owing to the fact that $C_{60}F_{36}$ has a higher fluorine content, and a higher energy input is needed in order to generate the pure carbon fragments necessary for coalescence to occur. At a laser irradiance of approximately 1.11×10^{8} W cm^{-2}, the spectrum shown in Figure 2b was recorded. C_{60}^{4+} may be seen to undergo increased fragmentation as a result of the higher laser irradiance, and the appearance of the distribution of higher fullerenes has radically altered. The clusters of enhanced intensity between the masses of 800 and 1400 Da are no longer present, and higher fullerenes between the masses of 800 Da and 4000 Da can be seen, where the intensity decreases with increasing mass. This change in appearance mirrors the change seen between Figure 1a and 1b; at lower laser irradiance, a distinct distribution is favored due to the limited variation in size of the fragments available, while at higher laser irradiance, a range of carbon clusters of roughly equal intensity is present because of the wide variety of highly energized fragments that are available for coalescence. An explanation for this trend may be that the increased energy supplied to the sample increases fragmentation, leading to a

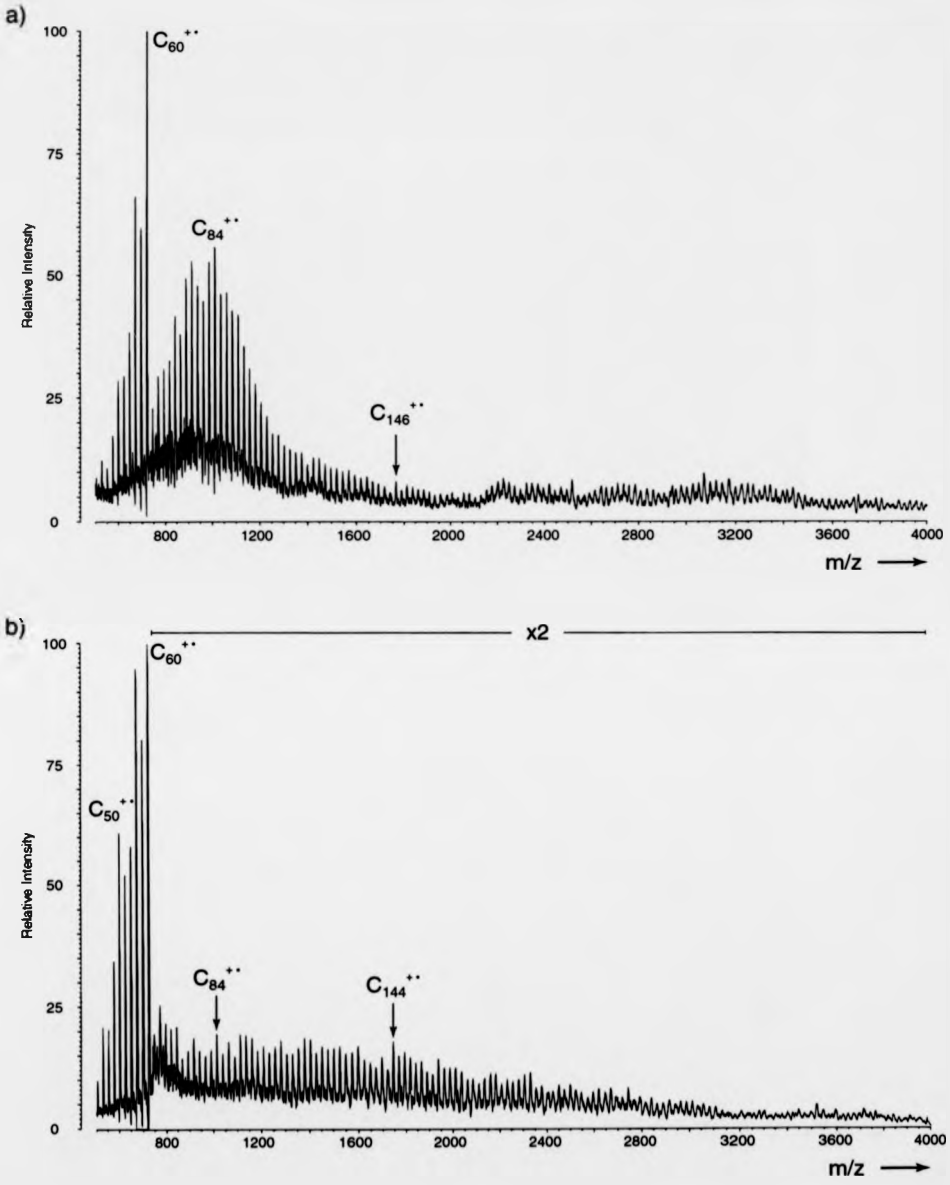

Figure 2: Positive-ion mode mass spectrum acquired using $C_{60}F_{36}$. Laser irradiances of 7.02×10^{7} W cm^{-2} and 1.11×10^{9} W cm^{-2} were used to produce spectra a and b, respectively.

larger variation of fragment sizes and with fragments of smaller size becoming increasingly intense. Increasing the fluorine content also leads to a requirement for an increasing energy input in order for pure fullerene fragments to be produced, and the argument becomes a circular one. As an increased number of fragments of smaller sizes become favored, a wider range of clusters are generated following coalescence reactions so that higher fullerenes become less selectively formed in the gas-phase. At lower laser irradiances, specific fragments such as $C_{60}^{+\bullet}$, $C_{58}^{+\bullet}$, $C_{56}^{+\bullet}$ and the like are favored, and this narrow range of precursors therefore leads to the selective production of higher fullerenes. A slight increase in the laser irradiance may only increase the fragmentation of coalesced species, due to the increase in their internal energy, while larger changes in the laser irradiance (or indeed fluorine content) will result in an obvious increase in the range of fragments, and hence precursors for coalescence, and in their abundance.

$C_{60}F_{48}$ was the final compound in the series of fluorinated C_{60} samples. Figure 3a shows the mass spectrum acquired at a laser irradiance of around 1.30×10^{8} W cm^{-2}. The threshold laser irradiance was determined during other experiments (spectra not shown). It may be noted that both $C_{60}F_{36}$ and $C_{60}F_{48}$ displayed similar tendencies at threshold laser irradiances, producing very weak carbon cluster signals which were present in a wide distribution similar to that observed when fusing pure fullerenes. However, it was noticeable that use of $C_{60}F_{36}$ yielded a distribution at higher mass (with the maximum intensity in a region of over 2400 Da) than the clusters generated when using $C_{60}F_{48}$, appearing with a maximum amongst the distribution closer to approximately 1300 Da. The spectra were not of sufficient quality to warrant presentation, and it was found that increasing the laser irradiance resulted in the enhanced signals seen in Figure 3a, while the distribution-like appearance was no longer present. There does not appear to be a stage at

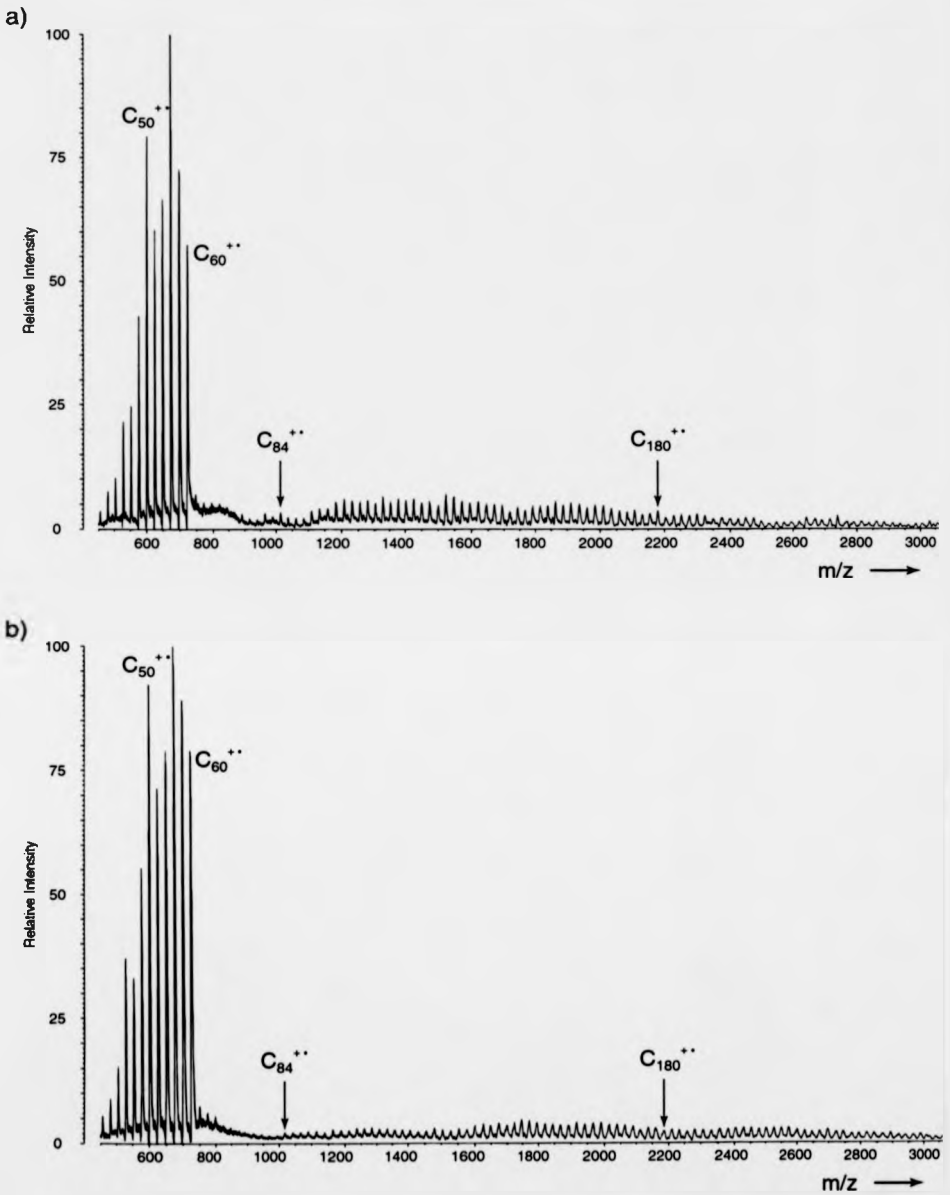

Figure 3: Positive-ion mass spectrum obtained using $C_{60}F_{48}$. Laser irradiances of 1.30×10^9 W cm^{-2} and 3.80×10^8 W cm^{-2} were used to produce spectra a and b, respectively.

which a distribution of higher carbon clusters are clearly generated, as are seen in Figures 1a and 2a, although it is possible to observe very weak signals in which such a trend is evident. Once a sufficient signal intensity has been obtained, the Gaussian distribution like appearance of the higher fullerenes disappears. A comparison with Figure 2b reveals that the fragmentation of $C_{60}^{+\bullet}$ is similar, although more marked in Figure 3a owing to the higher laser irradiance used, and that the patterns for the fullerenes formed in the gas-phase are not dissimilar. The greater fluorine content of $C_{60}F_{48}$ would mean that a greater energy is required to remove the extra fluorine atoms, compared to $C_{60}F_{36}$, and so the probability of increased fragmentation of pure fullerene fragments is also increased, purely on statistical grounds. In line with the hypothesis stated earlier, the generation of smaller fragments appears to lead to the lack of selective formation of specific carbon clusters. Figure 3b shows the spectrum procured at a laser irradiance of approximately 3.80×10^{8} W cm^{-2}, which is the maximum laser output for this particular laser cartridge. There is little difference compared to Figure 3a, except that the fragmentation of $C_{60}^{+\bullet}$ is enhanced further and the intensities of the higher fullerenes are perhaps more even. It is possible that fluorinated samples of a high fluorine content become less likely to selectively form particular carbon clusters due to the fact that such a high energy input is required to fragment the sample and to enable coalescence to take place. It must be assumed that a major component of the expanding material plume is constituted by smaller fragments, displaying behavior that is indicative of a lack of selective formation of higher carbon clusters.

Figure 4 shows a plot of the threshold laser irradiance required for coalescence reactions to occur versus the fluorine content of the C_{60} based sample. Only three samples are plotted here ($C_{60}F_{18}$, $C_{60}F_{36}$, and $C_{60}F_{48}$), and to increase the reliability of the plot, a greater range of samples must be investigated so that more data points may be plotted.

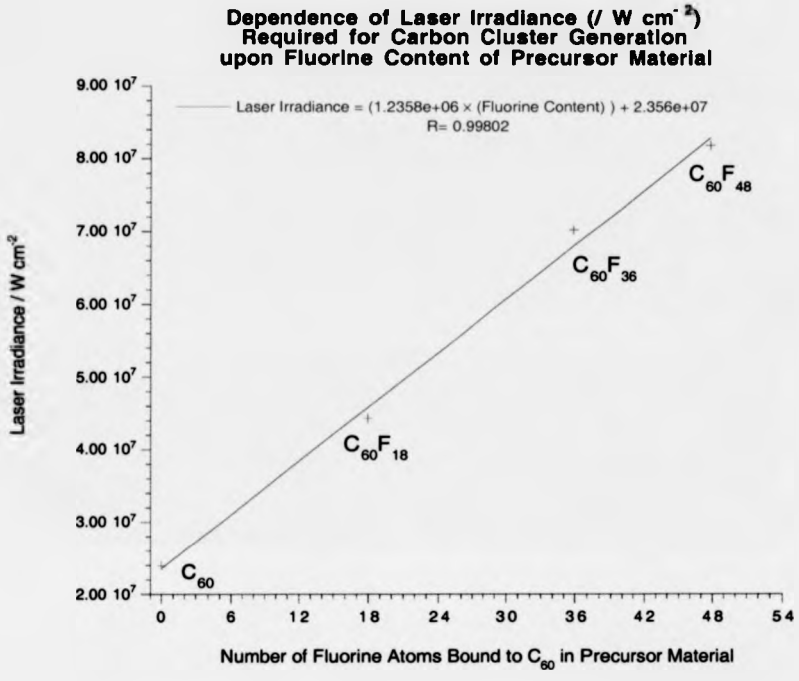

Figure 4: Graph showing the dependence of the laser irradiance required to form higher carbon clusters as a function of the fluorine content of the precursor used.

However, though the graph only displays such preliminary results, a linear dependence can be clearly seen. Increasing the fluorine content of the sample effectively increases the laser irradiance required for the initiation of coalescence reactions. From the results obtained so far, the following hypothesis may be proposed. Increasing the fluorine content of a sample of a given number of carbon atoms, for example increasing the fluorine content of C_{60}, increases the energy requirements for the fragmentation of the molecular ion to lead to the generation of the bare carbon cage. Increasing the energy supplied to a sample will also increase the statistical probability that fragments of smaller sizes will be formed and

will increase the viability of such dissociation channels. Fluorinated fullerenes may dissociate via more than one pathway, including loss of atomic fluorine radicals, loss of F_2, and, possibly as seen for ionized species, by the loss of perfluoroalkyl radicals; it is important to note this latter fragmentation route will lead to the shrinkage of the carbon cage size. Hence by increasing the fluorine content, the energy requirements for coalescence are increased as, for example, increased fluorine loss must occur prior to coalescence. This increased energy requirement therefore results in a net increase in the total internal energy of the sample, following laser ablation at increased laser irradiances. An increase in the net internal energy of the fullerene core, once fluorine loss has taken place, leads to increased fragmentation and thus the increased probability of the generation of smaller carbon fragments. The end result is the generation of smaller carbon fragments when increasing the fluorine content, due to the larger energy uptake required for coalescence. Therefore, the formation of smaller fragments and the formation of fragments over a greater variety of sizes makes the formation of favored carbon clusters less likely; there is a much wider range of possible precursors for coalescence. It is possible that once a certain fluorine content has been reached, the coalescence reactions are less varied, as the fragments produced prior to coalescence begin to vary in size and abundance less, and so the coalesced species formed become less varied in size and are relatively even in intensity. At higher laser irradiances, there will be increased fragmentation of initially generated coalescence products, which might also contribute towards the appearance of less selective cluster formation. A comparison may be drawn between the laser ablation of graphite and the laser ablation of fluorinated fullerene samples. Figure 5 shows the mass spectrum acquired by a research group working at Exxon in 1984,[16] prior to the discovery of C_{60} by Kroto et al.[15] The mass spectrum was obtained utilizing time-of-flight analysis following the laser ablation of a graphite surface. The trend is similar, but Figure 2a most of all shows a

remarkable similarity to Figure 5; the formation of carbon clusters of higher masses (not shown in Figure 5) following the laser ablation of graphite is well known, and the relative intensities of these species are similar to those observed for the coalescence products resulting from the use of fluorinated fullerenes. The laser ablation of a carbon surface, leading to the formation of many fragments of varying sizes is perhaps analogous to the mechanism postulated for the LDI of fluorinated fullerenes, where pure carbon fragments of varying sizes are formed prior to coalescence, and hence fullerene formation in the gas-phase.

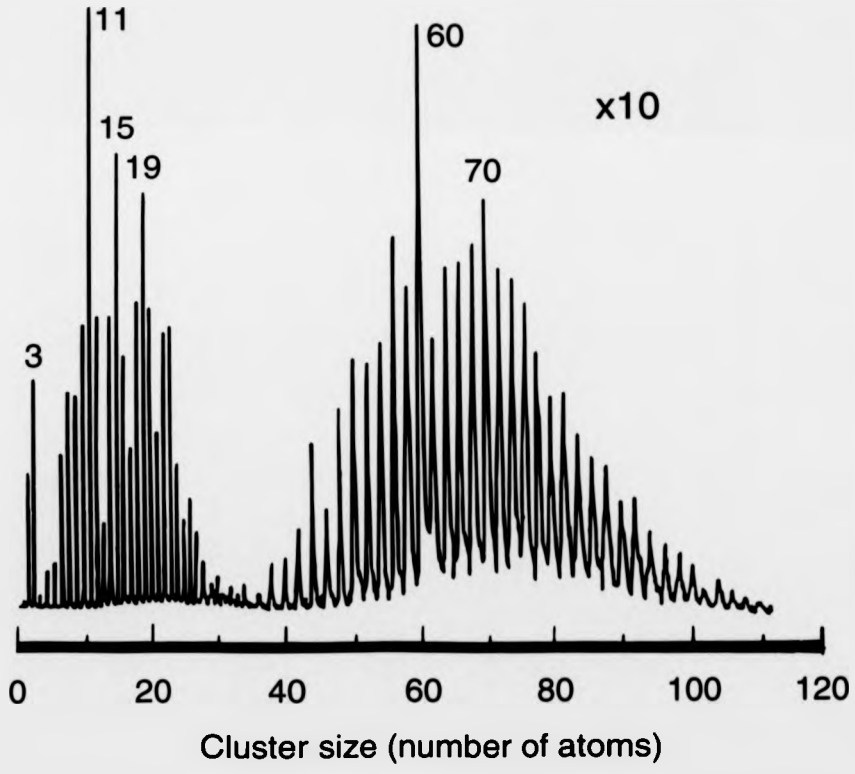

Figure 5: Positive-ion time-of-flight mass spectrum demonstrating the generation of carbon clusters in the gas-phase following the laser ablation of a graphitic surface.

A final investigation involved the coalescence of $C_{70}F_x$ for comparison, where the fluorine content varies as the sample is a mixture of compounds; possible compounds present included $C_{70}F_{52}$ and $C_{70}F_{56}$, although it is difficult to establish how many species were present. Figure 6 shows the resulting spectra. Figure 6a was acquired using a laser irradiance of about 6.02×10^7 W cm^{-2} while Figure 6b was obtained using a laser irradiance of approximately 1.51×10^8 W cm^{-2}. A weak distribution of favored products may be seen between the masses of $C_{70}^{+\bullet}$ and in the region of 1400 Da. These carbon clusters are only slightly more pronounced than others, but the extent of clusterization appears to be less than when C_{60}-based fluorinated samples were used. Carbon cluster signals become very weak after about m/z 2200, and it seems that no carbon cluster signals are detected by m/z 3000. Figure 6b shows that the extent of fullerene formation has greatly increased upon increasing the laser irradiance. This spectrum perhaps most closely resembles Figure 2b, where $C_{60}F_{36}$ was used, and this is not entirely unexpected as the laser irradiances used were similar. The difference between Figures 6a and 6b are analogous to the mass spectra of the other fluorinated compounds, where certain cluster sizes are favorable at a lower laser irradiance, but increasing the laser irradiance increases the range of fullerene fragment sizes, and so many more reaction pathways become available. A balance exists where, on the one hand, increasing the laser irradiance decreases the fragment sizes, but on the other hand, increasing the laser irradiance also increases the number of highly energized fragments available for reactions.

These experiments also answer the initial question about whether or not "Teflon balls"[31] can be generated by laser induced coalescence. Under the present conditions, the answer is certainly that they cannot be formed. A rationalization of this possibly has to be seen in the manner that energy is transferred to the system. The laser provides the system

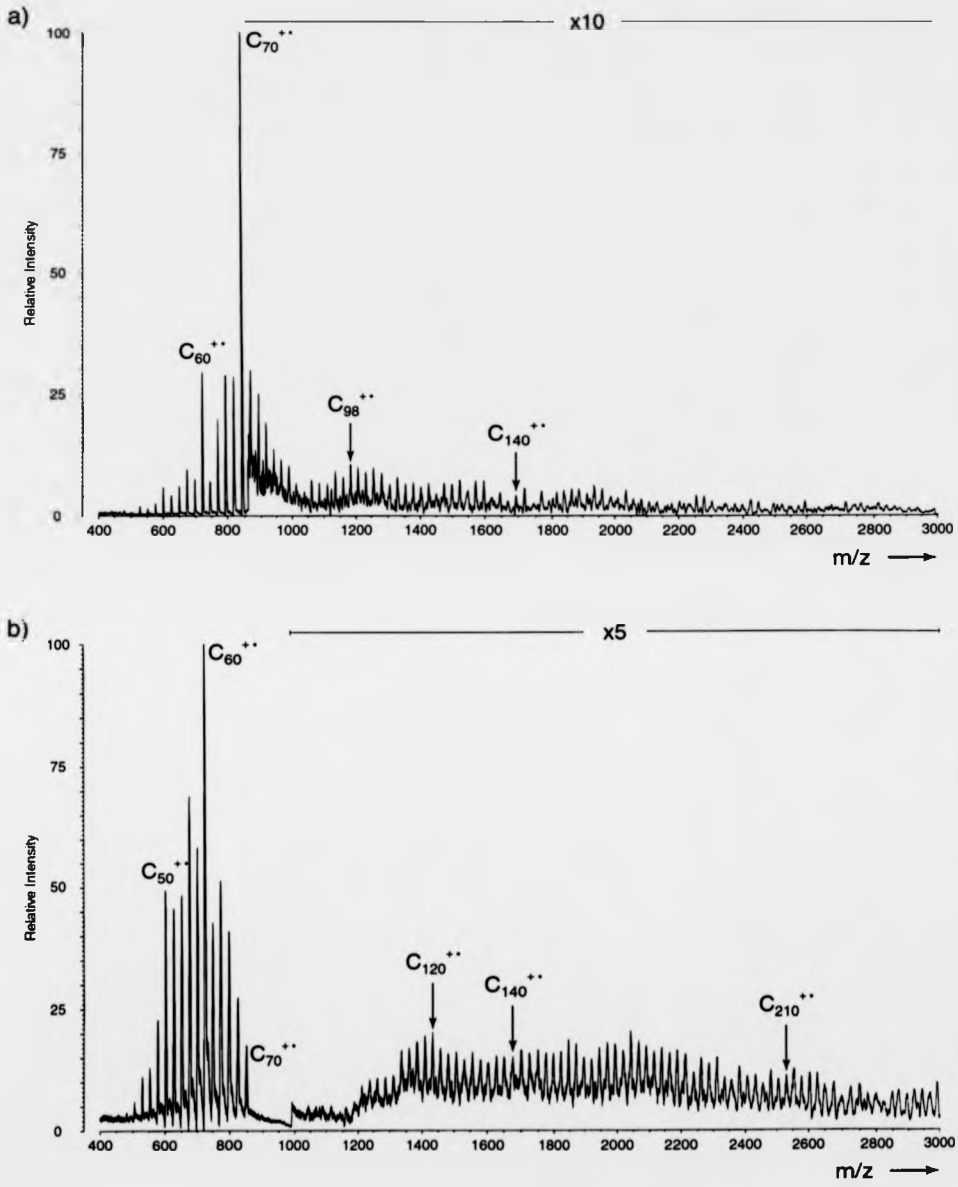

Figure 6: Positive-ion mass spectra acquired using $C_{70}F_x$, where the major components of the mixture are believed to be $C_{70}F_{62}$ and $C_{70}F_{66}$. Laser irradiances of 6.02×10^7 W cm^{-2} and 1.51×10^8 W cm^{-2} were used to produce spectra a and b, respectively.

with quanta of energy (in the present case, photons of wavelength 337 nm each deliver 3.6 eV of energy), and enough photons must be absorbed to overcome the ionization potential which acts as the energetic barrier to ionization. However, the ionization energies of fluorinated fullerenes are the highest established for any fullerene compounds. The removal of an electron from $C_{60}F_{48}$, for instance, requires 12.0 eV which is equal to approximately 3.3 photons; therefore, if the fluorinated fullerene were to exist in its ground state during the course of the experiment, four photons would be required for direct ionization. The decomposition of the neutral fluorinated fullerene by F_2 loss, for instance, is less energetically demanding; Dunlap et al. found that both the C-F bond, for fluorinated fullerenes, and C-H bond, for hydrogenated fullerenes, are reduced in strength by between 15% and 40%, compared to smaller, alkane based systems.[37] The C-F bond dissociation energy has been studied and, though such the value depends on the fullerene used and the extent of fluorination, has typically been found to be located around the region of approximately 4 - 6 eV[4,9,37,38] and proceeds in preference to ionization.

5.4 Summary

Four fluorinated fullerene samples were investigated, three of which were based on a C_{60} core and possessed differing fluorine contents. When examining the three $C_{60}F_x$ derivatives, it was found that, for each one, increasing the laser irradiance used for the LDI process altered the distribution of clusters generated in the ion source. At the lower laser irradiance for two of the three compounds, a discrete distribution of higher carbon clusters could be observed, and increasing the laser irradiance led to the observation of a extended distribution where each signal was of roughly equal intensity. The compound with the highest fluorine content did not appear to be greatly affected by an increase in the

laser irradiance used; at threshold values of the laser irradiance, spectra obtained (not shown) did display a distribution-like appearance, but were very low in intensity. Small increases in the laser power dramatically changed this appearance, after which change the appearance of the carbon clusters no longer seemed to be affected by increases in the laser irradiance. It was determined that the threshold laser irradiances required for carbon cluster formation display a linear relationship with fluorine content, when keeping the carbon core size constant. It also became apparent that fluorinated fullerenes of larger fluorine contents tend to more readily undergo coalescence and tend to form a wide range of aggregates, of roughly equal intensity; specific cluster sizes become less longer favored. Hence, LDI of $C_{60}F_{18}$ at a low laser irradiance results in the production of coalesced species which resemble the products of coalescence when using C_{60} as the precursor material, while laser ablation of a $C_{60}F_{48}$ target results in the production of a wide range of carbon clusters of similar intensities. It has been proposed that the dependence of the threshold laser irradiance upon fluorine content signifies the increased energetic demands for fragmentation with increasing fluorine content. The distinctive coalescence distribution of fluorinated fullerenes, which differs strongly when compared with the behavior of pure fullerenes under similar conditions, is explained by the decomposition of these compounds into smaller fragments. Due to fluorination of the carbon core, higher laser irradiances are required and weakening of the overall bonding within the cage structure occurs, and both factors contribute to enhance the dissociation of the target material. As a result, smaller, more highly energized fragments become more common with increased fluorine content of the precursor and hence coalescence will differ between the different samples used. A brief comparison with $C_{70}F_x$, where the sample contained species with a range of fluorine contents, showed similar tendencies, where increasing the laser power changed the appearance of the signals arising from the detection of coalesced species. It has also been

noted that time-of-flight mass spectra acquired following the laser ablation of a graphite surface displays many striking similarities to the mass spectra obtained using fluorinated fullerene precursors. This can be seen as an indication that both mechanisms involve the coalescence of many, highly energetic, carbon fragments, encompassing a variety of of different sizes. Finally, the unprecedented observation of fluorinated fullerene cations generated by LDI has also been noted.

5.5 References

1) Boltalina, O. V. *J. Fluorine Chem.* **2000**, *101*, 273-278.

2) Vasil'ev, Y. V., personal communication

3) Steger, H.; Mische, U.; Kamke, W.; Ding, A.; Fieber-Erdmann, M.; Drewello, T. *Chem. Phys. Lett.* **1997**, *276*, 39-46.

4) Vasil'ev, Y. V.; Boltalina, O. V.; Tuktarov, R. F.; Mazunov, V. A.; Sidorov, L. N. *Int. J. Mass Spectrom. Ion Processes* **1998**, *173*, 113-125.

5) Lichtenberger, D. L.; Nebesny, K. W.; Ray, C. D.; Huffman, D. R.; Lamb, L. D. *Chem. Phys. Lett.* **1991**, *176*, 203-208.

6) Zimmerman, J. A.; Eyler, J. R.; Bach, S. B. H.; McElvany, S. W. *J. Chem. Phys.* **1991**, *94*, 3556-3562.

7) de Vries, J.; Steger, H.; Kamke, B.; Menzel, C.; Weisser, B.; Kamke, W.; Hertel, I. V. *Chem. Phys. Lett.* **1992**, *188*, 159-162.

8) Lifshitz, C. *Mass Spectrom. Rev.* **1993**, *12*, 261-284.

9) Mitsumoto, R.; Araki, T.; Ito, E.; Ouchi, Y.; Seki, K.; Kikuchi, K.; Achiba, Y.; Kurosaki, H.; Sonoda, T.; Kobayashi, H.; Boltalina, O. V.; Pavlovich, V. K.; Sidorov,

L. N.; Hattori, Y.; Liu, N.; Yajima, S.; Kawasaki, S.; Okino, F.; Touhara, H. *J. Phys. Chem. A* **1998**, *102*, 552-560.

10) Bulusheva, L. G.; Okotrub, A. V.; Boltalina, O. V. *J. Phys. Chem. A* **1999**, *103*, 9921-9924.

11) Boltalina, O. V.; Bühl, M.; Khong, A.; Saunders, M.; Street, J. M.; Taylor, R. *J. Chem. Soc. Perkin Trans. 2* **1999**, 1475-1479.

12) Fowler, P. W.; Sandall, J. P. B.; Taylor, R. *J. Chem. Soc. Perkin Trans. 2* **1997**, 419-423.

13) Heine, T.; Fowler, P. W.; Rogers, K. M.; Seifert, G. *J. Chem. Soc. Perkin Trans. 2* **1999**, 707-711.

14) Neretin, I. S.; Lyssenko, K. A.; Antipin, M. Y.; Slovokhotov, Y. L.; Boltalina, O. V.; Troshin, P. A.; Lukonin, A. Y.; Sidorov, L. N.; Taylor, R. *Angew. Chem. Int. Ed.* **2000**, *39*, 3273-3276.

15) Kroto, H. W.; Heath, J. R.; O' Brien, S. C. O.; Curl, R. F.; Smalley, R. E. *Nature* **1985**, *318*, 162-163.

16) Tuinman, A. A.; Mukherjee, P.; Adcock, J. L.; Hettich, R. L.; Compton, R. N. *J. Phys. Chem.* **1992**, *96*, 7584-7589.

17) Yeretzian, C.; Hansen, K.; Diederich, F.; Whetten, R. L. *Nature* **1992**, *359*, 44-47.

18) Yeretzian, C.; Hansen, K.; Diederich, F.; Whetten, R. L. *Supplement to Z. Phys. D.* **1993**, *26*, S 300-304.

19) Hunter, J. M.; Fye, J. L.; Bolvin, N. M.; Jarrold, M. F. *J. Phys. Chem.* **1994**, *98*, 7440-7443.

20) Zhu, L.; Wang, S.; Li, Y. *J. Chem. Phys.* **1994**, *101*, 8592-8595.

21) Liu, Z.-Y.; Wang, C.-R.; Huang, R.-B.; Zheng, L.-S. *Int. J. Mass Spectrom. Ion Processes* **1995**, *145*, 1-7.

22) Xie, Z. X.; Liu, Z. Y.; Wang, C. R.; Huang, R. B.; Lin, F. C.; Zheng, L. S. *J. Chem. Soc. - Faraday Transactions* **1995**, *91*, 987-990.

23) Onoe, J.; Takeuchi, K. *J. Mass Spectrom.* **1998**, *33*, 387-391.

24) Beck, R. D.; Weis, P.; Bräuchle, G.; Kappes, M. M. *J. Chem. Phys.* **1994**, *100*, 262-270.

25) Mitzner, R.; Winter, B.; Kusch, C.; Campbell, E. E. B.; Hertel, I. V. *Z. Phys. D* **1995**, *37*, 89-95.

26) Beck, R. D.; Stoermer, C.; Schulz, C.; Michel, R.; Weis, P.; Bräuchle, G.; Kappes, M. M. *J. Chem. Phys.* **1994**, *101*, 3243-3249.

27) Beck, R. D.; Weis, P.; Hirsch, A.; Lamparth, I. *J. Phys. Chem.* **1994**, *98*, 9683-9687.

28) Barrow, M. P.; Tower, N. J.; Taylor, R.; Drewello, T. *Chem. Phys. Lett.* **1998**, *293*, 302-308.

29) Al-Jafari, M. S.; Barrow, M. P.; Taylor, R.; Drewello, T. *Int. J. Mass Spectrom.* **1999**, *184*, L1-L4.

30) Cozzolino, R.; Belgachem, O.; Drewello, T.; Käseberg, L.; Herzschuh, R.; Suslov, S.; Boltalina, O. *Eur. Mass Spectrom.* **1997**, *3*, 407-414.

31) Curl, R. F.; Smalley, R. E. *Fullerenes*, 1991; Vol. 265, pp 32-41.

32) Hansen, K.; Yeretzian, C.; Whetten, R. L. *Chem. Phys. Lett.* **1994**, *218*, 462-466.

33) Boltalina, O. V.; Sidorov, L. N.; Bagryantsev, V. F.; Seredenko, V. A.; Zapol'skii, A. S.; Street, J. M.; Taylor, R. *J. Chem. Soc. Perkin Trans. 2* **1996**, 2275-2278.

34) Boltalina, O. V.; Borschevskii, A. Y.; Sidorov, L. N.; Street, J. M.; Taylor, R. *J. Chem. Soc. Chem. Commun.* **1996**, 529-530.

35) Boltalina, O. V.; Markov, V. Y.; Taylor, R.; Waugh, M. P. *J. Chem. Soc. Chem. Commun.* **1996**, 2549-2550.

36) Rohlfing, E. A.; Cox, D. M.; Kaldor, A. *J. Chem. Phys.* **1984**, *81*, 3322-3330.

37) Dunlap, B. I.; Brenner, D. W.; Mintmire, J. W.; Mowrey, R. C.; White, C. T. *J. Phys. Chem.* **1991**, *95*, 5763-5768.

38) Boltalina, O. V.; Ponomarev, D. B.; Borschevskii, A. Y.; Sidorov, L. N. *J. Phys. Chem. A* **1997**, *101*, 2574-2577.

Chapter Six

Gas-Phase Aggregation of C_{60} Oxides and C_{70} Oxides Under Matrix-Assisted Laser Desorption/Ionization Conditions

6.1 Introduction

Fullerene oxides have recently been the subject of much investigation. Many synthetic methods have been developed with the goal of creating epoxide functional groups on pure fullerenes. Fullerene oxides were amongst the first known fullerene derivatives, produced and discovered accidentally following the use of the Krätschmer-Huffman method[1] for fullerene production. The products of the synthesis were found to possess up to five oxygen atoms.[2] The oxidative stability of fullerenes has followed on to become a topic of great interest.[3,4] The role of singlet oxygen in the photochemical oxidation of C_{60} has been studied.[5] One surprising investigation demonstrated that C_{60} degrades under ambient conditions, in the presence of light and air, to produce $C_{120}O$,[6] as discussed in Chapter Seven. It is therefore apparent that pure fullerenes readily undergo oxidation. Though initially discovered as an unwanted by-product of the synthetic process, attempts to deliberately oxidize fullerenes using a variety of methods have become increasingly common. Modern synthetic methods include photooxygenation,[7] ozonolysis,[8-11] and reactions with peroxy acids such as m-chloroperoxybenzoic acid.[12] A range of products, containing differing numbers of oxygen atoms, consisting of different isomers, will be produced. High performance liquid chromatography (HPLC) is required for the separation and purification of the products.

The study of fullerene oxides has revealed many interesting characteristics. Thermal decomposition of fullerene oxides leads to the production of odd numbered carbon clusters, via the loss of CO[13-16] or CO_2.[17,18] Reactions may be carried out involving $C_{60}O_n$ and C_{60} which result in the formation of $(C_{60})_xO_n$ species. Examples of such compounds include $C_{120}O$,[19,20] $C_{120}O_2$ (where two isomers have been characterized so far),[20,21] $C_{120}O_3$,[20] and

$C_{180}O_2$.[22] It has been shown that such structures consist of distinct, intact C_{60} moieties and that these moieties are bridged by bonds that resemble furanoid rings.[20,23] The production of dimeric oxide species in the solution phase has been an area of particular recent interest. Kappes and co-workers have managed to isolate and characterize three isomers of a $(C_{60})O(C_{70})$ dimer, following the reaction of $C_{60}O$ with C_{70}, and vibrational spectroscopy has been used to investigate the dimer.[24] In addition, analogous species have also been studied using vibrational spectroscopy, including $(C_{60})_2O_n$[24,25] and $(C_{60})O(C_{70})$,[24] but $(C_{70})_2O_n$ has not yet been studied. This is due to the fact that attempts to synthesize it in the solution phase have failed. Early attempts to synthesize $(C_{60})O(C_{70})$ failed when using $C_{70}O$ as the oxidized moiety, and from this it can be extrapolated that the difficulty lies in using the $C_{70}O$ species as a starting material for the production of the dimer. $C_{70}O$ was found to lose the oxygen atom even more readily than $C_{60}O$. This lability is the reason for the failure of synthetic approaches which have relied upon the use of $C_{70}O$ as a reactant. The degradation of pure fullerenes in air[3,4] is well known, and in follow up to the recent discovery that oxidation may lead to the formation of dimeric species,[6] one group has very recently investigated the degradation of higher fullerenes which were obtained from fullerene soot, produced using the Krätschmer-Huffman method.[1] Under similar conditions, species such as $C_{152}O$ were observed in addition to $C_{120}O$ and $C_{120}O_2$.[26]

Many attempts have been made to synthesize fullerene oxides in the gas-phase, such as through reactions with oxygen in an ion trap,[27] reactions with molecular oxygen within the collision cell of a mass spectrometer,[28] or thermally induced oxidation.[29] Increasing attention, however, has been paid to analysis of fullerene oxides that have been produced through synthetic processes described earlier, and though nuclear magnetic resonance (NMR) has been used during such investigations,[30] mass spectrometry is the most common

technique used for studying such derivatives. Due to the fact that fullerene oxides are so labile, soft ionization methods have been used during mass spectrometric analysis. Fast atom bombardment (FAB),[31] electrospray ionization (ESI),[22,32,33] and matrix-assisted laser desorption/ionization (MALDI)[19-21] have all been implemented during the gas-phase analysis of fullerene oxides, and most studies are conducted using the negative-ion mode. This investigation involved the use of MALDI[20] and laser desorption/ionization (LDI)[32,34] conditions for the analysis of $C_{60}O_n$ and $C_{70}O_n$ samples. Coalescence[35,36] of these samples in the gas-phase was attempted, and comparisons between the different ionization techniques have shown that under the relatively mild conditions associated with MALDI, it is possible to generate ions of the structure $(C_{60})_xO_n$ in the gas-phase. It was possible to generate the dumb-bell like species, bridged by a furanoid ring geometry, each of which consists of C-O-C bonding and a σ C-C bond, that have been synthesized in the solution phase. Using the harsher conditions associated with LDI, coalescence was also observed, but the products were pure carbon clusters rather than bridged species. Noting that $(C_{70})_xO_n$ had not yet been synthesized in the gas-phase nor the solution phase, $C_{70}O_n$ was used as a precursor with the objective of producing the $(C_{70})_xO_n$ structure in the gas-phase under MALDI conditions. The investigation proved to be successful, resulting in the first experimental evidence for the existence of the $(C_{70})_xO_n$ species.

6.2 Experimental

The different oxides were prepared in a similar manner to each other. The C_{60} and C_{70} oxides were obtained from R. Taylor (University of Sussex, Brighton, UK). They were prepared by treating C_{60} or C_{70} with m-chloroperoxybenzoic acid and heated to ~80 °C for 24 hours, in accordance with the synthesis outlined by Balch et al.[12] The resulting

oxides were then separated and purified using HPLC, following prewashing with a base and drying of the toluene layer. The multistep separations were performed using both a 25 cm × 10 mm Cosmosil Buckyclutcher column and a Cosmosil Buckyprep column, with toluene or a toluene/heptane mixture as the eluent.

Mass spectrometric analysis was performed using a Kratos Kompact MALDI IV. The ionization source of the Kompact MALDI IV incorporates a nitrogen laser (337 nm, 3 ns pulse width) and constant accelerating potential of 20 kV, and ions are then extracted into the linear flight tube, which includes a curved field reflectron. All spectra obtained during the course of this investigation represent the accumulation of individual spectra following 200 laser pulses, and the reflectron was also used in every case in order to improve resolution. For matrix-assisted laser desorption/ionization (MALDI) experiments, the sample was dissolved in toluene and mixed with a solution of 9-nitroanthracene, which was used as the matrix during such experiments. The solution of 9-nitroanthracene was created by dissolving it in acetone (ratio of 10 mg of matrix per 1 mL of acetone). The final solution comprised a ratio of matrix to analyte of 20 μL to 1 μL. This solution was then spotted on to a stainless steel slide and dried prior to analysis. In the case of laser desorption/ionization (LDI) experiments, the sample preparation is carried out in the same manner. The toluene solution of the sample is spotted directly on to the stainless steel slide, the solvent evaporated, and then inserted into the ion source.

6.3 Results and Discussion

Figure 1 shows the mass spectra obtained using the $C_{60}O_n$ sample. Figure 1a shows the negative-ion MALDI mass spectrum, which provides an indication of the oxygen content of the sample. Contributions from $C_{60}O^{-\bullet}$, $C_{60}O_2^{-\bullet}$, $C_{60}O_3^{-\bullet}$, $C_{60}O_4^{-\bullet}$, and $C_{60}O_5^{-\bullet}$ can be

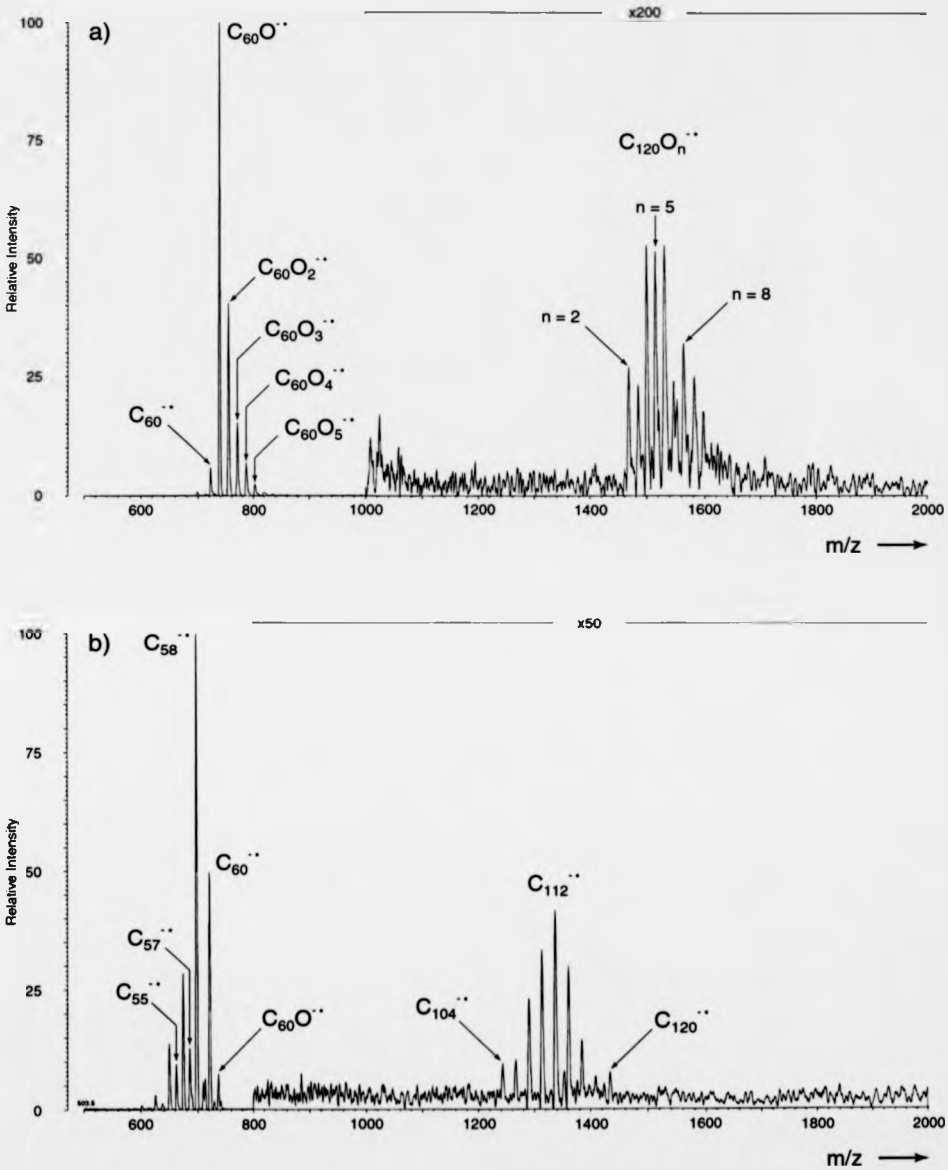

Figure 1: Negative-ion mass spectra acquired using a sample of $C_{60}O_n$, where n ≤5. Spectrum a was obtained under matrix-assisted laser desorption/ionization (MALDI) conditions, using 9-nitroanthracene as the matrix. Spectrum b was obtained under laser desorption/ionization conditions. Comparing the two mass spectra, it is evident that employment of differing ionization conditions leads to the formation of carbon clusters of differing structures.

observed, with a small contribution from $C_{60}O_6^{\bullet}$. Unfortunately, 9-nitroanthracene is known to oxidize fullerene samples during the laser desorption/ionization process, and so the exact oxygen content cannot be established beyond doubt. It is believed that the sample consisted of a range of fullerene oxides up to approximately $C_{60}O_5$, with fragmentation enhancing the signal intensities of fullerenes with lower oxygen content; previous experience with the study of the oxidizing ability of the matrix would suggest that the $C_{60}O_6$ signal is most likely to originate from oxidation of the sample. Any higher oxides arise from oxidation during the desorption/ionization process, and the lower oxides and $C_{60}^{\bullet}$ are produced by fragmentation processes. At higher mass, a distribution can be observed which can be assigned as arising from the formation of a dimeric species. However, the spacing between the signals is not the characteristic 24 Da (C_2) that would be expected for a pure fullerene. The signals are in fact separated by 16 Da, and $C_{120}^{\bullet}$ is not observed; the lowest m/z ratio observed in the distribution is 1472 ($C_{120}O_2^{\bullet}$), not 1440 ($C_{120}^{\bullet}$). It can be concluded that the dimeric species is formed in the gas-phase and is not present in the sample itself (due to its purity) and that the coalesced species are not pure, higher fullerenes which possess epoxide groups. If the coalesced species were indeed closed caged structures, pure fullerene fragments would be expected to be produced through C_2 loss, but no C_2 loss is apparent. The fact that C_2 loss is absent implies that a much weaker bond exists, and it is this bond which is broken in preference to C_2 loss.

It can be deduced that oxygen is involved in the formation of the dimeric species, and that not all oxygen atoms are present as epoxide groups, as a minimum of one oxygen atom must be present in order for the dimeric species to be observed at all. Fusion of fullerene oxides under such mild ionization conditions results in the production of a dumb-bell like species which consists of two, distinct C_{60} moieties, bridged by one or two

oxygen atoms, and further oxygen atoms may be present as epoxide groups on the exterior of the fused structure; the bridge between the two moieties consists of one or two furanoid ring geometries,[20,23] each of which entails C-O-C bonding and one σ C-C bond. No more than three furanoid bridges have been observed to date for steric reasons.[20] It is during desorption and ionization that many oxygen neutrals or ions may be liberated in the plume produced from the target, following each laser pulse. These oxygen atoms may attach themselves to the exterior of coalesced species, forming the epoxide groups observed on the exterior of the dimeric species. It is highly unlikely that more than two oxygen atoms are involved in the actual bridging of the two C_{60} moieties, however, due to strain considerations. Semiempirical calculations show that furanoid rings are the most energetically favorable way of linking the moieties.[23] These two, most probable, core structures can be seen in Figure 2. These predictions are supported by the recent isolation of $C_{120}O_2$ isomers by Krätschmer and co-workers,[21] which has revealed that one isomer possesses a single furanoid bridge, while the other isomer possesses two furanoid bridges. The assignment is based on an instrumental mass accuracy of ± 1 Da and the fact that the sample should be composed of only carbon and oxygen. As the instrumental resolution is too low to observe the individual isotopic patterns, it is impossible to discount a theoretical hydrogen contribution, arising from the matrix. It should also be noted that O_3 and C_4 moieties are isobaric, which can cause difficulty during mass assignment, but because C_4 loss is almost absent in the spectrum, interference between C_4 unit and O_3 units at higher mass is unlikely. The discovery that laser-induced, gas-phase aggregation of fullerene oxides leads to the formation of such bridged species is unprecedented.

Figure 1b shows the negative-ion LDI spectrum obtained using the same sample. Due to the fact that LDI conditions are harsher than MALDI conditions, it may be noted

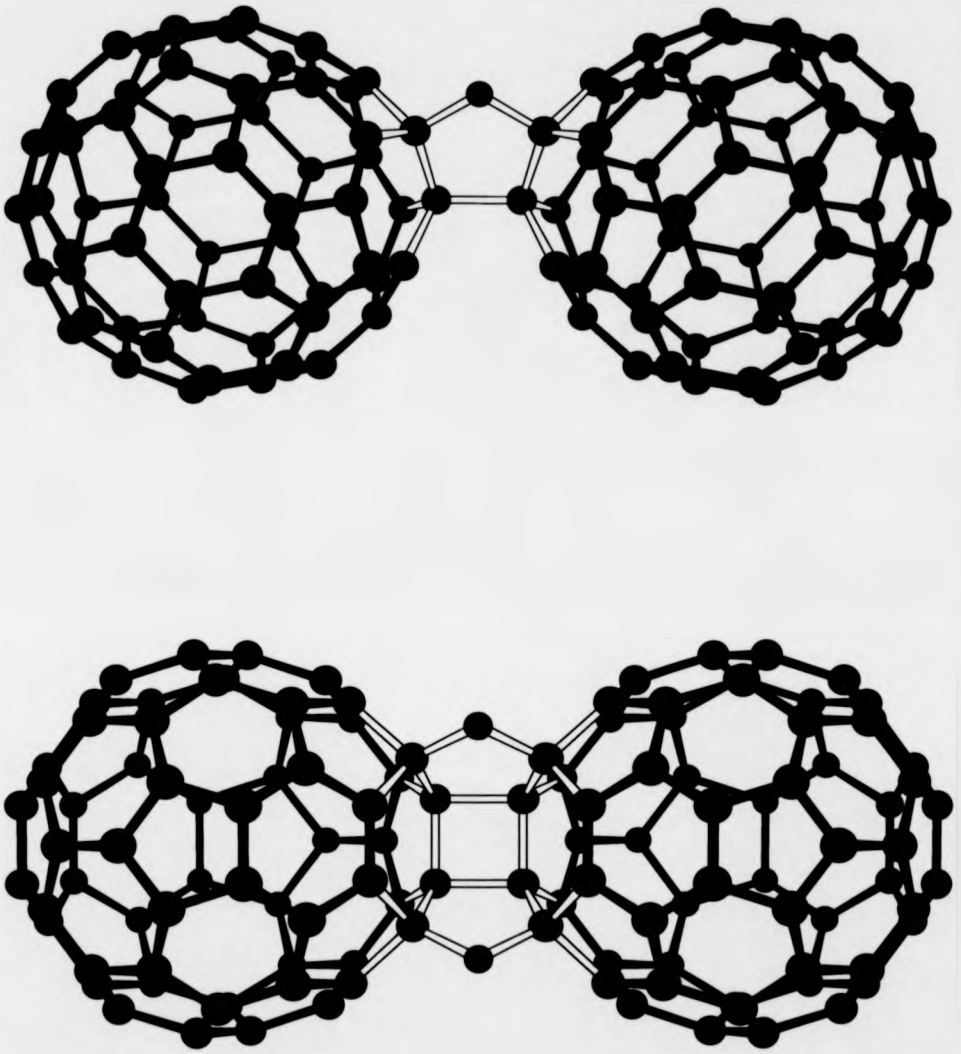

Figure 2: Proposed structures of the carbon clusters $C_{120}O$ and $C_{120}O_2$. These structures form the postulated core of the $C_{120}O_n$ species which are observed following gas-phase coalescence under MALDI conditions.

that even $C_{60}O^{+}$ is low in intensity and fragmentation in this mass region leads almost exclusively to the production of pure fullerenes. A careful analysis of the spectrum also revealed that odd numbered carbon cages were present, produced during fragmentation where CO loss occurs. At higher mass, a distribution can be observed which, again, must result from gas-phase interactions as the sample had been purified before analysis. In contrast to the dimeric species observed under MALDI conditions, the spacing between the signals is 24 Da (C_2 loss) and therefore is characteristic of a pure fullerene. No oxygen is present in this dimeric species, again in contrast to the structure generated under MALDI conditions. The reason for the difference between the LDI spectrum and the MALDI spectrum is the difference in the precursors generated, prior to coalescence. MALDI is a soft ionization technique, and therefore the precursors formed will be C_{60} oxide neutrals and anions, which then coalesce and result in the bridged species observed. Due to the more vigorous conditions which are associated with LDI, the precursors generated are pure fullerene neutrals and anions, which go on to coalesce and form pure, higher carbon clusters. Odd numbered carbon clusters are observed at low mass, and there is therefore a possibility that odd numbered, higher carbon clusters would be produced at higher mass; signals can be observed in between the even numbered carbon cluster signals, but due to the fact that these signals are little more intense than the noise level, it is not possible to assign them with confidence.

Laser-induced coalescence of fullerene oxides has been previously investigated by Kappes and co-workers,[37] using $C_{60}O_n$ where n = 1, 2, and 3. Coalescence was determined to occur at much lower laser fluences, in comparison with pure fullerene samples. The products of these reactions were also determined to be pure carbon clusters, similarly to the spectrum shown in Figure 1b. Figure 3 shows a comparison of two laser

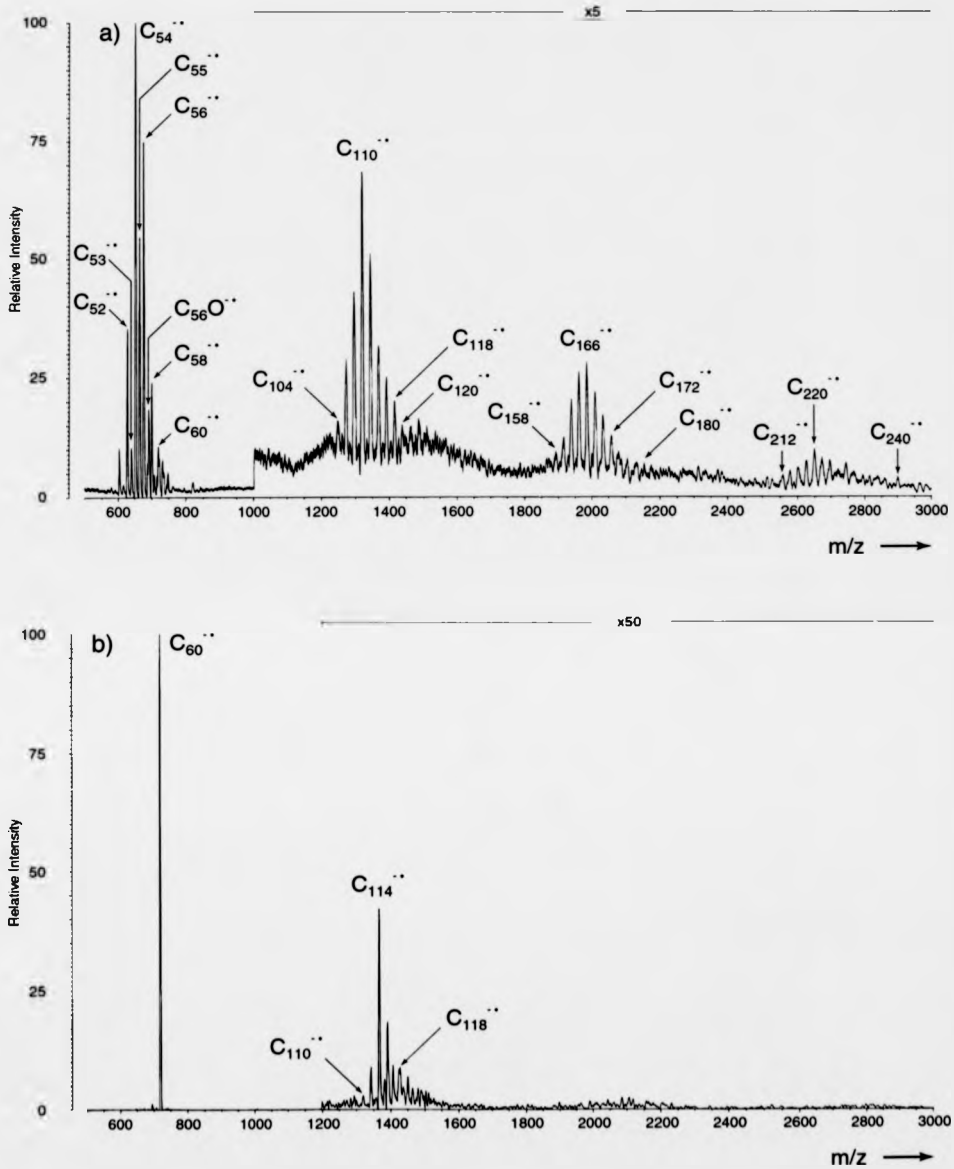

Figure 3: Negative-ion mass spectra demonstrating the differing efficiencies of gas-phase coalescence of $C_{60}O_n$ and pure C_{60} are shown in spectra a and b, respectively. The presence of epoxide groups on the fullerene core significantly increases the coalescence efficiency in the negative-ion mode.

desorption/ionization spectra, obtained using similar laser fluences, where Figure 3a was recorded using a $C_{60}O_n$ sample and Figure 3b was obtained using a pure C_{60} sample. Uneven carbon clusters can again be observed at low mass in Figure 3a, in similarity with the spectrum shown in Figure 1b, but a signal due to $C_{56}O^{-\bullet}$ can also be seen. At high mass, three distinct distributions can be observed with the general formula $(C_n)_x$ where x = 2, 3, and 4, generated from the fusion of pure fullerene fragments. In contrast, Figure 3b exhibits the formation of only dimeric species at high mass. The reason for the difference can be found when looking at the fragments of the two samples. While many pure fullerene fragments are observed in Figure 3a, which may then fuse to form higher fullerenes, the most intense signal in Figure 3b is that of $C_{60}^{-\bullet}$, with a minor contribution from $C_{58}^{-\bullet}$. Fullerene oxides will exhibit an increased inclination to coalesce due to the fact that the addition of epoxide groups will disrupt the bonding (and hence stability) of the fullerene cage, which will in turn result in a greater tendency to fragment under laser desorption/ionization conditions. It is the generation of excited species such as fragment neutrals and ions which is of primary importance for the fusion to produce higher fullerenes during coalescence reactions,[38,39] and this fact is further demonstrated by such a comparison of the gas-phase behavior of pure fullerenes and fullerene derivatives.

Further investigation was carried out using $C_{70}O_n$ samples, in order to compare the results with those obtained using $C_{60}O_n$. The primary goal of this investigation was the formation of a $(C_{70}O_n)_2$ structure, as this dimeric species had not yet been synthesized in the solution phase nor the gas-phase. Consequently, MALDI was the preferred ionization technique, as LDI would result in the formation of pure carbon clusters alone. The negative-ion MALDI spectra are shown in Figures 4a and 4b. The sample used in Figure 4a was $C_{70}O$, and the strongest signal is that due to $C_{70}O^{-\bullet}$. Small contribution from signals

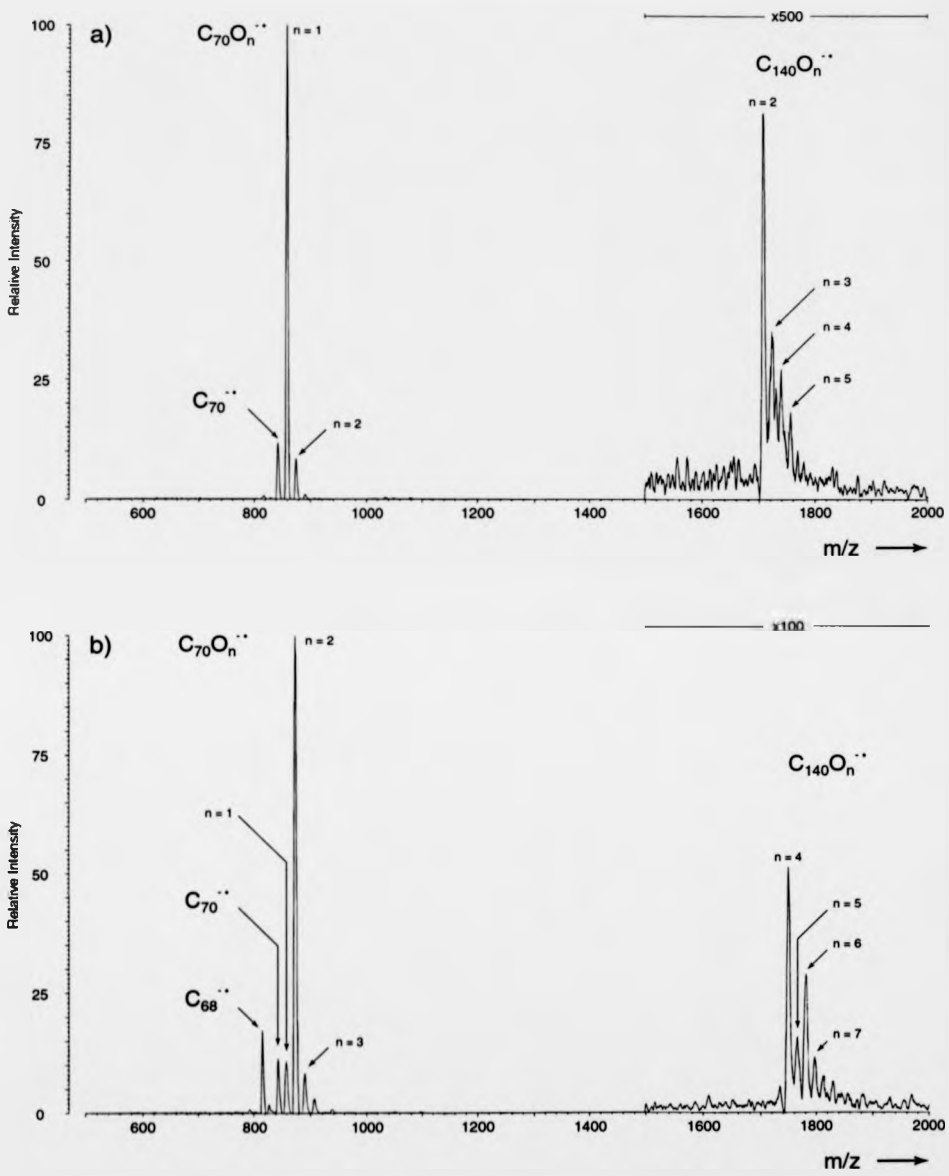

Figure 4: Negative-ion mass spectra of $C_{70}O$ and $C_{70}O_2$ are shown in spectra a and b, respectively. Both spectra have been obtained under MALDI conditions, using 9-nitroanthracene as the matrix. In similarity with the C_{60} oxides, use of MALDI conditions leads to the formation of carbon clusters which include oxygen. Variation of the oxygen content of the C_{70} oxides is also seen to affect the oxygen content of the coalesced carbon clusters.

arising from $C_{70}O_2^{-\bullet}$ and $C_{70}O_3^{-\bullet}$ can be observed, where $C_{70}O_2$ and $C_{70}O_3$ most probably originate from oxidation of the $C_{70}O$ sample in the gas-phase by 9-nitroanthracene. In Figure 4b, the most intense peak is that of $C_{70}O_2^{-\bullet}$, and the sample used was indeed $C_{70}O_2$, although small $C_{70}O_3^{-\bullet}$ and $C_{70}O_4^{-\bullet}$ peaks can be observed, which are again due to oxidation which occurs in the gas-phase, following reactions with the matrix. The high mass regions of both spectra reveal that $C_{140}O_n^{-\bullet}$ has indeed been produced in the gas-phase, although not as readily as was the case when using C_{60} oxide samples. As expected, the species formed are not pure fullerenes; the spacing between the signals is 16 Da and no pure fullerenes are observed in this mass region. In analogy with the C_{60} oxides, oxygen must again be involved in the linkage between the C_{70} moieties. MNDO calculations reveal the most likely structures[23] of these dimeric species to be similar to those of the dimeric species of the C_{60} oxides. Figure 5 shows the predicted, core structures for the $C_{140}O_n$ compounds. Again, the probability of more than two furanoid bridges being present is very low, due to strain considerations. Additional oxygen atoms may be present as epoxide groups on the exterior of the dimer. In analogy with the $C_{120}O_2$ compound investigated by Krätschmer et al.,[21] where two isomers were found to be present; it is possible that one isomer would possess one epoxide group and one C-O-C bridge, while the other isomer possessed two C-O-C bridging oxo-groups. Further analysis of $C_{140}O_n$ is likely to reveal the existence of more than one isomer.

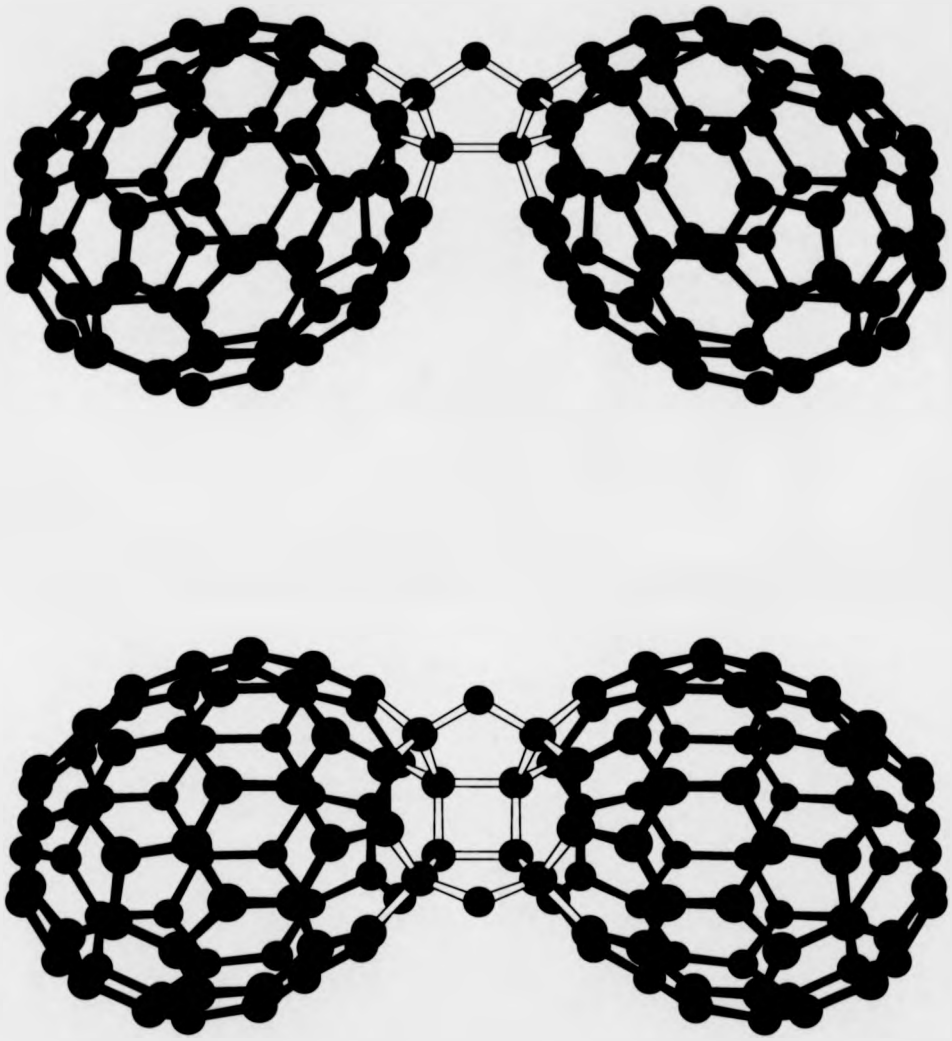

Figure 5: Postulated structures of the carbon clusters $C_{140}O$ and $C_{140}O_2$, which are believed to form the core of the coalesced carbon cluster species $C_{140}O_n$.

6.4 Summary

During the investigation of $C_{60}O_n$ and $C_{70}O_n$, two distinct coalescence reactions could be produced in the gas-phase using a laser desorption/ionization ion source. Use of MALDI results in the generation of dimeric species which consist of two moieties which retain the structural features of the pure fullerene core, where these two moieties are then bridged by an arrangement which resembles a furanoid ring, with one or two C-O-C based bridges and one σ C-C bond. The signals arising from the large aggregates are spaced by 16 Da, signifying oxygen loss, and no C_2 loss is observed, nor are any pure fullerenes; a minimum of one oxygen atom must be present to observe the dimer. These reactions have been observed for the first time in the gas-phase. Further oxygen atoms may be present as epoxide groups on the exterior of the dimer that has been formed. Use of LDI, by contrast, results in the generation of only pure carbon clusters. Signals resulting from the aggregate are spaced by 24 Da and signify C_2 loss, which is characteristic of a pure fullerene. This is further supported by the absence of any oxygen in the cluster species produced following LDI. Following on from the findings relating to $C_{60}O_n$, attempts were made to coalesce $C_{70}O_n$ for the first time. While other researchers had been unsuccessful in attempting to generate $(C_{70})_xO_n$ in the solution phase, it was possible, using MALDI conditions, to produce $C_{140}O_n^{\bullet+}$ in the gas-phase for the first time.

6.5 References

1) Krätschmer, W.; Lamb, L. D.; Fostiropoulos, K.; Huffman, D. R. *Nature* **1990**, *347*, 354-357.

2) Wood, J. M.; Kahr, B.; Hoke, S. H.; Dejarme, L.; Cooks, R. G.; Benamotz, D. *J. Am. Chem. Soc.* **1991**, *113*, 5907-5908.

3) Chibante, L. P. F.; Heymann, D. *Geochimica Et Cosmochimica Acta* **1993**, *57*, 1879-1881.

4) Scanlon, J. C.; Brown, J. M.; Ebert, L. B. *J. Phys. Chem.* **1994**, *98*, 3921-3923.

5) Schuster, D. I.; Baran, P. S.; Hatch, R. K.; Khan, A. U.; Wilson, S. R. *J. Chem. Soc. Chem. Commun.* **1998**, 2493-2494.

6) Taylor, R.; Barrow, M. P.; Drewello, T. *J. Chem. Soc. Chem. Commun.* **1998**, 2497-2498.

7) Creegan, K. M.; Robbins, J. L.; Robbins, W. K.; Millar, J. M.; Sherwood, R. D.; Tindall, P. J.; Cox, D. M.; Smith, A. B.; McCualey, J. P.; Jones, D. R.; Gallagher, R. T. *J. Am. Chem. Soc.* **1992**, *114*, 1103-1105.

8) Heymann, D.; Chibante, L. P. F. *Rec. Trav. Chim.* **1993**, *112*, 639-642.

9) Heymann, D.; Chibante, L. P. F. *Rec. Trav. Chim.* **1993**, *112*, 531-534.

10) Malhotra, R.; Kumar, S.; Satyam, A. *J. Chem. Soc. Chem. Commun.* **1994**, 1339-1340.

11) Deng, J. P.; Mou, C. Y.; Han, C. C. *Fullerene Sci. Tech.* **1997**, *5*, 1033-1044.

12) Balch, A. L.; Costa, D. A.; Noll, B. C.; Olmstead, M. M. *J. Am. Chem. Soc.* **1995**, *117*, 8926-8932.

13) McElvany, S. W.; Callahan, J. H.; Ross, M. M.; Lamb, L. D.; Huffman, D. R. *Science* **1993**, *260*, 1632-1634.

14) Beck, R. D.; Brauchle, G.; Stoermer, C.; Kappes, M. M. *J. Chem. Phys.* **1995**, *102*, 540-543.

15) Taylor, R. *J. Chem. Soc. Chem. Commun.* **1994**, 1629-1630.

16) Darwish, A. D.; Birkett, P. R.; Langley, G. J.; Kroto, H. W.; Taylor, R.; Walton, D. R. M. *Fullerene Sci. Tech.* **1997**, *5*, 705-726.

17) Callahan, J. H.; McElvany, S. W.; Ross, M. M. *Int. J. Mass Spectrom. Ion Processes* **1994**, *138*, 221-239.

18) Taylor, R.; Penicaud, A.; Tower, N. J. *Chem. Phys. Lett.* **1998**, *295*, 481-486.

19) Lebedkin, S.; Ballenweg, S.; Gross, J.; Taylor, R.; Krätschmer, W. *Tetrahedron Lett.* **1995**, *36*, 4971-4974.

20) Penn, S. G.; Costa, D. A.; Balch, A. L.; Lebrilla, C. B. *Int. J. Mass Spectrom. Ion Processes* **1997**, *169/170*, 371-386.

21) Gromov, A.; Lebedkin, S.; Ballenweg, S.; Avent, A. G.; Taylor, R.; Krätschmer, W. *J. Chem. Soc. Chem. Commun.* **1997**, 209-210.

22) Deng, J.-P.; Mou, C.-Y.; Han, C.-C. *Chem. Phys. Lett.* **1996**, *256*, 96-100.

23) Fowler, P. W.; Mitchell, D.; Taylor, R.; Seifert, G. *J. Chem. Soc. Perkin Trans. 2* **1997**, 1901-1905.

24) Eisler, H.-J.; Hennrich, F. H.; Werner, E.; Hertwig, A.; Stoermer, C.; Kappes, M. M. *J. Phys. Chem.* **1998**, *102*, 3889-3897.

25) Krause, M.; Dunsch, L.; Seifert, G.; Fowler, P. W.; Gromov, A.; Krätschmer, W.; Gutierez, R.; Porezag, D.; Frauenheim, T. *J. Chem. Soc. Faraday Trans.* **1998**, *94*, 2287-2294.

26) Akimoto, Y.; Kudoh, T.; Shinoda, K.; Jeyadevan, B.; Tohji, K.; Nirasawa, T.; Kasuya, A.; Nishina, Y.; Krätschmer, W. *Synthesis of Higher Dimeric Fullerene Oxides*: Toronto, 2000; Vol. 2000-I.

27) Watanabe, N.; Shiromaru, H.; Negishi, Y.; Achiba, Y.; Kobayashi, N.; Kaneko, Y. *Supplement to Z. Phys. D.* **1993**, *26*, S 252-254.

28) Stry, J. J.; Garvey, J., F. *J. Phys. Chem.* **1993**, *97*, 7910-7913.

29) Wohlers, M.; Bauer, A.; Schlögl, R. *Mikrochim. Acta* **1997**, *14*, 267-270.

30) Smith III, A. B.; Strongin, R. M.; Brard, L.; Romanow, W. J.; Saunders, M.; Jiménez-Vázquez, H. A.; Cross, R. J. *J. Am. Chem. Soc.* **1994**, *116*, 10831-10832.

31) Van Cleempoel, A.; Gijbels, R.; Claeys, M.; VandenHeuvel, H. *Rapid Commun. Mass Spectrom.* **1996**, *10*, 1579-1584.

32) Deng, J. P.; Mou, C. Y.; Han, C. C. *J. Phys. Chem.* **1995**, *99*, 14907-14910.

33) Liu, T.-Y.; Shiu, L.-L.; Luh, T.-Y.; Her, G.-R. *Rapid Commun. Mass Spectrom.* **1995**, *9*, 93-96.

34) Lu, W.; Huang, R.; Yang, S. *Chem. Phys. Lett.* **1995**, *241*, 373-379.

35) Yeretzian, C.; Hansen, K.; Diederich, F.; Whetten, R. L. *Nature* **1992**, *359*, 44-47.

36) Yeretzian, C.; Hansen, K.; Diederich, F.; Whetten, R. L. *Supplement to Z. Phys. D.* **1993**, *26*, S 300-304.

37) Beck, R. D.; Stoermer, C.; Schulz, C.; Michel, R.; Weis, P.; Bräuchle, G.; Kappes, M. M. *J. Chem. Phys.* **1994**, *101*, 3243-3249.

38) Beck, R. D.; Weis, P.; Bräuchle, G.; Kappes, M. M. *J. Chem. Phys.* **1994**, *100*, 262-270.

39) Mitzner, R.; Winter, B.; Kusch, C.; Campbell, E. E. B.; Hertel, I. V. *Z. Phys. D* **1995**, *37*, 89-95.

Chapter Seven

Degradation of C_{60} to $C_{120}O$ in the Solid State Under Ambient Conditions

7.1 Introduction

A collaborative effort with Taylor and co-workers at the University of Sussex led to the discovery of the dimerization of $C_{60}O_x$ and $C_{70}O_x$ in the gas-phase,[1,2] using laser desorption/ionization (LDI) and matrix-assisted laser desorption/ionization (MALDI), for which the results are detailed in Chapter Six. Following these investigations, Taylor informed the research group at the University of Warwick about his observation that pure C_{60} displayed unusual behavior when attempts were made to dissolve older samples of this fullerene in toluene. A proportion of the aged sample would not readily dissolve, though the solution itself was not yet saturated. Taylor collected this material and used high performance liquid chromatography (HPLC) to characterize and purify the sample, and used infra-red (IR) spectroscopy to further analyze the sample. Further structure elucidation was performed at the University of Warwick using MALDI time-of-flight mass spectrometry, and thus it was possible to identify one of the intrinsic impurities which accompanies pure C_{60} samples. The nature of the impurity and its formation yielded surprising results which could in turn present significant difficulties for the applications of fullerenes.

HPLC was used to analyze the samples and determined that a dimeric, oxygen containing species was present. Matrix-assisted laser desorption/ionization mass spectrometry was employed for verification and for structure elucidation. MALDI is a soft ionization technique, and so was the ionization technique of choice in order that the molecular ion could be established, without unwanted fragmentation. Infra-red (IR) spectroscopy was also used to further verify the results, comparing the IR spectrum of the isolated species with that of a synthetic sample in order to test the hypothesis.

Once the structure had been established, the investigation was extended by attempting to generate more of the contaminant species under similar, ambient conditions, as it is believed that the contaminant species is the product of the reaction between C_{60} and oxygen under ambient conditions. The stability and reactivity of fullerenes[3-7] and fullerene oxides[8,9] has always been a subject of much interest. In order to test the theory that the impurity that Taylor isolated was generated through oxidation, C_{60} samples were allowed to stand in light and air for 40 hours, and the resulting samples were then analyzed. The results showed that C_{60} does indeed undergo reactions with oxygen at room temperature in the presence of light and air, but the extent of the reactions were surprising. $C_{60}O$ is the first fullerene oxide to be produced synthetically[10] and since that time a variety of synthetic methods have been investigated including photooxygenation,[10] ozonolysis,[11-14] or reactions with peroxy acids such as m-chloroperoxybenzoic acid.[15] Although it has long been suspected that C_{60} also undergoes oxidation upon standing,[4,5] the findings of the following experiments revealed a surprising degree of reactivity under relatively mild conditions and the structures of the products were also unexpected. The results have serious implications for possible applications of fullerenes, as oxidation must now be a serious consideration.

7.2 Experimental

High performance liquid chromatography was carried out using a 4.6 mm × 25 cm Cosmosil Buckyclutcher column, using toluene as the eluent with a flow rate of 1 mL min^{-1}. Mass spectrometric analysis was performed using a Kratos Kompact MALDI IV. The sample was dissolved in toluene and mixed with a solution of 9-nitroanthracene, which was used as the matrix for matrix-assisted laser desorption/ionization experiments. The

solution of 9-nitroanthracene was created by dissolving it in in acetone (ratio of 10 mg of matrix per 1 mL of acetone). The final solution comprised a ratio of matrix to analyte of 20 μL to 1 μL. This solution was then spotted on to a stainless steel slide and dried. This slide was then inserted into the instrument prior to analysis.

7.3 Results and Discussion

The initial aim of the HPLC analysis of the C_{60} sample was to assess the purity, with particular attention being paid to any contamination arising from the presence of C_{70} or higher fullerenes. Figure 1 shows the results of the HPLC analysis. The peak resulting from C_{60} can be observed at a retention time of 7.4 minutes, and while a negligible C_{70} contribution could be seen, of much more interest was the peak associated with a time of 14.6 minutes. This time is identical to that of $C_{120}O$ carried out under identical conditions; retention times have been previously quoted as 7.8 minutes for C_{60} and 15.8 minutes for $C_{120}O$. It may be noted that retention times can be affected by ambient temperature, column condition, and injection volume. The eluent solution produced at 14.6 minutes was straw colored, and removal of the toluene resulted in a brown film which was much less soluble than C_{60} or C_{60} oxides.

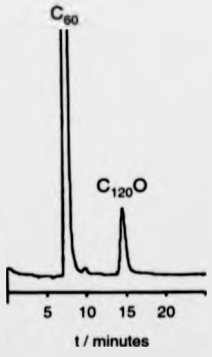

Figure 1: High performance liquid chromatography (HPLC) trace for a saturated solution of C_{60} sample. The presence of $C_{120}O$ as an impurity is clearly observable, as is the absence of contamination from C_{70}.

Mass spectrometric analysis provided further proof for the assignment of the oxidation product. Figure 2 shows the negative mode MALDI mass spectrum obtained on the Kratos Kompact MALDI IV. It should be noted that the unlabeled signals which lie approximately in the regions of m/z 600 - 700 and m/z 750 - 900 are known to arise from the matrix; such signals are well known. The presence of $C_{120}O^{-\bullet}$ (m/z 1456) is clearly evident. $C_{120}O_2^{-\bullet}$ (m/z 1472) is also present. As $C_{120}O_2$ was not detected using HPLC and as the matrix 9-nitroanthracene is known to oxidize samples to a small extent, this signal can be attributed to the further oxidation of $C_{120}O$ by the matrix, with the additional oxygen atom most likely forming an epoxide group on the surface of the molecule. $C_{60}O$ is believed to be strained and unstable relative to $C_{120}O$,[8] and the capture of another C_{60} molecule is therefore likely, resulting in the formation of the aforementioned dimeric species. When using a matrix that is known to oxidize samples, it is not surprising that $C_{120}O$ would readily undergo further oxidation, forming $C_{120}O_2$. Strong signals resulting from $C_{60}^{-\bullet}$ and $C_{60}O^{-\bullet}$ were also detected. As the sample should be pure following HPLC separation, C_{60} and $C_{60}O$ should not be present in the sample analyzed. Also, while the presence of $C_{120}O^{-\bullet}$ is detected, none of the characteristic C_2 losses (which may be used to identify closed-caged fullerenes) accompanies it; $C_{118}O^{-\bullet}$, for instance, is not detected. The lack of C_2 loss advocates a theory that the $C_{120}O$ species is not based on a pure, closed-caged, fullerene structure. The presence of $C_{120}^{-\bullet}$ is also not recorded, although it would be expected should the oxygen atom exist as an epoxide group on the exterior of a closed-caged C_{120} structure. It is therefore logical to conclude that the oxygen atom does not exist as an epoxide group on the exterior of a pure fullerene. It may be concluded that the $C_{120}O$ species consists of two distinct C_{60} moieties bridged by a single oxygen atom. It would therefore be most likely that this species fragments into two smaller molecules, C_{60} and $C_{60}O$, rather than undergo C_2 loss, and this accounts for the observation of $C_{60}^{-\bullet}$ and $C_{60}O^{-\bullet}$ (which could not

be present as impurities) and the lack of observation of C_2 loss. Also, this proposed structure would account for the fact that C_{120} was not observed; if the structure consists of two C_{60} moieties rather than a C_{120} core, and the bridging epoxide group is the most likely candidate for dissociation, it is therefore impossible to observe $C_{120}^{\cdot+}$ following fragmentation. Indeed, the structures of $C_{120}O$ and $C_{120}O_2$ are known to consist of two moieties which are bridged through C-O-C bonding and σ C-C bonds, where the bridge is similar in appearance to a furanoid ring.[8,16] Consequently, this mass spectrum provides further evidence for the proposed "dumb-bell like" structure.

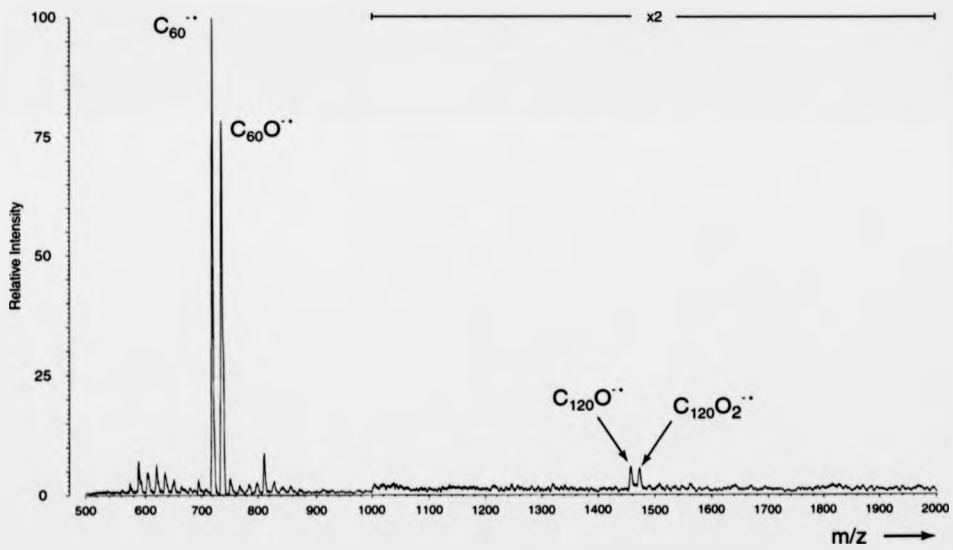

Figure 2: Negative-ion time-of-flight mass spectrum obtained on a Kratos Kompact MALDI IV under matrix-assisted laser desorption/ionization (MALDI) conditions. The presence of $C_{120}O$ is again noticeable; the presence of $C_{120}O_2$ is believed to result from oxidation of the sample by the matrix, 9-nitroanthracene.

An IR spectrum of the sample was obtained by R. Taylor (University of Sussex, Brighton, UK), and this spectrum was compared to the IR spectrum of a synthetic $C_{120}O$ sample. The synthetic $C_{120}O$ was synthesized according to the known reaction of $C_{60}O$

with C_{60}, leading to the production of $C_{120}O$, as detailed by Lebedkin et al.[17] The reaction may be carried out in solution or in the solid state. The comparison between IR spectra is shown in Figure 3, where Figure 3a shows an enlarged region of the IR spectrum of a synthetic $C_{120}O$ sample, and Figure 3b shows the same enlarged region of an IR spectrum of the assumed $C_{120}O$ species following HPLC separation. The common bands lie at the wavenumbers: 1632m, 1463m, 1456sh, 1429, 1384, 1307, 1218, 1183, 1166, 1101m, 1063, 1033m, 1016sh, 960, 849, 831, 807, 780, 765, 746, 711, 606, 589, 574, 551, 527, and 479 cm^{-1}. These absorption characteristics may be corroborated by those found in the literature.[18]

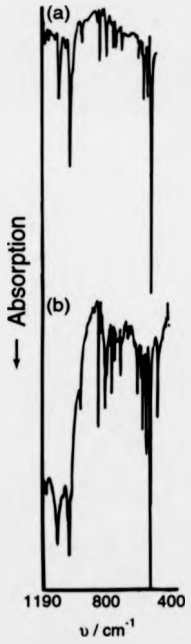

Figure 3: Infra-red spectra of a synthesized sample of $C_{120}O$ (spectrum a) and of the impurity, which is also believed to be $C_{120}O$, obtained from the C_{60} which has been exposed to light and air (spectrum b).

The oxidative stability of pure C_{60} has long been a topic of interest[4,5] and the role of singlet oxygen in the oxidation process has been studied.[19] It is believed that C_{60} oxidizes

under atmospheric conditions, reacting to form $C_{60}O$.[4] As the mono-oxide is strained and unstable relative to $C_{120}O$,[8] it is proposed that $C_{60}O$ reacts with C_{60} in a [2+2] manner, resulting in the formation of $C_{120}O$. This reaction scheme is shown in Figure 4. It is clear that such a reaction occurs under atmospheric conditions, after the C_{60} sample has been obtained. As $C_{120}O$ elutes after C_{70} during HPLC separation, the C_{60} samples were shown to be almost entirely free of contamination from C_{70}, and all commercial samples undergo HPLC separation in order to assure a high purity, it can confidently be stated that $C_{120}O$ is not produced in the arc-discharge process used to produce the pure fullerenes but after purchase. The absorption coefficient of $C_{120}O$ is not known, and so it is not possible to quantify the percentage of $C_{120}O$ present, but a visual estimate of the maximum percentage contribution has been stated to be 1%.

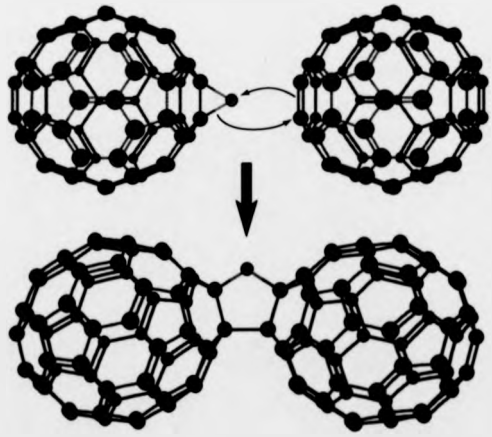

Figure 4: Proposed reaction scheme for the formation of $C_{120}O$ from $C_{60}O$ and C_{60} via a [2+2] cycloaddition

In order to verify further the belief that $C_{120}O$ is the result of oxidation under atmospheric conditions following the purchase of the sample, a further experiment was

designed by Taylor. Solid samples of HPLC purified C_{60} were exposed to air and light for 40 hours. Subsequent analysis using HPLC is shown in Figure 5. Figure 5a shows the HPLC spectrum for a C_{60} sample before exposure, and Figure 5b shows the HPLC spectrum following exposure for 40 hours. A small contribution from $C_{60}O$ is observed in Figure 5a (arising from the handling and concentration of the eluent prior to HPLC analysis), but this contribution becomes much larger in Figure 5b, and the most striking feature of Figure 5b is the presence of $C_{120}O$, which was previously not observable. Further oxidation of the mono-oxide under atmospheric conditions is also likely, and therefore a reaction between $C_{60}O_2$ and C_{60} is possible, leading to the formation of $C_{120}O_2$. Indeed, $C_{120}O_2$ was detected in some of the samples, albeit in much lower abundance than $C_{120}O$, with a retention time of 16.9 minutes; this retention time is identical to that of a synthetically produced $C_{120}O_2$ sample. It is interesting to note that the formation of $C_{120}O_2$ is energetically more favorable than $C_{120}O$,[8] but that $C_{120}O_2$ is much less abundant in the samples than $C_{120}O$. This is attributed to the fact that $C_{60}O_2$, a likely precursor for $C_{120}O_2$ formation, is less abundant than $C_{60}O$, which is more likely to rapidly react to form $C_{120}O$ than to undergo further oxidation to produce $C_{60}O_2$.

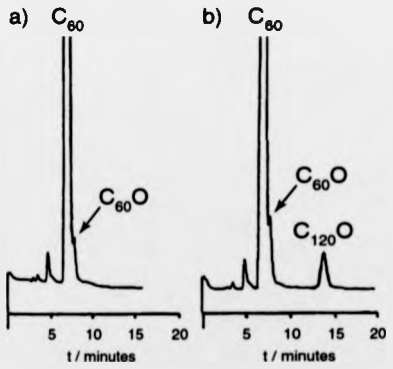

Figure 5: HPLC traces of saturated toluene solutions of C_{60}. Trace a was obtained from a sample of C_{60} which had been previously purified. Trace b resulted after the same sample had been exposed, in solid form, to light and air for 40 hours.

7.4 Summary

Following collaborative efforts with the research group at the University of Sussex which involved the research into fullerene oxides, a remarkable discovery was made. Samples of pure C_{60} which have been allowed to stand in air and in the presence of light are known to degrade over time, and it has long been assumed that the resulting products of degradation are fullerene epoxides such as $C_{60}O$. However, the dramatic discovery has been made that the fullerene oxides formed under ambient conditions may undergo further reactions, resulting in dimerization. Generation of $C_{120}O$ therefore occurs even in the solid state under ambient conditions. Such species have been referred to in Chapter Six and are believed to possess a "dumb-bell like" structure, where two C_{60} moieties are connected through a bridge which consists of one C-C bond and one C-O-C bond, resulting in a bridge that bears a resemblance to a furanoid ring. The discovery of this reaction, which occurs in the solid state and under mild conditions, is remarkable in itself. There are consequences of the discovery that fullerenes may oxidize and dimerize under such mild conditions. The purity level of pure fullerene samples, stated by manufacturers, refers to the compound at the time of purchase, and this purity level will change with time, following exposure to air and light. Perhaps the most serious consequence is that the stability of fullerenes with respect to oxidation must now be properly evaluated, with special attention being paid to potential applications of fullerenes, such as uses in nanotechnology. Oxidation of fullerenes under such mild conditions could prove to be a major problem that must be overcome before uses for fullerenes may be implemented. The findings detailed here have become the basis of another publication which claims to have settled the matter of the long-debated origin of the "spike" observed in the electron paragmagnetic resonance (EPR) spectrum of $C_{60}^{\bullet}$. Paul et al. stated that the observed

"spike" can now be shown to originate from the presence of $C_{120}O$ in the C_{60} sample, following degradation.[20]

7.5 References

1) Barrow, M. P.; Tower, N. J.; Taylor, R.; Drewello, T. *Chem. Phys. Lett.* **1998**, *293*, 302-308.

2) Al-Jafari, M. S.; Barrow, M. P.; Taylor, R.; Drewello, T. *Int. J. Mass Spectrom.* **1999**, *184*, L1-L4.

3) Tomanek, D.; Wang, Y.; Ruoff, R. S. *J. Phys. Chem. Solids* **1993**, *54*, 1679-1684.

4) Chibante, L. P. F.; Heymann, D. *Geochimica Et Cosmochimica Acta* **1993**, *57*, 1879-1881.

5) Scanlon, J. C.; Brown, J. M.; Ebert, L. B. *J. Phys. Chem.* **1994**, *98*, 3921-3923.

6) Aihara, J. *J. Phys. Chem.* **1995**, *99*, 12739-12742.

7) Austin, S. J.; Fowler, P. W.; Manolopoulos, D. E.; Orlandi, G.; Zerbetto, F. *J. Phys. Chem.* **1995**, *99*, 8076-8081.

8) Fowler, P. W.; Mitchell, D.; Taylor, R.; Seifert, G. *J. Chem. Soc. Perkin Trans. 2* **1997**, 1901-1905.

9) Taylor, R.; Penicaud, A.; Tower, N. J. *Chem. Phys. Lett.* **1998**, *295*, 481-486.

10) Creegan, K. M.; Robbins, J. L.; Robbins, W. K.; Millar, J. M.; Sherwood, R. D.; Tindall, P. J.; Cox, D. M.; Smith, A. B.; McCualey, J. P.; Jones, D. R.; Gallagher, R. T. *J. Am. Chem. Soc.* **1992**, *114*, 1103-1105.

11) Heymann, D.; Chibante, L. P. F. *Rec. Trav. Chim.* **1993**, *112*, 639-642.

12) Heymann, D.; Chibante, L. P. F. *Rec. Trav. Chim.* **1993**, *112*, 531-534.

13) Malhotra, R.; Kumar, S.; Satyam, A. *J. Chem. Soc. Chem. Commun.* **1994**, 1339-1340.

14) Deng, J. P.; Mou, C. Y.; Han, C. C. *Fullerene Sci. Tech.* **1997**, *5*, 1033-1044.

15) Balch, A. L.; Costa, D. A.; Noll, B. C.; Olmstead, M. M. *J. Am. Chem. Soc.* **1995**, *117*, 8926-8932.

16) Penn, S. G.; Costa, D. A.; Balch, A. L.; Lebrilla, C. B. *Int. J. Mass Spectrom. Ion Processes* **1997**, *169/170*, 371-386.

17) Lebedkin, S.; Ballenweg, S.; Gross, J.; Taylor, R.; Krätschmer, W. *Tetrahedron Lett.* **1995**, *36*, 4971-4974.

18) Krause, M.; Dunsch, L.; Seifert, G.; Fowler, P. W.; Gromov, A.; Krätschmer, W.; Gutierez, R.; Porezag, D.; Frauenheim, T. *J. Chem. Soc. Faraday Trans.* **1998**, *94*, 2287-2294.

19) Schuster, D. I.; Baran, P. S.; Hatch, R. K.; Khan, A. U.; Wilson, S. R. *J. Chem. Soc. Chem. Commun.* **1998**, 2493-2494.

20) Paul, P.; Bolskar, R. D.; Clark, A. M.; Reed, C. A. *J. Chem. Soc. Chem. Commun.* **2000**, 1229-1230.

Chapter Eight

Coalescence and Collision-Induced Dissociation of Three Bis(ethoxycarbonyl)methylene C_{60} Derivatives

8.1 Introduction

Laser desorption/ionization (LDI) mass spectrometry, often used in conjunction with a time-of-flight (ToF) mass spectrometer, has always been one of the most widely used techniques applied to the analysis of fullerenes. An interesting phenomenon was discovered by Yeretzian et al.[1,2] when using laser ablation of a C_{60} film, where the fullerenes were found to coalesce, forming higher fullerenes in the gas-phase. Since then, much interest in the coalescence reactivity of pure fullerenes[3-10] followed, and a variety of similar experiments have been performed which involved the use or production of a range of fullerene derivatives. Fullerene derivatives involved in such laser ablation based experiments have included: fullerene oxides,[11-15] fluorinated fullerenes,[16] hydrogenated fullerenes,[17] and metallofullerenes.[18,19]

Polyadducts of C_{60} which incorporate bis(ethoxycarbonyl)methylene ligands have also become a subject of recent interest. The biological activity of oligoadducts of C_{60} has attracted attention[20,21] as such compounds have been found to inhibit the HIV enzymes protease and reverse transcriptase. Three such compounds are shown in Figure 1: $C_{60}[C(COOEt)_2]$, $C_{60}[C(COOEt)_2]_2$, and $C_{60}[C(COOEt)_2]_3$; note that for the purpose of brevity, these three compounds shall simply be referred to as the mono-adduct, bis-adduct, and tris-adduct, respectively, throughout this report. The first example of this class of compound was synthesized in 1993 by Bingel,[22] and Paulus and Bingel later characterized the mono-adduct using X-Ray crystallography.[23] Guldi et al. investigated the redox properties of the mono-, bis-, and tris- adducts[21] and found that the redox properties are affected as the number of ligands is increased due to the increased disturbance of the π-system of the fullerene core. Hirsch et al. detailed the synthesis and spectroscopic investigation of a range of polyadduct species, determining the regiochemistry of the

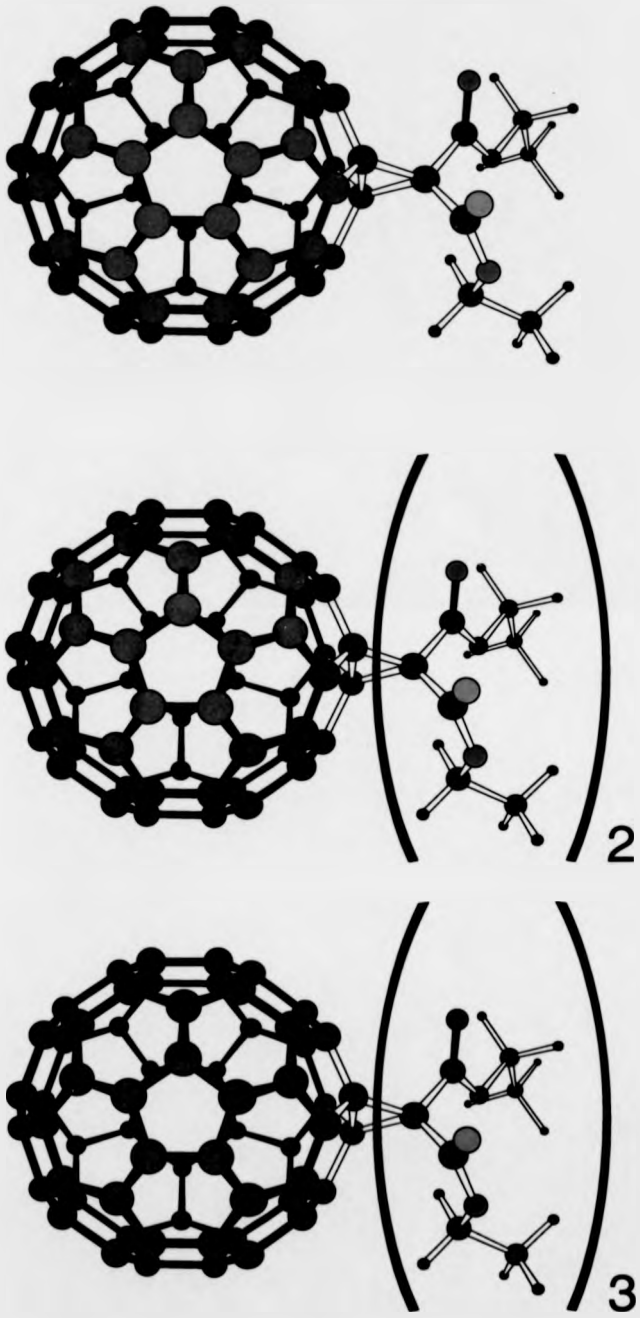

Figure 1: Structures of the mono-, bis-, and tris- adducts, respectively, of C_{60} possessing the bis(ethoxycarbonyl)methylene ligand.

synthetic products;[24] eight isomers of the bis-adduct resulted from the synthesis, but further reaction to generate the tris-adduct led to the preferential production of only two isomers. The regiochemistry of products following successive additions of the bis(ethoxycarbonyl)methylene groups to the C_{60} core was further studied by Hirsch et al.[20] Electron paramagnetic resonance (EPR) spectroscopy was used by Pasimeni et al. to monitor the triplet states of the tris-, tetra-, penta-, and hexa- adducts,[25,26] with the intention of differentiating between the regioisomers for each polyadduct. Three methanofullerene derivatives, which are similar to the three polyadducts studied during the following investigation, have been examined using ultra-violet-visible (UV-vis) spectroscopy.[27] It was found that varying the functional groups present within each ligand had little effect on the photophysical properties of the different derivatives. In their pioneering work, Beck et al. reported the coalescence of these three fullerene derivatives under LDI conditions,[28] and demonstrated that the size of the coalescence products depended strongly upon the size of the fragments generated by the laser ablation process; in addition, Beck et al. later proceeded to investigate the possibility of the bis-adduct undergoing delayed ionization.[29] The detection of carbon clusters possessing an uneven number of carbon atoms was also detailed,[28] and the structures of the higher fullerenes generated had not yet been established.

Building on the work of Beck et al.,[28] the following report aims to reveal more details concerning the structures of the higher fullerenes produced after the laser ablation of the mono-, bis-, and tris-adducts. With access to more recent technology, there are three goals of the investigation. The first is to examine the distribution of coalesced species formed in the gas-phase under LDI conditions, as the resolution of the mass spectrometer used by Beck et al. was a limiting factor in their work, and the precise number of species present was not always clear. It was assumed that fragmentation of the mono-adduct,

leading to the formation of C_{61}^{2+}, was the preliminary step prior to the formation of C_{122}^{2+}. However, as the resolution of the mass spectrometer employed was not great enough to establish beyond doubt that the precursors formed were pure carbon clusters; hence, there remains much that is unknown concerning the mechanism of coalescence, the precursors involved, and the products formed. Once the nature of the coalescence reactions has been established, such as the relative intensities of clusters possessing an even/uneven carbon content, the second goal is to determine whether or not hydrogen is present in the clusters or whether they are indeed pure carbon clusters. This can be accomplished by close scrutiny of the isotopic patterns for each carbon cluster; discrepancies between the relative intensities of the observed signals (within a given distribution) and the relative intensities of the predicted signals would provide the first evidence for the presence of hydrogen. Finally, the third goal of the investigation is to obtain insight into the structure of the coalesced species, and deduce whether they are closed cage entities or whether they are in fact dumb-bell like in structure. Collision-induced dissociation (CID) is the method of choice, by attempting to fragment the higher carbon clusters and determining whether they possess a "memory" of their precursors. Through the acquisition of the above information, it is possible to obtain insight into the structures of such species which are formed in the gas-phase, and hence provide more information regarding the nature of the precursors in the ion source.

8.2 Experimental

The three fullerene derivatives were provided courtesy of H. Hungerbühler (Hahn-Meitner-Institut Berlin, Germany) and had been synthesized using the method employed by Hirsch et al.[22,24] where C_{60} was cyclopropanated through the reaction with

diethyl bromomalonate. Mass spectrometric analysis of the compounds was performed using a Micromass AutoSpec oa-ToF, where an EBE geometry is coupled with an orthogonal time-of-flight region at the end of the instrument and spectra were obtained with the assistance of M. Green (Micromass Ltd., Manchester, UK). A schematic diagram of the instrument is shown in Figure 2. A laser desorption/ionization (LDI) ion source was used throughout the course of the experiments. The samples were dissolved in toluene, and the resulting solution was spotted on to the stainless steel target slide. Once the solvent had evaporated, the target slide was fixed to the source probe, which then entered the ion source. A nitrogen laser is used for the laser ablation of the target, and an 8 kV accelerating potential is used to extract the ions formed. Those ions possessing the full kinetic energy, provided through the acceleration process, must first traverse the first electrostatic sector, ESA1. Selection of ions of a certain mass may be carried out using the magnetic sector, B, before the ions pass through the second electrostatic analyzer, ESA2. Ions are usually selected prior to collision-induced dissociation (CID) experiments, and in the case of this instrument, the selected ions were slowed to 800 eV in an electrically floated collision cell prior to collision, involving a choice of collision gases. If the selection of ions is not warranted, all ions may be allowed to bypass the magnetic sector by using a "bypass tube," where the ions then pass through the second electrostatic sector, ESA2. Whether a "bypass" mass spectrum or a CID spectrum is being recorded, all ions then continue to the orthogonal ToF analyzer, where they are accelerated perpendicularly from their flight path by a "pusher" electrode. The instrument thus functions as a time-of-flight (ToF) mass spectrometer with mass selection (using the magnetic sector) or without mass selection (bypassing the magnetic sector). The pusher electrode is utilized to accelerate orthogonally an ion of a selected m/z value. An uncertainty is associated with the pusher electrode in that ions with a mass difference of ±4% from the selected ions are also orthogonally

accelerated into the time-of-flight region. The advantage of the orthogonal ToF arrangement is that an energy spread amongst ions of the same mass (and hence differing temporal displacements) is compensated for, as temporal spread is converted to angular spread, following acceleration perpendicular to the previous flight path. Angular spread (which becomes a temporal spread, following orthogonal acceleration) is not compensated for by an orthogonal ToF arrangement, but angular spread is more easily minimized by use of ion optics during flight.

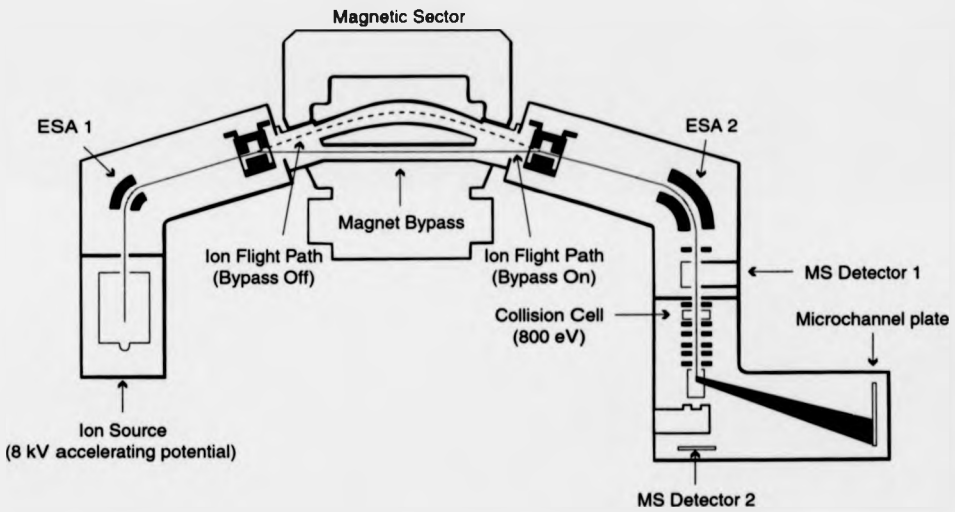

Figure 2: Schematic diagram of the Micromass AutoSpec oa-ToF

8.3 Results and Discussion

As stated earlier, the experiments can be classified as correlating with three, different investigations; the gas-phase coalescence of the three adducts, the investigation of the possible hydrogen content of the coalesced species, and finally the determination of whether

or not the coalesced species are indeed higher fullerenes. Laser ablation of the sample material was employed in order to attempt to coalesce each of the three derivatives in turn. These carbon clusters are then accelerated into the flight tube and bypass the magnetic sector, using the bypass tube, in order that a partial mass spectrum may be obtained. As explained earlier, in order to obtain a partial time-of-flight mass spectrum, the ions of interest must be orthogonally accelerated by the pusher electrode in the ToF section of the instrument, with a ±4% uncertainty in the selection accompanying the acceleration process; in other words, ions of a ±4% deviation from the m/z value of the selected ions will also be accelerated by the pusher electrode. For the following experiments which do not involve collision-induced dissociation, all ions leaving the source traverse the electrostatic sectors and have bypassed the magnetic sector, where the coalesced species of interest are subsequently orthogonally accelerated in the ToF section of the mass spectrometer, enabling further analysis. Figure 3 shows the mass spectra obtained when using the mono-adduct as the precursor. Figure 3b shows an enlarged mass region, taken from Figure 3a. The presence of $C_{60}^{+\bullet}$ in Figure 3a can be attributed to fragmentation of the coalesced species as it is impossible for it to be orthogonally accelerated in conjunction with the coalesced species of interest; the difference in mass is too great. Other fragment signals are also present such as $C_{61}^{+\bullet}$ (not labeled), but are more difficult to discern. The signals correlating with the carbon clusters generated in the ion source are spaced by 24 Da, which corresponds with the expected C_2 loss/uptake which is an indicative characteristic of fullerenes, but equally there is evidence to the contrary to this idea. The facts that fragments such as $C_{60}^{+\bullet}$ and $C_{61}^{+\bullet}$ are observed, following dissociation of the coalesced species, are indicative that the products of the coalescence reactions are not pure fullerenes. Unusually, weak signals at m/z 1452 and m/z 1476 may point to the presence of $C_{121}^{+\bullet}$ and $C_{123}^{+\bullet}$, respectively, and this appears to provide evidence for the formation of fullerene based products with an

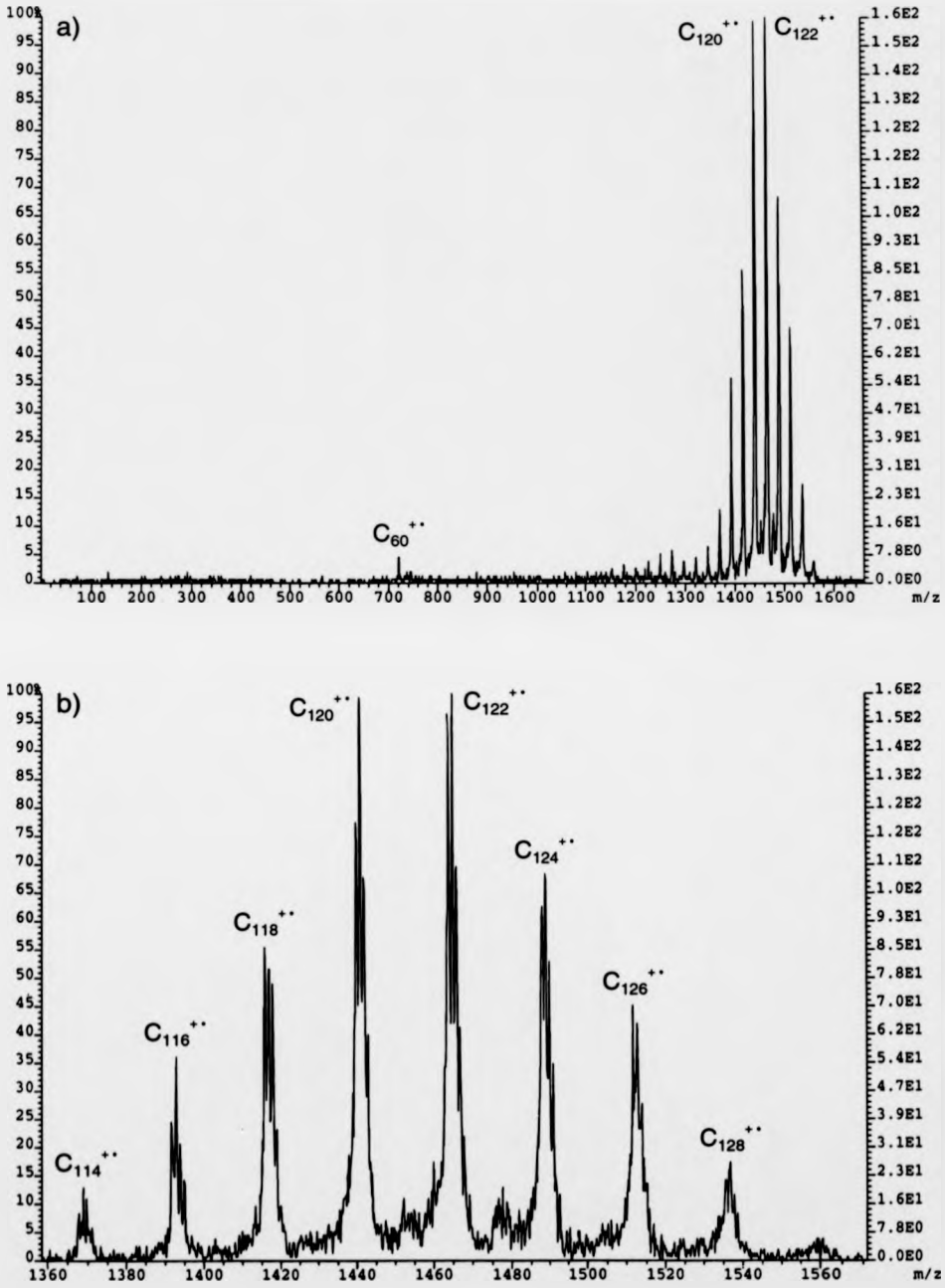

Figure 3: Positive-ion mass spectra of the coalescence products formed under laser desorption/ionization conditions, using the mono-adduct. Spectrum b shows a narrow mass range of coalesced carbon clusters, resulting from an enlargement of part of spectrum a.

uneven carbon content, but this is not conclusive evidence of their formation, as they are only slightly more intense than the noise level. Beck et al.[28] had shown that the production of carbon clusters possessing an uneven carbon content was indeed possible, and so the results detailed here would be in line with their published work. The most intense signals present in Figure 3 lie between $C_{114}^{+\bullet}$ and $C_{128}^{+\bullet}$, with the largest ion being $C_{130}^{+\bullet}$ and the smallest higher carbon cluster being $C_{96}^{+\bullet}$.

Figure 4 shows the partial mass spectra produced following the coalescence of the bis-adduct, where Figure 4b shows an enlarged mass region of Figure 4a. As can be seen from Figure 4a, $C_{60}^{+\bullet}$, $C_{62}^{+\bullet}$, and $C_{64}^{+\bullet}$ can be observed as fragments of the coalesced species. The carbon clusters produced using the bis-adduct as a precursor are of higher mass than those formed using the mono-adduct, and this is to be expected, as the bis-adduct has a greater carbon content, due to its extra ligand. Beck et al. postulated that fragmentation of the mono-adduct leads to the formation of $C_{61}^{+\bullet}$ as a precursor for coalescence reactions, and so, equally, it would be expected that dissociation of the bis-adduct would lead to the formation of $C_{62}^{+\bullet}$ as a precursor for gas-phase reactions, while use of the tris-adduct would lead to $C_{63}^{+\bullet}$ formation which may in turn coalesce in the ion source. Following the experiments performed using the bis-adduct, the most intense carbon cluster signals lie between $C_{118}^{+\bullet}$ and $C_{132}^{+\bullet}$, with $C_{134}^{+\bullet}$ being the largest carbon cluster detected and $C_{98}^{+\bullet}$ being the smallest. Besides the shift to higher mass, one of the most striking features of the carbon clusters observed in Figure 4b is again the presence of products with an uneven carbon content. Not only can they be clearly observed, but ions such as $C_{123}^{+\bullet}$ and $C_{125}^{+\bullet}$ are quite abundant, being approximately two thirds the intensity of neighboring signals resulting from fullerenes possessing an even carbon content.

uneven carbon content, but this is not conclusive evidence of their formation, as they are only slightly more intense than the noise level. Beck et al.[28] had shown that the production of carbon clusters possessing an uneven carbon content was indeed possible, and so the results detailed here would be in line with their published work. The most intense signals present in Figure 3 lie between $C_{114}^{+\bullet}$ and $C_{128}^{+\bullet}$, with the largest ion being $C_{130}^{+\bullet}$ and the smallest higher carbon cluster being $C_{96}^{+\bullet}$.

Figure 4 shows the partial mass spectra produced following the coalescence of the bis-adduct, where Figure 4b shows an enlarged mass region of Figure 4a. As can be seen from Figure 4a, $C_{60}^{+\bullet}$, $C_{62}^{+\bullet}$, and $C_{64}^{+\bullet}$ can be observed as fragments of the coalesced species. The carbon clusters produced using the bis-adduct as a precursor are of higher mass than those formed using the mono-adduct, and this is to be expected, as the bis-adduct has a greater carbon content, due to its extra ligand. Beck et al. postulated that fragmentation of the mono-adduct leads to the formation of $C_{61}^{+\bullet}$ as a precursor for coalescence reactions, and so, equally, it would be expected that dissociation of the bis-adduct would lead to the formation of $C_{62}^{+\bullet}$ as a precursor for gas-phase reactions, while use of the tris-adduct would lead to $C_{63}^{+\bullet}$ formation which may in turn coalesce in the ion source. Following the experiments performed using the bis-adduct, the most intense carbon cluster signals lie between $C_{118}^{+\bullet}$ and $C_{132}^{+\bullet}$, with $C_{134}^{+\bullet}$ being the largest carbon cluster detected and $C_{98}^{+\bullet}$ being the smallest. Besides the shift to higher mass, one of the most striking features of the carbon clusters observed in Figure 4b is again the presence of products with an uneven carbon content. Not only can they be clearly observed, but ions such as $C_{123}^{+\bullet}$ and $C_{125}^{+\bullet}$ are quite abundant, being approximately two thirds the intensity of neighboring signals resulting from fullerenes possessing an even carbon content.

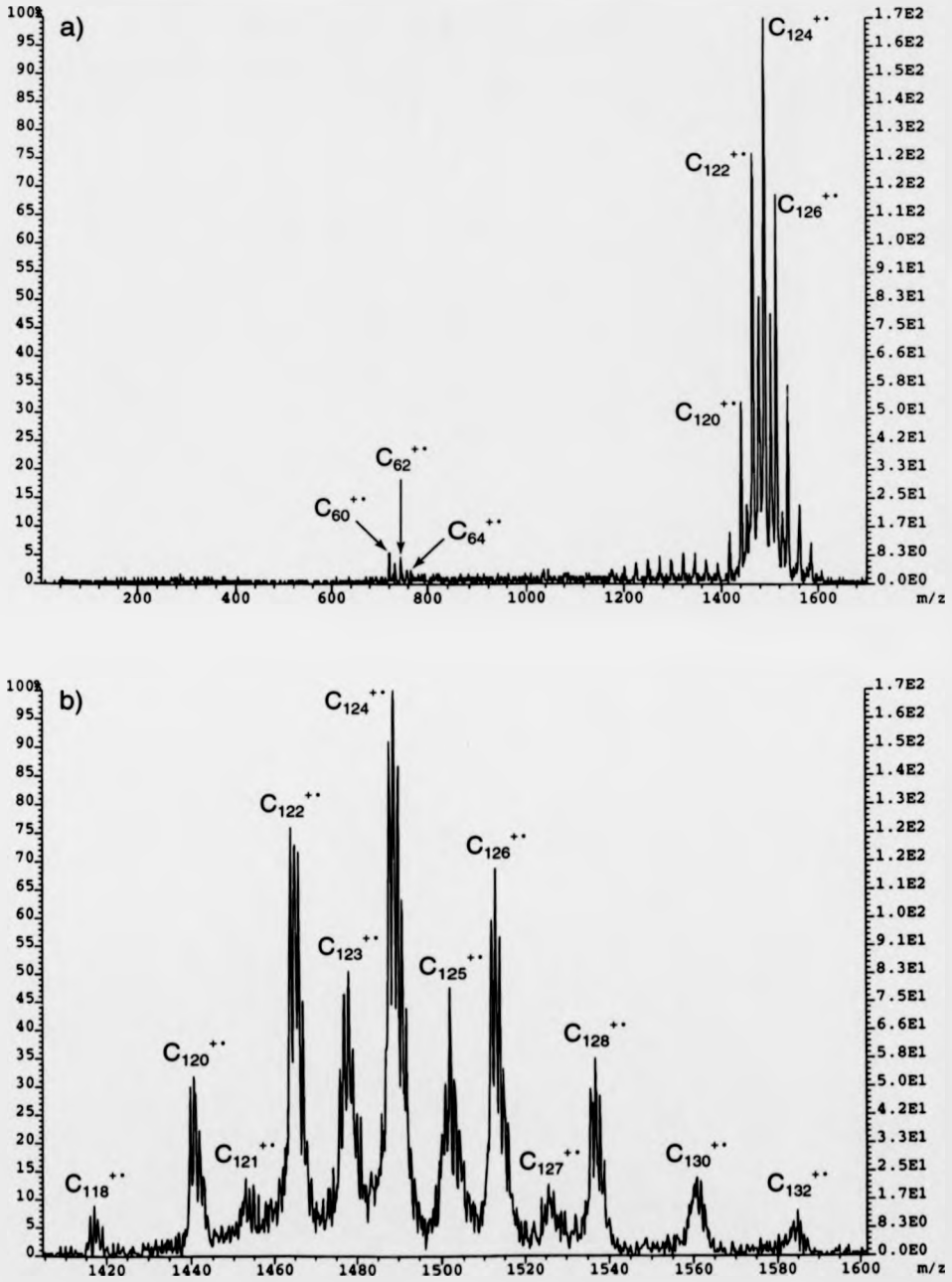

Figure 4: Positive-ion mass spectra of the coalescence products formed under laser desorption/ionization conditions, using the bis-adduct. Spectrum b shows a narrow mass range of coalesced carbon clusters, produced by enlarging part of spectrum a.

Figure 5 shows the mass spectra recorded after coalescence reactions using the tris-adduct as a precursor, where Figure 5b shows an enlarged mass region for the higher carbon clusters. (It should be noted that in the case of Figure 5 only, the enlarged mass region does not relate directly to the mass spectrum directly above it; Figures 5a and 5b actually result from different mass spectra. The reason for this fact is that the spectra were obtained with kind cooperation from Micromass Ltd. (Manchester, UK), and it was unfortunate than an enlarged mass region of Figure 5a was not available, and neither was a wider mass range for Figure 5b.) Fragments from the coalescence products, produced following use of the tris-adduct, appear to be almost absent; very weak signals between m/z 700 and m/z 800 can be discerned, but they are similar in intensity to the noise level present in the spectrum. Fragmentation of the higher carbon clusters also appears to be reduced when compared to Figures 3b and 4b. These observations may be explained by a lower laser fluence being used to produce Figure 5a and also possible differences between the densities of the compounds on the target slides. Figure 5b was recorded using the same laser fluence as was used to produce Figures 3 and 4, but the fragment ion signals in Figure 5b are still less intense than those observed in Figures 3 and 4, and this may signify a slight difference in the constitution of target material, as mentioned earlier. The range of carbon cluster masses lies between $C_{116}^{+\bullet}$ and $C_{132}^{+\bullet}$, and the carbon clusters with an uneven carbon content are even more pronounced than those observed when using the bis-adduct as the target material. However, as the signal intensities are lower, the isotope patterns for the carbon clusters tend to fluctuate more, and it becomes difficult to determine whether there is a chemical reason for this, or whether the signals are statistically unreliable due to the low sampling rate (i.e. low number of ions recorded).

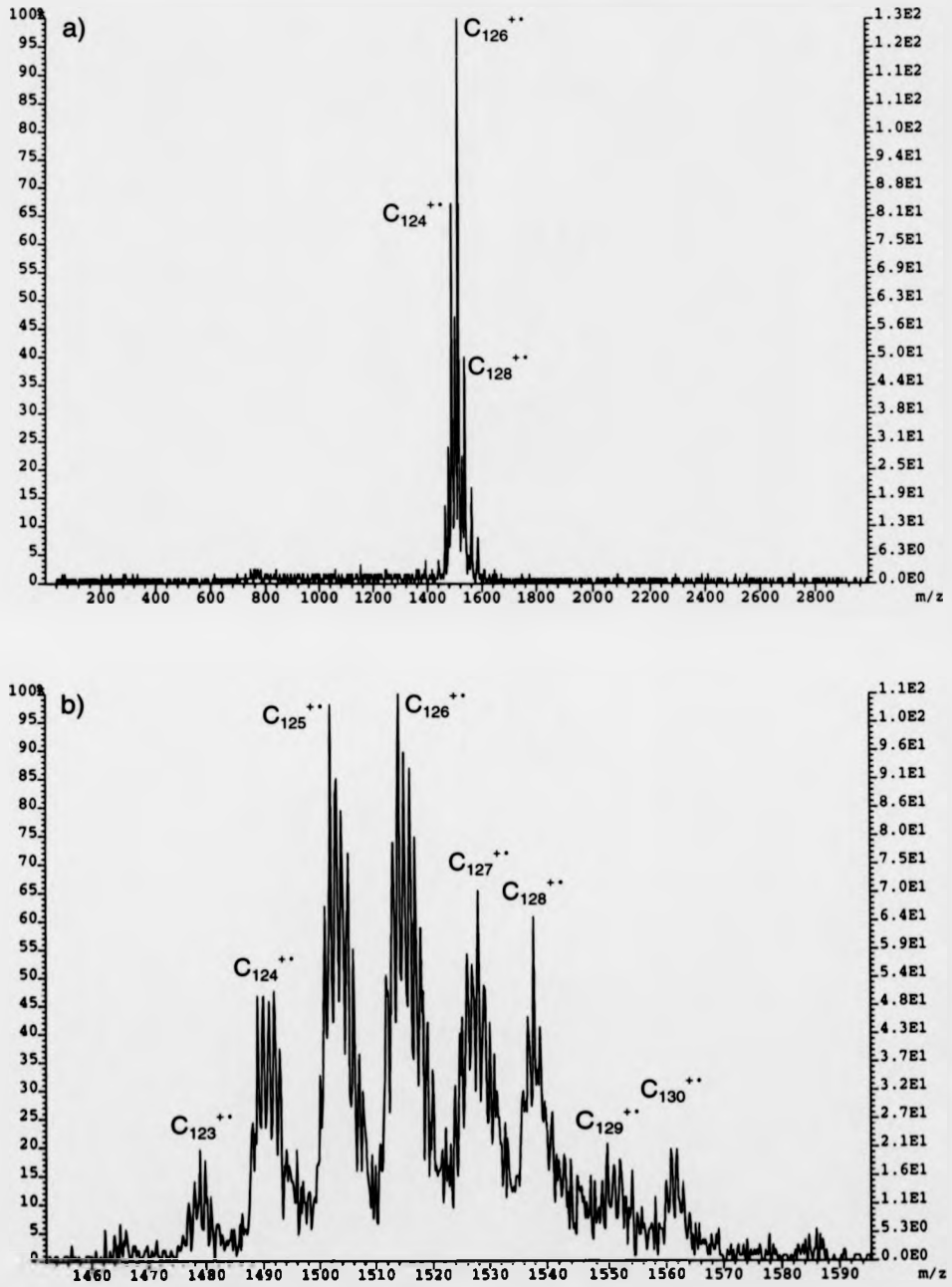

Figure 5: Positive-ion mass spectra of the coalescence products formed under laser desorption/ionization conditions, using the tris-adduct. Spectrum b shows a narrow mass range of coalesced carbon clusters, obtained by enlarging of part of spectrum a.

When comparing the spectra obtained using the mono-adduct, the bis-adduct, and the tris-adduct as precursors for higher carbon cluster generation, several observations may be made. The signal intensities present in the spectra obtained using the bis-adduct and the tris-adduct are similar, but the signal intensities obtained using the tris-adduct are slightly lower. While Figure 5a was obtained at a lower laser power than the other spectra, all other spectra were obtained under identical conditions. Regardless of this, the signal intensities observed in Figure 5b are also lower, and this appears to signify a difference in experimental conditions such as a lower density of target material on the slide. It is unlikely that the addition of a third ligand reduces the tendency towards coalescence to such an extent. It is noticeable that fullerenes possessing an uneven carbon clusters are not observed (or are very weakly observed) when using the mono-adduct as the precursor for coalescence, whereas higher carbon clusters with an uneven carbon content are clearly evident in spectra recorded using the bis-adduct and the tris-adduct. Also, fullerenes of uneven carbon content are proportionally more abundant when using the tris-adduct. It may be concluded that the addition of $(C(COOEt)_2)$ ligands increases the probability of the generation of higher carbon clusters possessing an uneven carbon content. The next stage of the investigation involves examining the isotope patterns of the carbon clusters to determine whether any of the peaks within a given distribution is enhanced, providing evidence for hydrogen content. An instrument that operates at very high resolution (e.g. approximately 183000 at m/z 1440) may be able to resolve peaks resulting from the presence of ^{13}C and from the presence of ^{1}H, but such a facility was not available at the time of investigation. One of the greatest problems faced was that the isotope patterns observed were not consistent and tended to fluctuate in intensities. This almost certainly arises from the fact that the species being analyzed must first be generated in the gas-phase, resulting in a relatively low signal, and with such a low sampling rate, the isotope patterns are less likely to statistically resemble

a proper cross section of these species. Consequently, the error is large enough to make quantitative analysis difficult, although qualitative analysis is less difficult.

The next stage of the experiments was to determine whether or not hydrogen was present in the coalesced species. This was done by obtaining enlarged mass regions of the coalesced species and by comparing the isotopic distributions for each ion with the expected isotopic distribution for that species. Isotopic patterns for the individual carbon clusters which contain hydrogen were incorporated into the calculations, making use of step wise increases in the number of hydrogen atoms present in each recalculation of the isotope pattern. By comparing the three mass spectra in this way, one mass spectrum for each of the precursors, it is possible to obtain insight into the structures of the coalesced species in each of the three cases. The first case to consider is that of the higher carbon clusters generated using the mono-adduct as the precursor. Figure 6 shows an enlarged mass range of Figure 3. Overlayed over the top of the spectrum are the isotope patterns expected for $C_{120}^{+\bullet}$, $C_{122}^{+\bullet}$, and $C_{124}^{+\bullet}$, respectively. The observed pattern for $C_{120}^{+\bullet}$ correlated closely with the predicted pattern, while the observed patterns for $C_{122}^{+\bullet}$ and $C_{124}^{+\bullet}$ correlate less well, but there is still a reasonable match. In each case, however, the M+3 signal is enhanced, but it is difficult to determine whether this is due to error or due to hydrogen content. It would not be possible for the M+3 signals to be selectively enhanced by the presence of hydrogen, while leaving other signals unchanged, as a new distribution would be overlayed (e.g. $C_{122}H_3^{+\bullet}$) rather than one, individual signal. The main differences between the predicted and observed patterns occur when the observed intensities are actually lower than the predicted intensities. There is no obvious explanation for this, other than the low signal intensities obtained which, in turn, are less reliable for the statistical analysis of a system. It would be unlikely that kinetic isotope effects are evident during coalescence reactions,

as, for instance, M+1 and M+2 signals may be less intense than expected while M+3 and M+4 signals may correlate more closely with the expected pattern; this selectivity is unlikely to be due to a genuine phenomenon and more likely to arise purely through error. From the results shown in Figure 6, it is reasonable to conclude that coalescence using the mono-adduct as the precursor results in the formation of pure carbon clusters of even carbon content; no hydrogen is present in the higher carbon clusters.

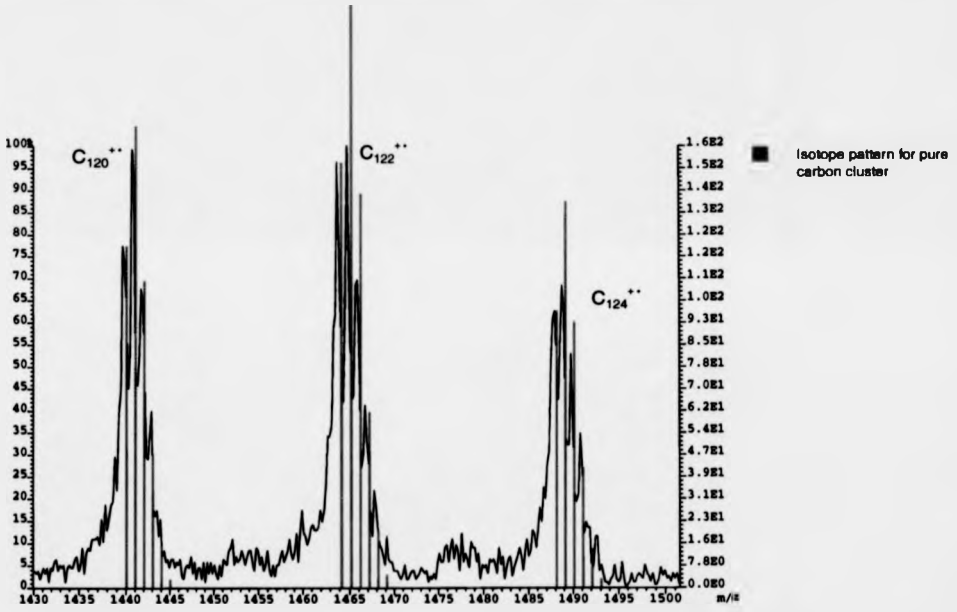

Figure 6: Comparison of experimental results with the predicted isotope patterns for coalesced carbon clusters generated following the laser ablation of the mono-adduct. Hydrogen does not appear to be present amongst the higher carbon clusters formed.

Analysis of carbon clusters resulting from coalescence of the bis-adduct revealed different tendencies. For all clusters with an uneven carbon content, the M+2 peak shows an increased intensity, and from then on within a given distribution, the observed pattern fits less well with the expected isotopic distribution. This immediately appears to indicate

the presence of species including two hydrogen atoms within each cluster, and so isotopic distributions for each $C_xH_2^{+\bullet}$ species were overlayed on top of each $C_x^{+\bullet}$ isotopic distribution. Figure 7 shows one such enlarged mass region, where derivatives of $C_{123}^{+\bullet}$ and $C_{125}^{+\bullet}$ are suspected of containing two hydrogen atoms. Though the total intensity of the M+3 peak for $C_{125}^{+\bullet}$ does not fit very closely with the observed intensity, the predicted intensity of the M+3 peak for $C_{125}^{+\bullet}$ alone (i.e. without the presence of hydrogen) does not correlate very closely either. Clusters with an even carbon content, by contrast, do not display an enhanced M+2 signal. $C_{124}^{+\bullet}$ and $C_{122}^{+\bullet}$ do possess enhanced M+3 peaks, and other clusters of even carbon content also exhibit this tendency albeit to a lesser degree. It is therefore possible that the fullerenes of even carbon content may include a contribution from a species of the same carbon content but containing three hydrogen atoms in addition. The overlayed pattern for $C_{124}H_3^{+\bullet}$ can be seen in Figure 7. Again, one of the limiting factors during the investigation of possible hydrogen content is the lack of strong and consistent signals for further analysis. Signals which are more intense than expected may contain hydrogen or they may be more intense due to experimental error; signals which are less intense than expected will almost certainly be less intense purely as a result of experimental error. However, because the clear trend for carbon clusters of uneven content is to display enhanced M+2 signals within the isotopic distributions, it is reasonable to assume that this is a result of the presence of two hydrogen atoms in these species. The enhancement of the M+3 peaks for carbon clusters of even carbon content is less clear, but could signify the presence of three hydrogen atoms in such species.

The final clusters to analyze were those generated using the tris-adduct as the precursor. Figure 8 shows the enlarged mass region for such species. These higher fullerenes were the most difficult to analyze of the three. This is because the signals fluctuate more

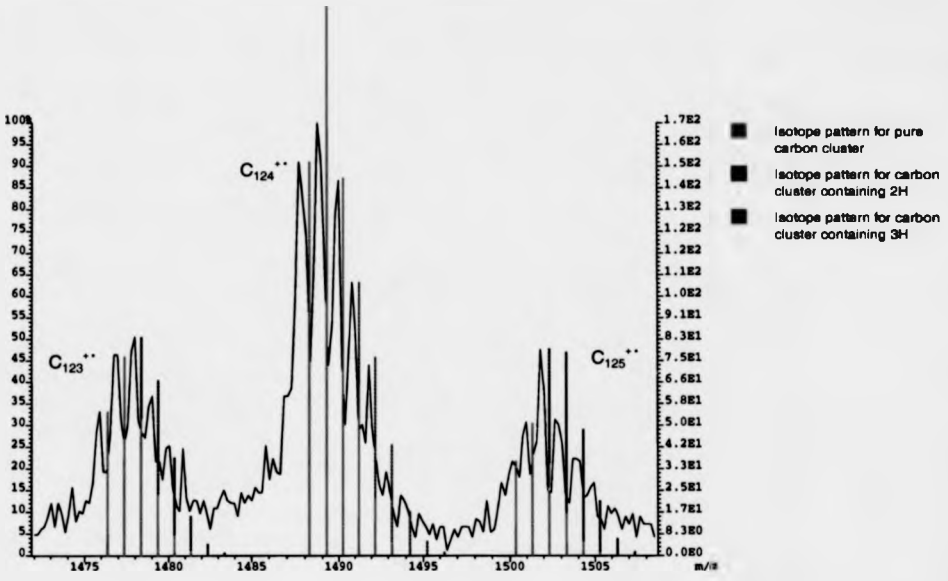

Figure 7: Comparison of experimental results and the predicted isotope patterns for higher carbon clusters, which both do and do not possess hydrogen, produced following the laser ablation of the bis-adduct. In contrast to the higher carbon clusters produced using the mono-adduct, these coalescence products appear to contain hydrogen.

and because the signals are lower in intensity than signals observed in Figures 6 and 7. An example of this problem can be seen in Figure 5b, where the signals that constitute the isotopic distribution for $C_{124}^{+\bullet}$ are almost equal in intensity; this would be unexpected even when allowing for the presence of hydrogen containing species, and surely indicates that the error associated with this mass spectrum may be greater than that associated with the other mass spectra. It is also difficult to be certain of the mass accuracy for Figure 5b (and hence Figure 8), as the intensity of what may constitute the first peak of a given distribution varies greatly, and it is therefore difficult to assign the first peak of each distribution. It may be that the calibration is accurate, or it may be that all masses have been shifted by 1 Da to higher mass. With these sources of error, it is therefore possible to assign a range of species within a given distribution and so a thorough, quantitative analysis becomes almost

impossible. It is clear that hydrogen is present and that the hydrogen content is greater than that observed in clusters generated from the bis-adduct, and hence also the mono-adduct (where no hydrogen content was discovered), but the number of hydrogen atoms contained by species present in each cluster distribution is unclear. At a minimum, species including three hydrogen atoms are present in every cluster, including clusters of even carbon content, but up to seven hydrogen atoms may be present in some of the species. A conclusive assignment is not possible, because of the number of sources of error and the magnitudes of the errors involved, and it is difficult to establish a trend even amongst the clusters within the same spectrum. However, it is possible to deduce that the hydrogen content for clusters generated using the tris-adduct as a precursor is greater than the hydrogen contents observed for clusters produced using the mono-adduct and the bis-adduct.

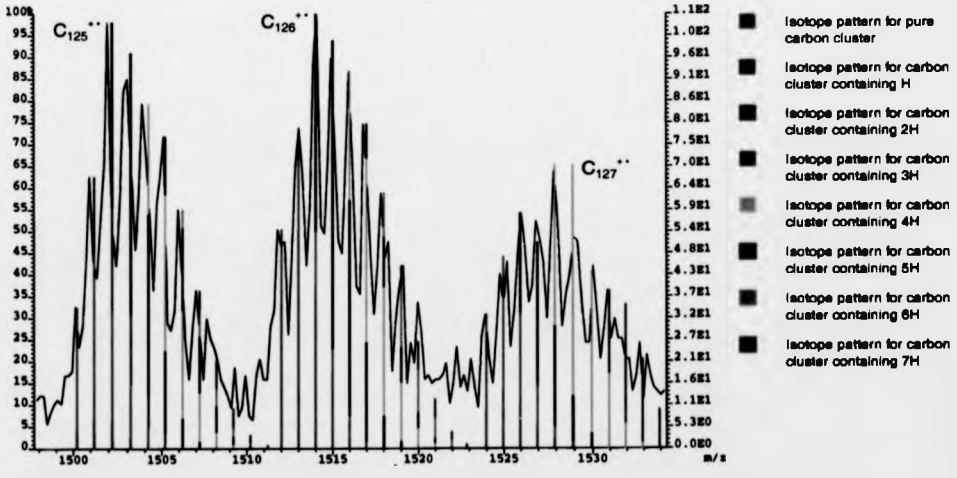

Figure 8: Comparison of experimental results and predicted isotope patterns for the coalescence products formed after the laser ablation of the tris-adduct. In contrast to the products formed following the laser ablation of the mono-adduct and in similarity to results obtained using the bis-adduct, these higher carbon clusters appear to possess hydrogen.

Under the applied experimental conditions, laser ablation of the mono-adduct leads to the formation of pure carbon clusters, and these clusters all consist of species which are constituted by an even number of carbon atoms. There are no signs of hydrogen-containing species within the distribution of products. Laser ablation of the bis-adduct leads to the production of clusters of both even and uneven carbon content. Clusters of uneven carbon content appear to include species which possess two hydrogen atoms, while clusters of even carbon content may include species which possess three hydrogen atoms, but this has not yet been established beyond doubt. Mass spectra recorded using the tris-adduct incorporate variation of signal intensities and unexpected isotopic patterns which are difficult to account for, and this coupled with the low signal-to-noise ratio mean that a larger error is involved. Despite these facts, it has been possible to demonstrate that hydrogen is indeed present, and species containing at least two to three hydrogen atoms were present in every cluster distribution. It is possible that species containing up to seven hydrogen atoms were present amongst some distributions, although quantitative analysis was hampered by the fact that a wide variety of equally viable isotopic patterns may be overlayed to account for the observed patterns.

The final stage of the structural analysis of the carbon clusters generated in the gas-phase is the examination of the fragmentation dynamics of these clusters. Pure fullerenes are known to coalesce to form larger, closed cage carbon clusters following high collision energies while dimeric, bridged species result from low energy collisions.[30] Fullerene oxides tend to form pure fullerenes under the relatively harsh laser desorption/ionization (LDI) conditions, though under matrix-assisted laser desorption/ionization (MALDI) conditions, it has been shown that coalescence results in the formation of dumb-bell like species, consisting of two, distinct moieties, bridged by

C-O-C and C-C bonds. The mono-, bis-, and the tris-adducts are fullerene derivatives that readily undergo coalescence reactions,[28,29] but the precise structures of the coalesced species has never been established. Apart from the possible presence of hydrogen, these clusters consist entirely of carbon atoms, and therefore any possible bridging bonds must be C-C bonds. The C_2 losses evident in Figures 3a, 4a, and 5a would appear to indicate that the clusters are pure, closed cage fullerenes at first glance. However, the presence of fragment ions which do not arise through sequential C_2 loss, such as $C_{60}^{+\bullet}$ and $C_{61}^{+\bullet}$, may be used as counter evidence for this theory or as an indication of the presence of at least one other isomeric form possessing a non-fullerene structure. To attempt to establish the structures of the carbon clusters generated in the gas-phase using these three fullerene derivatives, CID was selected as the method of choice. For each of the fullerene derivatives, a carbon cluster, formed in the ion source following laser ablation, would be selected using the magnetic sector and then collided with xenon in the collision cell. Xenon was chosen as the collision gas in order that a higher center of mass collision energy would result, thus inducing greater fragmentation and providing greater insight into the structure of the selected species.

Figure 9 shows the resulting CID spectrum following the selection of $C_{122}^{+\bullet}$ (m/z 1464), generated using the mono-adduct as the target material in the ion source. The pressure before the introduction of the gas to the collision cell was 5×10^{-8} mbar and after the introduction it rose to 1×10^{-6} mbar. Fragmentation of the selected ion via C_2 loss is evident in Figure 9, but at lower mass, $C_{62}^{+\bullet}$ and $C_{60}^{+\bullet}$ can also be observed. The production of $C_{62}^{+\bullet}$ and $C_{60}^{+\bullet}$ as fragments despite the fact that C_2 loss does not continue down to that mass range implies that it is possible to fragment the higher carbon cluster, producing fragments which may closely resemble the constituent moieties. The coalescence products,

generated in the gas-phase following laser ablation of a fullerene derivative, thus do not possess any "memory" of the formal precursor, $C_{61}^{+\bullet}$, but do in fact dissociate in a manner unlike closed cage fullerenes. This may be taken as evidence for the formation of structures which are "dumb-bell like" and consist of distinct moieties. $C_{60}^{+\bullet}$ may result from C_2 loss from $C_{62}^{+\bullet}$ or it may also be one of the moieties present in the $C_{122}^{+\bullet}$ ion. The formation of a $C_{62}^{+\bullet}$ fragment ion from $C_{122}^{+\bullet}$ would lead to the production of a C_{60} neutral, while the formation of a $C_{60}^{+\bullet}$ fragment ion from $C_{122}^{+\bullet}$ would result in the generation of a C_{62} neutral. As C_{60} possesses an unusually high ionization potential with respect to similar sized carbon clusters,[31] it is more probable that the other fragment would carry the positive charge.

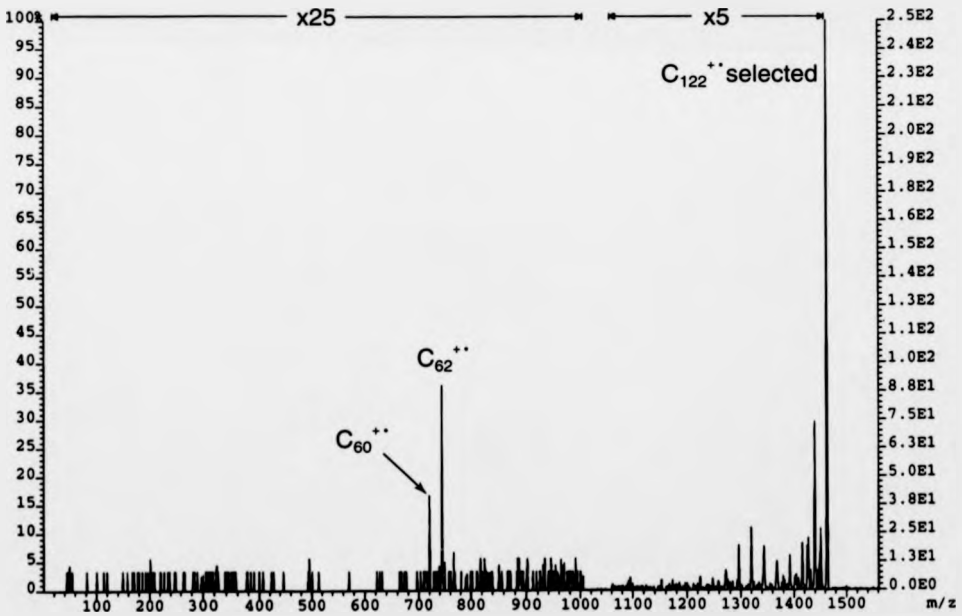

Figure 9: Collision-induced dissociation spectrum of the $C_{122}^{+\bullet}$ ion, generated following coalescence reactions resulting from the laser ablation of the mono-adduct. Fragment ions are clearly evident, indicating that not all the coalescence products are pure fullerenes; the higher carbon clusters must possess a dimeric structure, consisting of two moieties.

Figure 10 shows the CID spectrum resulting from the selection of $C_{124}^{+\bullet}$ (m/z 1488), which was formed following laser ablation of the bis-adduct as the target material. The conditions used for this experiment were the same as those used for the previous experiment, using the mono-adduct. C_2 loss is again evident as one of the primary fragmentation channels of the selected ion. At the lower mass range, $C_{64}^{+\bullet}$ and $C_{62}^{+\bullet}$ can be observed. Unexpectedly, $C_{60}^{+\bullet}$ is not observed as a fragment. In analogy with the earlier results, it can be inferred that this fragmentation pattern results from the dissociation of the $C_{124}^{+\bullet}$ species into its species which resemble the constituent moieties, though the fragments may not be identical to these moieties. Formation of a $C_{64}^{+\bullet}$ fragment ion from $C_{124}^{+\bullet}$ would lead to the formation of a C_{60} neutral, which would not be detected, while loss of $C_{62}^{+\bullet}$ from $C_{124}^{+\bullet}$ would lead to the production of a C_{62} neutral. $C_{62}^{+\bullet}$ may result from C_2 loss

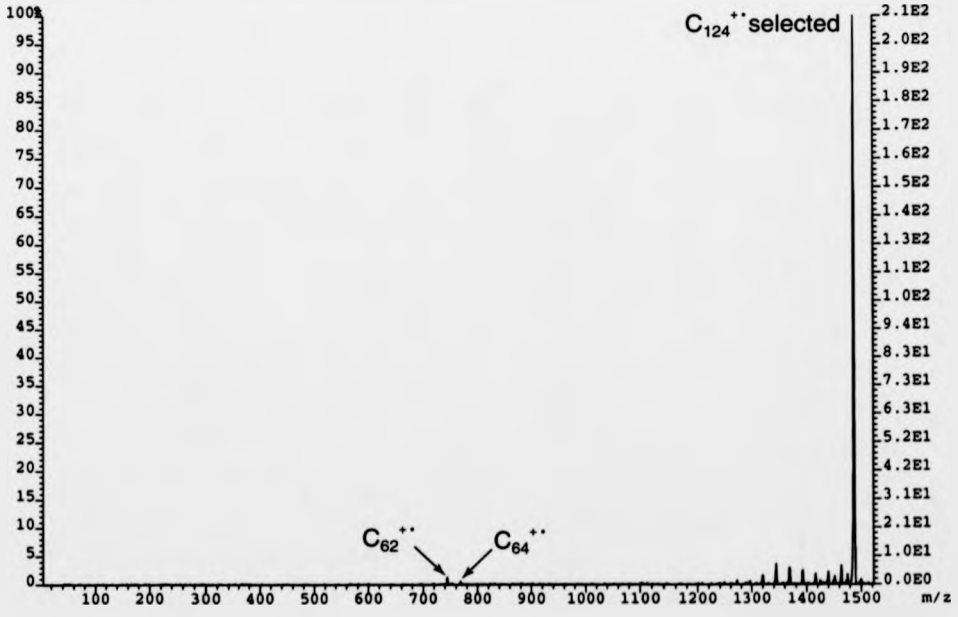

Figure 10: Collision-induced dissociation spectrum of $C_{124}^{+\bullet}$ formed after coalescence reactions resulting from the laser ablation of bis-adduct. Daughter ions are again in evidence, demonstrating that, in similarity with the coalescence products obtained using the mono-adduct, the higher carbon clusters cannot entirely consist of pure fullerenes.

from $C_{64}^{+\bullet}$ or it may result from the fragmentation of $C_{124}^{+\bullet}$, but it is not possible to distinguish between the two possible cases.

The CID spectrum of $C_{126}^{+\bullet}$, formed using the tris-adduct as the precursor, can be seen in Figure 11. Identical experimental conditions to those used for the mono-adduct and the bis-adduct were used during the recording of this spectrum. C_2 loss can be observed from $C_{126}^{+\bullet}$, in line with the previous two experiments. At lower mass, three fragments can be observed: $C_{66}^{+\bullet}$, $C_{64}^{+\bullet}$, and $C_{62}^{+\bullet}$. In similarity to the experiment performed using the bis-adduct, $C_{60}^{+\bullet}$ is not observed as a fragment. The formation of $C_{66}^{+\bullet}$ from $C_{126}^{+\bullet}$ would yield a C_{60} neutral, the production of $C_{64}^{+\bullet}$ would lead to the generation of a C_{62} neutral, and the formal loss of a $C_{62}^{+\bullet}$ fragment ion would result in the formation of a C_{64} neutral.

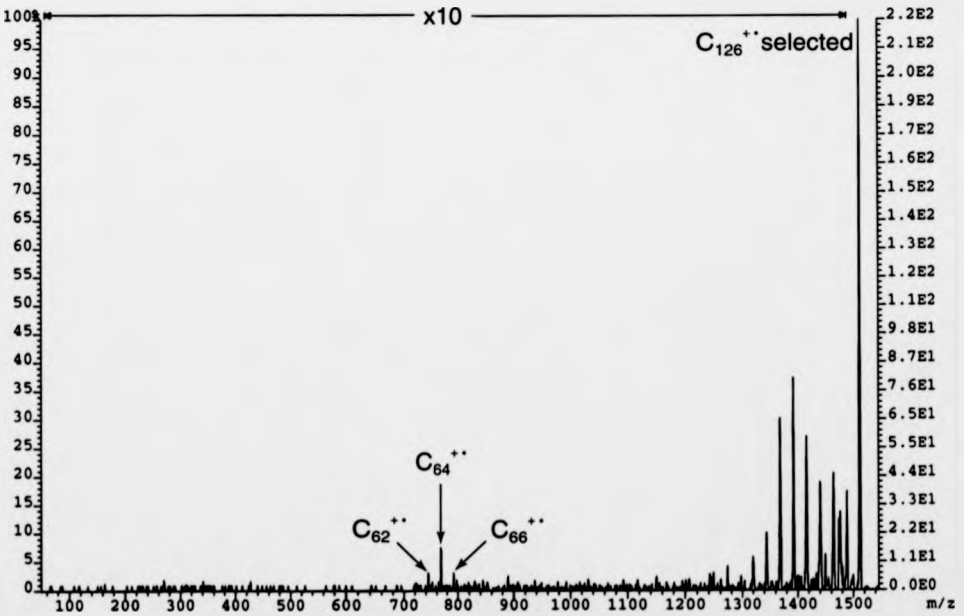

Figure 11: Collision-induced dissociation spectrum of the $C_{126}^{+\bullet}$ ion, which has been selected following coalescence reactions after laser ablation of the tris-adduct. Fragmentation is observed which, in similarity with results obtained using the mono- and bis- adducts, demonstrate that the higher carbon clusters generated through coalescence reactions cannot entirely consist of pure fullerenes.

Again, it is not possible to distinguish between whether $C_{62}^{+\bullet}$ and $C_{64}^{+\bullet}$ result from C_2 loss from $C_{66}^{+\bullet}$, or whether they are produced directly from the fragmentation of $C_{126}^{+\bullet}$.

From these three experiments, it is possible to observe a trend. In each case, the largest fragment at low mass is equal to the mass of the selected ion following the loss of a C_{60} neutral. It is possible to conclude that the two or three fragments within this mass range in each case result from direct dissociation of the selected ion, as C_2 loss from the selected ion in each case does not continue to occur down to such a low mass range. Other fragments within this mass range are separated by 24 Da (C_2) and could result from either C_2 loss from the low mass fragment (e.g. $C_{60}^{+\bullet}$, $C_{64}^{+\bullet}$, or $C_{62}^{+\bullet}$) or equally from direct dissociation of the selected ion. Owing to the fact that in two of the three experiments, $C_{60}^{+\bullet}$ is not observed, it would be inconsistent to conclude that $C_{60}^{+\bullet}$ is observed due to direct fragmentation of $C_{122}^{+\bullet}$ in Figure 9; $C_{60}^{+\bullet}$ is not observed when selecting $C_{124}^{+\bullet}$ although $C_{64}^{+\bullet}$ is seen, and $C_{60}^{+\bullet}$ is not observed when selecting $C_{126}^{+\bullet}$ although $C_{66}^{+\bullet}$ is present. $C_{60}^{+\bullet}$ is less likely to be observed as a daughter ion due to the fact that it will possess a higher ionization potential than the other fragment, and therefore the other moiety is likely to carry the charge and be observed as a fragment ion, while C_{60} would be produced as a neutral species. It is more consistent to conclude that the $C_{60}^{+\bullet}$ observed in Figure 9 results from C_2 loss from $C_{62}^{+\bullet}$. Similarly, $C_{62}^{+\bullet}$ would result from C_2 loss from $C_{64}^{+\bullet}$ in Figure 10, and $C_{64}^{+\bullet}$ and $C_{62}^{+\bullet}$ would be observed as fragments following C_2 loss for $C_{66}^{+\bullet}$ in Figure 11. In keeping with this hypothesis, the fragments $C_{62}^{+\bullet}$ (Figure 9), $C_{64}^{+\bullet}$ (Figure 10), and $C_{66}^{+\bullet}$ (Figure 11) may be said to result from direct dissociation of the selected ion, while all lower mass fragments in each, respective CID spectrum are most likely to result from C_2 loss, although a direct fragmentation route cannot be ruled out entirely as a competing reaction. The deduction that the selected ions dissociate to form fragments which closely

resemble their formal precursors has structural implications. The higher carbon clusters generated using the three fullerene derivatives must possess a "dumb-bell like" structure, rather than resemble a closed cage fullerene. Though the relative positions of the ligands on the C_{60} core for the bis-adduct and the tris-adduct are not known, it is believed that the isomers used are the same as used by Beck et al. and were produced using the same synthetic method. However, if carbon atoms formed a "bridge" between two fullerene cores in the higher carbon clusters, the fragment ions observed following collision-induced dissociation may be more readily explained as entities which closely resemble the moieties present in the higher carbon cluster. Furthermore, the fact that the selected carbon clusters dissociate to produce such fragments may be taken as an indication that the exohedrally bound carbon atoms (present following loss of the majority of the ligands, of which they were part) remain externally bound and have not become incorporated into the fullerene core. Were these carbon atoms to become incorporated into the fullerene core, the fusion products would be more likely to be closed cage fullerenes, as this would be in line with the observed coalescence behavior of other, pure fullerenes. The selective formation of specific fragments may be seen as evidence for two, distinct moieties being bound to each other via C-C bonds.

The mechanism for coalescence of these derivatives will involve the loss of $(COOEt)_2$ from each $(C(COOEt)_2)$ ligand as an early step. The mono-adduct will dissociate to form $C_{61}^{+\bullet}$ as a reactive precursor for coalescence, while the bis- and tris- adducts equally dissociate to form $C_{62}^{+\bullet}$ and $C_{63}^{+\bullet}$, respectively. The favored products of the fusion reactions are thus expected to be based upon $C_{122}^{+\bullet}$, $C_{124}^{+\bullet}$, and $C_{126}^{+\bullet}$ for the mono-, bis-, and tris-adducts, respectively. The presence of hydrogen amongst the carbon clusters has been noted and so it may no longer be assumed that the products of coalescence reactions are

pure carbon clusters; equally, the precursor species generated through the dissociation of the molecular ion may also contain hydrogen. The precise hydrogen content for each species is difficult to ascertain, but it is probable that two or three hydrogen atoms may be present for the coalescence products formed following laser desorption/ionization of the bis-adduct and the tris-adduct. Though it is not possible to establish the hydrogen content of each species beyond doubt, and therefore not possible to accurately determine the structures of the coalesced species, it would be reasonable to assume that the hydrogen is most likely to be bound to the exohedral carbon atoms which remain. Thus, a possible mechanism for coalescence of the three samples is that the adducts dissociate following laser desorption/ionization to form precursors for coalescence which possess "dangling" carbon atoms (equivalent to a carbene), which may in turn be bound to hydrogen atoms. Two or more precursors must collide in the gas-phase and bond to one another. The fragmentation of the coalesced carbon clusters does not lead to the production of the original precursor moieties. Dissociation of $C_{122}^{+\bullet}$ generates $C_{62}^{+\bullet}$ as fragment ions, and not $C_{61}^{+\bullet}$. This strongly suggests that the initially "dangling" carbon atoms of the two C_{61} units may form a bridging connection between the two fullerene cores. Indeed, Segura and Martín have detailed syntheses of fullerene dimers which proceed via the production of a carbene intermediate, where the fullerene cores of the products are bridged by exohedral carbon atoms.[32] One possible account for the observations could involve a -C=C- bridge. Such a method for bridging the two moieties would similarly be in line with the observed fragmentation patterns for $C_{124}^{+\bullet}$ and $C_{126}^{+\bullet}$. For the latter two clusters, it is not clear whether a single, long chain of carbon atoms or several, smaller carbon chains would constitute the connection between the two fullerene cores. To allow for the formation of such bridges, it has to be assumed that the "dangling" carbon atoms migrate from their initial locations on the surface of the fullerene core to a position where they may partake in the aggregation of

the two moieties. The migration of carbon atoms in ionized hydrocarbons is a well-known process which occurs spontaneously. The assumption that -C=C- bridges are involved in the bonding between two fullerene cores would thus be in line with the observations made during the course of these experiments, though the structures of the coalesced species cannot be established beyond doubt. It may be noted that collision-induced dissociation experiments were attempted using coalesced, carbon clusters of uneven carbon content, but the resulting signals were so weak that meaningful data could not be extracted. In support of the theory that the coalescence products consist of two moieties, bridged by exohedral carbon atoms, dimeric fullerene species are known to exist and have been studied by Jarrold and co-workers using ion mobility experiments.[8,33] Further evidence has been provided in the form of the dissociation patterns of selected coalesced species which were observed by Martin and co-workers.[34] Xia et al. have demonstrated that the collision energy and impact parameter during collision are crucial; collisions at high energy tend to result in the formation of pure fullerenes, while collisions at low energy tend to lead to the production of dimeric species.[30]

8.4 Summary

The coalescence reactions of three fullerene derivatives were investigated. Coalescence of the mono-adduct was seen to result in the formation of carbon clusters, with $C_{122}^{+\bullet}$ being preferentially formed. The presence of hydrogen was not observed amongst such higher carbon clusters. The coalescence of the bis-adduct led to the production of range of higher carbon clusters, including those with an uneven carbon content, and $C_{124}^{+\bullet}$ was the favored product of coalescence. Hydrogen was observed to be present in the higher fullerenes formed, where clusters of uneven carbon content may include two

hydrogen atoms; clusters of even carbon content may contain three hydrogen atoms, but this cannot be established beyond doubt, considering the experimental error involved. Coalescence of the tris-adduct led to the formation of higher carbon clusters where $C_{126}^{+\bullet}$ was the coalescence product that was favored, and clusters of uneven carbon content were observed in increased abundance when compared to those observed using the bis-adduct. Due to the large variation in the isotopic patterns and the lower signal-to-noise ratio, quantitative establishment of the hydrogen content of these clusters was difficult. It can be concluded that hydrogen was indeed present, and species containing at least two to three hydrogen atoms were present in every cluster distribution, and it is possible that species containing up to seven hydrogen atoms were present amongst some distributions. Moving from the mono-adduct to the tris-adduct, the following trends may be observed: the product cluster size increases, the presence of hydrogen increases, and the abundance of clusters with an uneven carbon content also increases. Collision-induced dissociation experiments have revealed that a considerable fraction, if not all, of the higher clusters produced are not closed cage fullerenes but are "dumb-bell like" in structure, consisting of two moieties. While the mechanism of their coalescence is not yet fully understood, a mechanism of formation has been proposed which includes dissociation of the sample neutral to form a reactive precursor which possesses externally bound carbon atoms; such carbon atoms of one precursor may be directly involved in the formation of bridging bonds with the other precursor species. These findings obtained during the course of this investigation provide greater insight into the precursors required and the final structure of the coalesced species.

8.5 References

1) Yeretzian, C.; Hansen, K.; Diederich, F.; Whetten, R. L. *Nature* **1992**, *359*, 44-47.

2) Yeretzian, C.; Hansen, K.; Diederich, F.; Whetten, R. L. *Supplement to Z. Phys. D.* **1993**, *26*, S 300-304.

3) Zhu, L.; Wang, S.; Li, Y. *J. Chem. Phys.* **1994**, *101*, 8592-8595.

4) Beck, R. D.; Weis, P.; Bräuchle, G.; Kappes, M. M. *J. Chem. Phys.* **1994**, *100*, 262-270.

5) Hansen, K.; Yeretzian, C.; Whetten, R. L. *Chem. Phys. Lett.* **1994**, *218*, 462-466.

6) Mitzner, R.; Winter, B.; Kusch, C.; Campbell, E. E. B.; Hertel, I. V. *Z. Phys. D* **1995**, *37*, 89-95.

7) Liu, Z.-Y.; Wang, C.-R.; Huang, R.-B.; Zheng, L.-S. *Int. J. Mass Spectrom. Ion Processes* **1995**, *145*, 1-7.

8) Hunter, J. M.; Fye, J. L.; Bolvin, N. M.; Jarrold, M. F. *J. Phys. Chem.* **1994**, *98*, 7440-7443.

9) Xie, Z. X.; Liu, Z. Y.; Wang, C. R.; Huang, R. B.; Lin, F. C.; Zheng, L. S. *J. Chem. Soc. - Faraday Transactions* **1995**, *91*, 987-990.

10) Onoe, J.; Takeuchi, K. *J. Mass Spectrom.* **1998**, *33*, 387-391.

11) Beck, R. D.; Stoermer, C.; Schulz, C.; Michel, R.; Weis, P.; Bräuchle, G.; Kappes, M. M. *J. Chem. Phys.* **1994**, *101*, 3243-3249.

12) Beck, R. D.; Weis, P.; Rockenberger, J.; Kappes, M. M. *J. Phys. Chem.* **1995**, *99*, 3990-3999.

13) Taylor, R.; Barrow, M. P.; Drewello, T. *J. Chem. Soc. Chem. Commun.* **1998**, 2497-2498.

14) Al-Jafari, M. S.; Barrow, M. P.; Taylor, R.; Drewello, T. *Int. J. Mass Spectrom.* **1999**, *184*, L1-L4.

15) Barrow, M. P.; Tower, N. J.; Taylor, R.; Drewello, T. *Chem. Phys. Lett.* **1998**, *293*, 302-308.

16) Cozzolino, R.; Belgachem, O.; Drewello, T.; Käseberg, L.; Herzschuh, R.; Suslov, S.; Boltalina, O. *Eur. Mass Spectrom.* **1997**, *3*, 407-414.

17) Möder, M.; Nüchter, M.; Ondruschka, B.; Czira, G.; Vékey, K.; Barrow, M. P.; Drewello, T. *Int. J. Mass Spectrom.* **2000**, *195/196*, 599-607.

18) Hopwood, F. G.; Fisher, K. J.; Greenhill, P.; Willett, G. D.; Zhang, R. *J. Phys. Chem. B.* **1997**, *101*, 10704-10708.

19) Kimura, T.; Sugai, T.; Shinohara, H. *Int. J. Mass Spectrom.* **1999**, *188*, 225-232.

20) Hirsch, A.; Lamparth, I.; Grösser, T. *J. Am. Chem. Soc.* **1994**, *116*, 9385-9386.

21) Guldi, D. M.; Hungerbühler, H.; Asmus, K.-D. *J. Phys. Chem.* **1995**, *99*, 9380-9385.

22) Bingel, C. *Chem. Ber.* **1993**, *126*, 1957-1959.

23) Paulus, E. F.; Bingel, C. *Acta Cryst.C* **1995**, *51*, 143-146.

24) Hirsch, A.; Lamparth, I.; Karfunkel, H. R. *Angew. Chem. Int. Ed. Engl.* **1994**, *33*, 437-438.

25) Pasimeni, L.; Hirsch, A.; Lamparth, I.; Maggini, M.; Prato, M. *J. Am. Chem. Soc.* **1997**, *119*, 12902-12905.

26) Pasimeni, L.; Hirsch, A.; Lamparth, I.; Herzog, A.; Maggini, M.; Prato, M.; Corvaja, C.; Scorrano, G. *J. Am. Chem. Soc.* **1997**, *119*, 12896-12901.

27) Bensasson, R. V.; Bienvenüe, E.; Fabre, C.; Janot, J.-M.; Land, E. J.; Leach, S.; Leboulaire, V.; Rassat, A.; Roux, S.; Seta, P. *Chem. Eur. J.* **1998**, *4*, 270-278.

28) Beck, R. D.; Weis, P.; Hirsch, A.; Lamparth, I. *J. Phys. Chem.* **1994**, *98*, 9683-9687.

29) Beck, R. D.; Weis, P.; Rockenberger, J.; Kappes, M. M. *Surface Review Letters* **1996**, *3*, 771-775.

30) Xia, Y.; Xing, Y.; Tan, C.; Mei, L. *Phys. Rev. B* **1996**, *53*, 13871-13876.

31) Zimmerman, J. A.; Eyler, J. R.; Bach, S. B. H.; McElvany, S. W. *J. Chem. Phys.* **1991**, *94*, 3556-3562.

32) Segura, J. L.; Martin, N. *Chem. Soc. Rev.* **2000**, *29*, 13-25.

33) Shvartsburg, A. A.; Hudgins, R. R.; Dugourd, P.; Jarrold, M. F. *J. Phys. Chem. A* **1997**, *101*, 1684-1688.

34) Tast, F.; Malinowski, N.; Billas, I. M. L.; Heinebrodt, M.; Branz, W.; Martin, T. P. *J. Chem. Phys.* **1997**, *107*, 6980-6985.

Chapter Nine

Metal-Catalyzed Coalescence Reactions of Metallofullerenes

9.1 Introduction

In 1985, Smalley and co-workers attempted to provide evidence for the closed cage nature of Buckminsterfullerene.[1] The method employed was the formation of fullerene complexes which contained a single lanthanum atom, proving that the metal atom was encapsulated by a carbon cage. Since these early experiments, interest in "endohedral" fullerene complexes, where an atom or atoms are enclosed in (but not bound to) a fullerene cage, has rapidly grown.[2-20] Synthesis of endohedral fullerenes frequently involved the use of collision experiments using mass spectrometers, where the collision gas atoms (typically small, noble gas atoms) became trapped inside fullerene ions.[2,4-7,9,21,22] Other synthetic methods have included the generation of fullerenes in an inert atmosphere,[13] such as helium, or using high pressure to insert small gas atoms into the cage.[23] Formation of fullerenes using a doped, carbon-based surface, where some of the fullerenes generated will contain the dopant, has also been shown to be an effective method for endohedral fullerene production.[8,24-27] Other groups have been interested in improving metallofullerene yield by synthesizing new precursor materials.[28] The area of endohedral fullerene research that has been gaining the most interest is that of metallofullerenes. Although such compounds have been synthesized early on during the course of fullerene research,[1] it was the inclusion of noble gas atoms which became the topic of greater interest for many years and it is only comparatively recently that the subject of metallofullerenes has become as intensively investigated as it is now.

Metallofullerenes are a specific class of endohedral compounds, where the endohedral atom is a metal, typically from Group 3 or else the lanthanide series of the periodic table. $M@C_{82}$ and $M_2@C_{80}$ have been found to be particularly common synthetic products,[8,26]

though other structures such as $Ca_2@C_{72}$ have also been observed to be preferred.[25] Collisions with molecular oxygen showed that metallofullerenes may undergo oxidation in the same way as pure fullerenes, but that metallofullerenes which were the most frequently extracted from solution were the least likely to undergo oxidation.[29] Other collision experiments have shown that metallofullerenes fragment via C_2 loss, analogously to pure fullerenes, usually without the loss of the metal atom.[30,31] Computational approaches have been used by many research groups, as discussed by Andreoni.[32] An investigation by Kobayashi et al. into the structures of $Sc_2@C_{84}$ and $La_2@C_{80}$ revealed that the metal atoms have enough freedom to move inside the carbon cages[33]; this movement has even been noted to result in the presence of a small magnetic field, leading to speculation about possible applications of such compounds. Further theoretical studies of metallofullerenes led to the discovery that a heptagonal ring is present in one of the isomers of $Ca@C_{72}$.[34] More recently, Kobayashi et al. have determined that the metal atom present in a $M@C_{82}$ species (where M = Sc, Y, La, and lanthanides) electrostatically interacts with the fullerene cage, and such interactions lead to the stabilization of the structure,[35] as additionally noted by Laskin et al.[31] It was further shown that metal atoms including Y, La, Ce, Pr, Nd, and Gd favorably donate three electrons to the carbon cage, but that considerable back donation of electron density from the carbon cage leads to the more accurate description of $M^{2+}@C_{82}^{2-}$ when M is Ce, Pr, Nd, and Gd. In contrast, Sc, Eu, Yb, and Lu prefer to donate two electrons to the encapsulating fullerene structure. The findings of Kuran et al.[26] and Laskin et al.[31] have further supported these proposals, determining experimentally that donation of three electrons is common, although donation of two electrons is also possible, with the charge state depending on the redox properties of the metal species and the carbon cage size. Kimura et al. have revealed that cluster size is important is important in determining whether the metal atom is networked into the carbon cage or whether the metal atom is

present endohedrally.[27] It was also shown that formation of metallocarbon clusters in the negative-ion mode differs from that observed in the positive-ion mode; negative cluster ions were produced following electron attachment to neutral clusters while positive ions were produced following clustering around a positive metal ion core. Thus, the positive metal ion plays a crucial role in the formation of metallofullerenes.[27]

Interest in such a class of fullerene derivative has increased because of the fact that this species is one of the most promising with regards to applications of fullerene science. Perhaps the most commonly investigated application with regards to metallofullerenes is the potential use as superconductors.[17,25,36,37] Ways of increasing the critical temperature, T_c, of metallofullerenes are continually investigated, and with the significant, potential economic and technological gains to be made in this area, it is little surprise that there is considerable impetus in this field. Doped nanotubes have been seen as potential "nanowires" effectively.[37] One particularly visionary publication outlined a design that incorporated both a metallofullerene and a nanotube, with the metallofullerene being enclosed by the nanotube.[38] By the application of an electric field, the metallofullerene could be made to travel from one end of the nanotube to the other and this arrangement could be implemented as a memory device, with particular reference to RAM used in computers. With these potential applications in mind, it becomes clear that further characterization of metallofullerenes is important.

This chapter encompasses the investigation of three metallofullerenes, where the metals are all lanthanide metals. The cluster sizes were not initially known, and therefore required determination through mass spectrometric analysis as the first step. The initial purpose of the study was the determination of an ionization technique that may be applicable

to the structure elucidation of metallofullerenes. However, it was soon clear that these three compounds behaved in a remarkable manner in the gas-phase, in that they coalesced under relatively gentle matrix-assisted laser desorption/ionization (MALDI) and laser desorption/ionization (LDI) conditions. Consequently, the following study can be considered in two parts: the gas-phase behavior of the three compounds and the search for a suitable ionization technique.

9.2 Experimental

The metallofullerene compounds that were provided courtesy of C. Lebrilla (University of California, Davis, USA) had been dissolved in dimethylformamide (DMF), following purification using high performance liquid chromatography (HPLC), and the precise concentration was not known. The metal atoms involved were known to be gadolinium (RAM of Gd = 157.25 Da; six isotopes), terbium (RAM of Tb = 158.93 Da; one isotope), and erbium (RAM of Er = 167.26 Da; four isotopes). Experiments were performed using four different mass spectrometers. A Kratos Kompact MALDI IV (reflectron time-of-flight) was used for most of the laser desorption/ionization (LDI) and matrix-assisted laser desorption/ionization (MALDI) experiments. This instrument incorporates a nitrogen laser (337 nm, 3 ns pulse width), a 20 kV accelerating potential, and a curved field reflectron. All spectra recorded using this instrument result from the sum of 200 laser pulses. Further high resolution LDI experiments which were required for verification purposes, which therefore required a higher resolving power, were performed using a Bruker Reflex (reflectron time-of-flight) with the assistance of J. Jarvis (Bruker, Coventry, UK). The Reflex also uses a nitrogen laser and a 20 kV accelerating potential, but the ion source incorporates delayed extraction for improved resolution and the reflectron

uses a linear field. The negative-ion spectrum recorded using the Reflex is the result of 130 laser pulses, and the positive-ion spectrum represents the sum of 110 laser pulses.

In the case of either instrument, LDI work was conducted by first placing a small droplet of the metallofullerene solution on each target on a stainless steel slide, and the solvent was allowed to evaporate. The slide was then inserted into the ion source of the instrument. When performing MALDI experiments, the matrix 9-nitroanthracene was used. 9-nitroanthracene was dissolved in acetone (ratio of 10 mg of matrix per 1 mL of acetone) and then a final solution, comprising a ratio of matrix to analyte of 20 μL to 1 μL, was created. This solution was then spotted on to the stainless steel slide and then dried in the same manner as for LDI experiments.

Electrospray ionization (ESI) analysis was conducted using a VG-manufactured ESI source, coupled with a VG Platform (quadrupole), and the spectra were provided courtesy of Prof. R. Herzschuh (Universität Leipzig, Leipzig, Germany). The sample was mixed with toluene in order to increase the total volume used during analysis, and the resulting solution was directly sprayed, with no modification to the sample and no other cosolvents. Negative-ion electron ionization (EI) experiments were carried out using a Micromass EI source coupled with a Micromass AutoSpec (EBE geometry), with the assistance of I. Katyal.

9.3 Results and Discussion

Prior to further analysis, it would be preferable if the identity of the molecular ions could be established beyond doubt and if the purity of the samples could also be established.

It has been known that many fullerene derivatives are difficult to analyze and that many traditional ionization techniques are too violent for the analysis of such compounds. Therefore, it is important that another, softer, ionization technique can be successfully implemented in order that fullerene derivatives may be investigated. As outlined in Chapter Ten, a recent investigation by this research group has shown that it is possible to analyze fullerenes and their derivatives using ESI on a routine basis. The spectra produced demonstrated that there was very little degree of fragmentation, and that the molecular ions could easily be established, using the unmodified sample solution. It therefore follows that ESI is the best method for identifying the derivatized fullerene. Due to the limitations of the sample quantities and the available time for the utilization of other instruments, only one of the metallofullerene compounds was studied, and the compound of choice was the terbium-based metallofullerene sample. In contrast to previous work, a VG manufactured ESI ion source was used, coupled to a VG Platform, and the resulting negative-ion spectrum is shown in Figure 1a.

The resulting ESI spectrum comprises only three signals. The signal due to $Tb@C_{82}^{-\bullet}$ was expected, as this was believed to be the molecular ion, judging by the MALDI results. However, $Tb_2@C_{80}^{-\bullet}$ was also apparent, and this may be a contaminant, as it is highly implausible that $Tb@C_{82}^{-\bullet}$ is produced during gas-phase reactions of $Tb_2@C_{80}^{-\bullet}$ and vice versa. $Tb_2@C_{78}^{-\bullet}$ is also observed, but this has been assigned as a fragment of $Tb_2@C_{80}^{-\bullet}$, following expected C_2 loss, as the fullerene cage fragments and retains the endohedral, metal atom. It is encouraging that ESI has been shown to be a viable method for the analysis of this metallofullerene species; it is therefore possible that ESI may be used to analyze other metallofullerenes on line in direct combination with high performance liquid chromatography. The ability to produce molecular ions with very little degree of

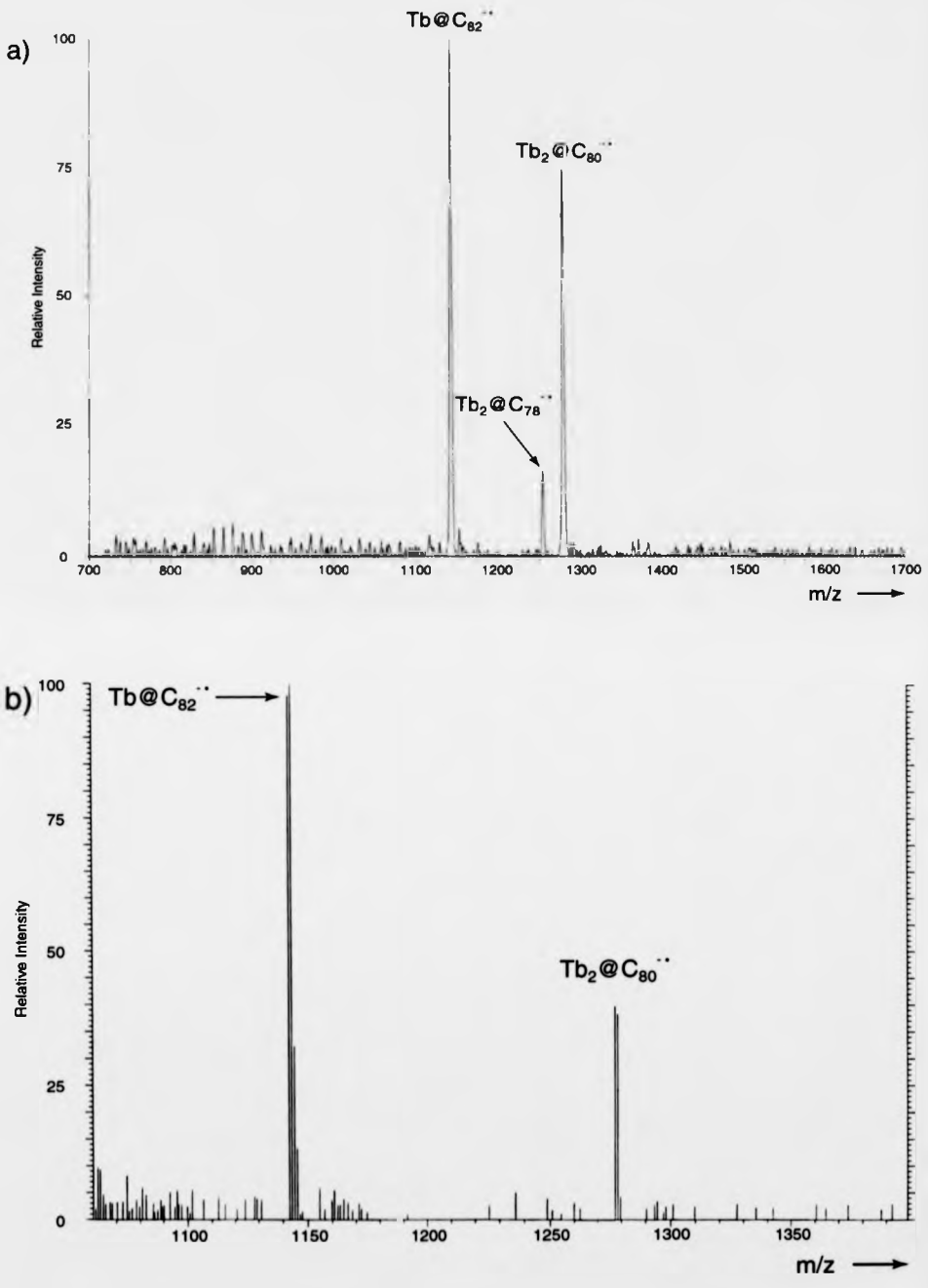

Figure 1: Negative-ion mode mass spectra of the terbium-based metallofullerene sample. Spectrum a was obtained following electrospray ionization (ESI) on a VG Platform. Spectrum b is a single scan, taken from the 200 initially acquired, produced through electron ionization (EI) on a Micromass AutoSpec.

fragmentation (or other side reactions) has been one of the strengths of the ionization method when it comes to the analysis of labile fullerene derivatives, such as fluorinated fullerenes, which are liable to undergo thermal decomposition. For comparison, an EI spectrum was obtained using a Micromass AutoSpec. Figure 1b shows the resulting EI spectrum in the negative-ion mode. It must be noted that this spectrum resulted from only one scan of the 200 scans acquired during thermal desorption of the sample, but the signal-to noise-ratio was very poor, and it was only possible to produce this spectrum by selecting one good scan. The results shown are very similar to the ESI spectrum obtained, but the relative difficulty with which the EI spectrum was obtained is evidence that EI is not the most suitable ionization technique for the study of this species. The attempts to identify the molecular ion indicate that is is likely that the sample comprised two, distinct constituents: $Tb@C_{82}$ and $Tb_2@C_{80}$. This finding would be in line with the observation that $M@C_{82}$ and $M_2@C_{80}$ are two of the most abundant metallofullerene species formed,[8,26] and it is therefore a possibility that the other two samples may comprise analogous components.

Positive-ion mass spectra obtained for the erbium based metallofullerene sample (shown in Figure 2), using MALDI and LDI conditions on the Kratos Kompact MALDI IV, revealed an extensive degree of clusterization. The formation of these higher carbon clusters occurs in the gas-phase following laser ablation, and is a well known phenomenon.[39,40] The laser irradiance used in each case was only a threshold value, and the intensity of the carbon clusters formed is therefore unexpected. For a new laser, the power setting chosen using the software would correspond to an irradiance of approximately 3×10^7 W cm^{-2}, but in this case the laser was approximately two years old and so the laser irradiance value quoted is only an approximation. The threshold setting for the laser

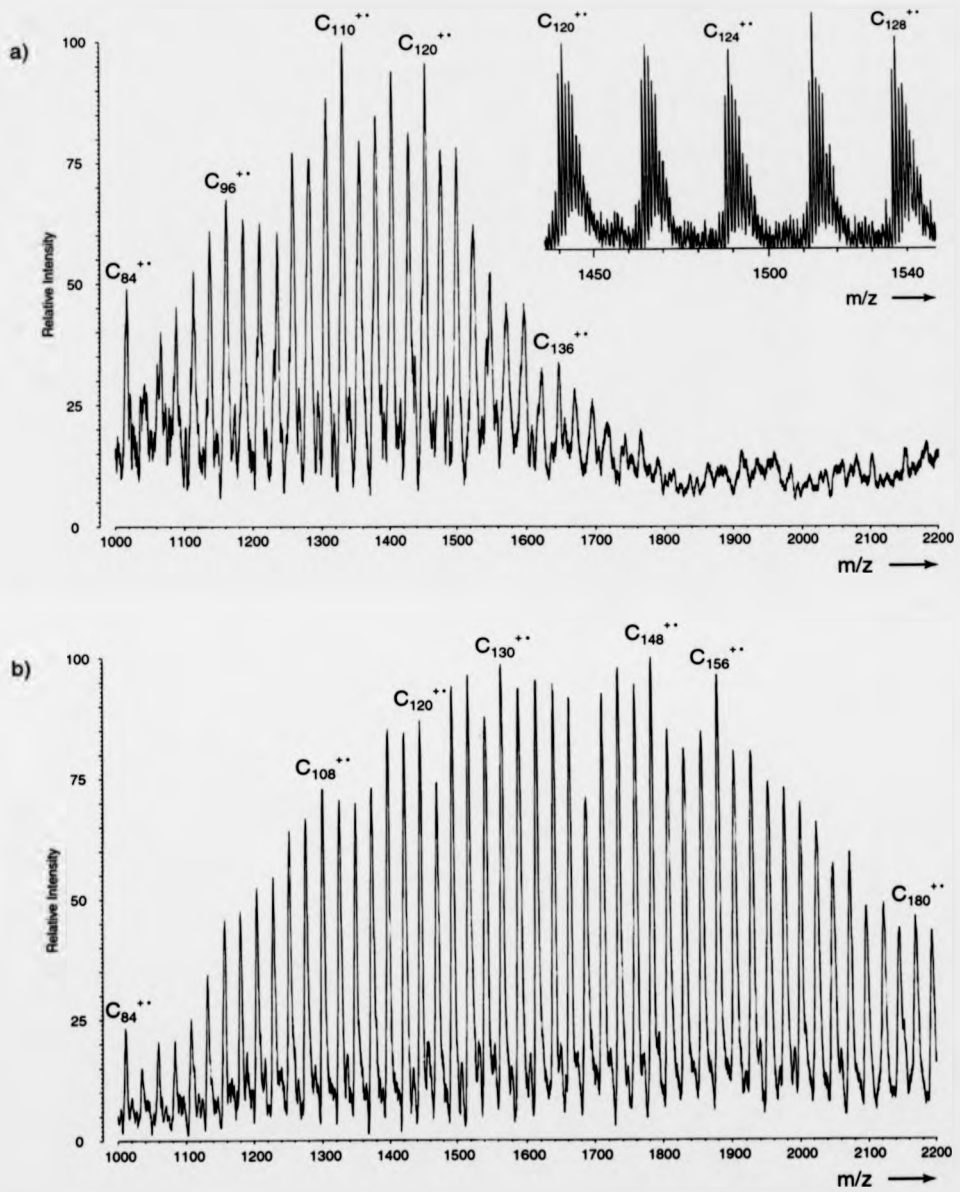

Figure 2: Positive-ion mass spectra acquired using the erbium-based compound. Spectrum a was produced through laser desorption/ionization (LDI) on the Kratos Kompact MALDI IV; the inset was obtained under similar conditions using the Bruker Reflex for a higher resolving power. Spectrum b resulted from matrix-assisted laser desorption/ionization (MALDI) on the Kratos Kompact MALDI IV.

irradiance is not much greater than used for recording spectra of C_{60} ions (positive or negative) at the time, when intending to avoid carbon cluster generation. It must be emphasized that though output power from the laser at that point in time could not be known exactly, it is known that such a laser irradiance setting on the instrument would not be enough to perform similar coalescence reactions using a pure C_{60} sample; such a laser irradiance setting would indeed only be high enough to observe the $C_{60}^{+\bullet}$ ion with a small degree of fragmentation via C_2 loss, with fragments such as $C_{54}^{+\bullet}$ being observable. Figure 2a shows the positive-ion LDI spectrum obtained on the Kompact MALDI IV, and only pure fullerenes can be seen. The signals within the distribution of carbon clusters are most abundant for ions between $C_{110}^{+\bullet}$ and $C_{120}^{+\bullet}$, and no carbon clusters larger than approximately $C_{148}^{+\bullet}$ are observed. All signals result from higher fullerenes, generated in the gas-phase; the facts that the samples were separated using HPLC and that other mass spectra confirm that these species are indeed generated in the gas-phase verify the hypothesis that they are not byproducts of the synthesis. It is possible that a signal resulting from the parent ion is present, but overlaps with $C_{96}^{+\bullet}$ (m/z 1152), as the parent ion signals due to $Er@C_{82}$ would lie between m/z 1150 and m/z 1156 when allowing for the isotopic distribution that results. Therefore, due to the limitations of the resolution of the Kompact MALDI IV, it is not possible to determine whether or not a parent ion signal was present.

The higher carbon cluster ion signals are separated by 24 Da, corresponding to C_2 loss/uptake in the gas-phase. C_2 loss is a characteristic of pure fullerenes, indicating that the carbon clusters are indeed larger fullerenes. No smaller, pure fullerenes are observed as fragments of these higher carbon clusters, providing further evidence that these coalesced species are indeed close caged entities, rather than bridged species which possess "dumb-bell-like" structures. The inset shows a partial mass spectrum obtained using the

Bruker Reflex at a later date, in order to verify the results obtained on the Kratos Kompact MALDI IV. Again, higher fullerenes are observed and constitute the greatest number of signals present in the spectrum. The Reflex is known to have a higher sensitivity and resolving power than the Kompact MALDI IV, and the higher resolution is clearly evident in the inset. It should be noted that the parent ion signals were indeed detected using the Reflex. The isotope pattern relating to the coalesced species does not match the expected isotope pattern and it can therefore be postulated that such signals do not result from one species alone, but from the overlap of signals arising from at least two species. Nine signals appear to be detected amongst each isotope pattern, which increases support for the theory that more than one species is involved, as six signals tend to be observed for pure carbon clusters, judging by previous experience. It is proposed that contributions from several species do indeed result in the patterns observed, and that three of the most likely species include: pure carbon clusters of even carbon content ($C_{2n}^{+\bullet}$), carbon clusters of even carbon content and containing one erbium atom ($Er@C_{2n}^{+\bullet}$), and carbon clusters of uneven content with the presence of one oxygen atom and containing one erbium atom ($Er@C_nO^{+\bullet}$). Unfortunately, as the isotope patterns are inconsistent with the patterns of similar sized carbon clusters (e.g. $\pm C_2$) and the signal-to-noise ratio is relatively high for such precise measurements, the experimental error associated with these spectra make it impossible to assign the structures of the contributing species with confidence.

Figure 2b shows the resulting positive-ion MALDI spectrum for the erbium based compound. A parent ion is not observed, possibly because of the limiting resolution of the instrument, as stated previously. It is notable that the degree of clustering is higher under MALDI conditions, compared to LDI conditions. This can be attributed largely to the fact that the laser irradiance was slightly higher, and so a higher degree of fragmentation and

more extensive gas-phase reactions would be expected. In general, as the laser irradiance is increased, coalescence reactions become less selective, with products being generated over a wider mass range, as a greater variety of carbon fragments become available for reaction. Indeed, though the precursor carbon cages were determined to be C_{82}, higher fullerenes such as C_{180} can be observed in the spectrum shown, although carbon clusters as large as C_{324} have been observed (not shown). The usual route for coalescence to occur is via the fusion of two or more fragments, and can be followed by C_2 loss/uptake, according to reports in the literature which concern the mechanism of coalescence of fullerenes in the gas-phase. Current theories suggest that coalescence results from the fusion of one neutral species and one charged species[41] following laser ablation, followed by C_2 loss/ uptake, or the coalescence of two, excited, neutral species[42] and that the coalesced structures are also stable. The manner in which the metallofullerene sample fuses under such gentle conditions, using a threshold laser irradiance in conjunction with both MALDI and LDI, suggests that the metal atom plays a pivotal role in catalyzing the coalescence, although the exact nature of this role is yet to be determined.

Figure 3 shows the negative-ion spectra resulting from the analysis of the metallofullerene sample which incorporates erbium. The negative-ion LDI spectrum is shown in Figure 3a, and the intensity of the signals resulting from coalesced species is evident. Again, due to the fact that the parent ion signals would overlap with $C_{96}^{-\bullet}$ in the Kompact MALDI IV spectrum, it is not possible to determine whether or not the parent ion was present. The maximum intensity of the distribution of carbon clusters lies around $C_{108}^{-\bullet}$, with carbon clusters extending up to cluster sizes of $C_{214}^{-\bullet}$ (not shown) for example. The inset shows a spectrum obtained on the Reflex for comparison, and the results appear to verify those obtained on the Kompact MALDI IV, with the addition of the detection of

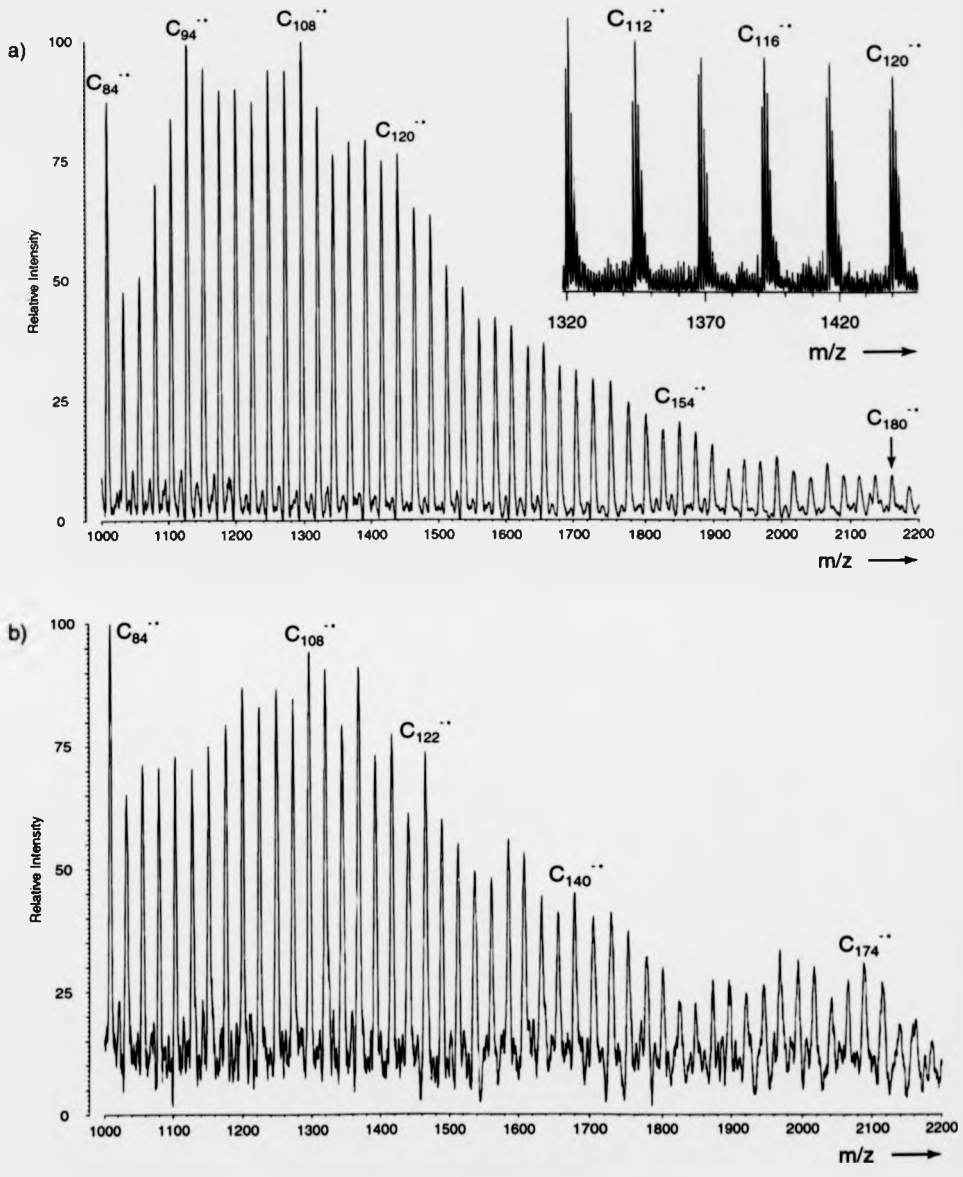

Figure 3: Negative-ion mass spectra acquired using the erbium-based compound. Spectrum a resulted from laser desorption/ionization on the Kratos Kompact MALDI IV; a mass spectrum of higher resolution is shown in the inset, acquired on the Bruker Reflex. Spectrum b was acquired on the Kratos Kompact MALDI IV following matrix-assisted laser desorption/ionization.

the parent ion signals. In contrast to the positive-ion spectra, the isotope patterns for the carbon clusters in negative-ion mode do correlate with the expected isotope pattern, and typically consist of six signals. This would suggest that the anionic species observed are pure carbon clusters. The negative-ion MALDI spectrum, shown in Figure 3b, displays a similar degree of clusterization, and the anions detected may also be assumed to be pure carbon clusters. No parent ion can be observed, possibly due to the instrumental limitations discussed earlier. The maximum of the distribution of higher fullerenes produced is located around $C_{108}^{-\bullet}$, and $C_{196}^{-\bullet}$ (not shown) is approximately the largest carbon cluster observed.

The results of the analysis of $Tb@C_{82}/Tb_2@C_{80}$ in the positive-ion mode are shown in Figure 4. For this particular sample and when using LDI conditions, shown in Figure 4a, clustering is first observable with a carbon cluster size of $C_{96}^{+\bullet}$, and the maximum of the distribution appears around $C_{128}^{+\bullet}$, and the largest carbon cluster generated was $C_{346}^{+\bullet}$ (not shown). The parent ion can be observed at m/z 1143 and can be confidently assigned as being $Tb@C_{82}^{+\bullet}$, as there is no overlap with other carbon clusters. A second distribution of signals can be observed, with the signals lying between those associated with the carbon clusters. Whereas the first distribution consists of pure carbon clusters, this second distribution consists of carbon clusters that retain the metal atom. It is not improbable that higher carbon clusters are formed which retain this metal atom, as, indeed, previous endohedral fullerene research has shown that fullerene fragments often retain the endohedral atom. In fact, this characteristic has been exploited when trying to determine whether an atom is endohedral or exohedral; collision induced dissociation (CID) of a suspected endohedral compound can be used to determine the position of the atom in question. If the atom is readily lost during CID experiments, it is likely that it is exohedral (bound externally to the carbon cage), but if the atom seems to be readily retained by the carbon cluster

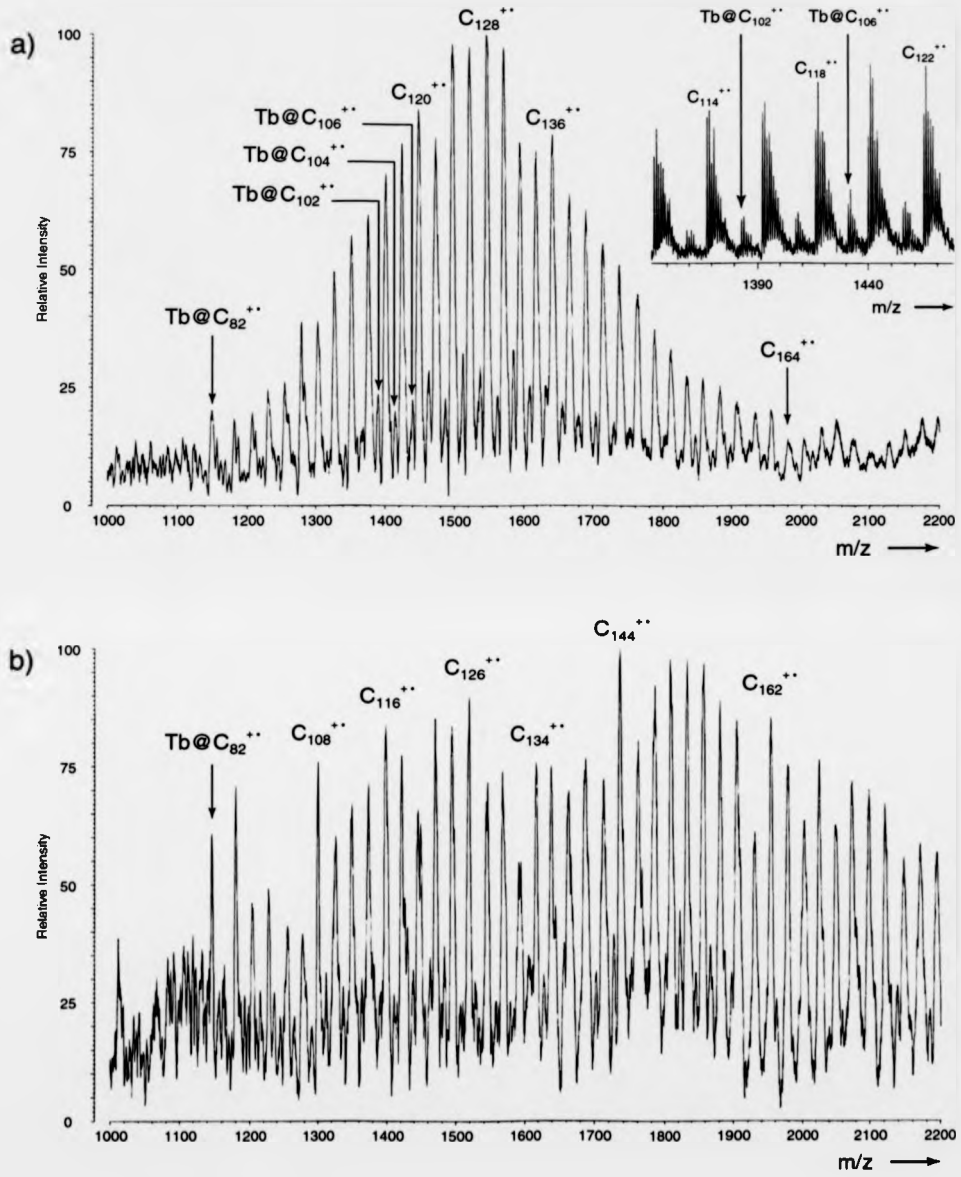

Figure 4: Positive-ion mass spectra acquired using the terbium-based compound. While spectrum a was obtained on the Kratos Kompact MALDI IV following laser desorption/ionization, the inset shows a mass spectrum produced under similar conditions on a Bruker Reflex in order to achieve a higher resolution. Spectrum b was produced following matrix-assisted laser desorption/ionization on the Kratos Kompact MALDI IV.

fragments, it is most likely that the atom is enclosed by the carbon cage. The mechanism for coalescence of fullerenes is most likely to involve fusion of one fullerene neutral and one fullerene ion[41] or, alternatively, the reaction of two excited neutrals in the gas-phase,[42] where cooling is effected by C_2 loss in either case. Therefore, as fragments provide the most abundant source of ions in this case, it follows that these fragments, which retain the endohedral metal atom, can be involved in coalescence with fullerene neutrals, leading to the formation of carbon clusters that contain Tb.

Due to the poor resolving power of the Kompact MALDI IV, further experiments were performed on a Bruker Reflex in order to provide verification. The inset in Figure 4a shows a partial mass spectrum obtained using the Reflex. The better resolution is immediately evident, with the ability to resolve unit masses, and these results do indeed provide further confirmation. The isotope pattern does not correlate with the predicted isotope pattern, and typically nine signals are present in each pattern. It can therefore be concluded that signals arising from two or more species overlap, resulting in the anomalous pattern observed. Due to the higher signal-to-noise ratio and the relatively more consistent isotope patterns that are observed, it is possible in the case of the $Tb@C_{82}/Tb_2@C_{80}$ sample to attempt to assign the structures of the overlapping species with more confidence. In each case, it appears as though at least three species are present in each isotopically resolved pattern. The three species that are almost certainly involved are a pure carbon cluster with an even number of carbon atoms ($C_{2n}^{+\bullet}$), a carbon cluster with an uneven carbon content and containing one terbium atom ($Tb@C_n^{+\bullet}$) (in contrast to the behavior of the erbium species), and a carbon cluster with an even number of carbon atoms and containing two terbium atoms ($Tb_2@C_{2n}^{+\bullet}$). It is also possible that other species contribute to the distribution observed. The existence of some of the species that have been proposed are less probable,

such as $C_{119}O^{+\bullet}$ when studying the distribution around m/z 1440, but the expected pattern for these species would be in excellent agreement with the pattern obtained experimentally. Unfortunately, it cannot be confidently determined whether these unusual species genuinely contribute to the signal intensities or whether experimental error is the reason for the discrepancy between predicted (when disregarding the less probable species) and experimental results. All of these species will be formed in the gas-phase, as stated previously. A reaction between two, metal containing carbon clusters, followed by fragmentation, could proceed by several different reaction pathways. One of these reactions could lead to the production of a carbon cluster that contains two metal atoms, where the other fragment is a pure carbon cluster, and another possible reaction pathway results in the formation of two carbon clusters, of different carbon contents, that each contain one metal atom.

The corresponding negative-ion MALDI spectrum is shown in Figure 4b. Again, it is possible to observe the parent ion at m/z 1143. Coalescence is again prominent, with the maximum of the distribution of carbon clusters being located around $C_{144}^{+\bullet}$ and the largest carbon cluster is approximately $C_{212}^{+\bullet}$ (not shown). Similarly to the analysis of the erbium based metallofullerene, the laser irradiance required for positive-ion MALDI analysis was slightly higher than for positive-ion LDI analysis. This difference in laser irradiance can account for some of the differences between Figure 4a and 4b. The distribution of carbon clusters is shifted to a slightly higher mass due to the fact that laser ablation is performed using a higher laser irradiance, but it can be noted that the largest carbon cluster formed following MALDI analysis is in fact smaller than following LDI analysis. This can be attributed to the lower density of sample material on the sample slide, due to the requirement for a high matrix to analyte ratio, so the sample material is

less dense on the sample slide when performing MALDI, compared to LDI. There have been many investigations into the mechanism of fullerene coalescence,[41-43] and the density of the plume of fullerene fragments following laser ablation is believed to play a crucial role in the rate of coalescence. Therefore, a higher laser irradiance is required to produce coalescence reactions, as MALDI is a comparatively soft ionization technique, but the lower density of fullerene neutrals and ions produced by ablation results in a much lower intensity of higher fullerenes; the lower probability of collision in the gas-phase, due to the lower density in the plume, also accounts for the fact that the higher fullerenes produced are of a lower mass that produced following LDI.

The negative-ion mode mass spectra are shown in Figure 5. The results in Figure 5b (MALDI) appear to indicate very strongly that the parent ion is $Tb@C_{82}^{-\bullet}$, as the signal due to this species is the sole metallofullerene species observed and the signal itself is intense. Should the sample indeed be pure as expected, it is possible to come to the conclusion from Figure 5b, Figure 4a, and Figure 4b that the sample is in fact $Tb_2@C_{80}$. The shape of the distribution of carbon clusters in Figure 5b is more pronounced than in the positive-ion mode, but the carbon cluster distribution is centered more around the lower mass region than in the positive-ion mode.

Figure 5a shows the LDI mass spectrum obtained in the negative-ion mode, and the signals due to carbon clusters are very intense, as were these signals in the positive-ion mode. Clustering again appears to begin with the formation of $C_{96}^{-\bullet}$, analogous with the positive-ion mode. The maximum of the distribution is around $C_{120}^{-\bullet}$, as opposed to $C_{128}^{-\bullet}$, but this difference can again be accounted for by a slight increase in the threshold laser irradiance required. The major difference between this spectrum and the one shown in

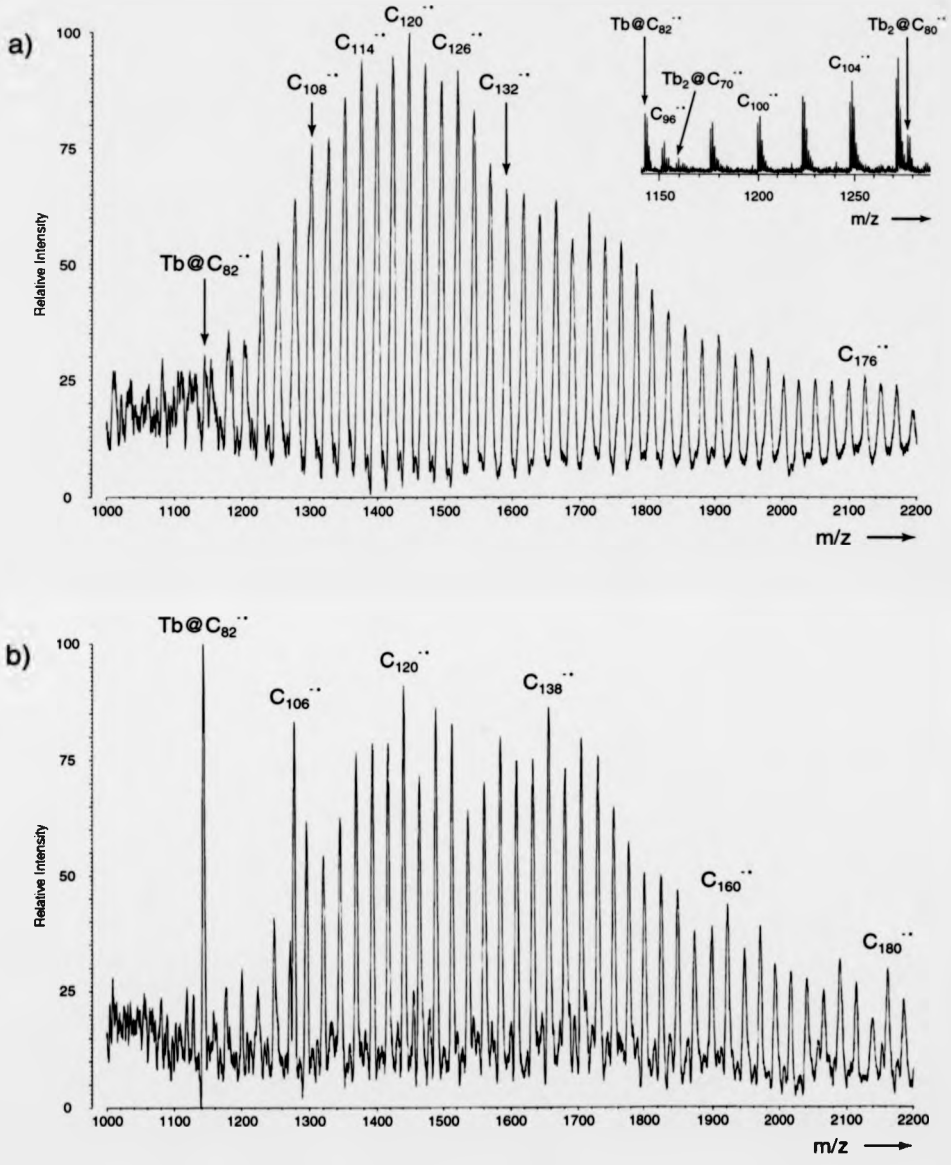

Figure 5: Negative-ion mass spectra acquired using the terbium-based compound. The Kratos Kompact MALDI IV was used to obtain spectrum a following laser desorption/ionization; the inset is a mass spectrum acquired under similar conditions on a Bruker Reflex, which operates at a higher resolving power. Spectrum b was produced on a Kratos Kompact MALDI IV following matrix-assisted laser desorption/ionization.

Figure 4a is the absence of metal-containing carbon clusters generated under laser ablation. The largest carbon cluster was possibly $C_{322}^{+\bullet}$ (not shown), as the carbon cluster signals begin to merge with the baseline of the spectrum. The inset in Figure 5a is a partial mass spectrum obtained on a Bruker Reflex, again to provide verification, and the results appear to be the same with only two exceptions; signals from two, metal-containing species; $Tb@C_{82}^{+\bullet}$ and $Tb_2@C_{80}^{+\bullet}$ are also present in the spectrum. These two species are believed to comprise the two components of the terbium based metallofullerene sample. The isotope patterns exhibited in the inset do correlate with the predicted isotope patterns and tend to consist of six signals, leading to the conclusion that the signals are due to pure carbon clusters observed which are free from interference from other species.

Analysis of the gadolinium compound was less successful than the analyses of the other two samples in the positive-ion mode. The resulting positive-ion LDI and MALDI spectra for $Gd@C_{82}$ revealed very little. Figure 6a shows the positive-ion LDI spectrum for this sample that was obtained using the Kratos Kompact MALDI IV, and no information can be reliably gathered from it. As a comparison, the inset shows the positive-ion LDI spectrum obtained on the Bruker Reflex at a later date, which is known to have a much higher sensitivity than the Kompact MALDI IV. The signal-to-noise ratio for this sample was lower when compared to the other two samples, but the signals were nevertheless stronger than those obtained on the Kompact MALDI IV. Coalescence can clearly be observed in the inset, where the resulting, coalesced species are indeed larger fullerenes. The isotope patterns exhibited by the carbon cluster signals, typically around nine signals, again do not fit with the predicted pattern. It is possible to propose that pure carbon clusters of even carbon content ($C_{2n}^{+\bullet}$) contribute to the pattern, but, in contrast to the other samples, it is unlikely that there is any contribution from carbon clusters of even carbon

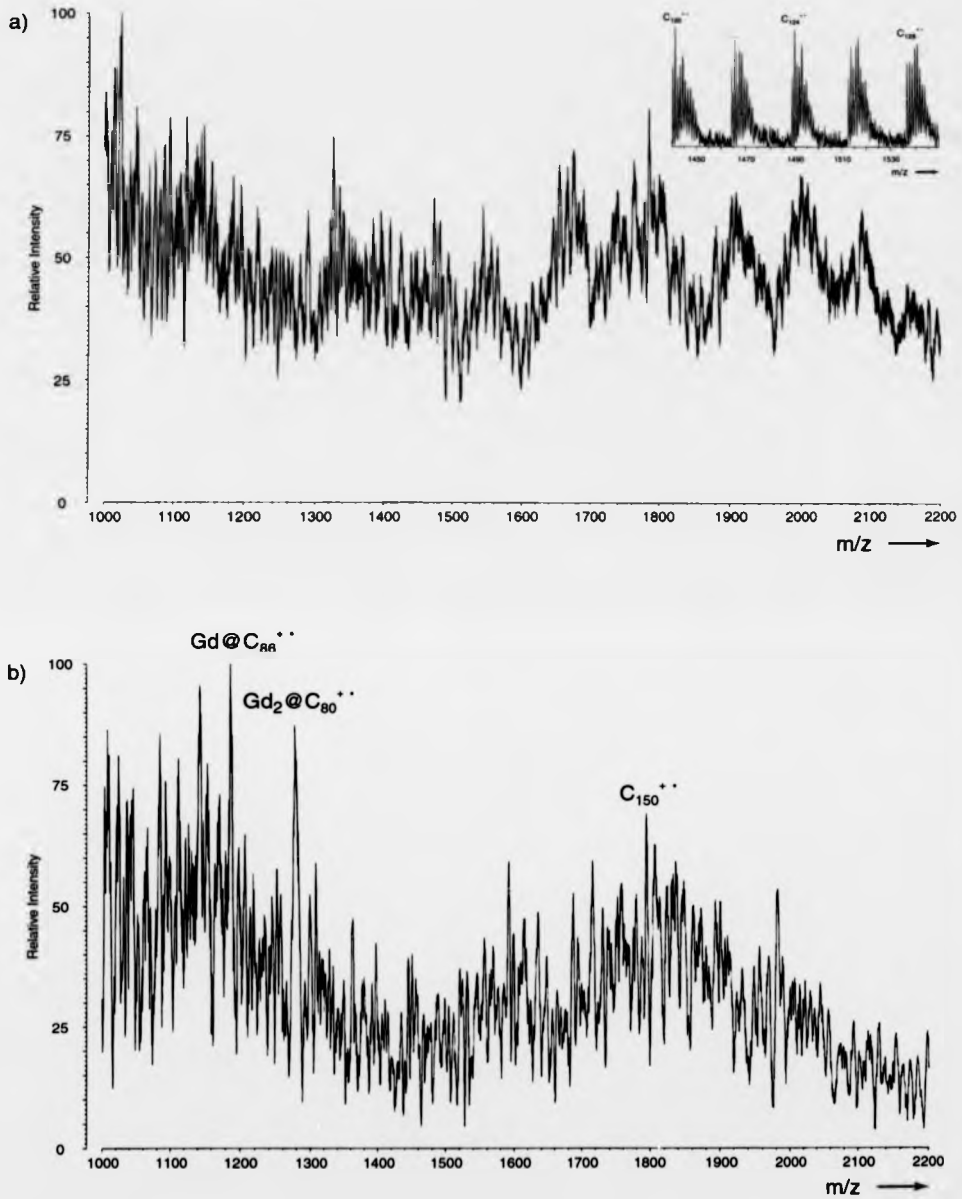

Figure 6: Positive-ion mass spectra acquired using the gadolinium-based compound. The Kratos Kompact MALDI IV was used to acquire spectrum a under laser desorption/ionization conditions, while the inset was obtained on a Bruker Reflex in order to produce a mass spectrum of higher resolution. Spectrum b resulted from the use matrix-assisted laser desorption/ionization conditions on the Kratos Kompact MALDI IV.

content which contain one gadolinium atom ($Gd@C_{2n}^{+\bullet}$) and also from carbon clusters of uneven carbon content with one gadolinium atom ($Gd@C_n^{+\bullet}$). The poor signal-to-noise ratio and the lack of consistency among the carbon cluster isotope patterns make it impossible to assign the structures of the species involved with confidence, and the patterns observed for this sample are the most inconsistent and difficult to assign of the three samples. Figure 6b shows the positive-ion MALDI spectrum obtained, and though it is better than the LDI spectrum, the signals are too weak to obtain much reliable information from them.

Analysis of the metallofullerene incorporating gadolinium in the negative-ion mode, especially under LDI conditions, was more successful. Figure 7 shows the negative-ion spectra, and Figure 7a shows the negative-ion LDI mass spectrum. An intense signal due to the detection of $Gd_2@C_{80}^{-\bullet}$ is immediately apparent, and a signal due to $Gd@C_{82}^{-\bullet}$ is also evident. The largest carbon cluster detected was $C_{202}^{-\bullet}$ (not shown) and the maximum of the pure carbon clusters is centered around $C_{116}^{-\bullet}$. The inset shows the spectrum obtained on the Bruker Reflex, which supports results obtained on the Kompact MALDI IV. The isotope patterns also correlate well with the expected isotope patterns, and consist of approximately six peaks, again leading to the conclusion that carbon cluster isotope patterns do not overlap with signals arising from other species in the negative-ion mode. This is in stark contrast to isotope patterns observed in positive-ion mode, throughout the investigation. Figure 7b shows the negative-ion MALDI spectrum. Coalescence can be observed, and the largest carbon cluster observed was $C_{166}^{-\bullet}$, which can be seen in the Figure, and the distribution of carbon clusters appears to be centered around $C_{110}^{-\bullet}$. It is clear that it is possible to observe higher fullerenes when using negative-ion LDI conditions during the investigation of the gadolinium based metallofullerene, but that positive-ion

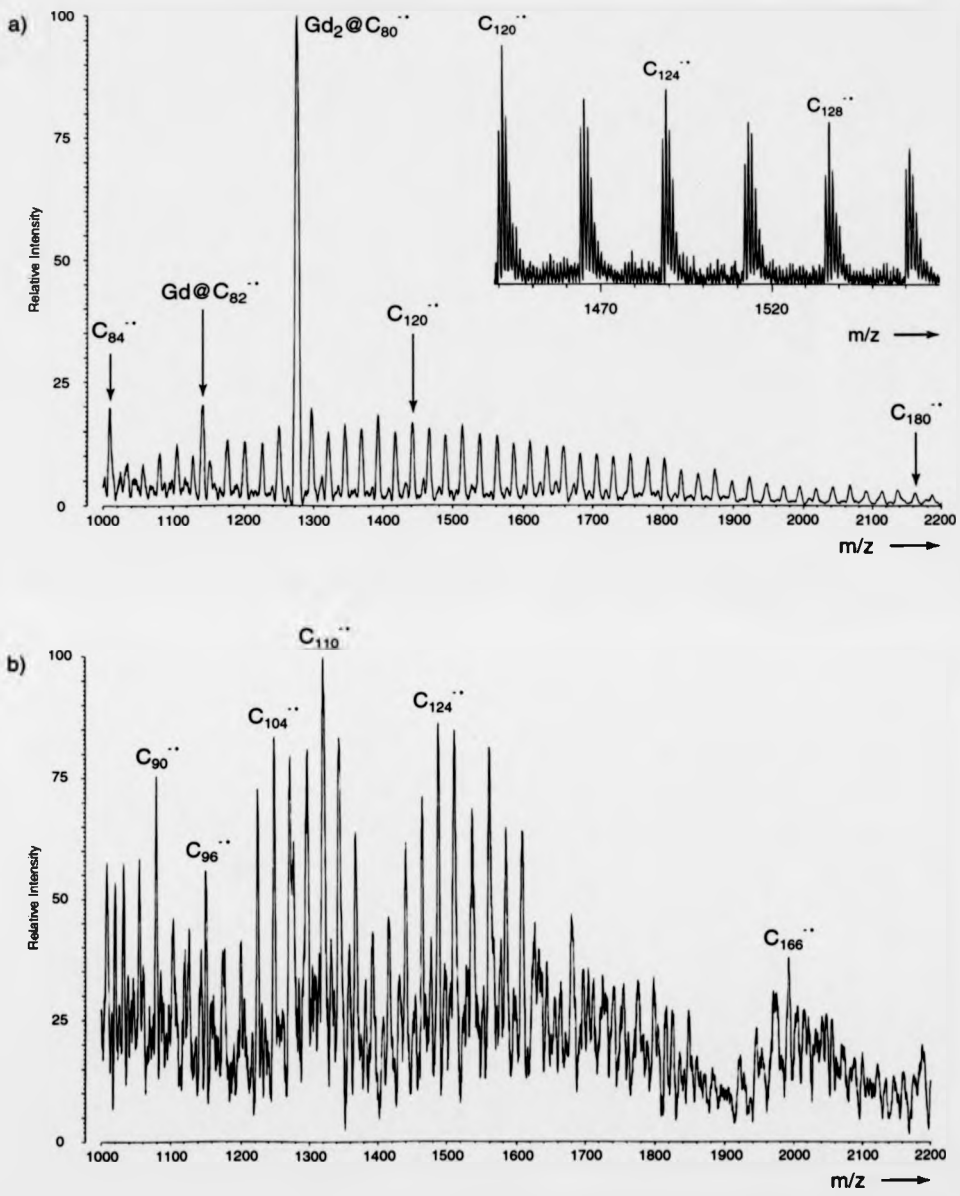

Figure 7: Negative-ion mass spectra acquired using the gadolinium-based compound. Spectrum a resulted from the use of laser desorption/ionization conditions on the Kratos Kompact MALDI IV and the inset shows a spectrum obtained under similar conditions on the Bruker Reflex in order to achieve a higher resolving power. Spectrum b was acquired using matrix-assisted laser desorption/ionization on the Kratos Kompact MALDI IV.

LDI and MALDI conditions are very inefficient on the Kompact MALDI IV. Negative-ion MALDI may be less efficient for the generation of higher fullerenes from the gadolinium based metallofullerene, compared to the other two samples, but it is indeed possible to perform such coalescence reactions.

It has become apparent that metallofullerenes undergo coalescence reactions to much greater extent than pure fullerenes. Even when using a threshold laser irradiance and when using MALDI, coalescence can be observed, despite such gentle conditions, which, by comparison, would only lead to molecular ions of $C_{60}^{+/-}$ with perhaps a small degree of fragmentation. It is even more difficult to coalesce larger fullerenes such as C_{70} and C_{84}. It is known that the metal atoms donate electron density to the fullerene cage and aid in stabilizing the fullerene structure.[26,31,35] By comparison with pure fullerenes, it is possible to conclude that the metal atoms must play a role in catalyzing the coalescence of metallofullerenes,[27] although the exact nature of this role has not been determined during these experiments. It can also be seen that the three metallofullerenes undergo coalesce with differing ease, and a trend begins to emerge. $Tb@C_{82}/Tb_2@C_{80}$ and the erbium based sample readily undergo aggregation, where $Tb@C_{82}/Tb_2@C_{80}$ displays the higher reactivity. The gadolinium based metallofullerene does coalesce, although it does so to a much lower extent than the other two samples. Almost exclusively pure carbon clusters are observed when using the negative-ion mode. Signals due to more than one species appear to overlap with the signals resulting from pure carbon clusters when using the positive-ion mode, leading to the conclusion that several different species may be generated during gas-phase reactions in the positive-ion mode.

9.4 Summary

Three metallofullerene samples were investigated, with the initial objective of establishing their composition and determining which ionization method is most suitable. It rapidly became apparent that these compounds readily undergo coalescence reactions, displaying an enhanced reactivity when compared to pure fullerenes. The three metallofullerene samples did not undergo such reactions with the same degree of reactivity. It appears that the erbium and terbium based metallofullerenes are more reactive than the gadolinium based metallofullerene sample; it is actually difficult to coalesce the gadolinium based compound while coalescence of the other two samples occurs even when only trying to establish the identity of the molecular ion. At first, it appeared that the coalesced species generated in the gas-phase were pure carbon clusters. Further research using an instrument with a higher resolution soon revealed that the patterns did not correlate with the expected isotope patterns of pure carbon clusters, and it is probable that at least three species are involved. It would be possible to establish the structures of the contributing species with certainty only after further investigation; even higher resolution and more accurate mass assignment is necessary to resolve the individual species that constitute the signals observed, and it is clear that use of a Fourier Transform Ion Cyclotron Resonance (FT-ICR) mass spectrometer with a laser desorption/ionization source is required.

The gas-phase reactivity of these compounds is surprising and may be attributed to the presence of the metal, which must play a role in the fusion reactions. However, despite the fact that threshold laser irradiances were selected and that MALDI was used, it is clear that the structures of the parent ions in each case cannot always be easily assigned. In order to attempt to overcome this difficulty, an ESI source was employed with success.

This follows on from previous work which has shown that fullerenes and fullerene derivatives may be analyzed in an unmodified form using ESI, contrary to the literature. The ability to use ESI in conjunction with such samples has obvious applications, as many fullerene derivatives may easily decompose following heating or fragment applying other ionization conditions. It is clear that in the case of the metallofullerene samples, LDI and MALDI were not suitable ionization techniques due to the reactivity of the samples in the gas-phase. ESI has shown itself to be applicable in this area and is the ionization method of choice. A comparison with EI shows that it is possible to obtain similar spectra but that it is much more difficult to do so, and so ESI remains the preferable technique.

9.5 References

1) Heath, J. R.; O'Brien, S. C.; Zhang, Q.; Liu, Y.; Curl, R. F.; Kroto, H. W.; Tittel, F. K.; Smalley, R. E. *J. Am. Shem. Soc.* **1985**, *107*, 7779-7780.

2) Ross, M. M.; Callahan, J. H. *J. Phys. Chem.* **1991**, *95*, 5720-5723.

3) Weiske, T.; Böhme, D. K.; Schwarz, H. *J. Phys. Chem.* **1991**, *95*, 8451-8452.

4) Caldwell, K. A.; Giblin, D. E.; Hsu, C. S.; Cox, D.; Gross, M. L. *J. Am. Chem. Soc.* **1991**, *113*, 8519-8521.

5) Weiske, T.; Böhme, D. K.; Hrusák, J.; Krätschmer, W.; Schwarz, H. *Angew. Chem. Int. Ed. Engl.* **1991**, *30*, 884-886.

6) Mowrey, R. C.; Ross, M. M.; Callahan, J. H. *J. Phys. Chem.* **1992**, *96*, 4755-4761.

7) Weiske, T.; Wong, T.; Krätschmer, W.; Terlouw, J. K.; Schwarz, H. *Angew. Chem. Int. Ed. Engl.* **1992**, *31*, 183-185.

8) Gillan, E. G.; Yeretzian, C.; Min, K. S.; Alvarez, M. M.; Whetten, R. L.; Kaner, R. B. *J. Phys. Chem.* **1992**, *96*, 6869-6871.

9) Caldwell, K. A.; Giblin, D. E.; Gross, M. L. *J. Am. Chem. Soc.* **1992**, *114*, 3743-3756.

10) Breton, J.; Gonzalezplatas, J.; Girardet, C. *J. Chem. Phys.* **1993**, *99*, 4036-4040.

11) Schwarz, H.; Weiske, T.; Böhme, D. K.; Hrusák, J. *Exo- and Endohedral Fullerene Complexes in the Gas Phase*; Billups, W. E. and Ciufolini, M. A., Ed.; VCH Publishers: New York, 1993, pp 257-283.

12) Ugarte, D. *Chem. Phys. Lett.* **1993**, *209*, 99-103.

13) Saunders, M.; Jiménez-Vázquez, H. A.; Cross, R. J.; Poreda, R. J. *Science* **1993**, *259*, 1428-1430.

14) Pederson, M. R.; Laouini, N. *Phys. Rev. B.* **1993**, *48*, 2733-2737.

15) Bethune, D. S.; Johnson, R. D.; Salem, J. R.; de Vries, M. S.; Yannoni, C. S. *Nature* **1993**, *366*, 123-128.

16) Holleman, I.; Boogaarts, M. G. H.; Meijer, G. **1994**, *113*, 543-546.

17) Tomanek, D.; Wang, Y.; Ruoff, R. S. *J. Phys. Chem. Solids* **1993**, *54*, 1679-1684.

18) Davey, S. N.; Leigh, D. A.; Moody, A. E.; Tetler, L. W. *J. Chem. Soc. Chem. Commun.* **1994**, 7-8.

19) Nemecek, S. *A Tight Fit*, 1995.

20) Dagani, R. *C&E News* **1995**, *73*, 9.

21) Callahan, J., H.; Ross, M. M.; Weiske, T.; Schwarz, H. *J. Phys. Chem.* **1993**, *97*, 20-22.

22) Weiske, T.; Schwarz, H.; Giblin, D. E.; Gross, M. L. *Chem. Phys. Lett.* **1994**, *227*, 87-90.

23) Saunders, M.; Jiménez-Vázquez, H. A.; Cross, R. J.; Mroczkowski, S.; Gross, M. L.; Giblin, D. E.; Poreda, R. J. *J. Am. Chem. Soc.* **1994**, *116*, 2193-2194.

24) Hopwood, F. G.; Fisher, K. J.; Greenhill, P.; Willett, G. D.; Zhang, R. *J. Phys. Chem. B.* **1997**, *101*, 10704-10708.

25) Stevenson, S.; Burbank, P.; Harich, K.; Sun, Z.; Dorn, H. C.; van Loosdrecht, P. H. M.; de Vries, M. S.; Salem, J. R.; Kiang, C.-H.; Johnson, R. D.; Bethune, D. S. *J. Phys. Chem. A* **1998**, *102*, 2833-2837.

26) Kuran, P.; Krause, M.; Bartl, A.; Dunsch, L. *Chem. Phys. Lett.* **1998**, *292*, 580-586.

27) Kimura, T.; Sugai, T.; Shinohara, H. *Int. J. Mass Spectrom.* **1999**, *188*, 225-232.

28) Rubin, Y.; Parker, T. C.; Khan, S. I.; Holliman, C. L.; McElvany, S. W. *J. Am. Chem. Soc.* **1996**, *118*, 5308-5309.

29) Callahan, J. H.; McElvany, S. W.; Ross, M. M. *Int. J. Mass Spectrom. Ion Processes* **1994**, *138*, 221-239.

30) Lorents, D. C.; Yu, D. H.; Brink, C.; Jensen, N.; Hvelplund, P. *Chem. Phys. Lett.* **1995**, *236*, 141-149.

31) Laskin, J.; Peres, T.; Khong, A.; Jiménez-Vázquez, H. A.; Cross, R. J.; Saunders, M.; Bethune, D. S.; de Vries, M. S.; Lifshitz, C. *Int. J. Mass Spectrom.* **1999**, *185/186/187*, 61-73.

32) Andreoni, W. *Annu. Rev. Phys. Chem.* **1998**, *49*, 405-439.

33) Kobayashi, K.; Nagase, S.; Akasaka, T. *Chem. Phys. Lett.* **1996**, *261*, 502-506.

34) Kobayashi, K.; Nagase, S.; Yoshida, M.; Osawa, E. *J. Am. Chem. Soc.* **1997**, *119*, 12693-12694.

35) Kobayashi, K.; Nagase, S. *Chem. Phys. Lett.* **1998**, *282*, 325-329.

36) Dresselhaus, M. S.; Dresselhaus, G.; Eklund, P. C. *J. Mater. Res.* **1993**, *8*, 2054-2097.

37) Aldersey-Williams, H. *The Most Beautiful Molecule: The Discovery of the Buckyball*; John Wiley and Sons, Inc.: New York, 1995.

38) Kwon, Y.-K.; Tománek, D.; Iijima, S. *Phys. Rev. Lett.* **1999**, *82*, 1470-1473.

39) Yeretzian, C.; Hansen, K.; Diederich, F.; Whetten, R. L. *Nature* **1992**, *359*, 44-47.

40) Yeretzian, C.; Hansen, K.; Diederich, F.; Whetten, R. L. *Supplement to Z. Phys. D.* **1993**, *26*, S 300-304.

41) Mitzner, R.; Winter, B.; Kusch, C.; Campbell, E. E. B.; Hertel, I. V. *Z. Phys. D* **1995**, *37*, 89-95.

42) Beck, R. D.; Weis, P.; Bräuchle, G.; Kappes, M. M. *J. Chem. Phys.* **1994**, *100*, 262-270.

43) Hansen, K.; Yeretzian, C.; Whetten, R. L. *Chem. Phys. Lett.* **1994**, *218*, 462-466.

Chapter Ten

Evaluation of Electrospray Ionization as an Analytical Tool for the Analysis of Fullerenes and Their Derivatives

10.1 Introduction

The suitability of different ionization techniques for different samples is always a concern for those conducting research using mass spectrometry. One of the most difficult tasks is to acquire molecular ion signals without inducing fragmentation. Techniques such as matrix-assisted laser desorption/ionization (MALDI) and field desorption (FD) have been developed as "soft" ionization methods, in order to minimize fragmentation. Another relatively recent soft ionization method is electrospray ionization (ESI);[1-8] though the origins of electrospray ionization are not new,[9] it is only within recent years that electrospray has evolved to become a common ionization method and has even become used in conjunction with time-of-flight instruments.[10,11] Normally, electrospray ionization enables the transfer of pre-formed ions from the solution-phase to the gas-phase. The formation of molecular ions is nearly universal and is thus rarely reported. Multiple protonation or deprotonation of large molecules is frequently observed, leading to the formation of ions which possess a high numbers of charges or quasi-molecular ions which have undergone a single protonation of deprotonation event. These quasi-molecular ions generated using ESI can frequently be formed without inducing fragmentation, and Van Berkel et al. were the first to observe radical cations using ESI.[12] Although fragmentation can be desirable in many instances to aid in structure elucidation or to induce side reactions in the gas-phase, it can be undesirable when the species under investigation is labile or prone to thermal decomposition.

Current fullerene research is increasingly concerned with the study of fullerene derivatives. Fullerene oxides and fluorinated fullerenes are two classes of fullerene derivative which attract particular interest, but the investigation of such compounds can

be difficult, owing to their lability. "Soft" ionization techniques alone have been required for the analysis of fullerene derivatives, including the use of MALDI to study hydrogenated fullerenes,[13] fluorinated fullerenes,[14] and fullerene oxides,[15-17] and the use of FD to study hydrogenated fullerenes.[18] Fragmentation is easily induced, and there is increasing need for a soft ionization technique that is suitable for the analysis of many fullerene derivatives. It can be assumed that ESI would represent the ionization method of choice, but there has been little evidence to advocate the theory that it is indeed a viable method for the study of fullerene derivatives. Initial investigations into the use of electrospray ionization for the analysis of fullerenes were not very promising,[19,20] yielding largely unsuccessful results. Furthermore, there has been an increasing belief that electrospray ionization of fullerenes is not experimentally possible, unless modification of the sample or the sample solution is carried out prior to analysis.

Publications which cite the use of electrospray ionization of fullerenes or their derivatives had, to an overwhelming extent, detailed the use of a VG/Fisons-manufactured ESI source,[21-29] although other manufacturers also produce ESI sources. It is conceivable that this leads to the belief that ESI of such compounds is dependent upon source design. Also, it is the case that almost every one of these publications also details modification of the sample or sample solution, whether it be via the addition of crown ethers for the formation of metal complexes,[30,31] redox reactions,[32] or other reactions to promote ion formation.[25-27,29] By this method, "ESI-inactive" compounds may be made "ESI-active" compounds, as compounds which undergo redox reactions in solution are the most suitable for electrospray ionization; fullerenes are non-polar and exist as neutrals in solution, and so fullerenes can be seen as being less suitable than other compounds for ESI. Recently, Khairallah et al. have formed cyano based adducts of higher fullerenes in the solution-phase

in order to make the analytes ESI-active, and indeed the samples were successfully observed using ESI.[25-27,29] However, in 1995 of Liu et al.,[22] of the National Taiwan University, made a discovery of great significance when they published a paper describing the successful application of this ionization method to the analysis of toluene solutions of fullerenes, but without the need for prior modification of the sample. For the first time, it seemed that ESI could be applied to the study of the labile fullerene derivatives that were increasingly being synthesized. In 1995, Deng et al., also of the National Taiwan University and using similar if not identical instrumentation, analyzed fullerene oxides using ESI[23] and in 1996 demonstrated that $C_{180}O_2$ could be analyzed using electrospray ionization.[24] During the same year, Hummelen et al. managed to produce a mass spectrum of the highly labile dimeric species $(C_{59}N)_2$ using electrospray ionization, but the ion source design was not detailed[33] Despite these facts, there has been little support since then for the use of electrospray as a method for the analysis of fullerene based materials, and the widespread belief that this ionization technique was not applicable to the study of fullerene derivatives remained.

Should it be established that ESI is a viable method for the ionization of fullerenes and their derivatives, it would enable more detailed investigation of derivatives to be performed. The current investigation describes the use of an ion source manufactured by Analytica of Branford, rather than VG/Fisons, for the study of a range of fullerene derivatives. The samples were also "sprayed" directly as toluene solutions. Successful utilization of a non-VG/Fisons ion source and use of non-modified sample solutions should demonstrate that electrospray ionization is indeed a viable ionization technique which may be applied to the investigation of fullerene derivatives. The investigation, furthermore, provides a first account of the use of nanospray[34] in conjunction with fullerenes and

demonstrates that protonation or deprotonation are not prerequisites for ionization, and therefore another ionization mechanism must occur. The establishment of molecular ions with the occurrence of little or no fragmentation is of great importance in the field of fullerene research, and is especially of significance when side reactions may take place in the gas-phase when using other ionization methods such as MALDI, where the matrix may react with the sample in an undesirable manner.

10.2 Experimental

All experiments were performed using a Bruker 9.4 Tesla BioAPEX II Fourier Transform Ion Cyclotron Resonance (FT-ICR) mass spectrometer, coupled with an Analytica of Branford electrospray ion source. Due to low sample quantities, the nanospray configuration of the electrospray ion source was used, as shown in Figure 1. The bis(ethoxycarbonyl)methylene adduct was supplied by H. Hungerbühler (Hahn-Meitner-Institut Berlin, Germany), the fluorinated fullerenes were provided courtesy of O. Boltalina (Moscow State University, Moscow, Russia), and the C_{70} oxide sample was obtained from R. Taylor (University of Sussex, Brighton, UK). Samples were prepared by dissolving the solid in toluene, where the concentration of the resulting solution was 10^{-3} M in each case and no cosolvents were used. Approximately 5 μL of the solution was then pipetted into a glass needle which had a metal-coated tip, where the metal coating plays a role in more precisely defining the field strength and is typically a coating consisting of gold and palladium. Carbon dioxide gas is used to force the solution to the end of the needle, and, coupled with the potential difference between the needle and the entrance to the instrument, results in the emergence of a spray from the needle tip. The potentials V_n and V_c, at each end of a capillary further inside the ion source, may be varied during

optimization. V_n was typically maintained in the range of 1000 - 1500 V, while V_c was kept at 100 V and V_{skim} was maintained at 2 - 4 V at all times. The difference between V_c and V_{skim} may be varied in order to induce capillary-skimmer collision-induced dissociation (CID) as required. The pressure in the region between the capillary and the skimmer was of the order of 10^{-2} Torr, while the hexapole ion trap region was kept at approximately 10^{-6} Torr. After passing through a hexapole ion guide, the ions may then pass into the FT-ICR cell for mass analysis. All spectra were recorded in the negative-ion mode due to instrumental problems at the time in the positive-ion mode, and also due to the fact that anions are the more abundant species formed when using the samples investigated.

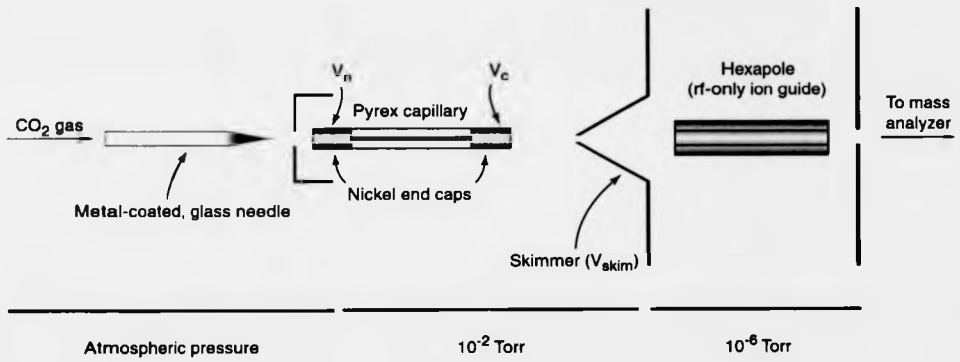

Figure 1: Schematic representation of the Analytica of Branford electrospray ionization (ESI) ion source.

10.3 Results and Discussion

Figure 2 shows the spectrum for C_{60} obtained in negative-ion mode. This result clearly shows that it is possible to use electrospray ionization for the analysis of pure fullerenes, despite little evidence for this in the literature. No cosolvents were used and no

sample modification was required in order to obtain the spectrum. Signals due to $C_{60}^{\bullet+}$ and its oxides are almost the only constituents of the spectrum. The inset shows an enlarged mass region which displays these signals. The high resolving power of the instrument is immediately evident. Oxidation of the sample upon standing is apparent, as signals due to $C_{60}O^{\bullet+}$, $C_{60}O_2^{\bullet+}$, and $C_{60}O_3^{\bullet+}$ are present. The intensity of these oxide signals is remarkable, as other soft ionization techniques such as matrix-assisted laser desorption/ionization usually results in much weaker oxide signals. This can be attributed to the fact that ESI is such a gentle ionization method, and molecular ions can be obtained without fragmentation, under the correct conditions. Indeed, no fragmentation of $C_{60}^{\bullet+}$ via C_2 loss was observed. It is possible that the oxides observed arise from fragmentation of higher oxides, however. The most important information that was obtained from this spectrum was that ESI is a viable technique for the analysis of fullerenes (despite not being a widely accepted idea), the signal-to-noise ratio was high and led to the recording of a spectrum at a high resolution, and that little fragmentation, if any, was observed. This makes ESI a potentially significant ionization method for the structure elucidation of fullerene derivatives, due to the fact that many fullerene derivatives are liable to thermal decomposition or are very labile under most ionization conditions.

Once it had been established that ESI is a viable technique for the analysis of pure fullerenes, the suitability of this ionization method for the analysis of fullerene derivatives was the next logical area of investigation. $C_{70}O$ was the next sample used, due to its similarity in structure to that of C_{60} and $C_{60}O_n$. As expected, a mass spectrum was successfully obtained, again with a high signal-to-noise ratio and a high resolving power. The mass spectrum of $C_{70}O$ is shown in Figure 3a. Again, no fragmentation occurs, due to the fact that the ionization process is so soft. The signals at slightly higher mass are

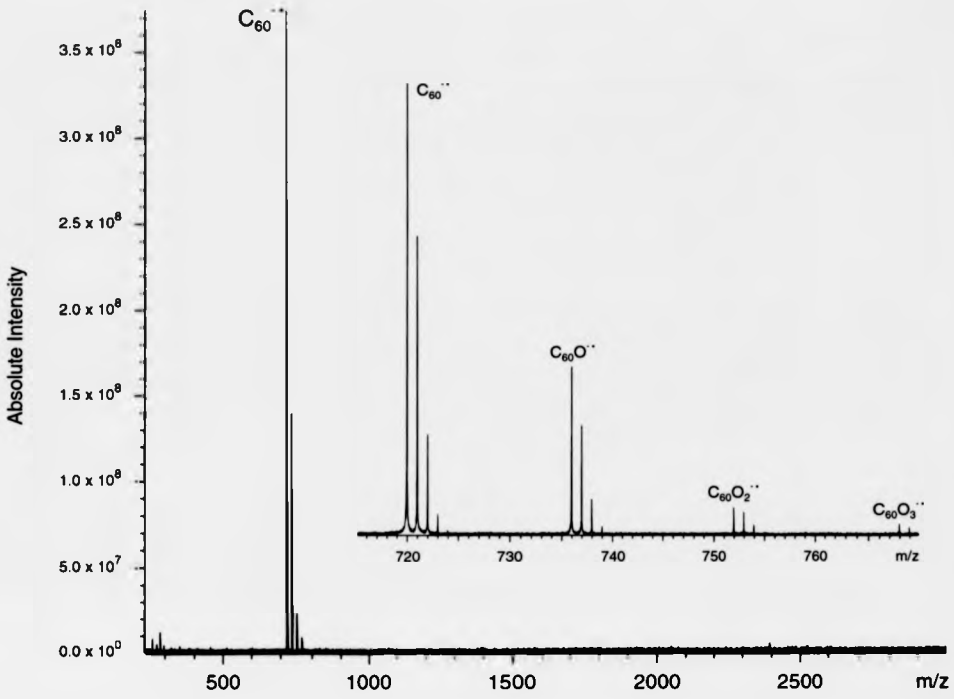

Figure 2: Negative-ion mass spectrum of C_{60} in toluene. C_{60} oxides are also present, resulting from oxidation of the C_{60} sample in the solid state when in the presence of air.

assigned as higher oxides of C_{70}. When using MALDI on other instruments, 9-nitroanthracene has been the matrix of choice for the study of fullerene oxides. The disadvantage of this matrix is that it can contribute towards further oxygen addition to the sample. Use of ESI does not oxidize the samples in this manner, and so is clearly a preferable ionization method. $C_{60}(C[CO2Et]_2)_2$ was the next sample chosen for analysis, as it possesses two ligands which are easily lost under many ionization conditions, including MALDI. The parent ion has never been observed using the Kratos Kompact MALDI IV, partly because of the ionization conditions and partly because of the low sensitivity of the instrument. The use of ESI on the BioAPEX II therefore represented an opportunity to

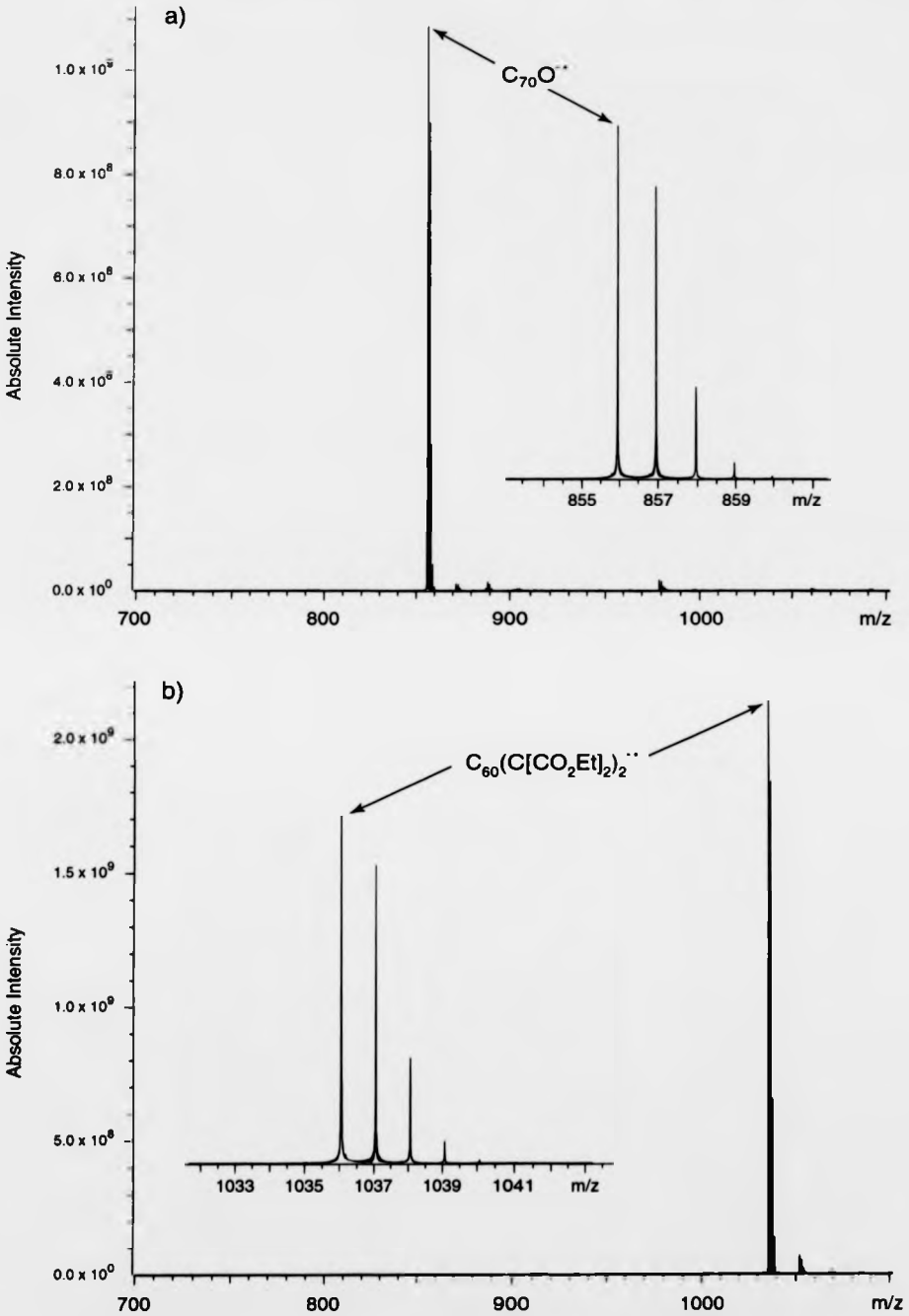

Figure 3: Mass spectrum a was acquired in the negative-ion mode using a sample of $C_{70}O$ dissolved in toluene. Mass spectrum b was obtained in the negative-ion mode, using a sample of $C_{60}[C(COOEt)_2]_2$ dissolved in toluene; the lack of deprotonation is particularly notable in this case.

observed the parent ion for the first time and to record a spectrum that is free from a high degree of fragmentation. Figure 3b shows the negative-ion mass spectrum for $C_{60}(C[CO_2Et]_2)_2$. No fragmentation is observed, and both a high signal-to-noise ratio and a high resolution are evident. Less intense signals appear at a higher mass than the parent ion, and these are assigned as the oxides of the sample, formed upon standing. In similarity with all other derivatives studied during the course of this investigation, the radical anions have been formed without the need for deprotonation, though deprotonation is indeed a possibility for this compound. This result leads to the conclusion that the ionization mechanism is similar for the different samples, regardless of whether or not hydrogen is present in the sample.

Another class of compounds that represents an analytical challenge is that of fluorinated fullerenes. Such compounds are extremely labile, and loss of fluorine radicals and C_nF_x units is difficult to avoid[35,36] when using techniques such as electron ionization (EI), chemical ionization (CI), matrix-assisted laser desorption ionization (MALDI), and laser desorption/ ionization (LDI). Fluorinated fullerenes are especially vulnerable to thermal decomposition, and ionization techniques such as CI and EI are therefore less suitable for the establishment of fluorinated fullerene parent ions. ESI again represents what may be the most suitable method for the analysis of such labile fullerene derivatives. Figure 4a and Figure 4b show the mass spectra obtained using $C_{60}F_{46}$[14,37-39] and $C_{60}F_{36}$,[32-41] respectively. Both spectra show a fluorine content higher than expected, but this will be due to a range of fluorinated products being formed during synthesis, and in each case, the signal arising from the expected product dominates the spectrum. It is reasonable to assume that ESI may be used during the course of analysis of a range of fluorinated fullerenes, and fragmentation has been minimized making the establishment of the parent ions in each

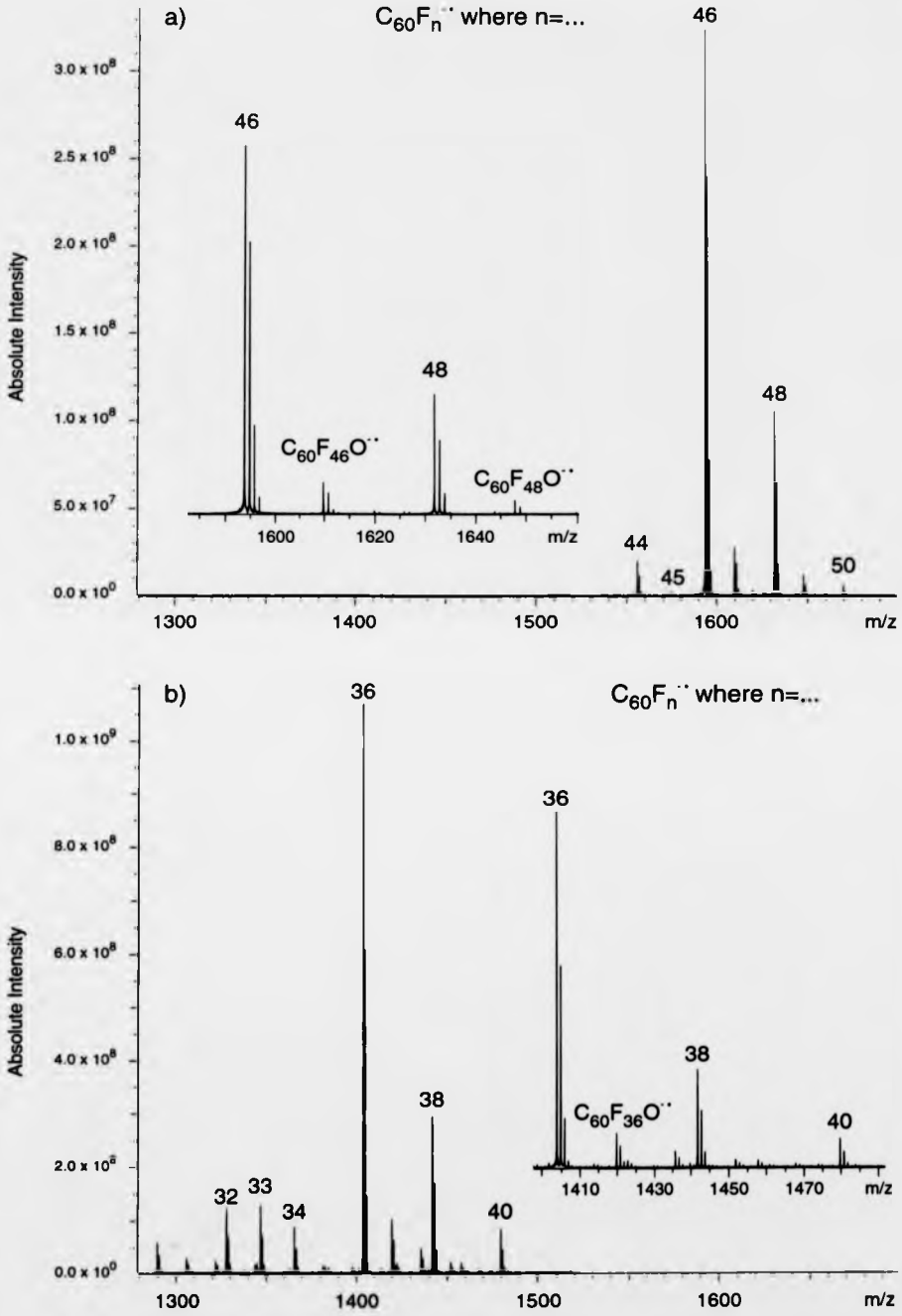

Figure 4: Negative-ion mass spectra of two fluorinated C_{60} samples, dissolved in toluene, are shown. The major reaction product present in the sample analyzed in mass spectrum a is demonstrated to be $C_{60}F_{46}$; the major reaction product present in the sample analyzed in mass spectrum b is shown to be $C_{60}F_{36}$.

case more reliable. Fullerenes containing an uneven fluorines content, such as $C_{60}F_{33}^{\bullet}$, may result from fragmentation processes, rather than being generated during synthesis. The high mass accuracy and high resolving power of the BioAPEX II proves to be extremely useful, and this is especially the case for these two spectra. From the expanded spectrum of Figure 4a, signals may be incorrectly assigned as being $C_{60}F_{47}^{\bullet}$ (m/z 1613) and $C_{60}F_{49}^{\bullet}$ (m/z 1651), but an enlarged spectrum shows that these signals in fact arise from $C_{60}F_{46}O^{\bullet}$ (m/z 1610) and $C_{60}F_{48}O^{\bullet}$ (m/z 1648) respectively. Similarly, in Figure 4b, the expanded mass spectrum may appear, at first glance, to also exhibit a signal correlating with $C_{60}F_{37}^{\bullet}$ (m/z 1423), but the enlarged spectrum shows that this signal can in fact be assigned as $C_{60}F_{36}O^{\bullet}$ (m/z 1420). The confidence with which these signals may be assigned is only made possible by the use of an instrument with a high resolving power and high mass accuracy; similar experiments using an instrument such as the Kompact MALDI IV, albeit with a different ion source, would not be possible.

It is notable in Figure 4a and 4b that molecular ions are again formed; it can be concluded that an ionization mechanism takes place which is different from the traditionally observed protonation/deprotonation mechanism. The mechanism of transfer of ions from the solution-phase to the gas-phase under electrospray conditions is a topic of great debate, with two competing theories. The model proposed by Iribarne and Thompson, entails the shrinkage of large droplets, which contain multiple ions, through evaporation of solvent molecules and the ejection of individual ions.[42,43] A second model was proposed by Dole et al., is based on the existence of droplets which contain a single ion, which is eventually ejected.[9] Along similar lines, Gomez and Tang have modeled the emission of small droplets from the solvent system under electrospray conditions,[44] and Fenn et al. have compared the proposed models which regard transfer of ions from the solution-phase to the

gas-phase.[3,34,45] These models solely concern the transfer of the ion to the gas-phase from the solution-phase, but do not address ion formation itself. Increasing support has been forthcoming for a model of the ionization mechanism where the electrospray ion source is treated analogously to an electrochemical cell,[21,46-53] leading to oxidation or reduction of the samples within the needle. Commenting on the observations of Liu et al.,[22] with regards to fullerene cation formation, Van Berkel proposed that the generation of C_{60} cations would most likely occur via the interaction of C_{60} with a corona discharge at the needle tip or through charge exchange between C_{60} and toluene.[48] His reluctance to accept that electrolytic ionization as the cause of cation formation for pure C_{60} was due in part to the fact that neat toluene, which is non-polar, was used as the solvent system and a very low cell current (the product of the rate of charged droplet formation and the number of charges per droplet) would occur. The possible mechanisms for ion formation proposed by Van Berkel would bypass the need for hydrogen transfer in solution and offer a possible account for the observations made thus far. However, the exact mechanism for ionization has not yet been established and is still under investigation.

10.4 Summary

Clearly, the coupling of ESI with an FT-ICR mass spectrometer represents a powerful tool for the structure elucidation of fullerenes and their derivatives, owing to the lack of fragmentation of even very labile structures, the high signal-to-noise ratio, the high resolution that may be obtained, the reliable mass accuracy, and the suitability for a range of compounds. Despite assumptions by many that ESI is not suitable for the direct "spraying" of fullerene related compounds, it has been shown that fullerene and fullerene derivatives may be sprayed as toluene solutions. No further modification of the sample or

of the solution is required in order to be able to acquire a strong enough signal intensity. It is also the case that only VG-manufactured electrospray ion sources are mentioned in publications where spray of fullerene samples has been successful. Though it has never been publicly stated, this has often led to the assumption by those involved in fullerene research that ion source design and sample modification are prerequisites for effective use of ESI in conjunction with fullerene samples. The experiments conducted have shown the first successful use of an electrospray ion source of different origin in conjunction with fullerene samples. The experiments also demonstrate the first use of nanospray as a viable technique for these samples, and again shows that such success is independent of the ion source manufacturer. Use of electrospray for the analysis of fullerenes and fullerene derivatives is likely to prove to be an invaluable tool for the structure elucidation of many, labile species. It is also clear that the evidence for the mechanism, by which ionization occurs in these experiments, is still pending. Further experiments are required in order to gain insight into the underlying principles of molecular ion formation under ESI conditions, in order to exploit the understanding for more efficient analyses in the future.

10.5 References

1) Yamashita, M.; Fenn, J. B. *J. Phys. Chem.* **1984**, *88*, 4671-4675.

2) Yamashita, M.; Fenn, J. B. *J. Phys. Chem.* **1984**, *88*, 4451-4459.

3) Fenn, J. B.; Mann, M.; Meng, C. K.; Wong, S. F.; Whitehouse, C. M. *Science* **1989**, *246*, 64-71.

4) Mann, M.; Meng, C. K.; Fenn, J. B. *Anal. Chem.* **1989**, *61*, 1702-1708.

5) Mann, M. *Electrospray Mass Spectrometry*; Gross, M. L., Ed.; Kluwer Academic Publishers: Netherlands, 1992; Vol. Chapter 8, pp 145-163.

6) Chapman, J. R. *Practical Organic Mass Spectrometry: A Guide for Chemical and Biochemical Analysis*; 2nd ed.; John Wiley and Sons Ltd.: Chichester, 1993.

7) de Hoffmann, E.; Charette, J.; Stroobant, V. *Mass Spectrometry: Principles and Applications*; John Wiley and Sons Ltd.: Chichester, 1996.

8) Gaskell, S. J. *J. Mass Spectrom.* **1997**, *32*, 677-688.

9) Dole, M.; Mack, L. L.; Hines, R. L.; Mobley, R. C.; Ferguson, L. D.; Alice, M. B. *J. Chem. Phys.* **1968**, *49*, 2240-2249.

10) Weickhardt, C.; Moritz, F.; Grotemeyer, J. *Mass Spectrom. Rev.* **1996**, *15*, 139-162.

11) Guilhaus, M.; Mlynski, V.; Selby, D. *Rapid Commun. Mass Spectrom.* **1997**, *11*, 951-962.

12) Van Berkel, G. J.; McLuckey, S. A.; Glish, G. L. *Anal. Chem.* **1991**, *63*, 1098-1109.

13) Rogner, I.; Birkett, P.; Campbell, E. E. B. *Int. J. Mass Spectrom.* **1996**, *156*, 103-108.

14) Cozzolino, R.; Belgachem, O.; Drewello, T.; Käseberg, L.; Herzschuh, R.; Suslov, S.; Boltalina, O. *Eur. Mass Spectrom.* **1997**, *3*, 407-414.

15) Lebedkin, S.; Ballenweg, S.; Gross, J.; Taylor, R.; Krätschmer, W. *Tetrahedron Lett.* **1995**, *36*, 4971-4974.

16) Penn, S. G.; Costa, D. A.; Balch, A. L.; Lebrilla, C. B. *Int. J. Mass Spectrom. Ion Processes* **1997**, *169/170*, 371-386.

17) Gromov, A.; Lebedkin, S.; Ballenweg, S.; Avent, A. G.; Taylor, R.; Krätschmer, W. *J. Chem. Soc. Chem. Commun.* **1997**, 209-210.

18) Rüchardt, C.; Gest, M.; Ebenhoch, J.; Beckhaus, H.-D.; Campbell, E. E. B.; Tellgmann, R.; Schwarz, H.; Weiske, T.; Pitter, S. *Angew. Chem. Int. Ed. Engl.* **1993**, *32*, 584-586.

19) Hiraoka, K.; Kudaka, I.; Fujimaki, S.; Shinohara, H. *Rapid Commun. Mass Spectrom.* **1992**, *6*, 254-256.

20) Fujimaki, S.; Kudaka, I.; Sato, T.; Hiraoka, K.; Shinohara, H.; Saito, Y.; Nojima, K. *Rapid Commun. Mass Spectrom.* **1993**, *7*, 1077-1081.

21) Dupont, A.; Gisselbrecht, J.-P.; Leize, E.; Wagner, L.; Van Dorselaer, A. *Tetrahedron Lett.* **1994**, *35*, 6083-6086.

22) Liu, T.-Y.; Shiu, L.-L.; Luh, T.-Y.; Her, G.-R. *Rapid Commun. Mass Spectrom.* **1995**, *9*, 93-96.

23) Deng, J. P.; Mou, C. Y.; Han, C. C. *J. Phys. Chem.* **1995**, *99*, 14907-14910.

24) Deng, J.-P.; Mou, C.-Y.; Han, C.-C. *Chem. Phys. Lett.* **1996**, *256*, 96-100.

25) Khairallah, G.; Peel, J. B. *J. Phys. Chem. A* **1997**, *101*, 6770-6774.

26) Khairallah, G.; Peel, J. B. *J. Chem. Soc. Chem. Commun.* **1997**, 253-254.

27) Khairallah, G.; Peel, J. B. *Chem. Phys. Lett.* **1997**, *268*, 218-222.

28) Khairallah, G.; Peel, J. B. *Chem. Phys. Lett.* **1998**, *296*, 545-548.

29) Khairallah, G.; Peel, J. B. *Int. J. Mass Spectrom.* **2000**, *194*, 115-120.

30) Wilson, S. R.; Wu, Y. *J. Am. Chem. Soc.* **1993**, *115*, 10334-10337.

31) Wilson, S. R.; Wu, Y. *J. Chem. Soc. Chem. Commun.* **1993**, 784-786.

32) Zhou, F.; Van Berkel, G. J.; Donovan, B. T. *J. Am. Chem. Soc.* **1994**, *116*, 5485-5486.

33) Hummelen, J. C.; Knight, B.; Pavlovich, J.; González, R.; Wudl, F. *Science* **1995**, *269*, 1554-1556.

34) Wilm, M.; Mann, M. *Anal. Chem.* **1996**, *68*, 1-8.

35) Selig, H.; Lifshitz, C.; Peres, T.; Fischer, J. E.; McGhie, A. R.; Romanow, W. J.; McCauley Jr., J. P.; Smith III, A. B. *J. Am. Chem. Soc.* **1991**, *113*, 5475-5476.

36) Tuinman, A. A.; Mukherjee, P.; Adcock, J. L.; Hettich, R. L.; Compton, R. N. *J. Phys. Chem.* **1992**, *96*, 7584-7589.

37) Boltalina, O. V.; Sidorov, L. N.; Bagryantsev, V. F.; Seredenko, V. A.; Zapol'skii, A. S.; Street, J. M.; Taylor, R. *J. Chem. Soc. Perkin Trans. 2* **1996**, 2275-2278.

38) Steger, H.; Mische, U.; Kamke, W.; Ding, A.; Fieber-Erdmann, M.; Drewello, T. *Chem. Phys. Lett.* **1997**, *276*, 39-46.

39) Boltalina, O. V. *J. Fluorine Chem.* **2000**, *101*, 273-278.

40) Boltalina, O. V.; Borschevskii, A. Y.; Sidorov, L. N.; Street, J. M.; Taylor, R. *J. Chem. Soc. Chem. Commun.* **1996**, 529-530.

41) Boltalina, O. V.; Bühl, M.; Khong, A.; Saunders, M.; Street, J. M.; Taylor, R. *J. Chem. Soc. Perkin Trans. 2* **1999**, 1475-1479.

42) Iribarne, J. V.; Thompson, B. A. *J. Chem. Phys.* **1976**, *64*, 2287-2294.

43) Thompson, B. A.; Iribarne, J. V. *J. Chem. Phys.* **1979**, *71*, 4451-4463.

44) Gomez, A.; Tang, K. Q. *Phys. Fluids* **1994**, *6*, 404-414.

45) Fenn, J. B.; Rosell, J.; Meng, C. K. *J. Am. Mass Spectrom.* **1997**, *8*, 1147-1157.

46) Blades, A. T.; Ikonomou, M. G.; Kebarle, P. *Anal. Chem.* **1991**, *63*, 2109-2114.

47) Kebarle, P.; Tang, L. *Anal. Chem.* **1993**, *65*, 972 A-985 A.

48) Van Berkel, G. J. *The Electrolytic Nature of Electrospray*; Cole, R. B., Ed.; John Wiley: New York, 1997; Vol. Chapter 2, pp 65-105.

49) Enke, C. G. *Anal. Chem.* **1997**, *69*, 4885-4893.

50) McCarley, T. D.; Lufaso, M. W., .; Curtin, L. S.; McCarley, R. L. *J. Phys. Chem. B* **1998**, *102*, 10078-10086.

51) Charbonnier, F.; Nicolas, J.-P.; Berthelot, L.; Hapiot, P.; Pinson, J.; Rolando, C. *Red-Ox Chemistry in the Electrospray Mist*: Orlando, Florida, 1998, pp 426.

52) Charbonnier, F.; Berthelot, L.; Rolando, C. *Anal. Chem.* **1999**, *71*, 1585-1591.

53) Jackson, G. S.; Enke, C. G. *Anal. Chem.* **1999**, *71*, 3777-3784.

Chapter Eleven

Conclusion

11.1 Overview

Throughout the course of these investigations, mass spectrometry has been successfully employed to gain further insight into the structure and gas phase behavior of pure fullerenes and fullerene derivatives. In particular, the coalescence reactivity of pure fullerenes, $C_{60}H_{36}$, oxides of C_{60} and C_{70}, metallofullerenes, fluorinated fullerenes, and three species based upon the formula $C_{60}[C(COOEt)_2]_n$ (where n = 1, 2, and 3) has been studied. The formation of pure fullerenes from an organometallic precursor may be considered to be an analogous concept, involving a non-fullerene precursor. The generation of dimeric species under ambient conditions, resulting from C_{60} samples which had degraded, can similarly be regarded as a class of coalescence reaction. The unimolecular dissociation of $C_{60}H_{36}$ was examined in order to gain insight into the gas phase behavior of the species, thus providing further information about the coalescence reactivity. The observation that many fullerene derivatives undergo extensive fragmentation or coalescence reactions under standard laser desorption/ionization (LDI) conditions provided impetus for the search for an ionization method which is suitable for the structure elucidation alone of such samples. This led to an investigation into the viability of electrospray ionization (ESI) for fullerene and fullerene derivatives analysis Although fullerenes are widely considered to be "ESI inactive," it is possible to obtain spectra which display molecular ion signals which are almost free of fragmentation. Finally, the careful analysis of post source decay spectra of fullerene ions that delayed ionization can interfere with the structure elucidation of higher fullerene species when using time-of-flight (ToF) instruments. Such an observation is of significance for much of fullerene research and the investigation led to novel methods of monitoring the delayed ionization of fullerenes on a time-of-flight instrument which employs a time-based method of mass selection of ions.

11.1A Chapter Two: "Laser-Induced Fullerene Production Using the Organometallic Precursor Penta(cyclopentadienyl)-η^5-cyclopentadienyl manganesetricarbonyl"

An organometallic compound of the structure [$Cp_5CpMn(CO)_3$] was synthesized by Prof. Vollhardt's group at the University of California at Berkeley and was analyzed using laser desorption/ionization mass spectrometry. The compound was considered to be a possible precursor for fullerene formation in the gas phase, as the Cp_5Cp ligand was seen to bear a resemblance to semibuckminsterfullerenes. In a collaborative effort, the structure of the organometallic compound, known as penta(cyclopentadienyl)-η^5-cyclopentadienylmanganesetricarbonyl, was analyzed using X-Ray crystallography and mass spectrometry. Utilizing laser desorption/ionization mass spectrometry, it was possible to fuse the ligands to form fullerenes. The products of fusion were known to be fullerenes due to the characteristic fragmentation pattern, involving the loss of C_2 units. $C_{50}^{+\bullet}$, $C_{60}^{+\bullet}$, and $C_{70}^{+\bullet}$ were observed to be amongst the most abundant products, though the yield was not high enough for this method to represent an efficient synthetic process for fullerene production. The reason for the low yields has been attributed to the large number of σ bonded hydrogen atoms, mirroring the reduced tendency for $C_{60}H_{36}$ to undergo coalescence to form higher fullerenes. Dissociation of the ligand bearing favorable structural features for the generation of fullerenes might also be of relevance to the low net yield of fullerenes. Further collaborative efforts involving the use of other polyaromatic hydrocarbons which bear a close resemblance to Vollhardt's compound revealed that it is not only the carbon content of the compound which is important, but also its structure. Greatly increased yields of fullerenes have been obtained using polyaromatic hydrocarbons in follow up investigations, and the original investigation, though shown not to be an efficient method

for fullerene synthesis, has led to new avenues of research with regards to synthetic methods for fullerene production.

11.1B Chapter Three: "Delayed Ionization as the Cause of Interference Signals Observed in the Post Source Decay Spectra of Coalesced Carbon Clusters"

Research into the structure of species formed through the coalescence of pure fullerenes in the gas phase led to an important discovery. The use of post source decay (PSD) as an analytical method, when utilizing a reflectron-ToF mass spectrometer equipped with a time-based "ion gate" and a continuous accelerating potential, soon led to the observation of artifact signals which could not be easily assigned. Though at first considered to be fragment ion signals, which would be in contradiction of evidence in the literature, it became apparent that these signals were associated with a known phenomenon which is almost unique to fullerenes, with the exception of metal clusters. "Delayed ionization" is a well documented occurrence where fullerenes may accommodate large amounts of internal energy, existing in excited states for long periods of time. Ions which resulted from delayed ionization drift through the ion source as neutrals initially, ionize at a lower potential within the source, and therefore leave with a lower kinetic energy than the corresponding prompt ions. As a result, delayed ions leave the source μs later and with a lower kinetic energy; the delay time itself constitutes the greatest component in the overall difference in flight time. A time-based pair of deflecting electrodes, known as the "ion gate," is frequently used for the selection of ions of interest and it is use of this instrumental feature which can lead to potential confusion. When the ion gate is employed to select ions of greater mass than the fullerenes present, there is the chance that delayed fullerene ions will traverse the

ion gate at the same time as the selected ions. The fullerene ion will possess a higher velocity than the selected ion (of higher mass), and therefore the delayed ion will arrive at the detector before the selected ion, thus initially appearing to be a fragment ion. The conclusions drawn have been supported by the facts that the artifact signals have not been observed when using the negative-ion mode, nor have they been obtained for intact, fullerene derivatives. This is a potentially misleading phenomenon which could have serious consequences for a wide range of instruments when investigating fullerene samples. The use of alternative instrument designs, such as the employment of an electrostatic sector to effectively act as a kinetic energy "filter," may minimize the presence of such artifacts. Alternatively, ToF instruments with a time-based method for ion selection, and in particular those instruments with delayed extraction ion sources which may be controlled by the user, represent an ideal experimental apparatus for studying delayed ionization of fullerenes.

11.1C Chapter Four: "Unimolecular Dissociation and Gas-Phase Coalescence of Hydrogenated Fullerenes"

The fragmentation dynamics of hydrogenated fullerenes were investigated applying electron ionization (EI), liquid secondary ion mass spectrometry (LSIMS), and laser desorption/ionization (LDI). Mass-analyzed ion kinetic energy (MIKE) and collision-induced dissociation (CID) spectra revealed that the hydrogenated fullerenes fragment in a similar manner regardless of hydrogen content; $C_{60}H_{18}$ and $C_{60}H_{36}$ both fragment via the loss of C_mH_n neutrals, resulting in the loss of both carbon and hydrogen from the parent ion. Using LDI, many hydrogen atoms remain attached to the carbon core, unlike fluorinated fullerenes under similar conditions. Pure fullerene fragments are produced as well as fragments which still possess hydrogen. Attempts to coalesce the hydrogenated fullerenes

revealed the decreased tendency to undergo such reactions. This is attributed to the fact that hydrogenated fullerenes have lower ionization potentials than pure fullerenes, which in turn have lower ionization potentials than fluorinated fullerenes. Therefore, hydrogenated fullerenes undergo ionization, in preference to dissociation, as the main channel for cooling the species. The resulting precursor for coalescence, with a significant number of hydrogen atoms still bound to the carbon core, therefore lacks a large number of π bonds which in turn assist coalescence reactions by providing suitable means for σ C-C bond formation during fusion. This can only serve to hinder the efficiency of coalescence reactions, making hydrogenated fullerenes a less viable precursor for such processes.

11.1D Chapter Five: "Coalescence of Fluorinated Fullerenes Using Laser Desorption/Ionization"

Fluorinated fullerenes were investigated using LDI ToF mass spectrometry during collaborative efforts with Dr. Boltalina of Moscow State University. The coalescence behavior of four fluorinated fullerene samples, $C_{60}F_{18}$, $C_{60}F_{36}$, $C_{60}F_{48}$, and $C_{70}F_{52,56}$, was studied and was determined to be unlike pure fullerenes and most fullerene derivatives investigated so far. Instead of the preferential formation of clusters which consisted of approximate multiples of the precursor carbon content, a large variety of carbon clusters of similar abundance was observed over a wide mass range. The carbon clusters formed were similar in distribution to those obtained following the laser ablation of a graphite surface. The laser fluence required for coalescence was also noted to linearly increase with fluorine content. Therefore, it was proposed that the difference in the coalescence products observed results from the increased energetic demands for the fusion of fluorinated fullerenes and that fluorine loss is the first step prior to coalescence. The possible formation

of highly energized fullerene cages and fullerene fragments, due to the high internal energy of the fluorinated fullerene neutral, paves the way for the formation of a wide variety of higher carbon clusters rather than the selective formation of particular coalescence products. The coalescence behavior of fluorinated fullerenes has thus far not been documented and this investigation therefore represents an unprecedented discovery which is of significance for the field of fullerene research.

11.1E Chapter Six: "Gas-Phase Aggregation of C_{60} Oxides and C_{70} Oxides under Matrix-Assisted Laser Desorption/Ionization Conditions"

Oxides of C_{60} and C_{70} were studied using laser desorption/ionization (LDI) and matrix-assisted laser desorption/ionization (MALDI) and it was shown that two distinct coalescence pathways exist. Use of LDI results in the expected production of pure carbon clusters, in line with the now well documented coalescence reactions. No oxygen is observed in these higher clusters, and the clusters fragment via the loss of C_2, indicating that they are indeed pure fullerenes and not bridged species. However, under MALDI conditions, which are known to be much milder, the fullerene oxides fused to form clusters which still possess oxygen and two initial fullerene moieties. The clusters do not fragment further than $C_{120}O^{+\bullet}$ when using C_{60} oxides and the lack of a $C_{120}^{+\bullet}$ signal was seen as additional evidence that the coalesced species were different from those generated under LDI conditions. Equally, $C_{140}^{+\bullet}$ is not observed when using C_{70} oxides and it is believed that the structure of $C_{140}O^{+\bullet}$ is analogous to $C_{120}O^{+\bullet}$. It was hypothesized that "dumb-bell like" species are formed when using MALDI, where two distinct, C_{60} or C_{70} moieties are effectively bridged by an epoxide group, involving C-O-C bonds and one σ C-C bond. Oxygen loss from the exterior of the coalesced species could occur but loss of the epoxide group between the fullerene

moieties would result in the cleavage of the bridge connecting them. This difference in coalescence behavior had been undocumented so far, and the fusion of C_{70} oxides represented the first time this had been achieved, though others had attempted to perform such a synthesis in the solution phase and had thus far failed.

11.1F Chapter Seven: "Degradation of C_{60} to $C_{120}O$ in the Solid State Under Ambient Conditions"

In a collaboration with Dr. Taylor from the University of Sussex, a study of the stability of pure C_{60} under ambient conditions led to a surprising discovery. While the degradation of pure C_{60} under ambient conditions to form C_{60} epoxides is known, it was unexpected that these epoxides would undergo further reaction in the solid state to form dimeric species. $C_{120}O$ was the resulting species generated as a consequence of the reaction between $C_{60}O$ and C_{60}, and it was shown that the most likely structure would be "dumb-bell like," with two C_{60} moieties bridged by an epoxide group through C-O-C bonds and one σ C-C bond. Mass spectrometry and infrared spectroscopy were used for the analysis of the product of degradation, once it had been purified using high performance liquid chromatography (HPLC), and the results of the analyses all supported the same conclusions. This finding has significant consequences for possible future applications of fullerene research, such as in the field of nanotechnology, as oxidation of fullerenes even under mild conditions must now be taken into consideration. Furthermore, it can be expected that the $C_{120}O$ "impurity" which is an intrinsic feature of aging C_{60} samples might be the cause of characteristics originally attributed to C_{60}. The illustrative example is the famous spike in the electron paragmagnetic resonance (EPR) spectrum of $C_{60}^{\bullet-}$, which has recently been shown to be caused by the presence of the $C_{120}O$ impurity.

11.1G Chapter Eight: "Coalescence and Collision-Induced Dissociation of Three Bis(ethoxycarbonyl)methylene C_{60} Derivatives"

One investigation involved the study of three fullerene derivatives of the formula $C_{60}[C(COOEt)_2]_n$ where n = 1, 2, and 3. The derivatives' coalescence behavior was of prime interest, and in particular whether or not hydrogen was present in the coalesced species. It was determined that hydrogen was indeed present in the higher carbon clusters, though previous publications in the literature had made the assumption that it was not. Studying the three compounds, it was found that moving to derivatives with a higher number of ligands attached led to the production of coalesced carbon clusters of greater size, the amount of hydrogen present in the clusters increased, and the probability of observing clusters with an uneven number of carbon atoms also increased. Collision-induced dissociation experiments also revealed that the coalesced species dissociated to form fragments which were not of equal size and that C_{60} was preferentially lost as a neutral in each case. This appears to indicate that the coalescence products consist of bridged species rather than single, closed cage entities and further corroborates the theory that fragmentation of the $C_{60}[C(COOEt)_2]_n$ compounds leads to the production of suitable precursors for coalescence. While the daughter ions generated following CID do not match the expected precursors formed in the gas phase, it is believed that the "dangling," exohedral carbon atoms of these precursors are crucial to the coalescence mechanism and that rearrangement of the bonding within the system leads to the dissociation of C_x^+ via the preferential dissociation into $C_{x-60}^{+\bullet}$ and a C_{60} neutral. The coalescence of these derivatives is still under investigation and is of importance due to the fact that a more comprehensive understanding of the structures of the coalescence products will provide insight into the reaction mechanism involved.

11.1H Chapter Nine: "Metal-Catalyzed Coalescence Reactions of Metallofullerenes"

Three endohedral metallofullerene species were studied originally for the purpose of structure elucidation and it immediately became apparent that all three underwent enhanced coalescence reactions. Indeed, coalescence occurred at much lower laser powers than would be required for pure fullerenes. In fact, the ease by which coalescence occurred prevented any structural assignment, so that other ionization methods had to be applied. Electron ionization and electrospray ionization were both used for the purposes of characterizing the precursor material and indicated that it was likely the three samples consisted of $M@C_{82}$ and $M_2@C_{80}$, where M is an endohedral metal atom and was Er, Tb, or Gd. The $Gd@C_n$ species coalesced less readily than $Er@C_n$ and $Tb@C_n$, though coalescence was still greatly enhanced. It is known from other studies that endohedral, lanthanide atoms donate electron density to the carbon cage, typically of an order of two to three electrons. As coalescence reactivity was greatly increased in each of the three cases, it is reasonable to propose that the reactions are metal catalyzed. The precise assignment of the coalescence products was difficult due to the limited resolution of the instrumentation used, but it is clear that the isotope patterns do not match with the distributions expected for pure carbon clusters in the positive-ion mode and therefore more than one species must be present within the distribution; by contrast, in the negative ion mode, the distributions appear to correlate much more closely with the expected values. It has been postulated that pure carbon clusters are observed in the negative ion mode, while other species such as metal-containing clusters may be present in the positive ion mode. Use must be made of a mass spectrometer with a higher resolution in future, in order to establish the constituent species within the distributions of coalescence products.

11.1l Chapter Ten: "Evaluation of Electrospray Ionization as an Analytical Tool for the Analysis of Fullerenes and Their Derivatives"

As pure fullerenes have become better understood over the years and the search for potential applications of this knowledge has increased, it is inevitable that research should be more directed towards the synthesis and analysis of fullerene derivatives. However, the lability of some derivatives, such as hydrogenated fullerenes with respect to heating, places restrictions upon what ionization techniques may be used. MALDI is one "soft" ionization technique which is frequently used, but reaction with the analyte, such as oxidation, can limit the usefulness of this method. One of the most promising ionization techniques is electrospray ionization due to its ability to produce molecular ions with little or no fragmentation, and the lack of heating or use of photoirradiation. It therefore represents one of the gentlest ionization methods. Analysis of fullerenes using ESI has always been problematic, however, and the samples have frequently been modified in order to make them "ESI-active." One group has thus far been able to analyze pure fullerenes straight from a toluene solution using ESI, but no support for such an experimental method has been found in the literature since that time. Conclusive evidence for the viability of ESI as an analytical method for the investigation of fullerenes and their derivatives is therefore much sought after. It was with this in mind that an study into the suitability of this technique was performed. It was shown that ESI is indeed a viable technique for the structural analysis and characterization of fullerenes and their derivatives. It was also shown that neither protonation nor deprotonation occurred prior to ionization, and only radical molecular ions were observed in most cases. The ability to establish the molecular ion so clearly is indeed significant and the evidence obtained during the research should provide

support for future fullerene research with the increased emphasis on synthetic derivatization and analysis of these derivatives.

11.2 Summary

The research detailed in this report represents a contribution to the advancement of fullerene science. The study of coalescence reactions has demonstrated the varying degrees of reactivity amongst differing fullerene derivatives, and the discussion of the relative ionization energies of the samples and possible precursors for coalescence reactions provides insight into the mechanisms of such reactions. The discovery of the formation of $C_{120}O$ under ambient conditions and in the solid state represents a surprising discovery which has consequences for future applications of fullerenes while also contributing to the understanding of coalescence which does not lead to pure carbon clusters. Frequent difficulties encountered during the analysis of fullerene derivatives, where the sample exhibits extensive and undesirable fragmentation, have been overcome through the demonstration that electrospray ionization can indeed prove to be a viable method for obtaining the molecular ion of pure fullerene and fullerene derivative samples. The study of delayed ionization has shown that mass spectrometrists must exercise caution when attributing signals obtained using ToF instruments as arising through fragmentation of larger species. The study also led to the discovery that the instrumental features may be used to an advantage, enabling the routine investigation of delayed ionization. New avenues of inquiry have been created within the research group as a result of the findings detailed. The study of coalescence has been widened to include new fullerene derivatives and new, non-fullerene precursors have also been used in the attempt to generate fullerenes through laser ablation. Delayed ionization is currently being examined for a range of fullerene

derivatives using the methods described earlier. Though the topics covered and the samples used in this report have varied, a continuous theme has always been present: the characterization of fullerenes and their behavior in the gas phase through the use of mass spectrometry; the body of this research contributes to a better understanding of the properties fullerenes and their derivatives and has already led to new avenues of investigation.

.3

DX

240334